AN ABSTRACT OF THE DISSERTATION OF

Claudia Gabriela Mayorga Adame for the degree of Doctor of Philosophy in
Oceanography presented on September 21, 2015.

Title: Modeled Larval Connectivity Patterns in two Coral Reef Regions: the
Western Caribbean and the Kenyan-Tanzanian Shelf

Abstract approved: ───────────────────────────────────────

Harold P. Batchelder   Yvette H. Spitz

Tropical coral reef ecosystems are very important from both the ecological and eco-
nomical points of view. However, they are also particularly fragile, and have been
declining in recent years in most regions of the world, since they are highly sus-
ceptible to anthropogenic stressors operating at global scales (e.g., global warming
and ocean acidification) and local scales (e.g., pollution/eutrophication, fishing, over-
commercialization for recreation). Coral reef ecosystems are complex communities
with very high species diversity. Most reef species have a bipartite life history with
a planktonic larval stage and a benthic associated adult life. Therefore most adult
reef organisms are distributed in metapopulations connected by pelagic larvae that
disperse subject to the ocean currents. Knowledge of population connectivity among
individual reef habitats within a broader geographic region of coral reefs has been
identified as key to developing efficient spatial management strategies to protect ma-
rine ecosystems. The study of larval connectivity of marine organisms is a complex
multidisciplinary challenge that is difficult to address with direct observations. This
research examines the temporal and spatial, physical and ecological processes influ-
encing connectivity of two important coral reef genera among isolated reef habitats
within two regions: the Kenyan-Tanzanian and the Western Caribbean coasts. High
resolution ocean circulation models were developed for each region and coupled to

individual based models (IBM) that track particles (virtual larvae) released from each reef habitat. The connectivity patterns for two coral reef species groups having contrasting larval behavior and development duration where characterized in the two study regions: *Acropora*, a genus of branching corals with passive larvae and fast development (pelagic larval duration (PLD)<12 days), and *Acanthurus*, a genus of highly mobile, herbivorous fish, with long PLD (>50 days). Additional simulations were done to represent better the complexity of the *Acanthurus* larval life: one experiment included an idealized ontogenetic vertical migration behavior; another experiment examined how temperature-determined larval duration influenced trajectories and settlement patterns. The more complicated behavioral and development models were evaluated by comparing connectivity matrices to the passively transported case. To investigate interannual variations in connectivity patterns and percentage of successful settlement experiments were done for two contrasting years 2000 and 2005. Environmental seasonal and interannual variability in the ocean circulation models was analyzed to detect the mechanisms controlling connectivity in the two regions. The connectivity patterns and the mechanisms causing them were compared among the two study regions. Results are interpreted in the context of marine spatial management, describing the implications of the modeled connectivity patterns for currently established Marine Protected Areas. The connectivity patterns, and the processes controlling connectivity for different taxa, provide policy relevant scientific information that enables managers and decision-makers to make more informed choices regarding the size, spacing and optimal spatial design of marine protected networks.

Modeled Larval Connectivity Patterns in two Coral Reef Regions:
the Western Caribbean and the Kenyan-Tanzanian Shelf

by

Claudia Gabriela Mayorga Adame

A DISSERTATION

submitted to

Oregon State University

in partial fulfillment of
the requirements for the
degree of

Doctor of Philosophy

Presented September 21, 2015
Commencement June 2016

Doctor of Philosophy dissertation of Claudia Gabriela Mayorga Adame presented on September 21, 2015.

APPROVED:

_____

Major Professor, representing Oceanography

_____

Dean of the College of Earth, Ocean and Atmospheric Sciences

_____

Dean of the Graduate School

I understand that my dissertation will become part of the permanent collection of Oregon State University libraries. My signature below authorizes release of my dissertation to any reader upon request.

_____

Claudia Gabriela Mayorga Adame, Author

ACKNOWLEDGEMENTS

all the difficulties and distress that this PhD of mine brought you. To my son Ian Giorgi Bravo-Mayorga, thank you for being so flexible and understanding, for your contagious happiness and unconditional love. It is because of you that I go on. Finally, to my mom, for always being there for me in the hardest times.

TABLE OF CONTENTS

TABLE OF CONTENTS (Continued)

TABLE OF CONTENTS (Continued)

LIST OF FIGURES

LIST OF FIGURES (Continued)

LIST OF FIGURES (Continued)

LIST OF FIGURES (Continued)

LIST OF TABLES

LIST OF APPENDIX FIGURES

Chapter 1: Introduction

Tropical coral reef ecosystems are among the most important living communities in the ocean, being the richest repositories of marine biodiversity [Spalding et al., 2001] They are also very complex and fragile ecosystems, highly susceptible to environmental changes that alter water temperature, pH (ocean acidity), sedimentation, pollutant concentrations and light availability, as well as changes in the reef community due to unsustainable fishing practices and the impacts of recreational tourism [Hughes et al., 2003; Pandolfi et al., 2003]. Less than 0.1% of the World Oceans are covered by coral reefs [Spalding et al., 2001], and these areas have been shrinking or their integrity threatened by direct anthropogenic activities and global climate change. While some coral reef systems, such as the Caribbean and Australian Great Barrier Reef are relatively well studied, other shallow water coral reefs, such as those off East Africa and most South Pacific Islands, are located in ocean regions where very few oceanographic studies have been conducted and where economic constraints are a major issue. However, the effort to protect these special areas has become global through international initiatives like the Reefs at Risk project [`http://www.wri.org/our-work/project/reefs-risk`], the Coral Reef Targeted Research (CRTR) program [`www.gefcoral.org`] and the International Reef Initiative [`http://www.icriforum.org/gcrmn`].

Despite the high diversity of coral reef organisms most species have in common a bipartite life history with a planktonic larval stage and a benthic associated adult life. As adults coral reef organisms exhibit various degrees of site attachment from completely sessile, like corals and sponges to highly mobile, like fish and crustaceans. However, even fish capable of swimming several kilometers in a few hours have restricted home ranges, since they are relatively territorial and are associated with specific reef habitats that are patchily distributed. Most adult reef organisms are distributed in metapopulations connected by pelagic larvae that disperse subject to the ocean currents.

Marine Protected Areas (MPAs, sometimes referred to as Marine Reserves) have been proposed as a spatially explicit approach to protect and restore populations of fished species, biodiversity, and the functional integrity of marine ecosystems, as well as to enhance fisheries yield beyond the boundaries of the MPAs [Agardy, 1997 as cited in Cowen et al., 2007; Sobel and Dahlgren, 2004]. MPAs have been implemented in coral reef regions worldwide. There are 2679 MPAs in coral reefs covering approximately 27% of the total area of tropical coral reef ecosystems [Burke et al., 2011]. However, the efficacy of MPAs as a spatial management strategy to guarantee sustainable marine resources is debatable, since the results of its implementation vary widely among different regions [Christie et al., 2010b; Fraschetti et al., 2006; Halpern, 2003; Maina et al., 2008; McClanahan et al., 1999]. According to the study of Burke et al. [2011], only 15% of the MPAs that contained coral reefs are effectively reducing the threat of overfishing, therefore only around 6% of the world's coral reefs are being effectively protected by MPAs. The level of protection provided by MPAs depends on their design and the effectiveness of their implementation. Often MPAs exist only as 'paper parks', since their management framework is not enforced by the implementing agencies, and/or the protection rules are ignored by local stakeholders that have conflicting interests resulting in obsolete policies and ineffective management strategies. Inconsistent results of the implementation of MPAs, even when properly enforced and monitored, indicate that the design (placing, size and separation distance) of individual MPAs within networks is not trivial and make evident the need for a comprehensive understanding of the spatial dynamics of marine populations. Several studies [e.g. McCook et al., 2009; Botsford et al., 2009 Botsford et al., 2003] emphasize the importance of connectivity of multiple types (larval dispersal, juvenile and adult swimming, and movement of fishers) in impacting the performance of MPA based spatial management for meeting population sustainability and fishery yield objectives. In a recent study using genetic parentage analysis, Harrison et al. [2012] documented (1) significant retention of larvae of two coral reef fish within their natal reserves, (2) connections among MPAs, and (3) a high proportion of fish export to adjacent fished areas. These results show that strategically designed and properly implemented MPAs can benefit both fish and fisheries and

highlight the importance of adequately designed MPA networks. Coral reef species with long larval durations (i.e. > 1 month) can travel long distances in the plankton before being competent to settle. Individual reserves may be unable to support self-sustaining populations of these species, but they may be able to persist locally through larval supply from other protected areas [Roberts, 2012].

Larval connectivity is vital to the survival of marine metapopulations, both at ecological and evolutionary time scales. Theoretical studies suggest that population connectivity plays a fundamental role in local and metapopulation dynamics, community dynamics and structure, genetic diversity, ecosystem responses to environmental changes, and the resiliency of populations to human exploitation [Cowen et al., 2007]. According to the same authors:

> "Population connectivity refers to the exchange of individuals among geographically separated subpopulations that comprise a metapopulation. Set in the context of benthic-oriented marine species, population connectivity encompasses the dispersal phase from reproduction to the completion of the settlement process (including habitat choice and metamorphosis)."

Connectivity among marine metapopulations is determined by physical transport and dispersion, temperature and biological processes such as the timing of spawning, pelagic larval duration (PLD), behavior, and mortality. The net effect of these processes determines the spatial scales over which a population is connected [Gawarkiewicz et al., 2007]. Connectivity is therefore a function of several interacting variables including species, geographical area, time of the year, and ocean conditions, and consequently is highly variable in both space and time [e.g. Christie et al., 2010a; Cowen and Sponaugle, 2009; Domingues et al., 2012]. Even for passively transported particles, it is difficult to adequately resolve time-varying three-dimensional dispersion over large enough spatial scales using direct measurements [i.e. Willis and Oliver, 1990], due to the very high spatial and temporal resolution needed. It becomes even more problematic for complex living particles that move, grow and die, making the estimation of connectivity among discrete habitat patches

using direct observations extremely difficult. Connectivity for some species has been established recently through genetic studies [Baums et al., 2005; Jones et al., 2005; Christie et al., 2010b; Hogan et al., 2012; Harrison et al., 2012], spatially varying natural bio-markers [Thorrold et al., 1998] or tagging of larvae [Jones et al., 2005; Almany et al., 2007]. These techniques are limited in the spatio-temporal scales they can resolve, and some of them are restricted to specific species or environments. The technical limitations of these methods led to the development of biophysical models that capture the spatial-temporal dynamics of marine populations, especially with respect to larval dispersal [Willis et al., 2003; Sale et al., 2005; Werner et al., 2007]. Individual based Lagrangian particle tracking models (hereafter, IBMs) coupled to realistic high resolution ocean circulation models offer great flexibility to study potential connectivity of marine organisms during their planktonic larval stage. Ocean circulation models are capable of providing a representation of the ocean state that the larvae experience at high spatial and temporal resolution. IBMs can incorporate life history traits and behavioral capabilities of the organisms at different developmental stages. By tracking each individuals life experience the variability within a population is represented in a more realistic way [Werner et al., 2001]. When coupled to high resolution ocean circulation models, IBMs are able to resolve time varying three-dimensional dispersion of planktonic larvae over large spatial scales with high spatiotemporal resolution, offering a viable method to obtain a more comprehensive understanding of the larval connectivity patterns that potentially links adult habitats; this could lead to more efficient design of MPAs. The goal of this study was to take advantage of the capabilities of biophysical modeling to study connectivity among coral reefs in the Kenya-Tanzania (hereafter KT) region off east Africa (Fig. 1.1), an economically and ecologically important coral reef region where larval connectivity studies are lacking. The information generated would be of prime interest to scientists seeking to understand the local populations of coral reef associated organisms, and to managers and decision makers seeking to (1) regulate the use of coral reef resources, (2) designate new MPAs, and (3) optimize the effectiveness of existing MPAs. While the coupled model can provide estimates of connectivity among coral reefs and estimate the potential of specific MPAs to seed other non-protected

regions, verifying these patterns in the KT region would be very difficult due to the lack of empirical field studies on ecological connectivity and recruitment of coral reef species. For that reason, a second study region in the Western Caribbean (hereafter WC; Fig. 1.2), with similar coastal morphology and general mesoscale circulation patterns selected to conduct parallel studies. The WC region has been the focus of many connectivity studies; therefore results generated for this region can be verified against observations from empirical studies and build confidence on the findings for both regions. The specific objective of my research was to develop high resolution ocean circulation model applications coupled with a Lagrangian particle tracking models to examine the potential (and expected) connectivity of isolated reef habitats within two coral reef ecosystem regions: the Kenyan-Tanzanian coast off east Africa (hereafter KT) and the Eastern coast of the Yucatan peninsula in the Western Caribbean Sea (hereafter WC). Connectivity patterns among coral reef patches at each site could be used to aid managers and decision makers regarding the size, spacing and optimum spatial arrangement of marine protected areas. The comparison of two similar, but not identical, regional scale coral reef ecosystems will identify similarities and differences between the connectivity patterns and provide insights on the generality of mechanisms controlling connectivity.

1.1 Study sites background

Coral reef ecosystems in both study regions (KT and WC) are important from both the economical and conservational points of view. Both study regions have been identified by the Coral Reef Targeted Research program (CRTR `www.gefcoral.org`) as key sites for the establishment of "Centers of Excellence". These centers form part of an international network, which has the aim of developing research, awareness and conservation strategies to preserve the coral reef environments around the world. The local economies of both Tanzania and Kenya depend strongly on their coastal and marine resources. Healthy and productive marine ecosystems are required to sustain tourism, fishing, pearl and seaweed farming activities. The coastal region of Tanzania contributes about one-third of the nations annual gross domestic product

(GDP) [Whittick, 2007], while Kenya coastal tourism accounts for 60-70% of the national tourism industry ($\sim 1/8$ of the national GDP) [Odido and Mazzilli, 2009], adding up to 17 billion dollars in 2013. The Mesoamerican Barrier Reef, the second largest barrier reef in the world lies along the WC coast of the Yucatan Peninsula [Cetina et al., 2006]. This ecosystem generates important tourism and fishing income to Mexico, Belize, Guatemala and Honduras. Cancun alone produces approximately 35% of the total annual tourism income of Mexico, more than 4.5 billion dollars in 2008. While the sand, sun and surf are the main attractions bringing tourists to the region, the diving, snorkeling, fishing and coral reef wildlife are also important attractions [Dupont and Thomas, 2004]. The two regions share similar coastal morphologies, characterized by narrow channels formed between the mainland and small islands, (Pemba, Mafia and Zanzibar Island, off of Tanzania (Fig. 1.1); Cozumel Island, Chinchorro Bank, Turneffe Island Atoll, Lighthouse Reef and Gladden Spit off of the Yucatan Peninsula (Fig. 1.2), surrounded by fringing reefs in addition to many other reef patches. Both sites are located in western boundary currents that flow northward throughout the year; the Caribbean Current (CC) on the Yucatan peninsula coast (Fig. 1.2) and the East African Coastal Current (EACC) on the Kenyan-Tanzanian coast (Fig. 1.1).

Many studies have examined the circulation in the Western Caribbean, based on direct observations [e.g. the CANEK project; Chvez et al., 2003; Cetina et al., 2006; Andrade et al., 2003; Richardson, 2005], satellite altimetry [e.g. Andrade and Barton, 2000], and modeling [e.g. Chrubin et al., 2008; Tang et al., 2006; Sheng and Tang, 2003]. Some observational studies used trajectories of subsurface Lagrangian drifters to describe the mean currents and eddies [Richardson, 2005]. The region has been the focus of many modeling studies, examining connectivity at fairly large scales [Treml et al., 2008; Cowen et al., 2006]. Few studies focus on particular species [e.g., Paris et al., 2005; Baums et al., 2006] or connectivity at scales small enough (~ 2 km resolution) to be useful for the design of marine protected areas [Paris et al., 2007; Tang et al., 2006]. A model that fuses both high resolution physics and particular species behavior is a logical next step that will provide results useful for management, while increasing the knowledge of the population ecology for particular species (see

Sponaugle et al. [2012] for an example in the Florida Keys). Compared to the Western Caribbean, there are few studies of the general ocean circulation in Kenya-Tanzania region. Those with an observational approach are based on very few measurements [e.g. Swallow et al., 1991; Shaghude and Wanns, 2000]. The Zanzibar region is included in some basin scale models [e.g.Hermes and Reason, 2008], and there are some ongoing efforts to model the ocean circulation on a regional [Manyilizu et al., 2014; Mayorga-Adame et al., accepted, also Chapter 2] and local scale [Mahongo and Shaghude, 2014; Zavala-Garay et al., 2015]. However the horizontal resolution of the regional scale models (ca. 4-5 km) is still insufficient to assess connectivity among individual coral reef habitats, which are of similar scale or smaller than these models. Local scale models have a more adequate horizontal resolution but are restricted to small areas.

1.2 Genus background

Two organism types (genera) with contrasting behavior and early life history traits were chosen for this connectivity study: *Acropora* corals and *Acanthurus* surgeon-fishes. These two genera were selected due to their ecological importance in coral reef systems, and because they have representative species in both the Kenya-Tanzania and Western Caribbean coral reef systems. There are regional and species specific variations in the biological and behavioral characteristics of the selected organisms at the genus level, however there is not enough information to study particular species. The details of the larval development of coral reef organisms are known for only a few species that are amenable to aquarium rearing, mainly demersal spawning species. Knowledge about larval behavior and ontogenetic changes is even more scarce [James et al., 2002]. This uncertainty made it impossible to focus on particular species, since not enough biological information (e.g., natural history knowledge) was available at that level. The genus *Acropora* was chosen because it is an ubiquitous species group and the dominant coral genus in many reefs. It is a fast growing branching coral that due to its intricate morphology provides shelter for many species of invertebrates and fish. Acropora are a highly resilient species group. Because of their high growth rate

they are known to quickly recover from stress and rapidly recolonize reefs after local mortality events due to bleaching and storm damage (Direct tracking of coral larvae: Implications for dispersal studies of planktonic larvae in topographically complex environments [Wallace, 2011]. For the purposes of this model study, they can be considered a model species whose larvae are passively dispersed (as if neutrally buoyant), and have a short pelagic larval duration (PLD). *Acropora* are hard branching corals, also known as staghorn corals, of the Acroporidae family (class Anthozoa, order Scleractinia of the phylum Cnidaria). They are colonies of small sac-like polyps that produce a calcium carbonate skeleton. They grow rapidly in many different intricate forms providing structure to the reef, shelter and habitat complexity for other reef biota, as well as food for corallivore species [Wallace, 2011]. *Acropora* are symbiotic corals, a primary initial link in the reef food chains, since they host zooxanthellae, endosymbiotic algae that fix light energy through photosynthesis [Richmond, 2002]. They are also capable of capturing and consuming plankton; different species depend to greater or lesser extent on direct heterotrophic consumption [Wallace, 2011]. The life cycle of *Acropora* corals consists of a dominant benthic polyp phase and a shorter planula larval stage (Fig. 1.3) [Harrison, 2011]. They are capable of asexual reproduction when branches break from the colonies, but sexual reproduction is more common in most species. They release gametes into the water column for external fertilization in broadcast spawning events [Wallace, 2011]. At mid latitude regions, like the Great Barrier Reef and Western Australia, *Acropora* species spawn as part of "mass spawning events"; large, multispecific coral assemblages release gametes synchronously in one evening between dusk and midnight (The life cycle of *Acropora* corals consists of a dominant benthic polyp phase and a shorter planula larval stage (Fig. 1.3) [Harrison, 2011]. They are capable of asexual reproduction when branches break from the colonies, but sexual reproduction is more common in most species. They release gametes into the water column for external fertilization in broadcast spawning events [Wallace, 2011]. At mid latitude regions, like the Great Barrier Reef and Western Australia, *Acropora* species spawn as part of "mass spawning events"; large, multispecific coral assemblages release gametes synchronously in one evening between dusk and midnight [Harrison et al., 1984]. Scleractinian corals in equatorial

reefs show less synchronous, protracted spawning seasons [Mangubhai and Harrison, 2008; Mangubhai, 2008]. Sexual reproduction in corals seems to be strongly influenced by environmental factors; seasonal changes in sea temperature, day length, wind or current patterns, lunar cycles of night irradiance, solar insolation cycles, duration of regional low wind periods and absence of heavy rainfall have been identified as cues that determine the timing of coral spawning events (briefly reviewed by Wallace, 2011). At low latitude, tropical Pacific reefs peak reproduction tends to occur in late spring to early summer. Subtropical and higher latitude reefs show later peaks in reproduction [Harrison, 2011]. In the Caribbean, A. cervicornis and A. palmata spawn between July and September [Van Woesik et al., 2006]. On equatorial reefs in Kenya *Acropora* species have been reported to spawn from October to April, with most colonies releasing gametes between January-March [Mangubhai and Harrison, 2008; Mangubhai, 2008; Harrison et al., 1984]. Scleractinian corals in equatorial reefs show less synchronous, protracted spawning seasons [Mangubhai and Harrison, 2008]. Sexual reproduction in corals seems to be strongly influenced by environmental factors; seasonal changes in sea temperature, day length, wind or current patterns, lunar cycles of night irradiance, solar insolation cycles, duration of regional low wind periods and absence of heavy rainfall have been identified as cues that determine the timing of coral spawning events (briefly reviewed by Wallace, 2011). At low latitude, tropical Pacific reefs peak reproduction tends to occur in late spring to early summer. Subtropical and higher latitude reefs show later peaks in reproduction [Harrison, 2011]. In the Caribbean, A. cervicornis and A. palmata spawn between July and September [Van Woesik et al., 2006]. On equatorial reefs in Kenya *Acropora* species have been reported to spawn from October to April, with most colonies releasing gametes between January-March [Mangubhai and Harrison, 2008; Mangubhai, 2008] A day or two after spawning the eggs develop into planulae larvae with limited motility [Babcock and Heyward, 1986]. Most *Acropora* planulae settle after 4-10 days in the plankton [Babcock and Heyward, 1986; Nishikawa et al., 2003; Nozawa and Harrison, 2008], however they can have settlement competency periods that extend several weeks if suitable benthic habitat for settlement is not available [Nishikawa et al., 2003; Nishikawa and Sakai, 2005]. Maximum PLDs of

ca. 100 days have been reported [Graham et al., 2008]. *Acropora* is considered a reef-front genus, since they prefer to settle near the outer edge of the reef, favoring sites with good circulation, high oxygen content, and access to food from oceanic waters [Wallace, 2011].

The surgeonfish genus *Acanthurus* was selected as a second target for dispersal studies because of their important ecological role as grazers on reefs; it is a common genus on coral reefs worldwide and is often very abundant. Surgeonfish are pelagic spawners and have larvae with long PLD. Fish with these characteristics are challenging to work with experimentally and have received minimal attention in potential connectivity studies because of the lack of observational data to compare model results, and the lack of behavioral and physiological data to characterize virtual larvae. Another reason for selecting this fish group was that their late larvae are one of the stronger swimmers among coral reef fish larvae, which both provides a contrast with coral larvae, and satisfies a settlement capability assumption commonly made when modeling coral reef larval fish. According to this assumption, larvae are able to detect, swim to and settle at reefs only when they are closer than a defined perception distance [Paris et al., 2007].

Acanthurus is the largest genus of surgeonfishes (family Acanthuride, distinguished by the possession of a knifelike spine or spines at the base of the tail). The genus contains 32 species, four of them inhabit the Atlantic Ocean and the remainders are found in the Indo-Pacific [Randall, 1961]. They are generally regarded as herbivorous although there are four zooplanktivorous species. Most of them feed on macrophytic (leafy/fleshy) and filamentous algae on reefs [Winterbottom and McLennan, 1993; Choat and Axe, 1996]. Their constant grazing helps keep algal populations in check and provides clear areas for invertebrate larvae to settle [Colin and Clavijo, 1988]. They play an essential role in coral reef ecosystems since low abundances of herbivorous fish potentially leads to the proliferation of macroalgae and decline of coral cover [Hawkins and Roberts, 2004]. In the Atlantic *Acanthurus* species are of minor commercial value, occasionally used as bait. In the Indo-Pacific they are more important as commercial species and often the bulk of artisanal fisheries. Craig et al. [1997] reported an annual catch of 28 metric tons of *Acanthurus*

lineatus in the artisanal fishery of American Samoa in 1994, which accounted for 39% of the fishery catch. Some species are targeted for the aquarium trade worldwide.

Acanthurus are broadcast-spawners that spawn year round in low latitudes with peak spawning during February and March [Randall, 1961;Munro et al., 1973; Craig, 1998]. Spawning time is likely determined by a combination of species specific diel rhythms and tidal phase, with most species spawning at sunset during ebb tides [Robertson, 1983; Myrberg et al., 1988; Craig, 1998]. They spawn both in pairs and in aggregations of up to several thousand individuals after a peculiar migration to open waters at reef edges [Robertson, 1983; Kiflawi and Mazeroll, 2006].

Eggs are approximately 0.7 mm in diameter, positively buoyant and transparent. After about one day, fertilized eggs hatch into yolk-sac larvae, which become negatively buoyant as they consume the yolk sac. Approximately four and a half days after hatching they become feeding larvae (see Randall, 1961 for details on A. triostegus). They start exhibiting swimming movements to maintain their vertical position 42.5 hours after hatching. Five-day-old larvae are capable of oriented swimming [Randall, 1961]. Older larval stages of *Acanthurus* are known as acronurus (Fig.1.4, conspicuous specialized planktonic larvae with strong swimming capabilities. Reported swimming speeds of acronuris from in-situ experiments range from 8.7 to 65.3 cm s^{-1} [Leis and Carson-Ewart, 1999; Leis and Fisher, 2006].

Diel vertical migration has not been reported for *Acanthurus* larvae [Huebert et al., 2011]. Ontogenetic vertical migration (OVM) has not been corroborated and studies show mixed results. The distribution of *Acanthurus* larvae in the Caribbean [Oxenford et al., 2008] and in French Polynesia [Irisson et al., 2010] at the family level indicate that OVM is highly likely [Huebert et al., 2011] did not observe an ontogenetic vertical shift for Acanthurid larvae in the Straits of Florida, however they captured only young larvae (smaller than 7 mm) found at the 45 26 m depth range. High densities of late acronurus larvae (9-41 mm) found in open waters of the eastern Caribbean, northeast and northwest of the Lesser Antilles, up to 200 km away from the nearest reef, were most abundant at 100-150 m and were found at 576 m depth [Oxenford et al., 2008]. Larvae of the family Acanthuridae collected around Tetiaroa (French Polynesia) displayed a vertical spread during ontogeny indicative

of a clear downward ontogenetic shift in the vertical distribution of the pre-flexion, flexion and post-flexion larvae. Median depth of the center of mass of larval patches increased from 35 m in the pre-flexion stage to 41 m in the flexion stage and 43 m in the post-flexion stage. Acanthuridae larvae were found between 0 and 90 m depth and the probability of encountering post-flexion larvae was equally high at 25 m and 60 m depth [Irisson et al., 2010]. Pelagic larval duration (PLD) for Caribbean species of *Acanthurus* ranges from 45-70 days with a mean of 56 days and an average length at settlement of 26.8 mm [Rocha et al., 2002]. The Indo-Pacific species A. triostegus has a mean PLD of 54 days (range of 44-83 days) and a mean length at settlement of 25.7 5mm [Randall, 1961; McCormick, 1999; Longenecker and Langston, 2008].

After settlement, *Acanthurus* quickly adapt to the benthic lifestyle. Lecchini [2005] reports that A. triostegus and A. nigricuda settled into benthic habitat occupied by juvenile conspecifics and that recently settled fish had similar behavior to older juveniles. Permanent migrations during adult life are not common especially for territorial species [Randall, 1961]. *Acanthurus* have potentially long life spans; [Choat and Axe, 1996] report life spans of 32 years for A. olivaceus and 46 years for A. lineatus. Most species reach sexual maturity between 3 and 7 years of age [Lecchini, 2005].

The objective of modeling two very different species groups with contrasting PLD, perception distances and swimming ability is to illustrate potentially different connectivity patterns among coral reef organisms, encompassing the wide spectrum likely generated by the highly diverse group of organisms living in coral reefs. Knowledge of the connectivity patterns of multiple species groups is essential when trying to design networks of MPAs that provide high connectivity for many species having different life history traits, particularly in the pelagic larval phase of the life cycle. By comparing and contrasting two coral reef regions with similar morphology and large scale circulation patterns I expect to develop more robust (e.g., general) insights on the mechanisms and tradeoffs that determine connectivity in coral reef regions. Identifying generalities and differences among the two regions will provide information about factors expected to have an important effect on coral reef connectivity in general, which will make this research relevant beyond the studied regions. My goal

is to make a significant contribution to the growing body of knowledge of larval connectivity in coral reef ecosystems and provide relevant information for managers and decision makers tasked with coral reefs conservation in the study regions, particularly in the design, placement and monitoring of MPAs.

In the following chapters I describe the circulation and hydrographic characteristics of the two study regions using the ocean circulation model applications developed; the Kenya-Tanzania Coastal Model (Chapter 2), and Mesoscale Caribbean Circulation Model (Chapter 4). Then I describe the particle tracking experiments accomplished to investigate the reef-to-reef and subregional connectivity of passive virtual larvae with life history traits of *Acropora* and *Acanthurus* larvae. Separate simulations of *Acanthurus* implementing an idealized ontogenetic vertical migration behavior and temperature dependent PLD were done to investigate the effects of behavior and environmentally controlled physiology on connectivity. Results of the particle tracking experiments for the Kenyan-Tanzanian region are reported in Chapter 3 and for the Western Caribbean region in Chapter 5. Lastly, in Chapter 6 the connectivity patterns of corals and surgeonfish from the two study regions are compared and contrasted and the implications of the results are discussed in the context of MPA management.
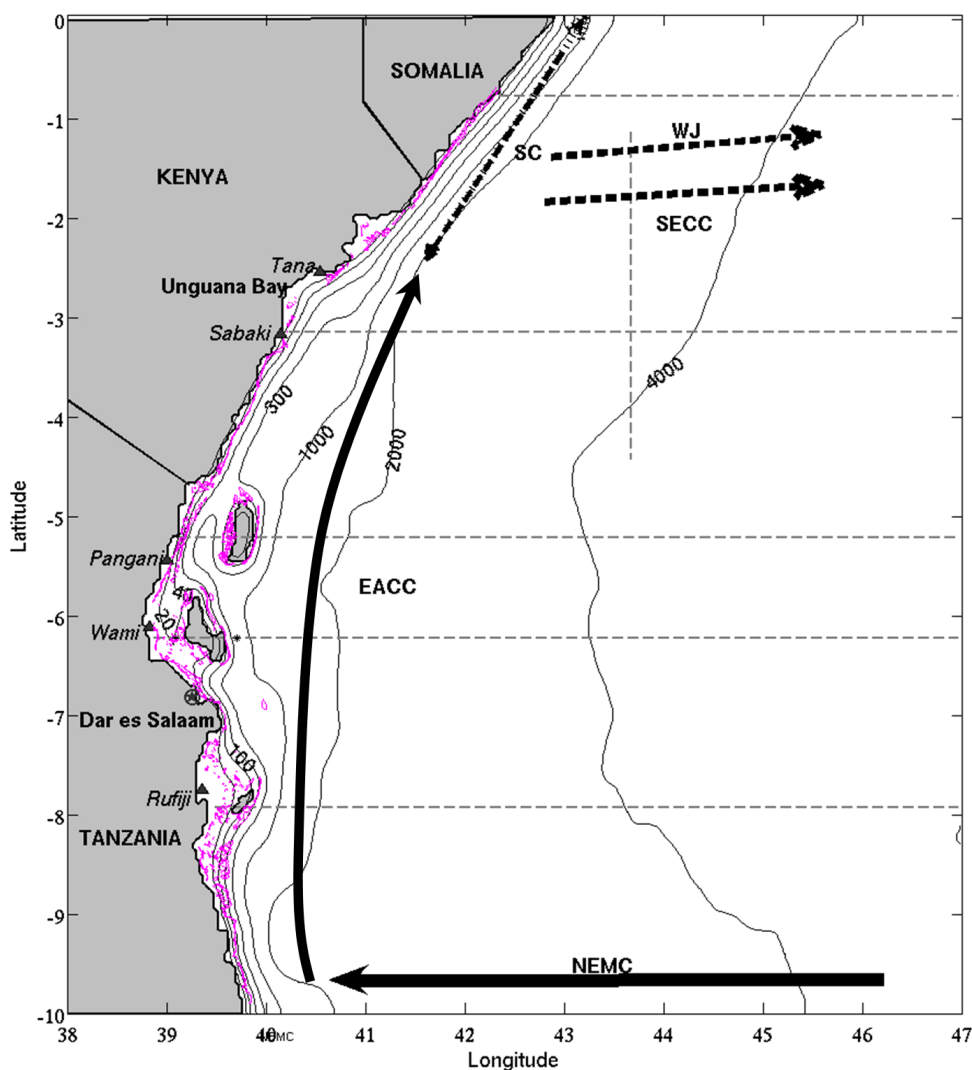
Figure 1.1: Map of the Kenyan-Tanzanian region showing the model domain with reefs in pink. Arrows are a schematic representation of the main surface currents: East African Coastal Current (EACC), Somali Current (SC), South Equatorial Current (SEC), South Equatorial Counter Current (SECC), and the Wyrtki Jets (WJ). Dashed lines mark currents that are not present year round. Triangles mark major river mouths. The model coastline, bathymetry, and some important locations are shown. Islands from north to south are Pemba, Zanzibar and Mafia. Light dashed lines mark locations where model-data comparisons where done (see Chapter 2).
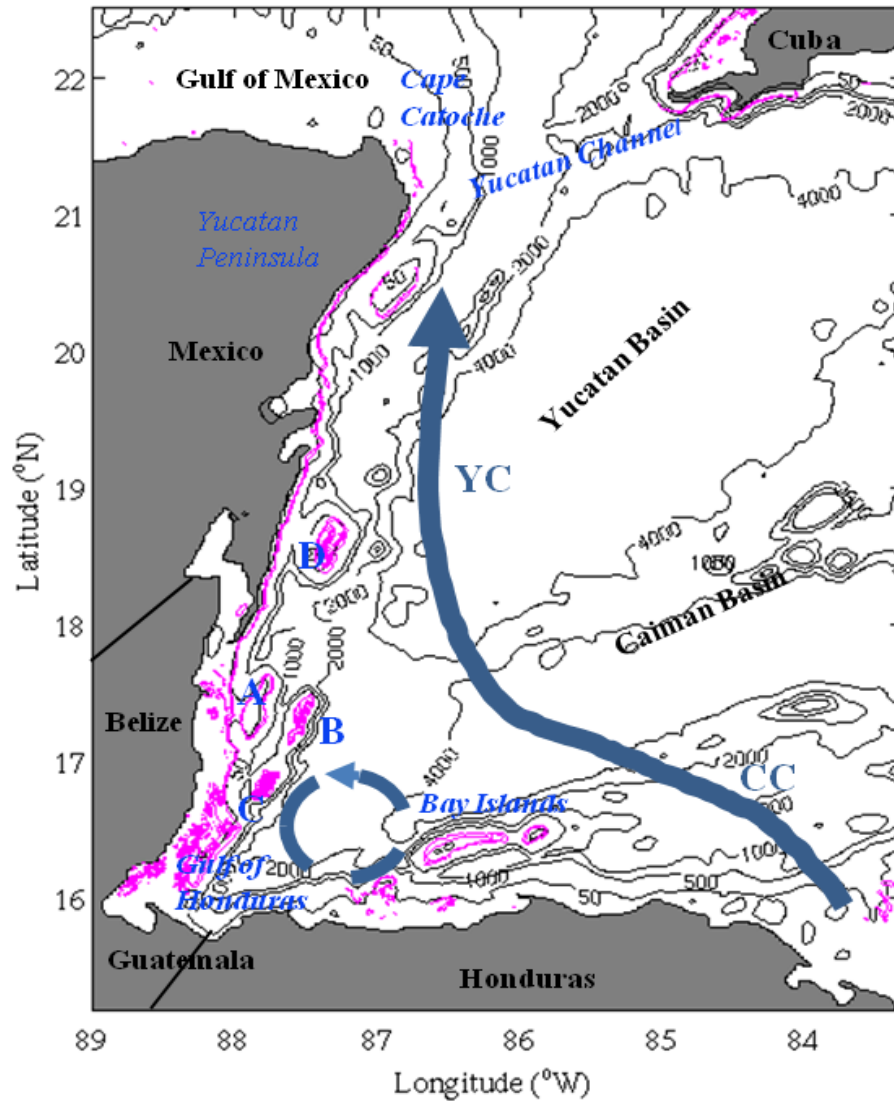
Figure 1.2: Map of the Caribbean region showing the model domain. The arrows represent schematically the main surface current: the Caribbean Current (CC), the Yucatan Current (YC) and an eddy that is often found in the Gulf of Honduras. Bathymetric contours and the main geographical features are labeled. Coral reefs are shown in pink with some important formations labeled by letters as follows: A. Meso-American Lagoon, B. Gladden Spit, C. Lighthouse Reef, D. Chinchorro Bank.
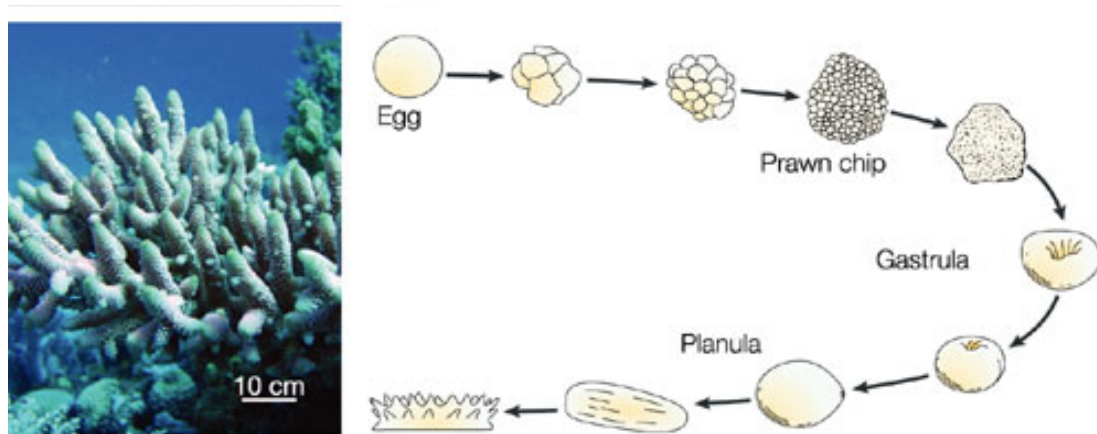
Figure 1.3: *Acropora millepora* life history. Drawings modified from Miller and Ball (2002). Photograph M. van Oppen.
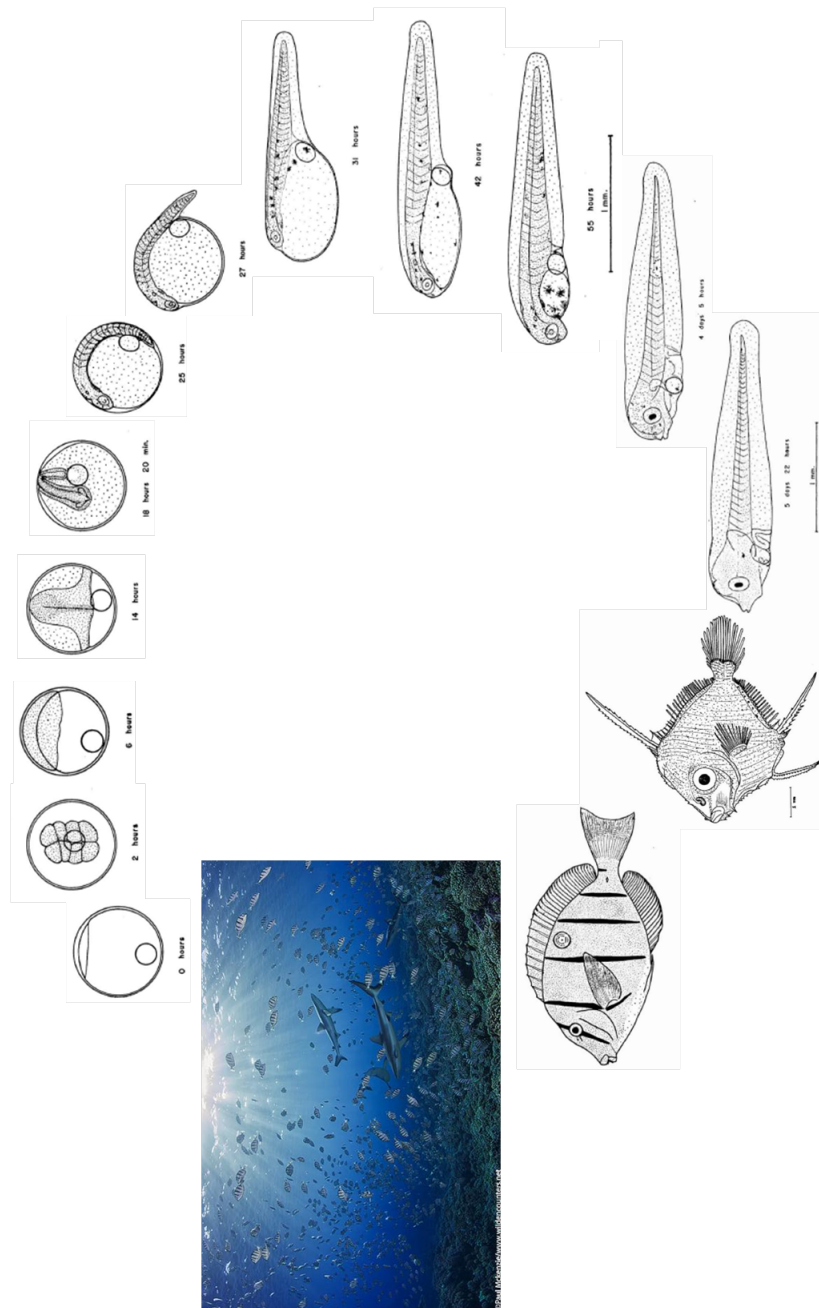
Figure 1.4: *Acanthurus triostegus* life history. Drawings from Randall (1961). Spawning aggregation photograph Paul Mckenzie.

Chapter 2: Characterizing the circulation off the Kenyan-Tanzanian coast using an ocean model

2.1 Abstract

The Kenyan-Tanzanian coastal region in the western Indian Ocean faces several environmental challenges including coral reef conservation, fisheries management, coastal erosion and near-shore pollution. The region lacks hydrodynamic records and oceanographic studies at adequate spatial and temporal scales to provide information relevant to the local environmental issues. We have developed a 4 km horizontal resolution ocean circulation model of the region: The Kenyan-Tanzanian Coastal Model (KTCM) that provides coastal circulation and hydrography with higher resolution than previous models and observational studies of this region. Comparisons to temperature profiles, satellite derived sea surface temperature and sea surface height anomaly fields, indicate that the model reproduces the main features of the regional circulation, while greatly increasing the details of the nearshore circulation. We describe the seasonal ocean circulation and hydrography of the Kenyan-Tanzanian coastal region based on a climatology of 8 years (2000-2007) of the KTCM simulations. The regional monsoon seasonality produces two distinct coastal circulation regimes: 1) During December to March there are relatively sluggish shelf flows; and 2) During April to November there are strong northward transports. Simulations from the model will be useful for examining dispersal of pollutants and spatial connectivity of coral reef species.

2.2 Introduction

Fishing, mangrove exploitation, tourism, and harbor services are important to the economies of Kenya and Tanzania. Approximately 20% of the gross domestic income of these countries is derived directly or indirectly from the coastal economies. Inade-

quate management of the marine resources has resulted in overexploitation, habitat destruction, pollution, and coastal erosion that diminish the value of coastal resources and activities [Odido and Mazzilli, 2009; Payet and Obura, 2004; Richmond, 2002]. A better understanding of the ocean circulation at temporal and spatial resolutions appropriate to these environmental issues will be valuable. However, this part of the East African coastal ocean has been grossly undersampled in comparison to neighboring areas such as the Somali coast and the Arabian Gulf [e.g. Vimal Kumar et al., 2008; Smith et al., 1998], the Red Sea [e.g. Roman and Lutjeharms, 2009] and the Mozambique Channel [e.g. Van der Werf et al., 2010; Ridderinkhof et al., 2010; Da Silva et al., 2009; Nauw et al., 2008; Matano et al., 2002]. Historically, the under-sampling is due to economical constraints of the local countries and the remoteness of the region, far from major oceanographic research institutes. Observational studies in the Kenyan-Tanzanian region continue to be a challenge, since most ships, including oceanographic research vessels, avoid the area due to concerns about piracy and high insurance expenses [Bendekovic and Vuletic, 2013].

Our knowledge of coastal dynamics off East Africa is based on limited observations [Manyilizu et al., 2014; Swallow et al., 1991; Shaghude et al., 2002]. The region is included in several basin-scale [Matano et al., 2008; Hermes and Reason, 2008; Mishra et al., 2007; Anderson et al., 1991] and global models [Sasaki et al., 2006; Chassignet et al., 2007], but their spatial resolution ($\sim$10-30 km) is too coarse to provide insight at the regional scale, and some important small-scale topographic features, like the Zanzibar Archipelago, are inadequately represented. Nearshore and shelf environmental issues, such as the threats imposed by pollution, overexploitation and habitat degradation and their potential impacts on water quality, health, eco-tourism, and sustainable recruitment of coral reef dependent species, require higher resolution physical models, capable of resolving small-scale transport processes. Near-field circulation profoundly influences dispersal and recruitment of coral reef organisms and the transport of pollutants. For example, in studies on coral reefs elsewhere, the important spatial scales for dispersal and recruitment of reef species varied from ¡5 km for coral larvae [Sammarco and Andrews, 1988] to 10-100 km for a variety of coral reef fish species [Cowen et al., 2006; Schultz and

Cowen, 1994]. Prior models [i.e.Manyilizu et al., 2014; Hermes and Reason, 2008 Pandey and Rai, 2008; Mishra et al., 2007; Xie et al., 2002; Lee and Marotzke, 1998; Anderson et al., 1991] that include the western Indian Ocean have not provided the resolution needed to address these environmental threats and enable assessment of their impacts.

The Tanzanian continental shelf is very narrow, with the 200 m isobath approximately 12 km offshore, except in the Mafia and Zanzibar Channels, where the shelf width extends ($\sim$60 km offshore (Fig. 2.1). Several islands in Tanzanian waters modify the coastal circulation and are of particular concern due to their rich coral reef ecosystems. The Zanzibar Archipelago, ($\sim$50 km offshore of the Tanzania mainland, is composed of several islets and two main islands: Unguja (also known as Zanzibar Island), and Pemba. Mafia Island is found farther south. Narrow channels ($<$60 km width) separate the islands from mainland Tanzania; the Mafia and Zanzibar Channels are shallow ($<$40 m depth), while the Pemba channel is much deeper ($\sim$500m maximum depth). The continental shelf north of Tanzania, off Kenya, is also narrow and protected by fringing coral reefs that stretch along the coast, except at the river mouths, where the continental shelf is wider (up to 15 km at the Tana River delta) [Odido and Mazzilli, 2009].

The monsoons are the dominant influence on the climate of the region generating a strong seasonality. The coastal circulation off Kenya and Tanzania is mainly influenced by (Fig. 2.1): (1) the northward flowing East African Coastal Current (EACC), fed by (2) the regionally westward flowing North East Madagascar Current (NEMC), (3) the seasonally reversing Somali Current (SC) and (4) local winds. The NE monsoon (November to February) is characterized by weaker winds ($\sim$6 m s $^{-1}$) from the NE, negative wind stress curl and upwelling along the coast. Farther offshore, wind stress curl is positive [Collins et al., 2012] and air temperatures are higher (22-34°C). During this period the SC flows southward across the Equator to meet the northward flowing EACC in a confluence zone between 2-4°S, supplying water for the eastward flowing surface South Equatorial Countercurrent (SECC). The SE monsoon (April to September) brings lower air temperatures (19-29°C) and stronger winds (up to 10 m s $^{-1}$) from the SE, positive wind stress curl and down-

welling along the coast, with negative wind stress curl farther offshore [Collins et al., 2012]. During this period, the EACC and the reversing SC create a continuous north-ward current adjacent to the Tanzanian and Kenyan coasts [Fieux, 2001], while the SECC becomes a subsurface current, masked by overlying westward Ekman currents [Schott et al., 2009]. The intermonsoon periods, March to April and October to November, are characterized by winds with lower speed and more variable direction [Schott et al., 2009; Odido and Mazzilli, 2009;Schott and McCreary, 2001]. At these times the Wyrtki Jets appear. These are strong eastward surface jets trapped within 2-3° north and south of the equator that uplift the thermocline in the western Indian Ocean (Fig. 2.1) [Fieux and Riverdin, 2001; Wyrtki, 1973]. There are two rainy seasons: the long rains during March to May and the short rains during November and December, with the maximum precipitation (approximately 20 cm month^{-1}) occurring during April and May [Odido and Mazzilli, 2009].

In addition to local atmospheric forcing and remote forcing created by the large-scale circulation, tidal currents are known to have an important effect on the inshore circulation of these regions [Shaghude et al., 2002; Van Katwijk et al., 1993; Mayorga Adame, 2007]. Freshwater inputs from rivers during the rainy seasons are also important in structuring shelf currents and hydrography [Van Katwijk et al., 1993], while diurnal variability of the local winds affects the nearshore surface currents.

Due to the challenges posed for field work in the region, our approach is to develop a high resolution model to characterize the circulation of the Kenyan-Tanzanian region at temporal and spatial scales relevant to local environmental issues. We developed a high resolution (4 km horizontal grid spacing) Regional Ocean Model System (ROMS) [Haidvogel et al., 2008] application and validate it with satellite observations and available in-situ measurements. This Kenyan-Tanzanian Coastal Model (KTCM) is used to investigate the influence of local atmospheric forcing, remote forcing through the model open boundaries and tidal forcing on the circulation and hydrography of the Kenyan-Tanzanian coast off East Africa. Forcing by freshwater input from rivers and the diurnal variability in local winds are not included in the present model.

The methods used are reviewed in Section 2.3, including descriptions of the model

(Section 2.3.1), the lateral boundary conditions (Section 2.3.2), the surface forcing (Section 2.3.3), initial conditions (Section 2.3.4) and the methods used to validate the model results (Section 2.3.5). Results are presented in Section 2.4, where we first compare model results to available satellite and in-situ observations (Section 2.4.1). The seasonality of the circulation and hydrography of the full model domain is presented in Section 2.4.2, followed by a detailed examination of the circulation of the coastal region within 60 km of land (Section 2.4.3). It is in the coastal region that the increased resolution of KTCM provides information relevant to the coastal environment of Kenya and Tanzania that is not available from previous studies [i.e. Hermes and Reason, 2008; Shaghude et al., 2002; Swallow et al., 1991]. In Section 2.5 we discuss the significance of our results and summarize our findings, and summarize our findings in Section 2.6.

2.3 Methods

2.3.1 Model overview

We use ROMS, a three dimensional, hydrostatic, terrain following, primitive equation model [Haidvogel et al., 2008] to simulate the circulation in the coastal ocean off Kenya and Tanzania. The model domain is a rectangular grid extending from 38° to 47°E and from the equator to 10°S (Fig. 2.1). It has a uniform horizontal resolution of 4 km and 31 vertical sigma levels with increased resolution towards the surface and the bottom. Inshore of the 500 m isobath, vertical resolution is finner than 20 m at intermediate depths; offshore, where depths exceed 3500 m, intermediate depths have ca. 300 m vertical resolution. Bathymetry for the region was created by fusing data from multiple sources: (1) ETOPO-02, (2) digitized nautical charts of the region and (3) sounder depth measurements collected by researchers of the Institute of Marine Sciences (IMS) of the University of Dar Es Salaam. This improved the bathymetry of the Zanzibar Channel, which is not accurately represented in the ETOPO-02 database. Near the eastern open boundary of the model domain ($\sim$920 km offshore), Aldabra and other smaller islands of the Comoros Archipelago were flattened to 4000

m depth to avoid numerical noise at the open boundary. Bathymetry was smoothed to meet a slope factor r <0.2, in order to reduce pressure gradient errors in terrain-following coordinates [Beckmann and Haidvogel, 1993]. The model coastline was manually modified to retain as many features as the 4 km horizontal resolution allowed. Only the islands of Zanzibar, Pemba and Mafia were included as dry cells in the land mask. The northern, southern and eastern edges of the model domain are open boundaries. A third-order, upwind-biased scheme is used for horizontal advection of momentum and tracers. Since clear water characterizes the region, Jerlov water type 1 was used [Jerlov, 1976]. A fourth-order, centered scheme was used for vertical advection of momentum and tracers. The generic length scale closure scheme [Warner et al., 2005; Umlauf and Burchard, 2003] with k-kl (Mellor-Yamada level 2.5) parameters [Mellor and Yamada, 1982] is used for vertical mixing. The Chapman open boundary condition is used for the free surface and the method of Flather is used for the depth-averaged velocities normal to the open boundaries [Marchesiello et al., 2001]. Radiation and nudging schemes are applied to the three-dimensional velocities and tracers at the boundaries. The nudging time scale is 20 days for outflow and 2 days for inflow. Since numerical noise was not generated at the open boundaries no sponge layer was used.

2.3.2   Boundary conditions

The boundary conditions provide tidal and remote forcing to the model. Tidal forcing was obtained from the TPXO7 [Egbert et al., 1994; Egbert and Erofeeva, 2002] Indian Ocean 2011 tidal solution atlas, with a resolution of $1/12^o$ in the study region. The tidal ellipse information and sea surface elevation harmonics were processed by ROMS to add the SSH and velocities contributed by tides to the boundary forcing. The 9 main tidal components: M4, K2, S2, M2, N2, K1, P1, O1, Q1 were included as forcing to KTCM.

Remote forcing at the open boundaries is driven by the gyre-scale wind stress curl and the resulting oceanic pressure fields that set up the large scale current system. Monthly open boundary conditions (temperature, salinity, sea surface height,

horizontal and vertical velocities) were extracted from the global Ocean General Circulation Model (OGCM) for the Earth Simulator (OFES) [Sasaki et al., 2006]. The OFES simulation has a horizontal grid spacing of $1/10^o$ (ca. 10 km in this region) and 54 fixed depth vertical levels. It was forced by daily mean QuickSCAT wind stress and atmospheric daily mean heat and salinity fluxes from the NCEP/NCAR reanalysis [Kalnay et al., 1996]. Remote forcing is summarized by examining the climatological volume transport across the open boundaries of the domain in the upper 500 m obtained from the parent model OFES (Fig. 2.2). The strongly seasonal flow and the abrupt transitions between monsoons broadly agree with observations [Schott et al., 2009]; [Schott and McCreary, 2001]. During the NE monsoon the primary transport balance is between inflow from the south and outflow to the east. During the SE monsoon the inflow from the south is joined by greater inflow from the east, from the seasonally broader NEMC, resulting in even greater outflow to the north (Fig. 2.2). The transport across the boundaries shows that the remote forcing imposes two main balances on the model: (1) during May-November (red arrows in Fig. 2.2 inset) inflow from the south and east is balanced by outflow through the northern boundary; and (2) during January-March (blue arrows) the inflow from the south is balanced by outflow through the eastern boundary since the outflow through the northern boundary is blocked by the influence of the southward flowing SC (Fig. 2.2, inset).

2.3.3   Surface forcing

Local atmospheric forcing consists of wind stress, heat and precipitation/evaporation fluxes that operate on the surface of the model domain. Surface forcing for KTCM was provided by daily mean atmospheric variables (air temperature and pressure, precipitation rate, relative humidity, solar radiation, downward longwave radiation, and the two components of the wind velocity) from the NCEP/NCAR reanalysis with a resolution of 1.8^o [Kalnay et al., 1996]. Atmospheric variables were bilinearly interpolated to the model grid. Wind stress, heat and fresh water fluxes were calculated by the ROMS atmospheric bulk formulation. Neither OFES nor KTCM

assimilate observations.

Of the local forcing variables, wind forcing has the strongest influence on the circulation of the modeled region. Collin et al. [2012] compared the NCEP wind product to QuickSCAT winds and concluded that despite its coarser resolution the NCEP reanalysis accurately represents the large scale wind patterns over the western tropical Indian Ocean. They describe important differences in the Somali Jet region north of our domain and around oceanic islands. QuickSCAT winds could make an important difference if the scatterometer was able to measure winds around the islands in our domain. However, there are no vectors inshore of these islands in the QuickSCAT wind product. Therefore we used NCEP winds for consistency with the other atmospheric forcing variables. The long term climatology of the wind forcing from 2000 to 2007 shows SE winds from April to November and NE winds in January and February (Fig. 2.3). The transition between SE and NE monsoons winds (and vice versa) happens very quickly. Intermonsoon conditions in the atmosphere, with weak onshore winds, are observed only in March and December.

2.3.4 Initialization

Transient model responses associated with initialization, were reduced by doing a 22-month ROMS spin-up from initial fields interpolated from the January 2000 OFES fields and climatological forcing (an average of 2000-2007 monthly boundary conditions from OFES and averaged daily surface forcing from the NCEP/NCAR reanalysis). Conditions at the end of the spin-up run were used as the initial conditions for an 8.25 year simulation (from October 1999 to December 2007). The first 3 months of the simulation were discarded to eliminate transient adjustments to the stronger and more realistic daily forcing. Results of the 8-year (2000-2007) simulation were averaged to form a monthly climatology. This yields a realistic representation of non-linear responses within the ocean to strong and rapidly changing surface forcing. The results describe the averaged response to energetic forcing, rather than the response to averaged (weaker and smoother) forcing obtained when forcing with climatological fields. We use this monthly climatology to examine the seasonal circulation off

Kenya and Tanzania.

2.3.5   Model validation

Year specific model results are compared with Pathfinder v5 satellite SST [`http://www.nodc.noaa.gov/sog/pathfinder4km/`], altimeter sea level anomaly (SLA) fields from AVISO [Archiving, Validation and Interpretation of Satellite Oceanographic data, `http://www.aviso.altimetry.fr/`] and World Ocean Database 2009 (WOD09) temperature profiles [`www.nodc.noaa.gov/OC5/WOD09/pr_wod09.html`]. Since there were too few salinity profiles in the WOD09 that overlapped our time period and they contained spurious data, we compared model salinity to a published salinity section [Swallow et al., 1991] that we consider representative of the subsurface salinity features, despite not corresponding to the modeled period. To make direct model-data comparisons, the model results were interpolated to the locations of the satellite gridded products using bilinear interpolation. The SST interpolation did not imply a change in resolution since both model and Pathfinder v5 SST have a grid spacing of 4 km. The AVISO SLA product has a grid spacing of $1/4^o$ (($\sim$30 km) therefore the interpolation was to the coarser AVISO grid. To provide comparable model SSH and altimeter SLA data, the long term mean SSH of the model was added to AVISO SLA to create absolute dynamic topography fields, which we simply refer to as SSH. Temperatures at standard hydrographic depths were extracted from the daily averaged model at the positions and dates of the observed WOD09 profiles within the modeled period (2000-2007).

To quantitatively assess the skill of the model to reproduce satellite SST and SSH we calculated metrics that summarize the variability, differences between modeled and observed values (after removing the mean of each field) and similarity of variability patterns, i.e. normalized standard deviations (σ), normalized root mean squared errors (nRMSE) and correlation coefficients (r), respectively [Taylor, 2000]. Agreement between model and satellite SSH was examined using an Empirical Orthogonal Functions (EOF) analysis on the detrended model and altimeter SSH.

Comparisons of the model and satellite fields should note the sources of error

in the satellite data, as well as in the model fields. The AVHRR SST fields, in particular, are subject to several types of error. The infrared (IR) signal from the sea surface originates in the top (1 mm or less) skin of the ocean, which can be either colder or warmer than the ocean in the upper several centimeters or meters. This can combine with warming of the top several meters of the water column during periods of calm winds, when a warm upper layer of the ocean develops that masks temperature signals associated with more dynamic processes such as upwelling and advection of SST gradients. In the tropics, there are also problems in the atmospheric correction due to the high humidity in the atmosphere. Atmospheric correction algorithms account for absorption by water vapor, but may be in error as humidity increases. Finally, the cloud mask is a notorious problem. The edges of clouds and small, sub-pixel sized clouds are especially difficult to detect, although algorithms attempt to do this. These problems are described in texts such as [Martin, 2014] and in chapters of [Barale et al., 2010]. Problems with the altimeter are greatest in the regions next to land, due to radar reflections from the land as described by [Gommenginger et al., 2011]. These potential problems with the satellite data should be kept in mind when comparing to the model fields. Below we note instances where these artifacts may affect the satellite data.

2.4   Results

2.4.1   Comparisons to observations

We start with an evaluation of model performance in its full domain, before presenting the model representation of seasonal changes in surface circulation, temperature and salinity. The goal is to represent the larger-scale circulation and water properties as well or better than previous regional models. We then focus on the seasonal cycles in the coastal region surrounding the islands off Tanzania, where the model provides details not available from earlier, coarser-scale models.

SST climatological means from 2000-2007 are shown in Figure 4 for months in which the correlations between the model and satellite SST fields are high (February,

r =0.78) and low (December, r=0.34). The KTCM's SST variability is more similar than OFES to the satellite SST in all months except March, when variability is slightly overestimated by our model. Although OFES SST fields produce a lower nRMSE when compared to Pathfinder SST than KTCM, the OFES SST has a cold bias relative to the satellite observations, with differences of up to 2.8^{o}C (Fig. 2.4). The smallest OFES SST biases occur during June to September (<1.5^{o}C) but bias relative to Pathfinder are never less than 0.5^{o}C. In contrast, KTCM SST fields are within 0.5^{o}C of the satellite observations in most of the domain during every month.

A cool SST band in the coastal shelf region extends from the northern boundary to 4.5^{o}S in February and to 6°S in December in the Pathfinder SST. This band stretches unrealistically along the entire coast in the OFES model. In KTCM the extension of this feature is very similar to that of Pathfinder in both months. In December, however, the across-shore temperature gradient in KTCM is weaker than in the satellite SST. KTCM SST is slightly cooler at the open boundaries, especially in the north, likely due to the influence of the OFES boundary conditions. This has only a minor impact on the interior of the domain where KTCM reproduces fairly well the satellite SSTs (Fig. 2.4).

Hövmuller diagrams in Figure 2.5c) and d) provide comparisons between monthly satellite and KTCM SST time series for the full east-west transect across the model domain at 6.2^{o}S for the 8 years modeled. Good agreement is observed between model and satellite annual cool and warm periods. KTCM slightly underestimates the magnitude and duration of warm periods in the deep basin east of the island. This transect is representative of the other four east-west transects examined, as well as the north-south transect at 43.3^{o}E in the northern half of the domain, where variability is maximum (gray dashed lines in Fig. 2.1). Point to point comparisons between monthly SST time series at several locations along these transects show similar results for all locations, indicating good agreement between modeled and observed SST temporal variations (r>0.85, p<0.01 for all locations). An example is shown in Figures 2.5a) and b) for two locations (marked with * in Fig. 1 at 6.2^{o}S), inshore and offshore of Zanzibar Island. Although the KTCM shows a tendency to slightly over or underestimate the magnitude of the seasonal extremes, it agrees

with the Pathfinder data in reproducing two relative maxima in SST in most years - a minor peak in December-January and a major peak in March-April (evident also in the Hövmuller diagrams). Years 2004 and 2006 are the exceptions for both KTCM and satellite SST, providing some confidence in the model's ability to capture interannual variability.

Looking next at sea surface heights, climatological monthly means of the "parent model" OFES, KTCM and altimeter SSH are shown in Figure 2.6 for June (early SE monsoon) when the model hindcasting skill is high (r=0.85) and March (late NE monsoon) when it is low (r=0.32). Correlation coefficients and nRMSE values comparing OFES and KTCM SSH to AVISO were very similar. However, the SSH variability from KTCM is more similar than OFES to the AVISO SSH in all months. The climatological mean SSH from KTCM and OFES compare well with AVISO in June (when nearshore-offshore gradients in SSH are strong and smaller-scale spatial variability is low); however, both models show less interannual variability than AVISO. For March (when gradients in SSH are weaker and local spatial variability is more prominent), the comparison of climatologies is less satisfactory. The mean SSH patterns of both models are poorly correlated with the mean satellite observations in the northern half of the domain (Fig. 2.6b). The positive SSH feature that extends from the northern coast to the center of the domain in AVISO is hardly noticeably in KTCM. OFES has this positive SSH feature but it occupies the entire northeastern corner of the domain. During this month altimeter SSH shows less interannual variability and both models are within a similar range, due to the direct influence of OFES boundary conditions on KTCM's SSH patterns.

The Hövmuller diagrams for the east-west transect at 8ºS (Fig. 2.7a, b) show a slightly larger amplitude seasonal cycle for the model than the altimeter. The model represents well the offshore extent of the EACC and its interannual variability, although there are examples of both under- and overestimates of the intensity of that variability. Several specific events with positive SSH extending far offshore are not reproduced by the model (e.g., in the first half of 2005 and again in 2007). At other times the model produces extended offshore features not found in the altimeter data. These discrepancies are typical of model simulations that produce features similar to

those found in observations but at different places and/or times. Such discrepancies are reduced in models that include data assimilation which is not incorporated into our model. At the beginning of the time series, AVISO SSH shows stronger negative values than KTCM in the open ocean, eastern side of the domain, a pattern that reverses by the end of the time series. This may results from the decadal trend in global sea level, which amounts to a rise of approximately 2 cm over the 8-year period. The AVISO data includes a band of low SSH at the far western boundary of the transect, next to the land. This is most likely an indication of land contamination of the altimeters radar signal [Gommenginger et al., 2011]. Comparisons shown in Fig. 2.7 are representative of other locations examined (gray dashed lines in Fig. 2.1).

The spatial patterns of the first EOF of SSH from AVISO and KTCM compare relatively well (Fig. 2.8a, b). Their time series capture many of the same events (r=0.43, p<0.01), although the mean of the model's time series is greater than that of AVISO. The first mode in both the model and satellite SSH explains approximately half of the overall variability. The spatial similarity of the first modes indicates that the KTCM captures the main SSH patterns seen by the satellite.

In order to assess the model representation of subsurface conditions, we plot KTCM temperatures vs. WOD09 in situ subsurface temperature observations from the same time and location (Fig. 2.9). This shows that the model does a reasonable job at representing observed subsurface temperatures (points cluster well along the 1:1 line). The model simulates vertical structure slightly better in coastal ocean regions shallower than 2000m (Fig. 2.9A and C). In the deeper regions it does a better job in the southern half of the domain (Fig. 9D) than in the north (Fig. 2.9B). The greatest discrepancies between model and observed temperatures are found in the main thermocline (75-250 m, gray circles). The low vertical resolution of our model at those depths (25-70 m offshore of the 2000 m isobath) may be responsible for the mismatch. The primary processes affecting temperature in the thermocline include vertical mixing of heat downward and internal displacements of isotherms caused by internal waves and tides, which we do not expect to be coherent in time between model and observations.

As a qualitative check on the model representation of subsurface salinity, given the lack of more representative observations, the modeled salinity climatology for April at 5°S was compared to a salinity section based on observations from April 1985 [Swallow et al., 1991] (Fig. 2.10). Several salinity features of the observed section are represented in the modeled April climatology low salinity surface water inshore, a strong halocline between 50 and 200 m depth, and an offshore core of high salinity near 200 m depth that extends eastward towards the surface. Interannual variability among the 8 model years is mainly observed in the offshore extent of the low salinity surface water and the tilting of the deep 35 and 34.9 PSU haloclines (not shown).

Only indirect comparisons of volume transports in our domain are possible since observed transports are reported for specific sections and times, while we have the climatological monthly mean transport across the model boundaries (Fig. 2.2). Flow through the southern boundary of the domain is inward throughout the year, but fluctuates between 8 and 15 Sv. The main contribution to this transport is the northward flowing EACC. Swallow et al [1991] report an observed EACC transport of 10 Sv in the upper 100m for April, 1985, at 5°S. Modeled transport through the northern boundary varies from ca. 2 Sv southward (inward) during February-March to 30-40 Sv northward (outward) during June-October (Fig. 2.2).

2.4.2   Seasonality of circulation, SST and SSS patterns

To describe the spatial and seasonal variability of the circulation, SST and SSS, we define the monsoon seasonality using the alongshore surface current patterns rather than the more commonly used wind patterns. Thus, April and November represent intermonsoon periods in the ocean, lagging the wind field by approximately one month. The SE monsoon season (May to October) is characterized by continuous northward flow along the entire coast; the NE monsoon season (December to March) has the southward flowing Somali Current intruding into the northern part of the modeled domain. The description that follows is based on the full monthly climatology (see Supplemental Materials).

2.4.2.1 Southeast Monsoon (May to October)

The circulation of the SE monsoon is represented by August in Figures 11 and 12. The EACC flows northward along the entire coast of the model domain (Fig. 11a, top row, Fig. 12a), reaching its maximum speed (>1 m s^{-1}) and offshore extent in the northern part of the domain in June (i.e. the 80 cm s^{-1} isotach at the surface is >150 km offshore). From May to July the northward flow occurs in the upper 300 m, but during September and October the 5 cm s^{-1} isotach extends down to >900 m depth. A north-south gradient of the northward alongshore transport is observed during this season, with slower velocities in the southern region of the domain and stronger velocities in the north (Fig. 2.11a, top row). This alongshore flow divergence is compensated by the westward inflow of the northward extended NEMC through the eastern open boundary between 8 and 10°S and even stronger inflow in the northern half of the domain with maximum currents between 2-4°S. The combination of this northern inflow and the northward flowing EACC produces a cyclonic feature in Fig. 2.11a (top row) known as the Southern Gyre (SG) [Schott and McCreary, 2001, Fig. 1a]. SST is uniformly "cold" in August ($\sim24^o$C), since it is austral winter and the water sources are the EACC and the NEMC (Fig. 2.11a, middle row). The uniformly cold temperature are only observed from July to September, after which warming begins. Low sea surface salinity (SSS <35.3 PSU) characteristic of the EACC is observed next to the coast during this period. The lowest SSS values are found along the shelf and in the band south of 9°S (Fig. 2.11a, bottom row) from May to July. The partial representation of the Southern Gyre during August has an intermediate salinity of <35.2 PSU, in agreement with observations reported by Schott and McCreary [2001].

2.4.2.2 Intermonsoon (November)

The intermonsoon that follows the strong SE monsoon is illustrated by November. It has weaker surface velocities in the offshore region, especially away from the Southern Gyre which is now fully inside the domain (Fig. 2.11b, top row). The offshore extent of the EACC core at the surface (> 80 cm s^{-1}) is much more coastal restricted, with

northward flow again restricted to the upper 400 m (Fig. 2.12b). The southward flowing Somali Current meets the EACC north of the equator (outside of our domain) in the OFES model. Therefore the EACC appears continuous through the KTCM domain, with an offshore jet at the northern boundary that supplies the SECC. SST increases to >27°C in the entire interior domain (Fig. 2.11b, middle row). The warmest and saltiest surface water occurs on the shelf where velocities are lower (e.g., with long residence time) and solar heating and evaporation is stronger. The lower salinity signature of the Southern Gyre is evident in the northern half of the domain (Fig. 2.11b, bottom row).

2.4.2.3   Northeast Monsoon (December to March)

During the NE monsoon from December to March the northward flowing EACC and the southward flowing SC meet inside the domain (at ca. 0-3°S). The SC flows southward in the upper ($\sim$60 m; below it, the EACC continues to flow northward, but lacks a surface expression. Thus, there is a strong vertical shear at ($\sim$70-80 m depth (Fig. 2.12c). The latitude where the currents meet progressively shifts southward from the equator in December to 3°S in March. Where the currents meet, an offshore jet forms the SECC. It flows directly eastward in December but rotates southward through time until it is aligned towards the south in February. A dipole is associated with the SECC jet, with an anticyclonic eddy to its north/east side and a cyclonic eddy (the former SG) to its south/west side. The dipole moves onshore and southward, and by March the cyclonic eddy is compressed against the coast. The dipole is fully inside the domain from January to March. The interaction of these eddies determines the location (latitude) of SECC outflow at the eastern boundary of the domain. The offshore position of the SECC jet at 47°E (our eastern model boundary) shifts southward from the equator in November to 4-6°S in January-March (Fig. 2.11c, top row). A strong north-south SST difference (of up to 3°C) is observed during the NE monsoon. Warm fresher water is advected into the domain from the south by the EACC, while the SC brings cold saltier water from the northern hemisphere (where strong coastal upwelling is occurring) (Fig. 2.11c, middle and

bottom row). The cold surface water feature extends to the confluence of the currents on the shelf (0° in December to ca. 3-4°S in February).

2.4.2.4 Intermonsoon (April)

In April the southward flow of the Somali current weakens and the continuous northward flow re-establishes along the northern region of the East African coast. The EACC becomes once again a surface current (Fig. 2.12d). The dipole and offshore jet that contributed to the SECC during the NE monsoon period disappear. Highest offshore velocities are now found in the westward flows at 7-10°S as the SEC feeding the NEMC strengthens (Fig. 2.11d, top row). The transition of the SST pattern from the NE monsoon to the SE monsoon condition is slower than the transition for the circulation and spans over three months (April-June). This transition is also slower than the one observed during the SE to NE intermonsoon season (November). In April as the inflow of the SC stops, SST in most of the domain warms to 29°C (Fig. 2.11d, middle row). In May the warm water is pushed towards the coast, as colder water advects into the domain through the southern and eastern open boundaries. By June the warm water (>28°C) has been flushed out through the northern open boundary by the EACC. The greatest salinity gradient is observed in April, with fresher water (34.8 PSU) along the southern boundary of the domain and saltier water (35.4 PSU) in the NE corner (Fig. 11d, bottom row). Fresher water extends along the shelf all the way to the northern boundary, showing the coastal influence of the EACC on the shelf water mass as well as the influence of local precipitation, which has an annual maximum in May.

2.4.2.5 Seasonal Variability of Shelf Circulation

As geostrophic currents approach the shelf, inshore of the 1000 m isobath, they accelerate due to conservation of volume and are deflected to follow lines of constant potential vorticity (here, constant depth). Inshore of the 100 m isobath, currents slow due to friction, the blocking effect of islands, and the barrier that shallow

bathymetry represents to deep flows. Between 4-8.5^{o}S the larger scale EACC flows northward year-round. The effect of the three large islands on the coastal circulation depends on the intensity of the EACC, the depth of the channels between the islands and the mainland (Pemba >100 m; Zanzibar and Mafia <40 m) and the coastline geometry. Therefore the circulation patterns around the islands vary both temporally and spatially along the Kenyan-Tanzanian shelf (Fig. 2.13). The coastal region is where higher resolution models, such as KTCM, enable a detailed look at the circulation, which is not well resolved by coarser resolution models.

During the SE monsoon and the two intermonsoon periods (throughout April-November, Fig. 2.13a, b, and d), the EACC is strong (>85 cm s^{-1}). Shelf flows are northward all along the coast, both inside and outside the channels since the EACC is able to overcome the obstacles that the shallow channels represent. During the NE monsoon (December-March, Fig. 2.13c), the EACC is slower (<75 cm s^{-1}) and the shallow channels inshore of Mafia and Zanzibar islands impede the northward flow, while channel flow inshore of Pemba continues. Shelf flow at the southern entrances of the channels differs among the islands during this period, since it depends on channel depth and coastline morphology.

Friction with the coast causes an across-shore gradient of the northward shelf currents. The positive curl in the currents generates small anticyclonic eddies where the coastline morphology allows it: at the southern tips of the islands, to the north of capes and in bays, especially during the NE monsoon when the EACC is slower. The gradient in the current velocities and conservation of potential vorticity causes a small portion of the northward flowing EACC to turn southward into the northern entrance of channels after it passes east of the islands. This return flow is minimal at the northern tip of Pemba Island but persistent year round, while to the north of Zanzibar Island it is strongest from December to March (NE monsoon). The cape near Dar es Salaam ($\sim$ 7°S) generates a permanent anticyclone in the southern entrance of the Zanzibar channel that partially impedes the flow through the channel year-round. The concave shape of the east coast of Zanzibar Island has a similar effect, which establishes a permanent anticyclonic eddy at 6°S, 39.5^{o}E (Fig. 2.13). Anticyclonic eddies are also present in Unguana Bay and at the south entrance of

the Mafia Channel but only when offshore velocities are less than 70 cm s^{-1} (i.e. from December to March).

From November to March the anticyclonic eddy in the southern entrance of the Zanzibar channel blocks most of the slow flowing EACC. The small northward flow that enters the Zanzibar channel from the south meets the return flow coming from the north, creating sluggish circulation inside the channel (<20 cm s^{-1}, Fig. 2.13 and 2.14). The waters of the Zanzibar channel are nearly isolated during this period. In April, offshore EACC speeds reach 1 m s^{-1} and northward along channel speeds increase to 28 cm s^{-1}, the southward return flow in the Zanzibar channel is restricted to the region near the northern entrance. In May, as its speed increases, the EACC is able to force itself into the southern entrance of the Zanzibar channel despite the blockage of the anticyclonic eddy and northward flow through the Zanzibar channel is re-established with velocities along the channel of up to 39 cm s^{-1}. The Mafia channel is similar in depth to the Zanzibar channel, and despite being narrower on its southern entrance, the northward flow through the channel is only completely blocked during January and partially blocked during December and February, since the eddy at its southern entrance is weaker and restricted to the upper ($\sim$10 m. The much deeper (>100 m) Pemba channel allows the EACC to continue northward through it all year round (Fig. 2.13).

Several processes are responsible for the east-west gradients of temperature in the region inshore of the three islands from November to February (Fig. 2.13b, c). The less intense circulation on the continental shelf allows temperatures in the shallow regions to evolve differently than in the rest of the domain. In November when currents relax the narrow shelf warms quickly until it starts being affected by the cooler SC in the north (Fig. 2.11b, c, center row). In the deep channel inshore of Pemba, temperature changes are mainly due to advection, which is not seasonally interrupted, and temperatures are more similar to those in the main offshore flows of the EACC. Circulation and water exchange in the Zanzibar channel are minimal during Nov-Feb; this allows the waters in the shallow channel to warm more than those outside the channel. The anticyclone in the southern entrance of the Zanzibar Channel generates localized upwelling of cooler waters next to the southern coast

of Zanzibar Island. Although the cooler temperatures next to the island are most evident during November to February (Fig. 2.13b, c), analyses of vertical velocities along a transect stretching from the southern coast of the island to the mainland (not shown) reveal positive vertical velocities throughout the water column next to the island in all months, along with downwelling in the core of the anticyclonic eddy, which is also present in all months. In the narrow region (∼10-20 km) next to the mainland coast, local heating warms shallow, sluggish regions, particularly during the onset of the monsoon periods (March-April and November-December) when wind forcing is at its minimum. The shallow bays along the mainland coast north and south of Mafia Island are always warmer than surrounding regions. Cooler SSTs are observed adjacent to the west coast of Mafia Island (Fig. 2.13, i.e. Nov, Feb), possibly due to localized upwelling as the northward flow passes around the islands [Hamner and Hauri, 1981].

2.5   Discussion

The interaction of the seasonally reversing SC with the more persistent flow of the EACC creates complex circulation patterns, especially when coupled with strongly seasonal monsoonal winds and the presence of islands with channels of various depths off Kenya and Tanzania. Previous ocean circulation models have not resolved the circulation inshore and around these islands. Our goal in developing the high-resolution KTCM is to more better resolve the details of the shelf circulation, while maintaining or improving shelf circulation connections with the broader forced dynamics caused by large scale wind and remote forcings. The results demonstrate success in achieving these goals with respect to seasonal patterns of surface circulation and water properties, with some caveats that warrant further discussion.

The KTCM SSTs compare well with satellite SST fields and provided regional improvement on the large scale OFES model SSTs along the western boundary (Fig. 2.4). The KTCM also eliminated the 1 to 2^oC cold bias from the global OFES model (Figs. 2.4 and 2.14). Below the sea surface, the KTCM adequately hindcasts vertical temperature profiles from the WOD09 from specific locations and times

(Fig. 2.9). Temperature hindcasts are least skillful at mid-depths (75-250 m), where there is increased temperature variability due to the coarser vertical resolution of the model and potentially differences in stratification, mixed layer depths and isotherm displacements by internal waves (Fig. 2.9). Although the scarcity of in situ salinity data in this region during the modeled time period prevent a thorough assessment of the fidelity of the model salinity, the general subsurface salinity structure agrees with published salinity sections from earlier periods [i.e. Swallow et al., 1991; Schott and McCreary, 2001; Schott et al., 2002].

The volume transports in the EACC, the SC and the offshore jet that contributes to the SECC in the model are seasonally consistent with prior field studies (Fig. 2.11) [Schott and McCreary, 2001; Reid, 2003; Schott et al., 2009]. Quantitative comparisons with observations of these large scale features are difficult, due to the lack of observations throughout the annual cycle and the lack of long time series that allow an observation-based climatology. However, the few observations of the magnitude and seasonality of volume transport of these currents suggest consistency of the model and observed transports. Surface circulation is also indicated by fields of sea surface height and the KTCM SSH fields reproduce the dominant statistical mode of SSH variability, as represented by AVISO altimetry. The ability of KTCM to reproduce monthly seasonal fields of SSH is similar to that of OFES. Both the KTCM and 10 km OFES reproduce the satellite fields during months when the SSH fields have strong gradients and relatively simple structure, but have difficulty reproducing the SSH patterns when smaller-scale spatial variability is high and horizontal gradients in SSH are weak (Figs. 2.6 and 2.8).

Direct comparisons of KTCM results to other models of the region are difficult due to differences in model resolution and simulated time. However, as far as the presence and characteristics of the main circulation features and seasonal timing, KTCM broadly agrees with coarser resolution OGCMs of Lee and Marotzke [1998] and Anderson et al. [1991], an earlier ROMS by Hermes and Reason [2008], and the Simple Ocean Data Assimilation (SODA) product evaluated by Xie et al. [2002]. Our model compares better to Levitus SST and ship-drift derived currents climatology used byMishra et al. [2007] to evaluate their global Modular Ocean Model (MOM3.0)

simulation of the Southern Indian Ocean, which does not perform well in our study region. KTCM SST and SSH seasonal cycles compares well to the larger scale ROMS model of Manyilizu et al. [2014]. Their climatological SST for the month of May shows a region of relatively cool surface water north of Madagascar. This is consistent with the April cooling we see in the southeast corner of our model domain (Fig. 2.11 and Suplemental Information.). The presence of this cool feature in the middle of Manyilizus larger model domain confirms that this is not an spurious feature in our model caused by the cold-biased boundary forcing from OFES, and verifies that the influence of the open boundary forcing on SST is restricted to regions less than 200 km wide around the perimeter of our model domain.

We did not find evidence in the Kenya and Tanzania region of a strong local influence of the zonal wind stress as was suggested by Pandey and Rai [2008] for the coasal regions of the tropical Indian Ocean north of 5^oS. They use a basin-scale Princeton Ocean Model (POM) with 5 resolution topography and no islands to discuss the large-scale coastal circulation. Based on a $1/6^o$ resolution ROMS model of the tropical Western Indian Ocean, Manyilizu et al. [2014] report that SST interannual variability in a region off southern Tanzania (40-42°E and 8-10°S) is weak in comparison to an offshore region and predominantly driven by surface heat flux. Their analysis focuses only on SST and does not investigate circulation patterns which are the main focus of our study. In the KTCM, the prevalence of northward flow along the coast south of 5^oS during January and February (Fig. 2.11 top row, and Fig. 2.13), when the local wind is blowing southward (Fig. 2.3) appears counterintuitive. In fact, it highlights the importance of large-scale remote forcing on the regional circulation. In this case, the southern hemisphere EACC opposes the northern hemisphere NE monsoonal winds, which cause the reversal of the Somali Current. The strong northern hemisphere winds and the southward equator crossing strong flows that result are the main influences over the modeled region, overpowering the effects of local winds on the circulation. However, neither diurnal variability in the wind forcing nor freshwater runoff are included in the KTCM, and either or both might influence coastal circulation. These forcings should be included in future model studies.

As intended, the KTCM significantly increases the spatial resolution of the circulation around the islands (e.g. Fig. 2.13 and 2.14). The coastal circulation patterns of the KTCM are likely to be more realistic than those of the OFES since bathymetry is represented more accurately, allowing nonlinear interactions between the flow and the bottom topography to be better resolved. However, coastal ocean observations off East Africa are too sparse to reliably validate nearshore coastal model results with observations. Without better velocity and hydrographic observations on the shelf, it is not possible to quantitatively assess the improvement provided by the KTCM. Thus, we present these patterns as working hypotheses, which could be verified by in situ observations, such as water temperature observations reported recently for a location in the Zanzibar Channel (Chumbe Island Coral Park) by Manyilizu et al. [2014]. The KTCM near bottom temperature agrees well with the in situ temperature from loggers at Chumbe Island Coral Park (Fig. 2.15). Thus, we have confidence that KTCM is reproducing well temperatures observed at one site in the Zanzibar Channel for which observations exist during our model time period.

While the KTCM better represents satellite SST compared to OFES over the broader model domain, the small-scale spatial SST patterns within the channels are not always in agreement with satellite observations. Figure 2.14 provides an example of this for the region surrounding Zanzibar Island. In October, when there is continuous northward flow through the Zanzibar Channel, both Pathfinder and KTCM show a small SST gradient inshore and offshore of the island with slightly warmer SST inshore, whereas the coarser resolution OFES shows uniformly colder SST (Fig. 2.14 top row). In December, when the circulation into the Zanzibar Channel in KTCM is largely blocked by eddies at both channel ends, Pathfinder shows stronger SST gradients with warmer water in the southern channel. KTCM however, shows cooler (warmer) water in the southern (northern) Zanzibar Channel. The gradients in OFES are minimal (Fig. 2.14 bottom row). The SST patterns in KTCM show localized upwelling of cooler water SW of the island, while westward flow of this cooler water displaces the warm surface water to the NW. As described above, the upwelling is present in all months, although its surface signature depends on stratification. Further studies at smaller spatial and temporal scales are needed to

determine the skill of KTCM to reproduce the small scale SST and circulation patterns and to assess biases in both satellite and model fields. Problems with infrared satellite SST retrievals are well known. Surface warming during calm periods produces warm and very thin skin layers that mask the more representative upper ocean temperatures beneath those layers. Atmospheric correction algorithms may also be in error due to small clouds and humid tropical conditions. These may keep the Pathfinder field in December from seeing the results of upwelling. Important sources of variability not included in the model like freshwater runoff and diurnal wind variability may modify the circulation pattern and SST, particularly in shallower coastal regions. Measurements of temperature, salinity and current velocities at higher spatial and temporal scales is crucial to corroborate nearshore circulation patterns and hydrography, especially in heterogeneous systems, where very local processes, such as small-scale upwelling may be important.

Coastal regions of Kenya and Tanzania depend heavily on their coastal resources for a variety of ecosystem services. The resources are vulnerable to both global and local anthropogenic stressors. Global stressors include excessive carbon dioxide emissions leading to global warming, sea level rise, water temperature increases and ocean acidification. Local stressors include pollution, and overfishing. Understanding coastal physical processes at the local scale, and having local-scale physical models of ocean circulation and hydrography are valuable for investigating the impacts of anthropogenic stressors in coastal systems and can help design strategies to mitigate their negative effects. For example, one of the primary findings of the KTCM simulation is the presence of a bimodal coastal circulation, with strong northward flow through the channels inshore of the islands during most of the year, but restricted channel through-flow inshore of Mafia and Zanzibar Islands during the northeast monsoon (Dec-Mar). Preliminary Lagrangian particle tracking experiments [Mayorga Adame, 2010] show that the strong northward flow during March to November implies shorter residence times of the water in the Zanzibar and Mafia Channels compared to the sluggish shelf circulation during the NE monsoon (Dec-Feb). This has important implications for ecological issues such as near-shore pollutant dispersal, mariculture operations, coral reef health and the connectivity of coral reef organisms.

Strong coastal flows are beneficial for coral reef health and mariculture operations since they constantly supply oxygenated, nutrient rich water to the organisms. They are also locally beneficial in reducing pollutant concentrations near their source due to rapid flushing, enhanced dispersion and strong mixing. Wide dispersal of pollutants during the strong flow regime will impact larger regions, including significant marine habitats such as mangroves and coral reefs. However, lower concentrations of pollutants in a larger area generally have lower negative effects on an ecosystem than higher pollutant concentrations in a smaller area [Pastorok and Bilyard, 1985], as would occur during the sluggish circulation regime. Slow flows promote retention which may benefit recruitment of coral reef associated species that need to find suitable habitat at the end of their pelagic larval phases. Rapid flows may imply losses for local populations but enhance one way connectivity between southern and northern reefs, and increase the probability of colonizing new habitat [Sammarco and Andrews, 1988; Cowen and Sponaugle, 2009].

For regions with limited observing capacity, such as East Africa, regional ocean circulation models like the KTCM offer a wide range of possibilities for examining physical phenomena despite a lack of in-situ physical observations, and provide opportunities for advancing our understanding of the regional ocean circulation and its effects on marine ecosystems. The hindcast ability of the KTCM could be used to address the effects of global climate changes on ocean circulation and environmental issues along the East African coast including sea level rise, coastal erosion, dispersion of pollutants, coral stress due to extreme temperatures, coral reef connectivity and the potential spillover effect of harvested and ecologically important species beyond the boundaries of Marine Protected Areas. KTCM can provide the velocity and temperature fields required by individual based biological models and other process-oriented models to test hypotheses about environmental stresses and ecological issues of the Kenyan-Tanzanian coastal region. Model simulations can also guide cost effective *in situ* observation campaigns to maximize available resources.

2.6   Summary

This paper presents results of the Kenya-Tanzania Coastal Model, a 4 km horizontal resolution ROMS application (Fig.1), forced locally by daily atmospheric fields from NCEP/NCAR reanalysis and remotely at the open boundaries by hydrography, SSH and velocity fields from the global model OFES and OTPX tidal forcing.

The KTCM's SST compares well with Pathfinder satellite observations improving the SST representation provided by the parent model OFES which has a cold bias (Fig. 2.4). Pathfinder SST seasonal and interannual variability is also adequately reproduced by our model (Fig. 2.5).

The climatological circulation patterns of the KTCM reproduce the main features reported for the region by previous observational and modeling studies. The KTCM SSH fields, reproduce the dominant statistical mode of SSH variability, as represented by AVISO altimetry (Fig. 2.8), which is indicative of the observed surface circulation.

A comparison to WOD09 temperature profiles shows that the model adequately hindcasts subsurface temperatures seasonally and spatially. Larger differences are observed at the main thermocline depth, where variability is expected to be high and the model has coarser resolution (Fig. 2.9). Due to the sparsity of salinity observations, model results were only qualitatively compared with a vertical salinity section reported in the literature. The main observed features are represented in the model climatology (Fig. 2.10).

KTCM adequately reproduces the main mesoscale features described for the region, while greatly increasing the details of the coastal circulation and hydrography in comparison to previous modeling and observational studies. We provide a climatological estimate of the seasonality of the ocean state based on an 8-year simulation of a dynamically coherent model (Fig. 2.13). This provides a working hypothesis for the seasonal coastal circulation in a region that lacks long term observations needed to define a reliable representation of the ocean on a typical year.

The KTCM monthly climatological fields (Fig. 2.11) describe the circulation. SW monsoon conditions: Strong continuous northward flow along the coast of the modeled domain and "cool" ($\sim$24°C) SST prevails from May to October. Intermonsoon conditions: Weakening of the EACC and surface velocities in the offshore region, with SST warming in November. NE monsoon conditions: From January to March, a strong north-south SST gradient is caused by the intrusion of the shallow, southward flowing, cold and salty Somali Current that meets the slow northward flowing, warm and fresh EACC. The convergence of the two currents forms the eastward flowing SECC. Intermonsoon conditions: The transition back to SW monsoon conditions occurs in April, with slow SST cooling and the re-establishment of northward flow all along the coast with the strengthening of the EACC.

The detailed shelf circulation consists of a bimodal coastal circulation pattern, with strong northward flow through the channels inshore of the islands during most of the year, but restricted channel through-flow inshore of Mafia and Zanzibar Islands during the northeast monsoon (Dec-Mar) (Fig. 2.13 and 2.14). This modeling study provides some guidance for future work. The shelf circulation patterns and hydrography of KTCM include a more accurate and detailed bathymetry, but do not include diurnal wind variability and local fresh water runoff. These should be included in future studies. At fine scales the KTCM SST fields on the shelf do not always agree with Pathfinder satellite observations (Fig. 2.14), which may be affected by a warm surface skin and errors in the atmospheric corrections due to small clouds and the humid tropical atmosphere. Concurrent direct measurements and satellite observations are needed to evaluate this further.

Implications of the shelf circulation patterns on various environmental issues affecting the Kanyan-Tanzanian coastal region are briefly discussed.
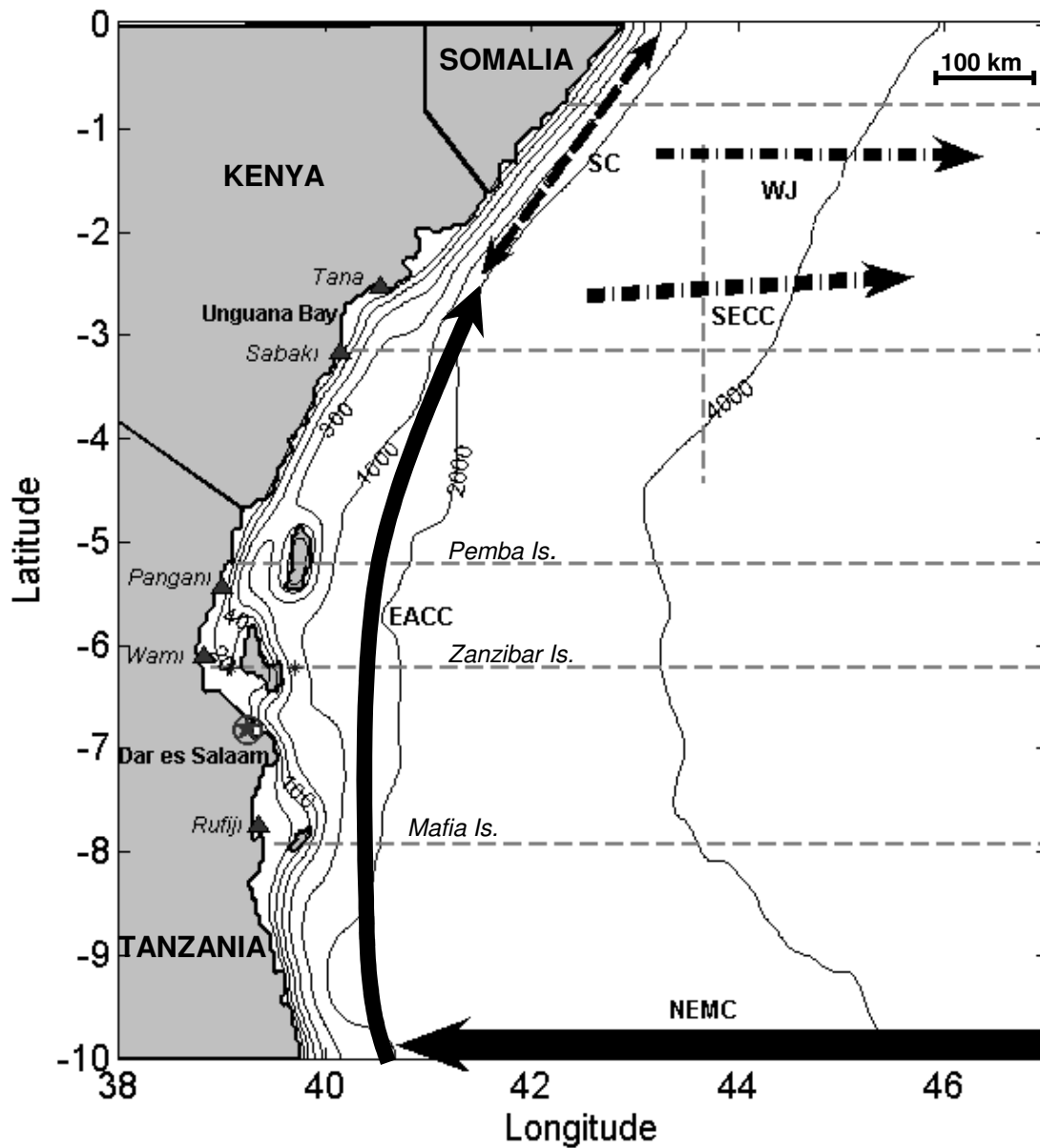
Figure 2.1: Model domain with schematic arrows showing the main surface currents, solid lines for year-round currents and dashed lines for seasonal currents (see text for details). Triangles mark river mouths. The model coastline and bathymetry are shown, along with locations named in the text. Starting at 5°S, the islands from north to south are Pemba, Zanzibar and Mafia. Grey dash lines and * mark locations examined for model validation. Bathymetric contours are: 20, 40, 100, 300, 1000, 2000 and 4000m.
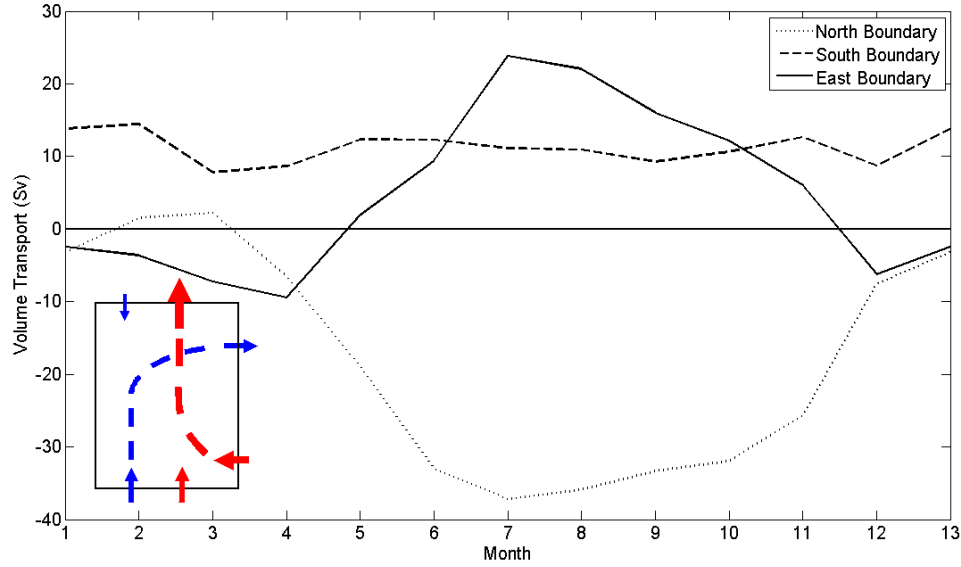
Figure 2.2: Volume transport in the upper 500 m in Sverdrup's (Sv=10 ^{6} m^{3}s^{-1}) across the 3 open boundaries of the model domain. Positive (negative) values represent transport into (out of) the domain. The inset represents the main flow balances in the model domain for January-March in blue and for May-November in red.
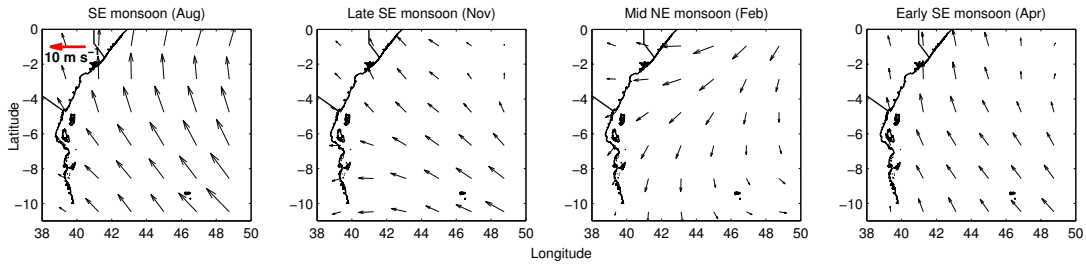
Figure 2.3: Climatological monthly mean of the NCEP-NCAR wind speed vectors used to force the model. Months shown are representative of the seasonality of the region: early (April), mid (August) and late (November) SE monsoon; NE monsoon (February).

47
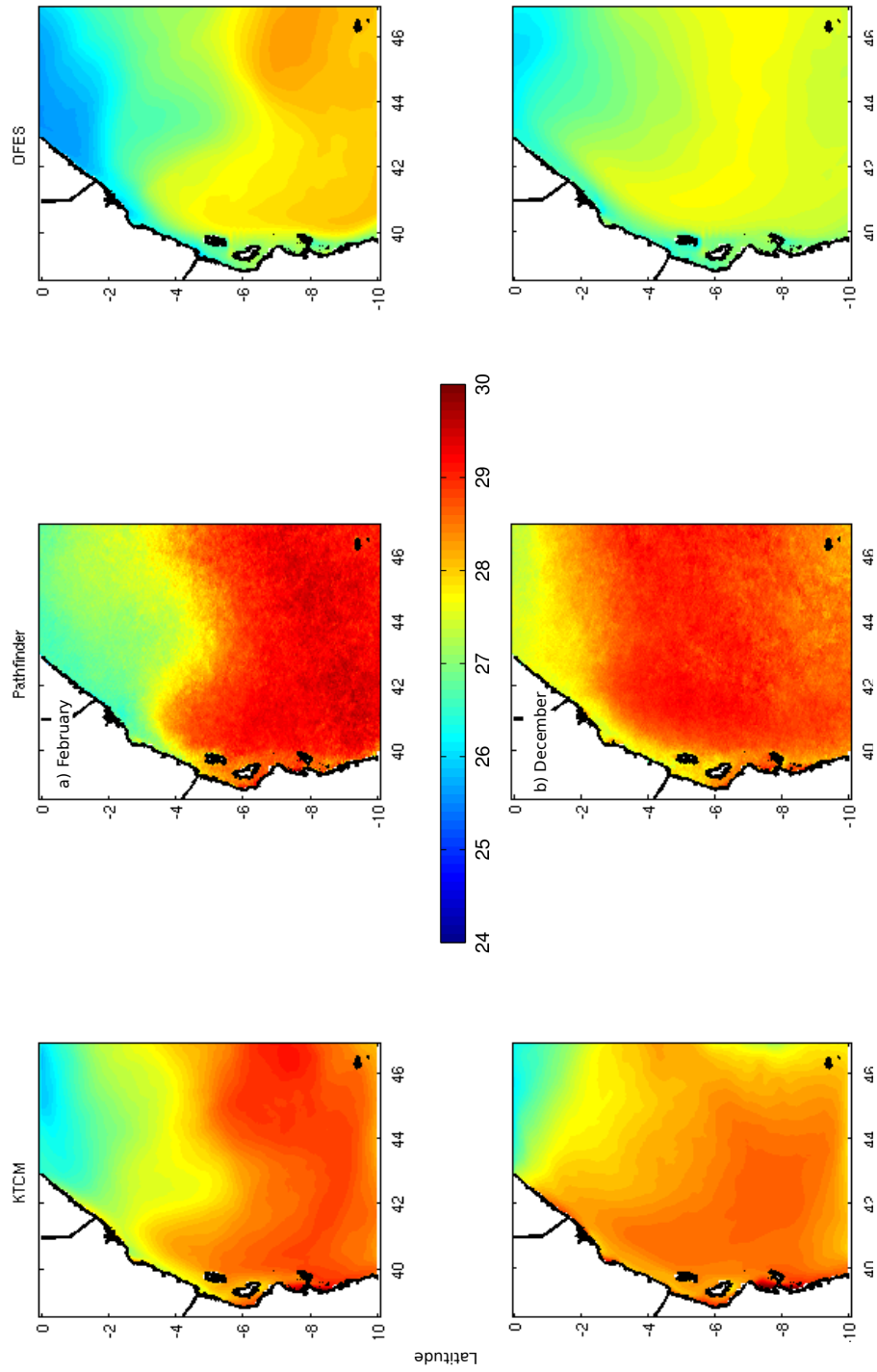
Figure 2.4: Sea surface temperature (°C) from KTCM, Pathfinder and OFES for two different months: a) February (NE monsoon) and b) December (transition).
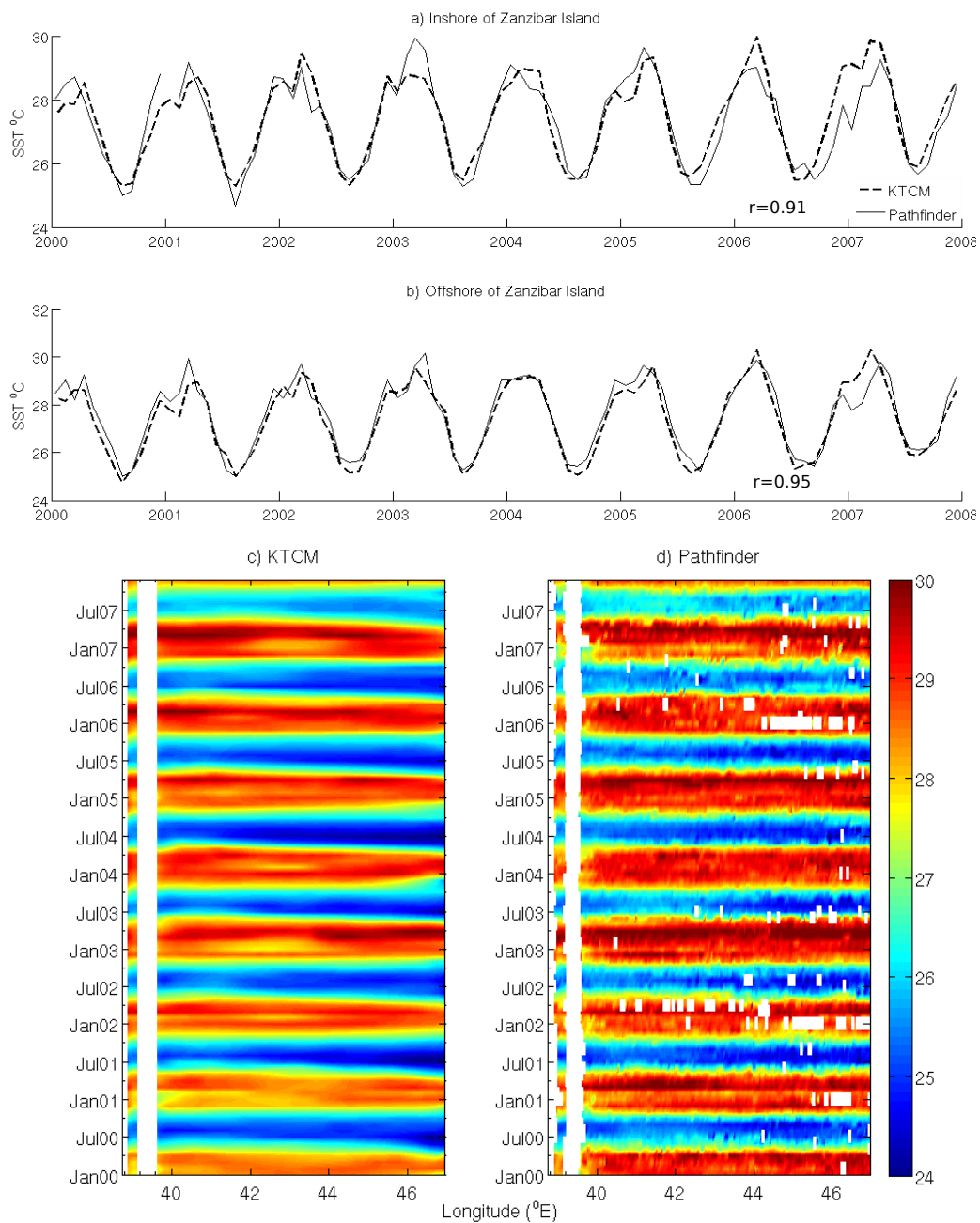
Figure 2.5: SST time series comparisons between KTCM and Pathfinder satellite observations: a) inshore and b) offshore of Zanzibar Island (6.2 °S). Hovmuller diagrams of SST along the transect at 6.2 °S from c) KTCM and d) Pathfinder satellite.

49
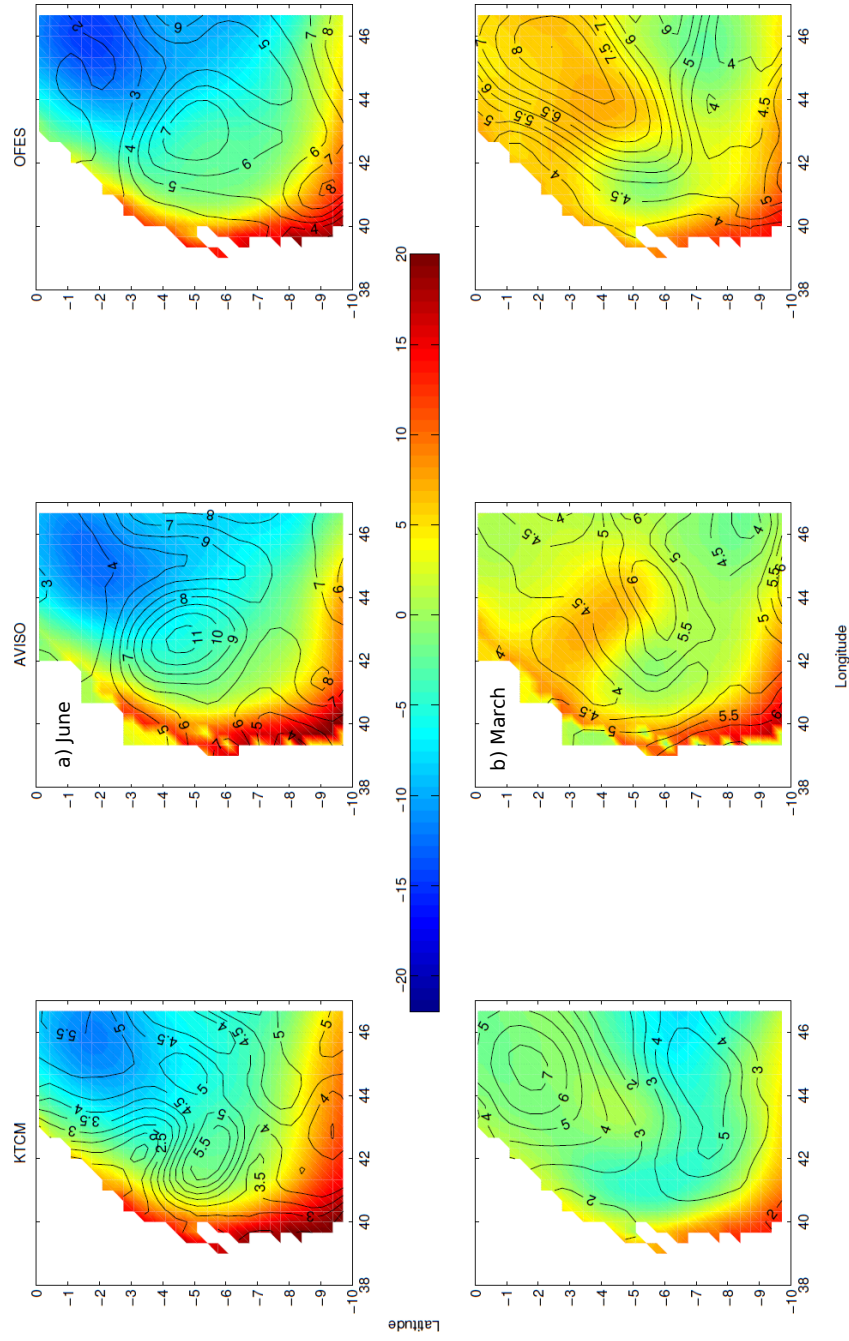
Figure 2.6: Sea surface height (colors) in centimeters from KTCM, AVISO and OFES for two different months: June (early SE monsoon, top) and March (late-NE monsoon, bottom), with overlaid contours of interannual variability (standard deviations) among the 8 years modeled.
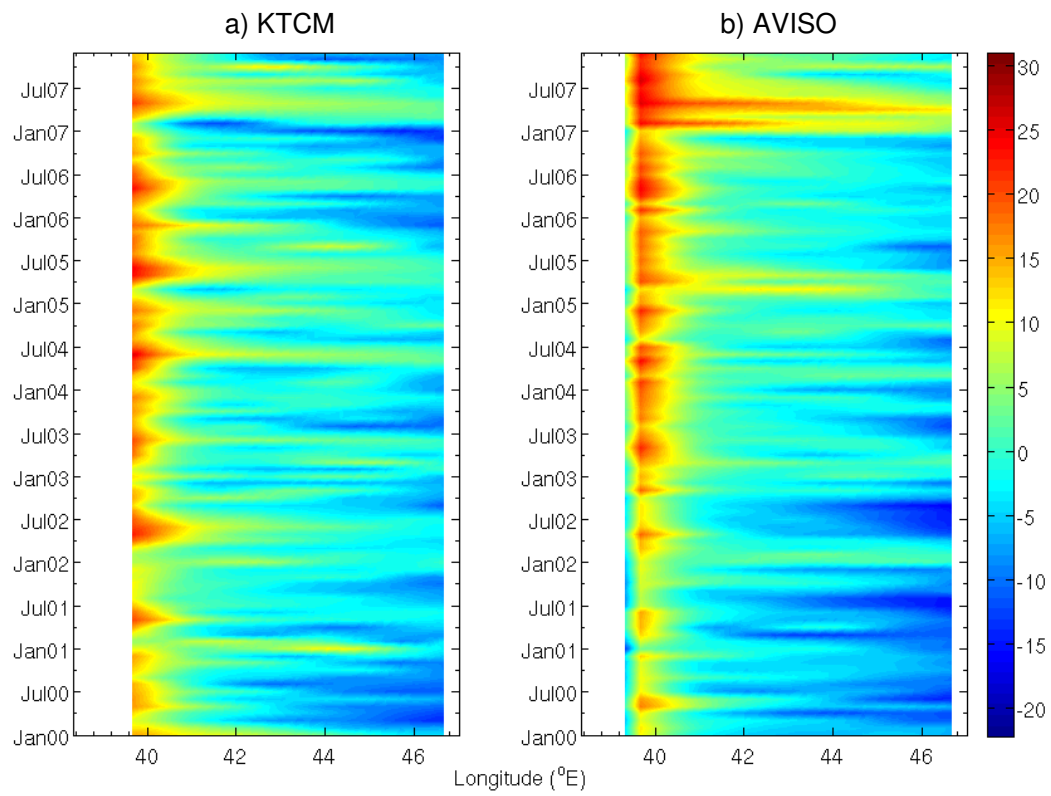
Figure 2.7: Hovmuller diagrams of SSH along a transect across the modeled region at 8°S from a) KTCM and b) AVISO.
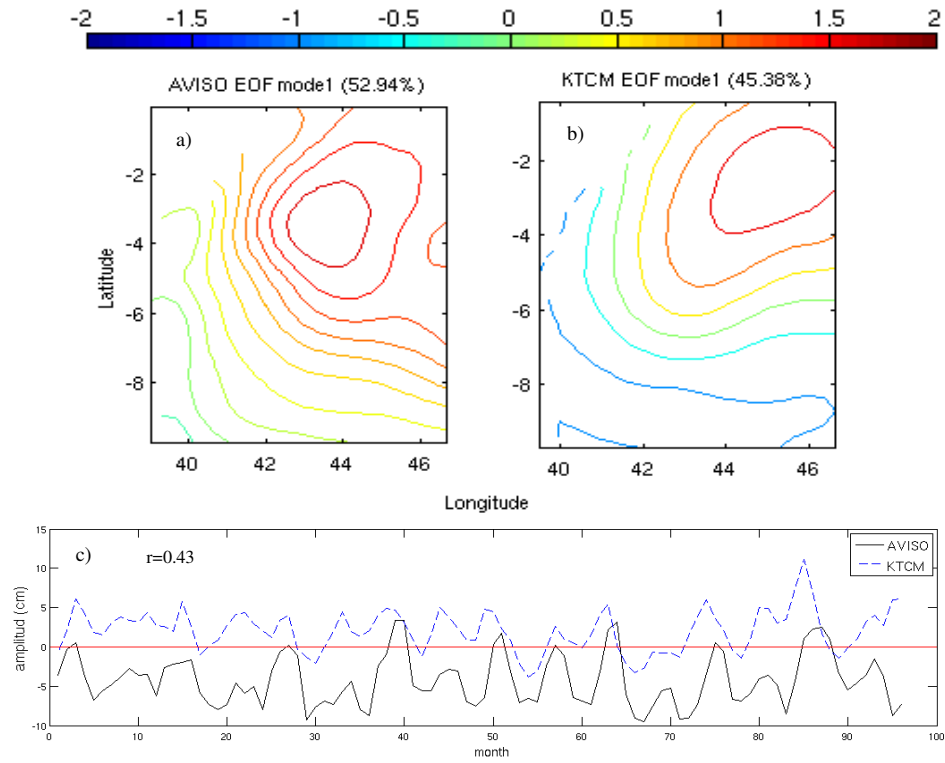
Figure 2.8: Spatial pattern of the first EOF mode of SSH (cm) for a) AVISO and b) KTCM. The amplitude and temporal variability of the patterns is shown this mode including the correlation coefficient (r) between the two time series in c). Colorbar at the top applies to a, b. Solid black line in c are AVISO time series; dashed blue lines are KTCM time series. .
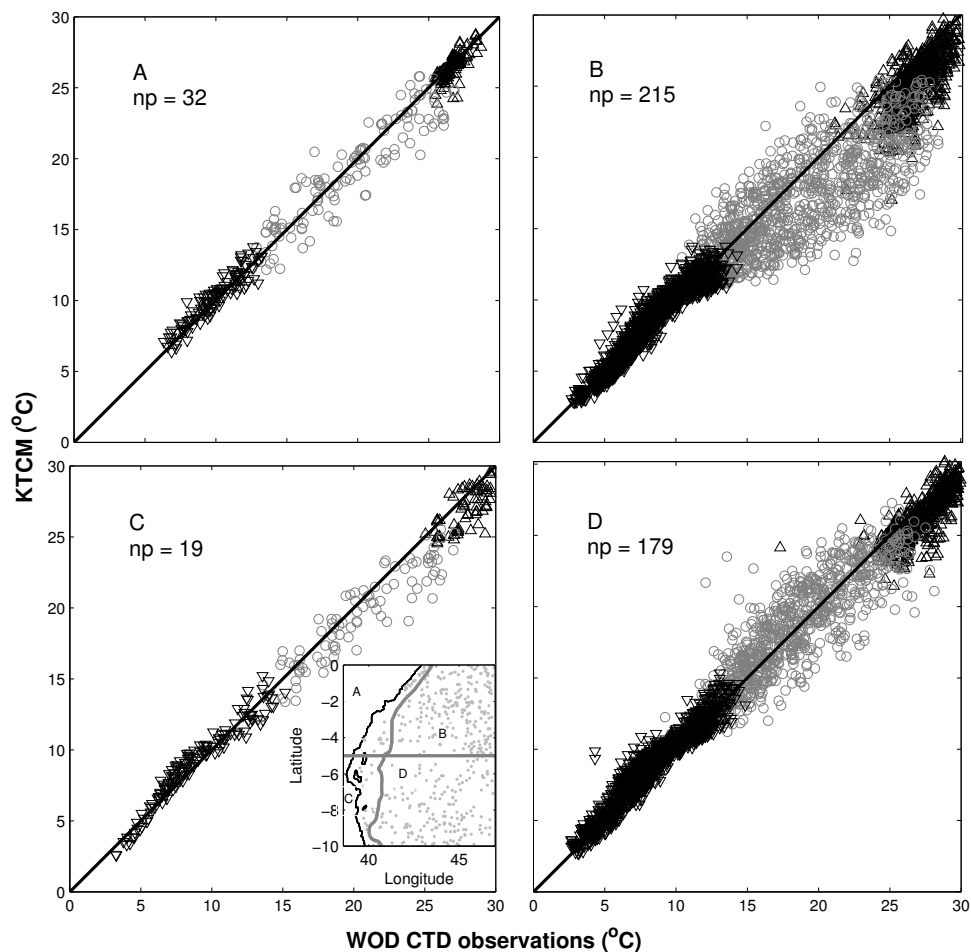
Figure 2.9: WOD observed temperature profiles at standard depths vs. KTCM modeled temperatures.Observed profiles are divided according to the bottom depth in water shallower (panels A and C) and deeper (panels B and D) than 2000 m and north (panels A and B) and south (panels C and D) of 5°S, as shown in the inset map on panel C. Different symbols mark temperatures at 3 different depth ranges: ($\triangle$) 0-75 m, ($\circ$) 75 to 250 m and (∇) deeper than 250 m, np=number of profiles. A diagonal 1:1 line is shown (not a regression line).
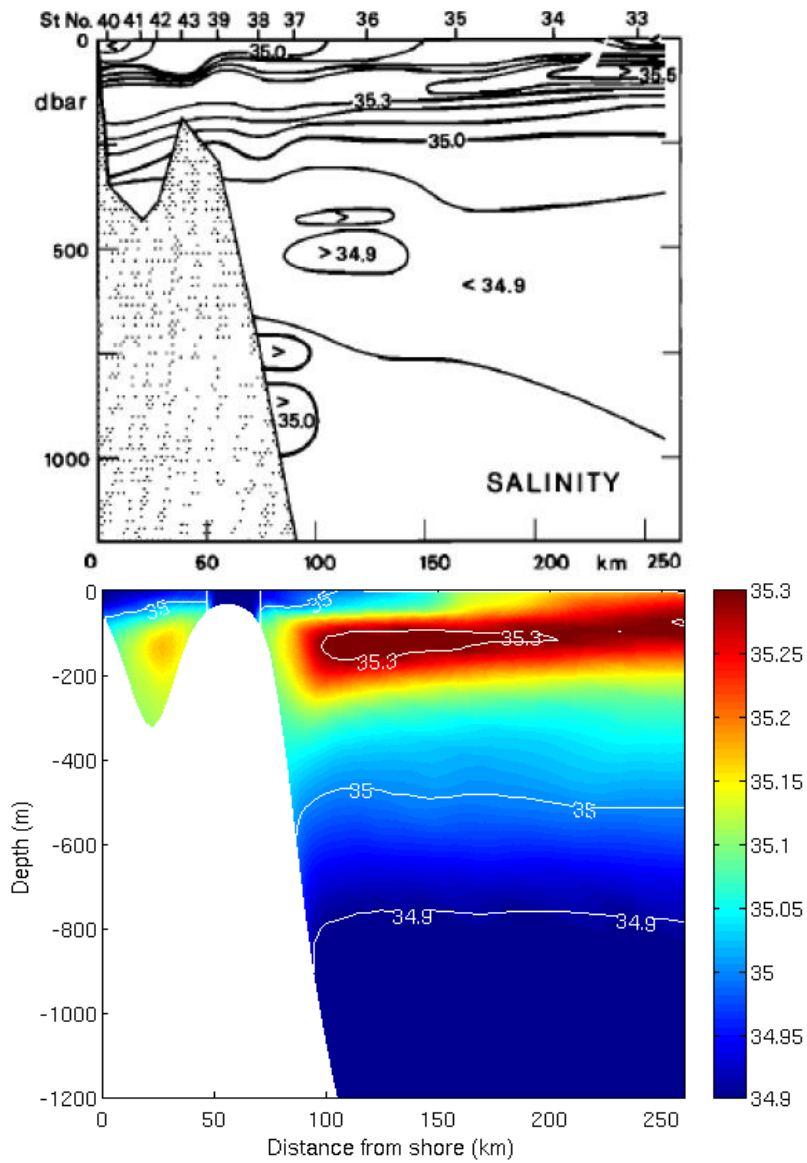
Figure 2.10: Salinity contours on a vertical section at ($\sim$5ºS. Top) Based on ship observations made in April 1985 [after Swallow et al, 1991]. Bottom) KTCM monthly mean April salinity for the same section.
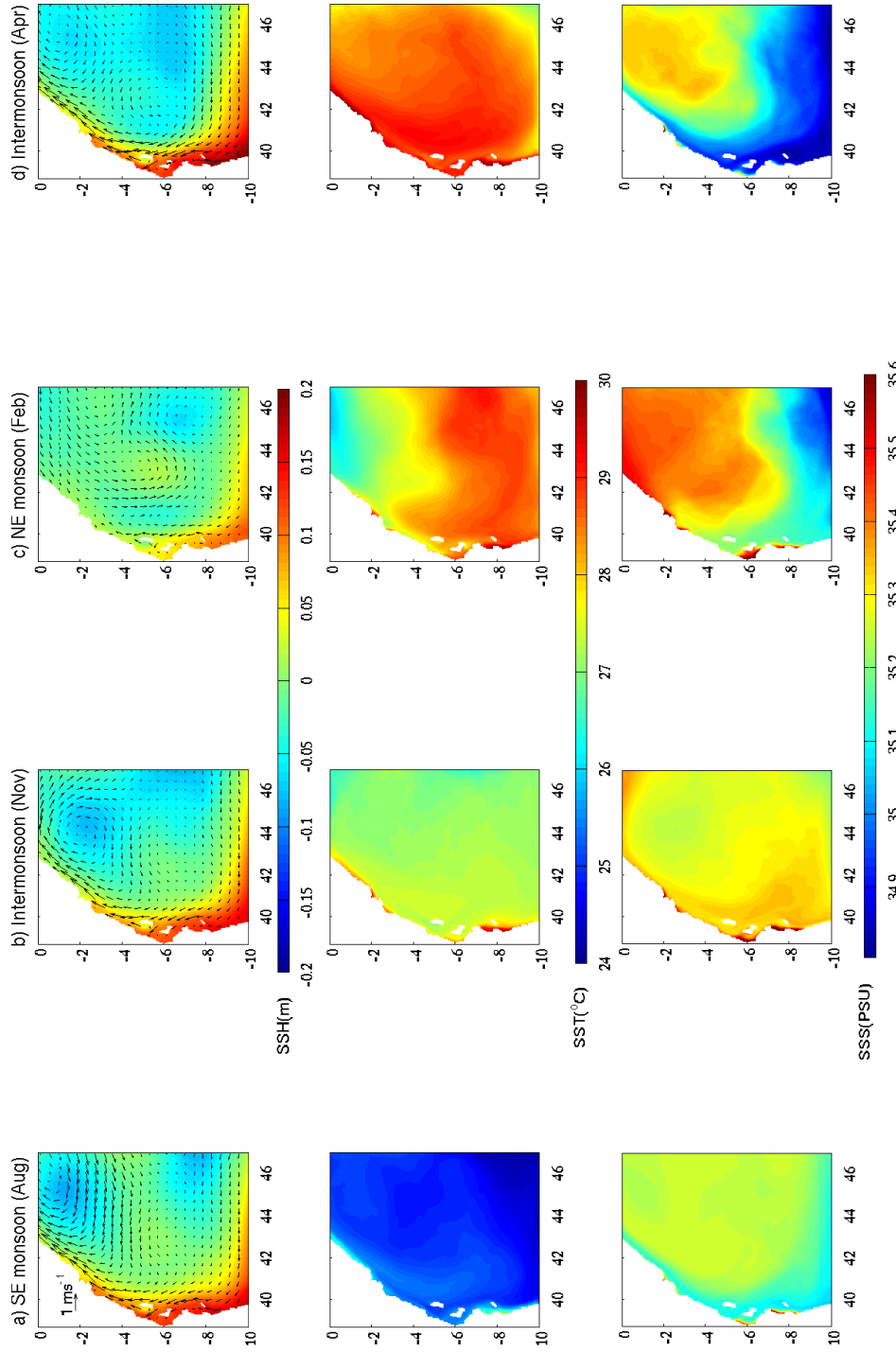
Figure 2.11: KTCM climatological monthly means representative of the seasonality of the modeled region: modeled SSH (m) with surface velocity vectors overlaid (top row), modeled SST (°C) (middle row), modeled SSS (PSU) (bottom row).

Figure 2.12: North-south (v) velocity (m s⁻¹) at 1°S, marked isotachs have a 10 cm s⁻¹ interval starting from ±5 cm s⁻¹; solid thick line is zero velocity, thin solid lines mark northward velocity contours, and dashed lines southward velocity contours.

56
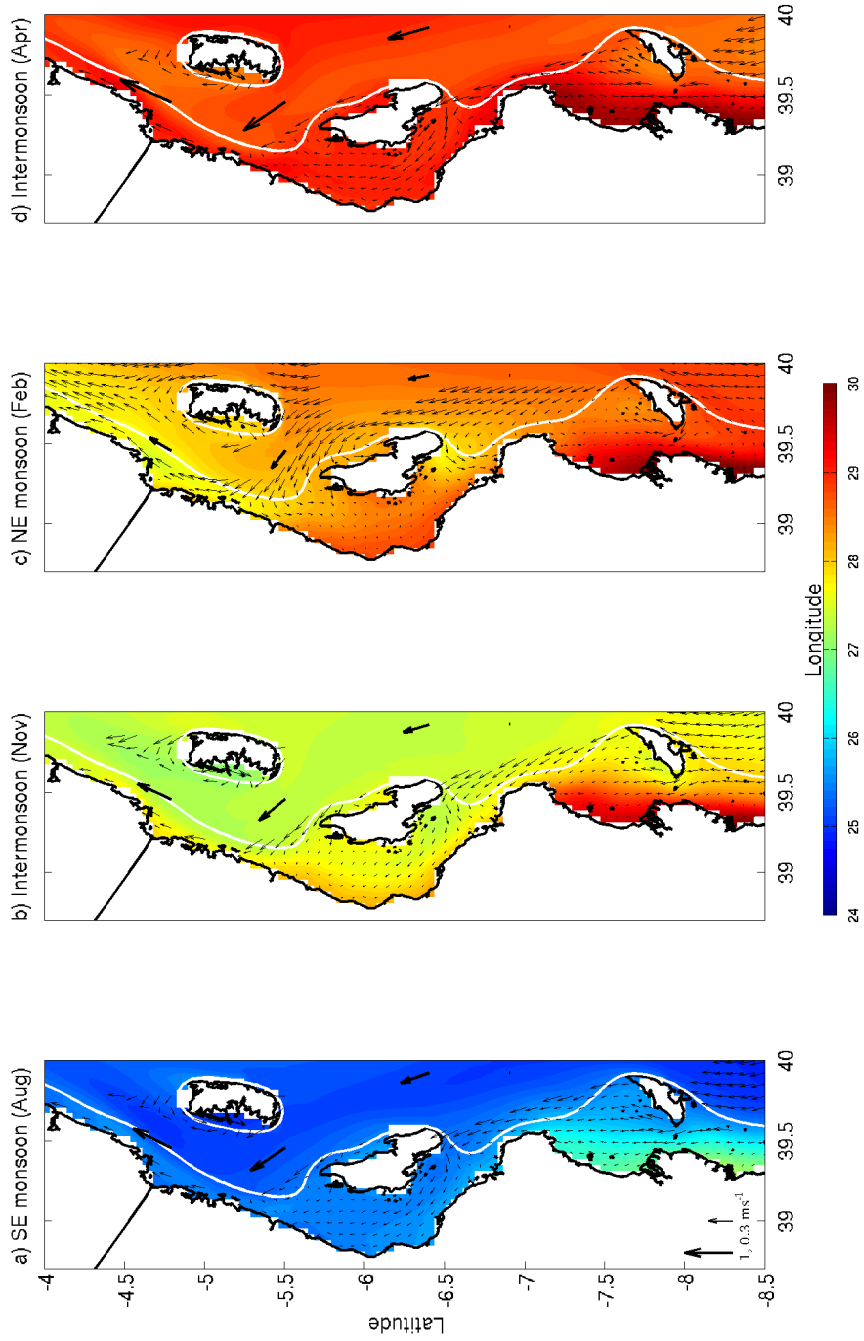
Figure 2.13: SST with surface velocity vectors overlaid for the Tanzanian shelf region. The islands from north to south are Pemba, Zanzibar and Mafia. For clarity only every third vector is shown and vectors with a speed greater than 0.4 m s⁻¹ were removed. Thick arrows show strong currents representing the removed vectors. Scale arrows in the left panel apply to all panels.

57
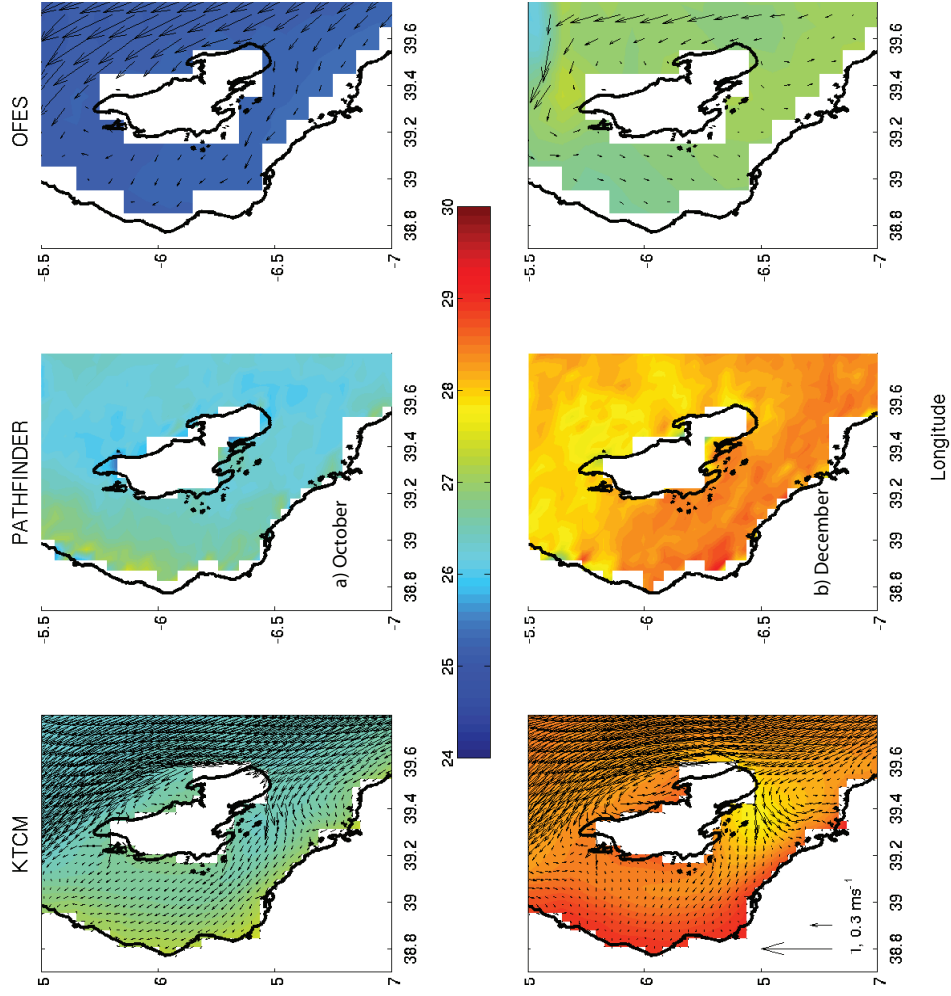
Figure 2.14: SST around Zanzibar Island is shown in color for a) October and b) December, from KTCM, the Pathfinder satellite product and OFES. Velocity vectors are shown at full resolution for both models. Scale arrows in the lower left panel apply to all panels
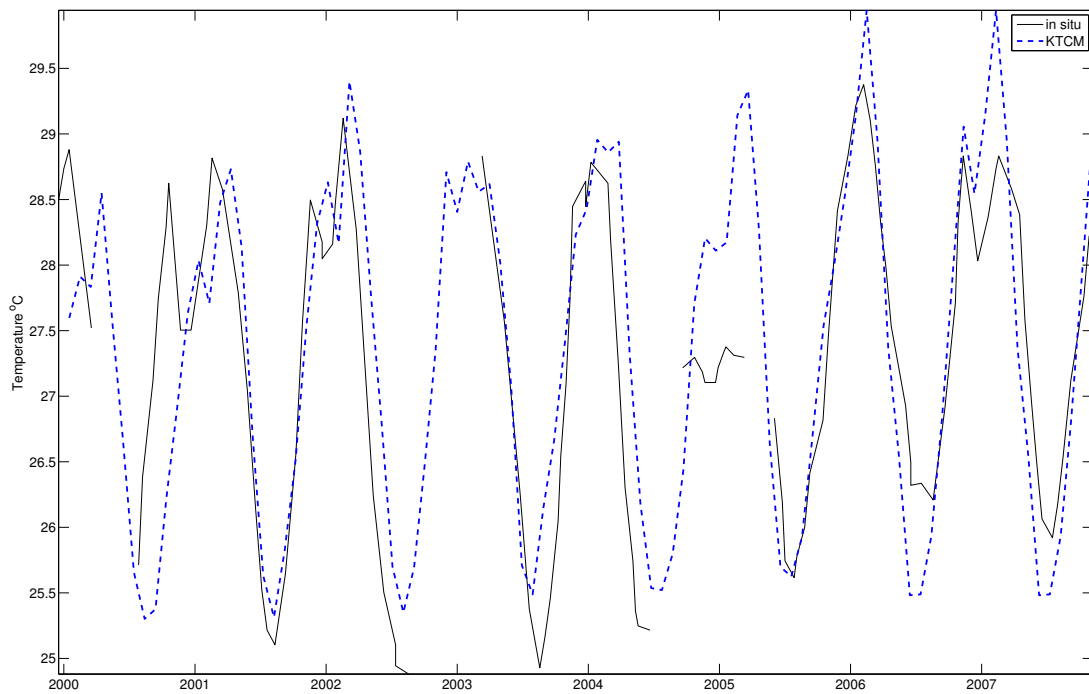
Figure 2.15: In situ near-bottom temperatures at Chumbe Island Coral Park in the Zanzibar Channel reported in Manyilizu et al., [2014] (black line) and concurrent temperature from the KTCM (blue dashed line).

Chapter 3: Modeling potential connectivity among coral reefs in the
Kenyan-Tanzanian region

.

3.1   Introduction

Coral reefs extend continuously along the coast of East Africa from the equator
to approximately 14ºS latitude; they are only interrupted at major river outflows or
Pleistocene river valleys. Fringing reefs are the most common but complex formations
occur around islands and other regions where the continental shelf extends more than
a few kilometers from shore. There is no significant reef development on the Somali
coast north of the equator due to seasonal upwelling of cold water. The southernmost
reef is found in Mozambique at 26ºS; but scattered colonies of scleractinian corals
occur down to 34ºS in South Africa [Day, 1974 cited in Hamilton and Brakel, 1984].
Western Indian Ocean coral reef communities are characterized by high levels of
species diversity and may be centers of biodiversity [Spalding et al., 2001].

Coastal communities of Kenya and Tanzania depend on the reef for food. Since
there is little control over the utilization of these resources through formal resource
management strategies, many reef areas have been degraded due to overfishing, de-
structive fishing techniques and other activities affecting the coastal environment
[Hamilton and Brakel, 1984; Spalding et al., 2001]. Growing interest in tourism ac-
tivities on coral reefs is simultaneously leading to increased pressure on some coral
reefs while providing a powerful local incentive for conservation [Spalding et al.,
2001]. There are 26 Marine Protected Areas (MPAs) in Kenya and Tanzania reported
in the Protected Planet Database [`http://www.protectedplanet.net/`; accessed
February 2013] that encompass coral reef habitat; some of them were established as
recently as 2010. Eight of the 26 MPAs are no-take areas, while 18 of them allow
extraction using traditional fishing methods like handlines and traps [Muthiga et al.,

2008]. The benefits for biodiversity conservation and fisheries management of the implementation of MPAs are well known [McClanahan and Mangi, 2000; Gell and Roberts, 2003; Roberts et al., 2005; Lester et al., 2009; Micheli et al., 2012]; however the design (spacing, size and separation distance) of effective MPA networks is not trivial [e.g. Botsford et al., 2003; McLeod et al., 2009; Edgar et al., 2014]. Several studies [e.g. McCook et al., 2009; Botsford et al., 2009] emphasize the importance of connectivity of multiple types (larval dispersal, juvenile and adult swimming, and movement of fishers) in the performance of MPA based spatial management for meeting population sustainability and fishery yield objectives.

With the exception of a few studies [McClanahan et al., 1994; McClanahan, 1994; Mangubhai, 2008; Yahya et al., 2011; Kruse et al., 2015], knowledge of reef biota ecology is lacking for much of the Western Indian Ocean region, due to the lack of infrastructure and indigenous expertise, combined with problems of national security in some areas [Spalding et al., 2001]. Few studies have examined larval supply and connectivity in coral reefs in the Western Indian Ocean [Kaunda-Arara et al., 2009]. Studies on connectivity of coral reef species in the Kenyan-Tanzanian reefs use genetic techniques to study connectivity at evolutionary time scales [Dorenbosch et al., 2006, Lutjanus fulviflamma;Visram et al., 2010, Scarus ghobban, and Muths et al., 2012, Lutjanus kasmira]. They report high gene flow and weak genetic structure within the populations of the fish studied, even among sites as distant as 4000 km [Muths et al., 2012]. These studies do not address ecologically significant timescales of a few generations, which would provide insights relevant to population demography at temporal and spatial scales relevant to the implementation of management and conservation strategies at a regional, national and international level. Only the Souter et al. [2009] study uses genetic techniques to examine both evolutionary and ecological connectivity of the coral Pocillopora damicornis in the MPAs of the Kenya-Tanzania (KT) region. They identify the Mnemba Conservation area in northeast Zanzibar as a potential source for the *P. damicornis* population, and Malindi Marine Narional Park and Reserve in north Kenya as a genetically isolated reef.

For decades connectivity of larval fish and invertebrates was thought to be a passive process governed by the ocean physics and the duration of the larval period

[Shanks, 2009]. The pelagic larval duration (PLD) of coral reef organisms varies greatly; from a few hours for some coral species to a few months for some fish and crustaceans [Shanks, 2009]. Among individuals of a species, PLD varies with temperature and food availability. Increased water temperature within the optimal species specific thermal range is expected to accelerate larval physiological processes, thus increasing developmental rates, which allows larvae to reach ontogenetic milestones, including settlement competency, earlier [Munday et al., 2009]. The relationship between PLD and temperature for coral reef fishes shows important variability [Munday et al., 2009]. O'Connor et al. [2007] examined the generality of the temperature-dependence of planktonic larval duration in marine species. They showed that PLD has essentially the same relationship with temperature across 69 species of marine invertebrates and fish from a variety of environments. Based on this finding they developed a mathematical model to represent this general relationship that can be adjusted based on observations to represent the effects of temperature on species specific PLD. Recent studies have shown that larval transport of most marine organisms is not strictly passive [i.e. Paris and Cowen, 2004; Shanks, 2009], and that there is an uncoupling between dispersal distance and PLD due to larval behavior, such as active depth selection. Nevertheless, PLD is still one of the most important factors determining the scale at which metapopulations are connected since it defines the time of exposure of larvae to the advective environment.

Discrepancies between the passive transport hypothesis and observed patterns of recruitment point to the importance of biological factors (i.e. behavior, predation, starvation, etc) controlling larval dispersal and connectivity [Cowen et al., 2006; Cowen and Sponaugle, 2009; Leis et al., 2007; Paris and Cowen, 2004; Sponaugle et al., 2012]. Even excluding mortality, the degree to which biological factors influence connectivity is greater than originally hypothesized. Recent studies have shown the importance of physiological and behavioral characteristics of larvae on influencing the connectivity and dispersal of species with a planktonic larval stage. Growth rates [e.g. Bergenius et al., 2002], ontogenetic and diel vertical migrations [Paris et al., 2007; Drake et al., 2013], swimming ability [e.g. Stobutzki and Bellwood, 1997; Wolanski et al., 1997; Leis et al., 2007], orientation through olfaction [Atema et al.,

2015, Atema et al., 2002; Gerlach et al., 2007] and audition [Tolimieri et al., 2000; Leis et al., 2003; Simpson et al., 2005, Heenan et al., 2009], and settlement strategies [Leis and Carson-Ewart, 1999; Lecchini et al., 2005] are important biological factors controlling connectivity of coral reef organisms.

Observational studies suggest that marked ontogenetic vertical zonation is important for larval transport [Boehlert and Mundy, 1993; Cowen and Castro, 1994]. In modeling studies, vertical migration has been shown to promote retention of pelagic larvae around suitable habitat and increase self-recruitment. The modeling study of the California Current System (CCS) by Drake et al. [2013] showed that larvae that remained below the surface boundary layer were 500 times more likely to be retained within 5 km of the coast after 30 days than larvae that remained near the surface. Settlement in the CCS increased by an order of magnitude when larvae remained at 30 m depth. Similarly, successful settlement in different regions of the Caribbean increased when a shallow ontogenetic vertical migration (OVM) behavior was added to the virtual larvae. Settlement increased up to 190% in the southern Florida keys with the OVM [Paris et al., 2007].

The influence of larval physiology and behavior on connectivity and dispersal of coral reef species is now well established. However biological characteristics are known with certainty only for a handful of species. Given the meager physiological and behavioral data for larvae of coral reef species, in this study, the approach to examine connectivity among coral reefs in the Kenyan-Tanzanian region is to conduct a series of idealized particle tracking experiments that simulate larvae with characteristics of two ubiquitous and ecologically important species groups: the *Acropora* branching corals with short PLD (ca. 12 days, [Babcock and Heyward, 1986; Nishikawa et al., 2003; Nozawa and Harrison, 2008] and the *Acanthurus* surgeonfish with long PLD (72 days, [Rocha et al., 2002]), during two years with contrasting ocean conditions. Particle tracking of individual organisms using the output of ocean circulation models is a suitable, cost effective tool to examine larval connectivity among coral reefs in large areas and at finer spatio-temporal scales relevant to the population ecology of coral reef species [Werner et al., 2001; Cowen and Sponaugle, 2009]. Insight developed from connectivity matrices generated from such studies can

aid local managers and decision makers in charge of regulating the use of marine resources in the Kenyan-Tanzanian region.

3.2   Methods

3.2.1   Hydrodynamic model

A 2 km horizontal resolution Regional Ocean Model System (ROMS) [Haidvogel et al., 2008] application including tidal signals, the 2 km Kenya Tanzanian Coastal Model (hereafter 2KTCM), was used to generate 3-dimensional ocean velocity fields. This ocean circulation model is an enhanced resolution version of the 4 km Kenyan-Tanzanian Coastal Model (KTCM) [Mayorga-Adame et al., 2015, provisionally accepted, also Chapter 2.], The model domain is a rectangular grid extending from 38° to 47^oE and from the equator to 10^oS (Fig. 3.1). It has 31 terrain following vertical levels. The model bathymetry is from the 30 sec global GEBCO product [`www.gebco.net/data_and_products/gridded_athymetry_data/`; accessed April 2011). The model coastline was manually edited to retain as many features as the 2 km resolution allowed. Only Pate Island in north Kenya, and Pemba, Zanzibar and Mafia Islands in Tanzania are included as dry cells in the land mask (Fig. 3.1). The atmospheric forcing (wind stress, heat and freshwater fluxes) is calculated by ROMS bulk formulation using atmospheric variables from daily NCEP/NCAR reanalysis [Kalnay et al., 1996]. The model is initialized from KTCM fields and forced at the boundaries by KTCM monthly outputs [Mayorga-Adame et al., 2015, provisionally accepted; also Chapter 2] and tides from the TPXO6 global tidal model [Egbert et al., 1994; Egbert and Erofeeva, 2002]. Freshwater inflows and diurnal wind variability are not included in the model. The ocean model was run continuously for 8.25 years from October 1999 to December 2007. Three-hourly averaged velocity and temperature fields for 2000 and 2005 are used for the particle tracking experiments.

3.2.2 Lagrangian particle tracking model

An Individual Based Model (IBM) [Batchelder, 2006] was run offline using previously stored 3-hour averages of the 3-dimensional 2KTCM velocity fields. The IBM interpolates tri-linearly in space and linearly in time the velocity and temperature fields from the ROMS simulation. Particle trajectories are computed using a 4th order Runge-Kutta algorithm. No explicit diffusion (e.g. random walk applied to the individual's position) is invoked since the 2 km horizontal resolution of the ocean circulation model is enough for significant eddy formation and horizontal mixing to occur around reefs, and the terrain following coordinates provide very high vertical resolution (<15 cm) in the shallow regions. An advection only version of the IBM was used to track forward in time the dispersal of particles (virtual larvae) originating at all reef polygons considered. The tracking was done using a 30 min time step. Coral larvae were tracked only under the 3-dimensional passive advection scenario. For surgeonfish, with longer PLDs and greater ability to control depth in the water column, especially for older larvae, two other more complex particle tracking scenarios were considered: an idealized ontogenetic vertical migration scenario and a temperature dependent PLD scenario.

3.2.3 Biological assumptions

In all experiments all reefs were seeded randomly with a density of 50 particles per square kilometer of reef. Reefs smaller than 1 km^2 were seeded with 50 particles. A total of 116 903 particles were released for each modeled spawning day, using the same seeding locations for all simulations. Spawning was assumed to take place at 5:30pm local time (~sunset) during February and March, the months of peak spawning for coral reef species in the Western Indian Ocean [Mangubhai and Harrison, 2008; Mangubhai, 2008]. Particles were released uniformly at 3 m depth. For the 3-dimensional passive experiments (reference experiments) virtual larvae were spawned from the randomly selected release locations at 3 day intervals starting on February 2nd for a total of 20 releases.

Acanthurus virtual larva were tracked for 72 days and considered competent

to settle 50 days after their release, giving them a competency period of 22 days. *Acropora* virtual larvae were tracked for 12 days and considered competent after 4 days giving them a competency period of 8 days. The ability of reef larvae to sense and swim towards settlement habitat is often represented in models as a sensory zone based on perception distance [Paris et al., 2007; Sponaugle et al., 2012], a buffer distance around suitable habitat that defines how far away from a reef polygon larvae are assumed to be able to settle. Based on observational studies of sensing, swimming and settling ability [[Atema et al., 2015]; Leis and Carson-Ewart, 1999;Leis and Fisher, 2006] perception distance was assumed to be 4 km for competent *Acanthurus* larvae, which is within the distance range used to model other coral reef fish [Paris et al., 2007; Sponaugle et al., 2012]. Perception distance for competent *Acropora* larvae was only 10 m since they have very limited swimming ability. Every night during their competency period virtual larvae were evaluated to determine if reefs were within their perception distance and for simplicity assumed to settle on the first reef they encountered. Sensitivity analysis was done to evaluate if the destination of larvae was affected by the time of evaluation during the dark hours. The effect of the time of evaluation turned out to be minimal; therefore for the experiments presented here virtual larvae were only evaluated once a day at 11:30 pm local time.

The *Acanthurus* ontological vertical migration experiment was set up as the passive experiment described above, but 20 days after spawning the depth of the virtual larvae was shifted to 50 m (or 3 m above the bottom when particles were found in areas shallower than 50 m). Virtual larvae continued to be passive in their horizontal movement but were kept at fixed depth for 20 days. Forty day old larvae migrated back to 3 m depth to find suitable reef habitat when reaching competency. After the migration larvae continue to advect passively in the three dimensions for the rest of their larval duration. They were analyzed for settlement as in the reference experiment, when they became competent, 50 days after spawning. This migration pattern is based on the increased depth of the *Acanthurus* larvae through ontogeny observed by Irisson et al. [2010]. The depth of the migration is not well defined and could be site dependent. For example, Irisson et al. [2010] reported post-flexion *Acanthurus* larvae in the 25-60 m depth range near reefs in French Polynesia, while Oxenford

et al. [2008] found aggregations of late larvae *Acanthurus* to be more abundant at 120 m in the eastern Caribbean Sea.

For the temperature dependent pelagic larval duration experiments the exponential-quadratic model derived by O'Connor (2007) (Eq.1) based on 69 species of invertebrates and fish was used.

$$ln(PLD) = \beta_0 + \beta_1 \times ln(T/T_c) + \beta_2 \times (ln(T/T_c))^2 \qquad \text{(Eq. 1)}$$

The parameter β_0 was fitted so that *Acanthurus* larvae exposed to the maximum temperatures experienced by successful settlers during the passive experiment would reach competency in 50 days. This constrained virtual larvae within the temperature range typical of the genus (20 to 33°C) to reported PLD values for *Acanthurus* (34 to 77 days; Fig. 3.2). The values used for the parameters in Eq. 1 are: β_0= 4.748, β_1= -1.344, and β_2= -0.278, with a reference temperature T_c=15°C. The fitted equation was coded into the particle-tracking model to control the development rate of virtual larvae depending on the environmental temperature experienced. Larvae were assumed to be competent when they reached 70% of their total development. Larvae that exceeded 70% of total development were evaluated for settlement every night during a 22 day competency period. Non-passive experiments (OVM and temperature dependent PLD) were run for the same February 5th to March 30th period as the passive experiments, but with larvae released only every sixth day (for a total of 10 release dates).

3.2.4   Seascape and visualization analysis

Kenya and Tanzanian have a very narrow continental shelf, with the 200m isobath only 12 km offshore, except at the Mafia and Zanzibar Channels. The shelf is protected by a virtually continuous chain of fringing coral reefs that stretch along the coast, only breaking at river mouths and estuaries. The coral reef polygons in the model domain were extracted from the Global Distribution of Coral Reefs 2010 database available at the Ocean Data Viewer webpage [`http://data.unep-wcmc.org/`]. After simplifying the polygons using ArcGIS, which implied merging adjacent

reefs, and discarding individual reefs smaller than 20 m^2. A total of 661 individual reef polygons were considered suitable reef habitat for larval settlement (Fig. 3.1.

A connectivity matrix showing the origin locations on one axis and destination locations on the other axis is fairly intuitive for visualizing the geographic connections among habitat patches for simple alongshore linear systems. However, because of the inherent two dimensional nature of the reef systems, with several reefs at the same latitude (i.e. mainland fringing reefs, atolls or patch reefs in the channels between the islands and mainland, fringing reefs in the west and east coast of the islands), simple reef to reef connectivity matrices organized by the latitude of the centroid of the reef polygons are not particularly informative regarding the connection on the longitudinal dimension (among inshore-offshore reefs). Because of the complexity of the habitat distribution and in order to synthesize the information from the reef to reef connectivity matrices and visualize the results in a more meaningful way, reefs were grouped into 15 geographical subregions (Fig. 3.1). The regional connectivity matrices are presented here for all simulations. To obtain the percentage of particles connecting from one reef or region to another the number of particles connecting was normalized by the number of particles released at the source reef or region. Therefore, adding the percentages in the horizontal direction on the connectivity matrices gives the percentage of successful recruits for each source reef or region.

In the results section the comparatives "weaker" and "stronger" are used to refer to the magnitude of connections between two specific sites, indicating the proportion of particles connecting from one reef or region to another. Strong connections appear as big circles in the connectivity matrices, while weak connections are small gray circles. Conversely "few" and "more/lots" are used to refer to the number of sites that are connecting to a reef or region. The number of connections for a region will be represented by the number of circles on each raw/column for origin/destination reefs.

3.3 Results

3.3.1 Passive particles

3.3.1.1 Settlement success

The percentage of surgeonfish *Acanthurus Spp.* virtual larvae that reach a reef during their competency period and are assumed to successfully settle varies between 13.5% and 31.9% among the 40 releases made during February and March of 2000 and 2005. The mean percentage of successful settlers was not significantly different between the two modeled years with 25.5% and 23.3% successful settlers during 2000 and 2005, respectively (Fig. 3.3a). Settlement success during 2000 shows two local maxima with values greater than 25% during February 8th to March 1st and from March 25th to 31st. The year 2005 shows a steady decline during the spawning period with a 31.55% maximum on February 6th and a minimum of 13.52% on March 31st. The highest percentage of success occurred during February in both years (on February 19th in 2000 and February 1st in 2005).

Acropora branching coral virtual larvae, with 12 days PLD and only near field (¡10m) habitat perception ability have much lower settlement success, fluctuating between 0.16% and 0.37% in the 2 years modeled, with very similar means: 0.27% and 0.28% for 2000 and 2005 respectively. The year 2000 shows small variations in settlement success among the 20 release days, with a slight decline from February to mid-March. Similarly to *Acanthurus*, the year 2005 shows more abrupt fluctuations on percentage of success (Fig. 3.3b).

3.3.1.2 Reef to reef connectivity matrices

The reef to reef connectivity matrices with reefs organized by the latitude of their centroid show that southern reefs providing larvae to northern reefs is the dominant connectivity pattern, as represented by the multitude of circles below the 1:1 diagonal line. This pattern is prevalent in both modeled years (2000 and 2005) for both larval types (*Acanthurus* and *Acropora*) (Fig. 3.4), and reflects the strong south to north

flows along much of the KT region (Chapter 2). The small number of circles above the 1:1 diagonal line of the connectivity matrices indicates north to south connections, which are much less common.

For the 2000 *Acanthurus* simulation (Fig. 3.4a) north to south connections occur in small proportions on reefs at almost all latitudes, but most north to south connections occurred at the northern (latitudes north of 3.3^oS) and southern most reefs (latitudes south of 7.9^oS). The connectivity pattern in these two regions is bidirectional with higher south to north connection strength. The highest magnitude of north to south connections occur in the north, on reefs around 1.4^oS where up to 10% of the *Acanthurus* virtual larvae released from a reef settles southward of their reef of origin. In 2005 (Fig. 3.4c) north to south connections were not observed at all latitudes. They concentrated mainly in Somali reefs (north of 2^oS), in small proportions among reefs with centroids between 2.5 and 3.5^oS, and among reefs between 5.2 and 7.7^oS. The highest probability of north to south connections occurred between 5.2 and 5.7^oS, the latitude of the northern entrance of the Zanzibar Channel.

In the two modeled years most connections concentrate in the southern half of the domain with strong northward connections among reefs between 5.2 and 9^oS. Reefs north of 5.2^oS are less likely to connect, since only a small number of reefs receive strong connections north of them (i.e. reefs around 1.5 and 3^oS). Source reefs of the 5.2 and 9^oS region are more likely to connect to reefs between 5.8 and 4.6^oS, which get settlers from most southward reefs in relatively high proportions (up to ($\sim$20%). During 2000, reefs around 7^oS show the highest probability of connecting (31%) primarily due to self and nearby recruitment. Reefs north of 2.6^oS, and south of 9^oS also have high probability (10-25%) of connecting to specific northern reefs (i.e. reefs centered at 8.9^oS, 1.5^oS, 1.7^oS, etc.). In 2005, larvae released south of 9^oS travel farther north than in 2000, being successful sources for reefs south of 4.6^oS. That year the reef with the highest probability of recruitment success (31%) is centered at 8.8^oS, its high probability of success is due to self-recruitment. Two reefs in the northern part of the domain (centered at ca, 1.5^oS) stand out for receiving settlers from more than 600 other reefs.

In *Acropora* corals (Fig. 3.4b) and d) most of the connections are due to self-

recruitment, or recruitment to nearby reefs. Most connections are restricted to 1 degree ($\sim$100 km) around the 1:1 diagonal line that indicates self-recruitment. Source reefs between 4.7 and 6.8^{o}S show the longest distance connections. Similar to *Acanthurus* there are more north to south connections in 2000 than in 2005. The main difference between the two years occur south of 8^{o}S where there is much more north to south connections in 2000 than in 2005. More long distance connections occurred in 2005 than in 2000, since flows were stronger in 2005 (Fig. A.1 and A.3). Small clusters of high connections are formed at various locations. The one at 5.2^{o}S (mid Pemba Channel) is the most prominent and is persistent in the two modeled years. During 2000, another cluster of similar magnitude is centered at 8.3^{o}S but its size is diminished in 2005. The reef centered at 2.6 ^{o}S has the highest probability of success ($>$1%) through self-recruitment in both modeled years. Two other reefs with high probability of success ($>$0.7%) are located at the northern and southern ends of the modeled domain (green circles).

The general pattern of more north to south connections during 2000 than during 2005 is explained by the influence of the mesoscale circulation on the shelf circulation pattern. In 2000 the northward flowing East African Coastal Current (EACC) was weak during the spawning months ($<$0.5 m s^{-1}) as is typical during the NE monsoon season. The Somali Current (SC) that flows southward at this time of the year was strong in February ($\sim$0.68 m s^{-1}) and its subsurface influence prevailed until April (Fig. A.2). The strong influence of the southward flowing SC current in the northern part of the domain is responsible for the north to south connections in that region. In the rest of the domain the weak EACC generates slower northward velocities on the shelf during the spawning months, especially February (Fig. A.1), allowing for some north to south connections at most latitudes.

In contrast, in 2005, the SC was weaker and only present during February and March since the transition to SW monsoon conditions happened very early in the year, with strong northward flow ($>$1 m s^{-1}) established in March and already re-established in the upper 300 m by April (Fig. A.4). The weak SC only promotes a few north to south connections in the northern part of the domain. The strong EACC intensifies the flow reversal north of the Mafia and Zanzibar Channels, which

is generated as the northward flow overshoots and turns southward into the channels when trying to follow the curved bathymetric contours past the islands (Fig. A.3). This small scale circulation pattern is responsible for the north to south connections observed south of 5.2 and 7.7ºS in 2000 for both *Acanthurus* and *Acropora* virtual larvae.

3.3.1.3   Regional connectivity matrices

Connectivity matrices with reefs grouped into subregions according to Figure 3.1 show that at a regional scale Kenya and Somali reefs receive *Acanthurus* virtual larvae from all other reef regions in both modeled years. In contrast regions around Pemba Island (eP, nP, wP) have very little *Acanthurus* larvae settlement (Fig. 3.5a) and c). Because of its oceanic location and its exposure to the strong northward flowing EACC, the reef offshore from Dar es Salaam peninsula (oR at ca. 7ºS) has potential for long distance connections. In 2000 it was a source for larvae settling on Kenyan and Somali reefs only, while in 2005 it exported larvae also to northern Tanzanian regions (central and north Tanzania and east Zanzibar regions; cT, nT, eZ). This offshore reef (oR) is not a common destination for *Acanthurus* larvae, but the origin of arriving larvae is diverse, coming from reefs to the south of it in 2000 and from most regions except east Zanzibar in 2005. The north Tanzania region is the destination region with the greatest diversity of origin reefs, followed by the south Kenya region. In 2000 the strongest connection was between the Dar es Salaam Peninsula (DP) region and the north Tanzanian region, followed in magnitude by the connection from the east Zanzibar region to the South Kenya region. In 2005 the strongest connection remains the same but the second strongest connection was between east Zanzibar and the north Tanzania region. During 2005 reefs around Zanzibar Island and the central Tanzania region had more connections to southern destination reefs. However the magnitude of self-recruitment by *Acanthurus* surgeonfish at the regional scale was larger in 2000.

   For *Acropora* corals (Fig. 3.5b and d) the highest proportion of successful settlement is due to self-seeding within the west Zanzibar and west Pemba regions in

both 2000 and 2005. In all regions except east Pemba and the offshore reef (oR), the probability of self-seeding is higher than the probability of connecting to another reef region. Similar to *Acanthurus* more north to south connections are observed in the regions between north Tanzania and the Dar es Salaam peninsula in 2005 than in 2000, when substantial north to south connection occurred only between Dar es Salaam and west Mafia. In 2000, the offshore reef (oR) connects to all Pemba regions and north Kenya while in 2005 it connects to all regions north of Dar es Salam except north and west Pemba. This offshore reef is the only source of *Acropora* larvae for the east Pemba region. North and west Pemba get recruits from all Pemba regions in both years.

3.3.1.4   Multiple origin and destination maps

Reefs that provide recruits to many other reefs have a reproductive impact beyond their local ecosystem and can help maintain and replenish multiple other metapopulations at the destination reefs. Distant origin reefs are vital to repopulate metapopulations that have been impacted by local environmental disturbances that limit local production of larvae (i.e. coral bleaching, overfishing). Even if the magnitude of the connections is not strong and only a few larvae get exchanged, reefs that provide larvae to multiple other reefs may have a significant impact for organisms repopulating deserted or degraded habitat.

Figures 3.6 and 3.7 show the origin reefs color coded by the number of destination reefs that receive 3D passive virtual larvae settlers from them. For these maps, the results from all particle releases in both 2000 and 2005 were merged. In general reefs south of Mafia Island (8^oS) provide larvae of both species groups to the greatest number of reefs. In the case of *Acanthurus* larvae (3.6) these reefs connect to more than 350 different reefs, for *Acropora* (Fig. 3.7) to more than 70 reefs. Reefs in the northern half of Tanzania are good sources of *Acropora* larvae, connecting to more than 50 reefs, while Kenyan reefs connect to approximately 30 different reefs. Somali reefs provide *Acanthurus* virtual larvae to less than 50 reefs and *Acropora* virtual larvae to less than 10 different reefs. This general pattern is consistent between the

short (*Acropora*) and long (*Acanthurus*) PLD groups simulated. The reefs providing larval settlers to the largest number of destinations are the same for both species groups: Juani Island reef (in purple) southeast of Mafia Island and Ocuz island reef (in pink) to the southeast of the later one. However, for *Acanthurus* there are many more reefs south of 8ºS that source multiple reefs in that same area.

Destination reefs receiving propagules from multiple origin reefs may have greater resilience to local environmental disturbances, since larval supply/recolonization is possible from multiple external sources unlikely to be affected simultaneously by a localized threat. At evolutionary time scales these reefs may have a diverse gene pool, which may increase their probability to adapt to new or changing environmental conditions. Figures 3.7 and 3.9 show destination reefs color coded by the number of reefs that provided settlers to them. The spatial distribution of these reefs is more variable between the two modeled PLD types than that of the origin reefs that provide larvae to multiple destinations. For *Acanthurus* destination reefs of multiple origins show the inverted pattern of the origin reefs sourcing multiple destinations: except for the northern tip of Mafia Island, the reefs of southern Tanzania, south of the Dar es Salaam peninsula receive virtual larvae from fewer than 100 reefs (Fig. 3.7). North Tanzanian reefs, including the Zanzibar Archipelago and coastal mainland reefs from the Dar es Salaam Peninsula to the Kenyan border receive larvae from 100-300 reefs with the exception of west Zanzibar and Pemba Island, which receive larvae from very few reefs. Kenya and Somali reefs especially those south of Unguana Bay, receive particles from 300-500 reefs.

The pattern of destination reefs receiving *Acropora* larvae from multiple origin reefs is patchy, with diverse origin reefs adjacent to reefs with relatively few origin reefs (Fig. 3.9). Regionalization is at a smaller scale (as expected from the shorter PLD). The reefs receiving *Acropora* larvae from most other reefs are located at the Kenya-Somalia border and receive virtual larvae from 60 reefs only. Northern Tanzania and South Kenya reefs receive *Acropora* settlers from many origins. Tumbatu Islands, northern Zanzibar and Bagamoyo (6.4ºS) on the Tanzanian mainland coast are also common *Acropora* destinations. *Acropora* larvae settling in West Pemba reefs originate from multiple different reefs, in contrast to *Acanthurus*. East Pemba

reefs receive settlers of both genera from relatively few origins.

3.3.2 Ontogenetic Vertical Migration Experiments

3.3.2.1 Settlement success

Experiments that include OVM exhibit greater variability in *Acanthurus* settlement success among the release dates and between the two modeled years in comparison to that observed for the passive experiments (Fig. 3.10 and Fig. 3.3, respectively). In the OVM scenario there is a marked decrease in settlement success from earlier to later spawning dates going from 28% for larvae released in February 5th to 5% for those released on March 30th in 2000, and from 42% to 16% for those same dates in 2005. The decrease in settlement success occurs earlier in 2005 than 2000, associated with the quick transition to SW monsoon conditions in 2005. In the northern part of the model domain the core of the northward flowing EACC is subsurface (below 70 m depth) at the beginning of the spawning season (NE monsoon), but it re-establishes in the upper 300 m by May in 2000 and April in 2005 (Fig. A.2 and A.4). This implied that 2005 larvae migrating down to 50 m are affected longer by the strong northward flow than the 2000 larvae. Three-dimensional passive larvae tend to stay near the surface and are therefore less likely to be carried away from suitable habitat (Fig. A.5) by the deeper strong northward flowing EACC core, which transitions from deep to shallow waters during the second half of the spawning season. Mean settlement success is similar in the two modeled years; 21.8% for 2000 and 21.3% 2005, but lower than for the passive scenario.

3.3.2.2 Reef to reef connectivity matrices

The patterns of reef connectivity for *Acanthurus* with OVM (Fig. 3.11) differ between the two modeled years. Weaker and fewer connections are observed in 2005 in comparisons to 2000. Similarly to the passive simulation, reefs south of 5.8ºS are likely to connect northward to reefs south of 4.5ºS, but in 2000 the origin region does not extend south of 9.2ºS, while in 2005 it extends south to 10ºS. The destination

region in contrast, spans from 4.5ºS down to 10ºS in 2000 while it is restricted to the region north of 8ºS in 2005. A northern reef centered at 1.6ºS stands out for receiving settlers from most other reefs during both simulated years.

In 2000 (Fig. 3.11a) small numbers of north to south connections occurred in the northern half of the domain (north of 6ºS) including long range connections originating at 1ºS and settling at 6ºS. North to south connections are also observed south of 8ºS. The greatest settlement success in 2000 was due to self or nearby recruitment at reefs with centroids around 6.8, 7 and 8ºS. Reefs between 8.2 and 8.6ºS are particularly successful at settling northward to reefs between 7.2 and 7.8ºS. Conversely larvae from reefs between 6 and 7ºS have high probabilities of settling at reefs between 4.5 and 6ºS.

In 2005 (Fig. 3.11b) fewer (less than 0.4%) north to south connections occur at most latitudes north of 8.2ºS. Longer-range north to south connections are frequent at reefs between 8.3 and 5ºS. The highest settlement success (27%) that year occurs at a reef centered at 9ºS due to self-seeding. This reef also receives settlers from most southward reefs and represents a settlement hot-spot during 2005. Other high settlement regions due to self and nearby recruitment are centered around 5.8 and 8ºS. Strong connections also occur among reefs between 8.1 and 8.6ºS (origin reefs) and reefs between 6.1 and 7.8ºS (destination reefs).

3.3.2.3 Regional connectivity matrices

When grouped at the regional level the *Acanthurus* OVM experiments show that in 2000 (Fig. 3.12a) the strongest connection is between central Tanzania (cT) and north Tanzania (nT). The north Tanzania region receives virtual larvae from all southward reefs. The south and north Kenya regions (sK, nK) and the south Somalia (sS) region receive settlers from all other regions. Southern Tanzania (sT), east and west Mafia (eM, wM) and the Dar es Salaam Peninsula (DP) regions are provide larvae to most other regions except the offshore reef (oR), but their probabilities of connecting to the Pemba regions are very low. The only destination regions for larvae coming from the offshore reef (oR) in 2000 are south and north Kenya (sK, nK) and

south Somalia (sS). Minimal north to south connections occur with larvae originating at east and west Mafia (eM, wM) and the Dar es Salam Peninsula regions (DP) in the south and north Kenya (nK) and south Somalia (sS) in the north connecting to southward regions.

In 2005 (Fig. 3.12b), in contrast, the reef offshore of Dar es Salaam (oR) connects to both Zanzibar regions and all reef regions to the north except those around Pemba Island. The strongest connections of 2005 occurred between the offshore reef (oR) and north Tanzania (nT) and south Kenya (sK) regions, and through self-seeding at the western Zanzibar (wZ) region. Most regions successfully connect to northward regions, except to the three Pemba Island regions, which get few recruits in both years modeled. Only west Pemba (wP) gets recruits, coming from itself and the two other Pemba regions. Small proportions of the larvae spawned at the Dar es Salaam Peninsula and north Tanzania regions connect southward to the west Mafia and west Zanzibar regions, respectively. Across shore connections are observed from west Mafia to east Mafia and from west Zanzibar to central Tanzania.

3.3.2.4   Multiple origin and destination maps

For the OVM experiment the distribution of reefs sourcing many different reefs (Fig. 3.13) is very similar to that of the passive experiment; The reefs providing virtual larvae to the greatest number of reefs are Juani (39.7°E and 8°S) southeast of Mafia Island and the large offshore reefs of the south Tanzania region (i.e. the Songo-Songo reef complex). The reefs providing virtual larvae to most reefs, however, connect to fewer reefs in the OVM experiment than in the passive experiment (i.e. 10 fewer reefs in the case of the reef with more different destinations).

The distribution pattern of reefs that received larval settlement from many sources (Fig. 3.14) is also similar to that of the passive experiment; reefs to the north of Dar es Salaam peninsula receive OVM *Acanthurus* virtual larvae from more than 150 different reefs. South of the Dar es Salaam peninsula only the reefs in northern Mafia receive propagules from more than 100 different reefs. The reef receiving settlers from the most different source reefs was the largest reef in south Somalia.

3.3.3   Temperature dependent Pelagic Larval Duration Experiments

3.3.3.1   Settlement success

In the *Acanthurus* experiments that include temperature-dependent PLDs, settlement success slightly decreases throughout the spawning period in both modeled years (Fig. 3.15). The patterns are similar to those observed for the passive experiment (Fig. 3.3a). Temperature-dependent PLD larvae starting at the same locations as the passive larvae will follow the same pathways but for a different amount of time due to the PLD variability introduced with temperature dependent development rates. Settlement on the first spawning date differs the most compared to the passive scenario and leads to the highest percentage of settlement success in 2000 (30.5%) and low settlement success in 2005 (17.5%) in this scenario. The March 13th release date, however, shows the opposite pattern with relatively low success in 2000 and high in 2005, which was also observed under the passive scenario. When including temperature dependent PLD, the mean settlement success is 25.6% for the 2000 spawning season and 27.4% in 2005, slightly higher than for the passive scenario.

3.3.3.2   Reef to reef connectivity matrices

When temperature dependent PLD is included, long distance dispersal from source reefs south of 7°S decreases, with successful settlement probability being much lower for reefs north of 4.5^{o}S in both modeled years (Fig. 3.16). This is consistent with PLD shortening due to the temperature dependence to less than the 50 days assumed in the passive experiment. The mean PLD of the successful larvae was 30 days for both modeled years, with very few individuals spending more than 50 days in the planktonic stage before reaching competency (Fig. 3.17). Similar to both the passive and OVM simulations, reefs south of 9°S have few connections in 2000 (Fig. 3.16a), restricted to south of 7.4^{o}S. In contrast, in 2005 (Fig. 3.16b) these southernmost reefs provide settlers to reefs south of 5.3^{o}S and some long distance connections all the way to the northernmost reefs. Self and nearby settlement is enhanced in comparison to the other scenarios in both years, but particularly in 2000. The strongest connections

are due to self-seeding at reefs around 7°S in 2000 and 9°S in 2005. The north to south connectivity pattern and its interannual variability are similar to that of the other two simulations. In 2000 north to south connections are common at all latitudes but more abundant at the northern- and southernmost reefs. In 2005 north to south connections are concentrated in central (between 5.5 and 8°S) and northern reefs (north of 3.2^{o}S), while no north to south connections occur south of 8°S.

3.3.3.3 Regional connectivity matrices

In the temperature dependent *Acanthurus* simulation, when reefs are grouped into regions (Fig. 3.18) the general pattern of connections for both years, without considering its magnitude, is very similar to that of the passive experiments. However under this scenario the north and west Pemba regions are likely to exchange recruits among themselves. Strong connections from central Tanzania to north Tanzania are observed in both years, although in 2000 the connection from Dar es Salaam Peninsula to north Tanzania is of similar strength.

In 2000 (Fig. 3.18a) strong connections also occurred between central Tanzania and south Kenya and were due to within region settlement (i.e. regional self-seeding) in the Dar es Salaam peninsula region. North to south connections occurred between the Dar es Salaam Peninsula region and west Mafia, from central Tanzania to Dar es Salaam Peninsula and in the north, from south Somalia to north Kenya and from north Kenya to south Kenya. In this scenario, within region settlement occurs in both years, but is stronger in 2000. The north Tanzania and south Kenya regions are remarkable destinations, getting settlers from all other regions to the south in both modeled years.

In 2005 (Fig. 3.18b) larvae from most regions connect to reefs in almost all northern regions. Only the three Pemba regions receive few settlers from other regions. North and west Pemba get recruits from themselves and each other, while east Pemba has minimal probability of getting settlers. Regions around the Zanzibar Channel (wZ, cT, DP) show north to south connections among themselves and down to the west Mafia region. In this scenario, within region settlement occurs in both

years, but is stronger in 2000.

3.3.3.4   Multiple origin and destination maps

The spatial patterns of reefs that provide/receive virtual larvae to/from multiple destinations/origins for the temperature dependent PLD experiment are similar to those of the other experiments. Reefs south of Mafia Island provide virtual larvae to the largest number of reefs (Fig. 3.19) while Somali reefs receive virtual larvae from the most different reefs. However in this scenario some reefs south of Unguana Bay in the south Kenya region are also among the most common destination reefs (Fig. 3.20). Destinations with multiple origin reefs extend southward to include reefs north of Mafia Island (Fig. 3.20). This is consistent with the fact that the variable PLD allows for both local retention of fast developing larvae (with PLD shorter than the standard 72 days for passive particles) and long distance dispersal of slow developing larvae, exposed to colder temperatures during their larval development.

3.4   Discussion

Mean settlement success varied greatly between the two passive larval types modeled, being ca. 100 times greater for the long PLD *Acanthurus* larvae than for the short PLD *Acropora* (Fig. 3.3). In addition to PLD, the larval types differ in the length of the competency period (22 days for *Acanthurus* and 8 days for *Acropora*) and perception distance (4 km for *Acanthurus*, and only 10 m for *Acropora*). Sensitivity analysis shows that the large difference in perception distance could be responsible for much of the intra-species variability in settlement success. A subset of the *Acropora* larval trajectories were analyzed for perception distances ranging from 1 m to 25 km. *Acropora* larvae settlement success increased rapidly with perception distances increasing from 1 m to 25 km, with success leveling off with far field perception. With a perception threshold of 4 km, the settlement success of *Acropora* was ca. 55%, or (~200 times higher than the settlement success at a perception distance of 10 m (Fig. 3.21). These large perception scenarios are not realistic for *Acropora*

larvae but provide insight on the causes of the persistently low settlement success in *Acropora*.

The dominant pattern of connectivity for both *Acanthurus* and *Acropora* in the KT region is south to north (Fig. 3.4). The scale of connectivity is much smaller for the short PLD coral group with connections restricted to a 1° radius (∼100 km) around origin reefs. In contrast, long distance connections from the southern- to the northern most reefs (∼950 km) are common for *Acanthurus*. 8.2% of *Acropora* larvae succeed by settling to their source reef (self-seeding), an important proportion compared to only 1-2% for *Acanthurus*. Some *Acropora* were capable of long distance dispersal, particularly larvae spawned at the reef offshore of Dar es Salaam peninsula (oR). This indicates that they can take advantage of the strong offshore EACC to reach distant northern reefs, and that even for short PLD, latitudinal isolation may be minimal, especially at longer (i.e. evolutionary) timescales.

North to south connections occur in regions of flow reversal: 1) the northern region, seasonally influenced by the southward flowing Somali current (SC), 2) the northern entrance of the Zanzibar Channel and the region south of the Dar es Salaam peninsula where nearshore flow reversal is promoted by strong northward offshore currents. Therefore, there is strong interannual variability in the amount and location of north to south connections depending on the strength of the offshore mesoscale currents. In 2000 when the SC is strong, short-distance north to south connections are common at most latitudes, but are most prevalent at the northern and southern edges of the study region. In 2005 when northward offshore flow is strong, sources of north to south connections are restricted to reefs in the wider shelf region between Pemba and Mafia Islands.

Interannual variability is observed in the connectivity patterns, especially with respect to the strength of the connections among reefs. In many cases the hot-spots in the connectivity matrices representing strong connections among reefs or regions are not persistent between the two modeled years; simulations of additional years are needed to see if more persistent patterns would emerge. Multi-year simulations would be helpful to identify connections that are of vital importance to maintain regional metapopulations of different species groups.

Contemporary gene flow results of Souter et al. [2009] for *Pocillopora damicornis* can be directly compared with results presented here to evaluate whether their genetic based patterns are confirmed by modeled connectivity patterns and whether the results for a different, shorter Pelagic Larval Duration (PLD) brooding coral species compares well with the longer PLD, broadcasting spawner *Acropora*. [Souter et al., 2009] identified first generation migrants of *P. damicornis* to 29 reefs sites in the KT region, and therefore determined the degree of isolation of the different reefs sampled. They found patchiness in the degree of isolation at very small scales, with marked differences even between lagoon and fringing reefs at Malindi Marine National Park and Reserve in south Kenya. The patchiness of the *Acropora* multiple origin and destinations maps is supportive of their finding, indicating strong spatial variability in the number of connections (degree of isolation) among nearby reefs. Souter et al. [2009] identified isolated reefs, highly dependent on self-recruitment for population renewal, in south Kenya, west Pemba, south Mafia and Mtwara (south of the model domain). In the *Acropora* simulation these regions receive virtual larvae from less than 10 different reefs (Fig. 3.9). The regional connectivity matrices (Fig. 3.5b) and d) show that self-recruitment is important for these regions. In this model, however only west Pemba, east Mafia and south Tanzania show relative isolation, receiving *Acropora* larvae from only three and two other regions respectively; south Kenya in contrast receives larvae from nine regions to the south and one to the north. In the *Acropora* simulation, the south Kenya region receive settlers from most southward regions; the discrepancy between our model and Souters results may reflect the different scales of the comparisons, since the regional grouping presented here conglomerates the connections for several reefs which might have different degrees of isolation. Souter et al. [2009] identify Mnemba Conservation Area as a strong source for other sampled sites. This site shows the highest genetic diversity and is similar only to one site in the Dar es Salaam Peninsula and one site in southeast Mafia Island. In the simulation *Acropora* larvae settling at the east Zanzibar region, which includes Mnemba Island come from few origin reefs. The Dar es Salaam Peninsula and east and west Mafia regions contribute the most settlers to the east Zanzibar region (Fig. 3.5b and d). The number of regions that receive *Acropora* larvae from

the east Zanzibar regions ranges between 3 and 5 in the 2000 and 2005 simulations. The multiple destinations map for *Acropora* (Fig. 3.8) shows that most reefs around Mnemba (east Zanzibar) provide larvae to approximately 30 to 60 different reefs. To the extent allowed by the comparison of this model with the results of Souter et al. [2009] sampling of specific reefs, the main connectivity patterns elucidated by their genetic study for an ecologically similar coral species are well represented in the connectivity results provided by the coupled biophysical model for *Acropora*. A discrepancy between the two studies is that the model results identify Juani reef to the southwest of Mafia Island and reefs further south as the main providers of *Acropora* larvae in the region while Souter et al. [2009] genetic study does not identify their south Mafia and Mtwara (further south)sites as important sources. This could be due to the high reef to reef patchiness of isolation identified by both studies, and the uncertainty of which specific reefs were actually sampled for the genetic study. Since the exact location of the reefs sampled by Souter et al. [2009] is not reported, this comparison is limited to the regional level. However, if the reef location information becomes available, it would be possible to examine the correspondence of the genetics and model studies on a reef-to-reef basis.

The ontogenetic vertical migration experiments of *Acanthurus* virtual larvae generated more successful settlers than the 3D passive scenario only at the beginning of the spawning season. This is inconsistent with prior reports in the literature for the Caribbean [Paris et al., 2007] and the California Current System [Drake et al., 2013], were OVM consistently increased settlement success. Differences in shear and stratification of the water column may be responsible for this marked difference among oceanographically distinct regions. The shelf circulation of the Kenya and Tanzania region is dominated by the strong offshore flows and a shallow (i.e. less than 50-100 m) wind driven mixed layer is not common. Northward velocities off Kenya and Tanzania dominate the upper 300 m of the water column during most of the year. Therefore a shallow vertical migration would have little effect. During the SE monsoon (Dec-Mar) the Somali Current flows southward in the upper 100 m north of ($\sim 3^o$S. During this period, which encompasses part of the spawning period, staying near the surface instead of migrating to deeper waters, would actually promote

north to south connections and retention if the duration of the pelagic phase includes the seasonal reversal to northward flow. Only during the transition between NE to SE monsoon conditions would a shallow migration result in significantly shorter displacements for *Acanthurus* larvae. Interannual variability increased greatly when the simple ontogenetic vertical migration behavior was implemented because the vertical structure of the velocities was markedly different in the two modeled years (Figs. A.2 and A.4). The implementation of vertical migration in these experiments was highly idealized, shifting all particles to a specific depth 20 days after release, ignoring their vertical position at that time. This meant that some larvae that had reached deeper depths than this fixed migration level while moving passively were actually displaced upward with this migrating behavior. The number of particles in this scenario was not an important fraction of the successful larvae since most larvae stayed in the upper 5 m when passively advected; a small proportion, however, reached depths below 100 m (Fig. A.5). Migrating only shallow particles downward would be a more realistic scenario as well as distributing the particles within a broader depth range as opposed to fixing all of them to a single specific depth. These more realistic approaches could be implemented in future experiments. The very simple scenario modeled here was to illustrate the effects on connectivity of a shallow ontogenetic vertical migration in a rapidly evolving water column with deep stratification and strong shear.

On average the proportion of successful settlers for the temperature dependent PLD experiments was similar to that of the passive experiments, but exhibited greater interannual and intraseasonal variability. Long distance connections were reduced in the temperature dependent PLD scenario in comparison to the other *Acanthurus* scenarios, particularly in 2000. This result is consistent with the suggestions that warmer water temperatures from global climate change projections are likely to reduce the scale of connectivity for long PLD species [Munday et al., 2009]. Ideally the intercept parameter of equation 1 should be fitted to observed PLD form rearing experiments at different temperatures, however, *Acanthurus* are particularly difficult to rear in an aquarium. As a sanity check the PLD-temperature relationship used in these modeling experiments was compared to one developmental series

of Acanthrus provided by Frank Baensch (personal communication, June 18, 2013) and a few otolith derived PLDs reported in the literature, the latter observations lacking an ontogenetic temperature time series. This PLD-temperature relationship is meant to be used for comparative model experiments (i.e. between different years, or against fix PLD scenarios) and is not expected to represent the real effects of temperature on PLD of *Acanthurus* larvae.

Real larvae are complex organisms, constantly reacting to their environment. Assuming that larvae are well adapted to the pelagic phase, larval behavior, particularly sensing, orientation and swimming abilities would aid them in finding suitable settlement habitat, which would reduce interannual variability in settlement success. However, when faced with increased environmental variability due to climate change effects, their strategies are not guaranteed to work. The experiments presented here, although idealized, serve as a starting point to develop hypotheses that should be verified using more complex models and empirical studies. Monitoring recruitment of coral reef organisms is basic to assess the effects of environmental variability on settlement success. Having long term time series of recruitment of coral reef dependent species in the Kenya-Tanzania region would be very useful for tuning models, as has been done for other coral reef regions [Sponaugle et al., 2012].

Observations of vertical distribution and abundance of pelagic larvae concurrent with hydrographic conditions are needed to design better vertical migration experiments, and to assess larval fish responses to temperature, light, or velocity shears; for some of these the fish may alter their preferred depth. With such knowledge, modeling experiments similar to those presented here, but better informed by empirical data, and including the capability of larvae to respond to the ocean conditions could be helpful to understand how larvae are interacting with their environment, and how individual responses produce the observed distribution patterns. This will provide greater detail on the complex biophysical interactions that occur in the sea, and render a more realistic, and less uncertain, representation of connectivity patterns.

The patterns of the multiple origin and destinations maps reefs are very similar and consistent among the three *Acanthurus* simulation scenarios. Reefs south of Mafia Island provide larvae to the highest number of destinations, while Somali

reefs are the most common destination reefs, receiving larvae from most other reefs. This reflects the strong mostly unidirectional south to north flow along this coast. Some north to south connections occur, mostly in inshore regions that experience substantial eddy flows and topographically steered flow reversals. For *Acropora* larvae, the origin and destinations maps are very patchy, reflecting the effects of their smaller scale of dispersal. It is important to consider interspecific variability when implementing conservation strategies to ecosystems as diverse as coral reefs, since spatial management strategies should be designed to enhance settlement success for a wide suite of species with different dispersal and perceptive capabilities. Origin and destinations maps are a good visualization tool to define strategic locations to apply spatial management conservation strategies and design effective marine protected areas that prioritize specific needs. For example, reefs that have high probabilities of settlement from multiple other reefs may be resilient, through frequent colonization opportunities, to short term calamities such as bleaching events and overfishing. The multiple origins maps are therefore indicative of how resilient individual reefs may be. They could be useful to identify vulnerable locations and to prioritize local spatial management conservation efforts. Results of this modeling study indicate that *Acanthurus* virtual larvae settling to coral reefs around Pemba Island come from relatively few origin reefs, which highlight the need for strong local protection since the resilience, e.g. potential recolonization, of the local *Acanthurus* populations is minimal. Reefs that receive settlers from many different reefs are more resilient to local and global stresses, since having multiple sources increases probabilities of getting recruits in any given year. Somalia and north Kenya reefs are examples of reefs with multiple origin settlers within the model domain. Maps of reefs providing settlers to multiple destinations give an indication of the importance of particular reefs to the regional ecosystem. Reefs that have the potential to provide settlers to many other reefs are important to protect from a larger ecosystem conservation perspective, since an increase of the local spawning population might positively impact a large number of reefs outside of the MPA. Reefs south of Mafia Island are the most important larval origins for the Kenyan-Tanzanian reefs, and most reefs in the region might benefit from their protection. The robustness of the information provided by multiple origin

and destinations maps needs to be corroborated by performing experiments for more years and longer spawning seasons, and by performing detailed sensitivity analysis to the model assumptions. After gaining more confidence in the modeled connectivity patterns, the information provided by origin and destination maps, could be carefully and critically evaluated, in order to be applied to optimize the effectiveness of spatial marine protected area management and other marine protection efforts.

Region to region connectivity matrices synthesize the information of reef to reef connectivity matrices making it more manageable and easy to interpret. While many of the decisions about which reefs to protect are based on a reef to reef basis, visualizing connectivity information by subregions is useful for presenting scientific results to diverse audiences. The regional summary offers an easier to assimilate, simplified picture of the regional connections and could assist managers, policy makers and the general public to understand the interconnectedness among coral reef regions due to their pelagic larval stages. Considering larval connectivity at regional levels is very important when trying to prioritize the implementation of management strategies for both conservation and fisheries enhancement goals. One of the insights of looking at connectivity at a regional scale was that international connections are very common. In all experiments Tanzanian reefs were an important source of settlers to Kenyan reefs; this hints on the scale at which management strategies are required and points to the need for international collaborations in order to protect the east African coral reef ecosystem. The results presented are expected to provide more specific guidelines for spatial management once the robustness of the connectivity patterns to the assumptions of the model is evaluated.
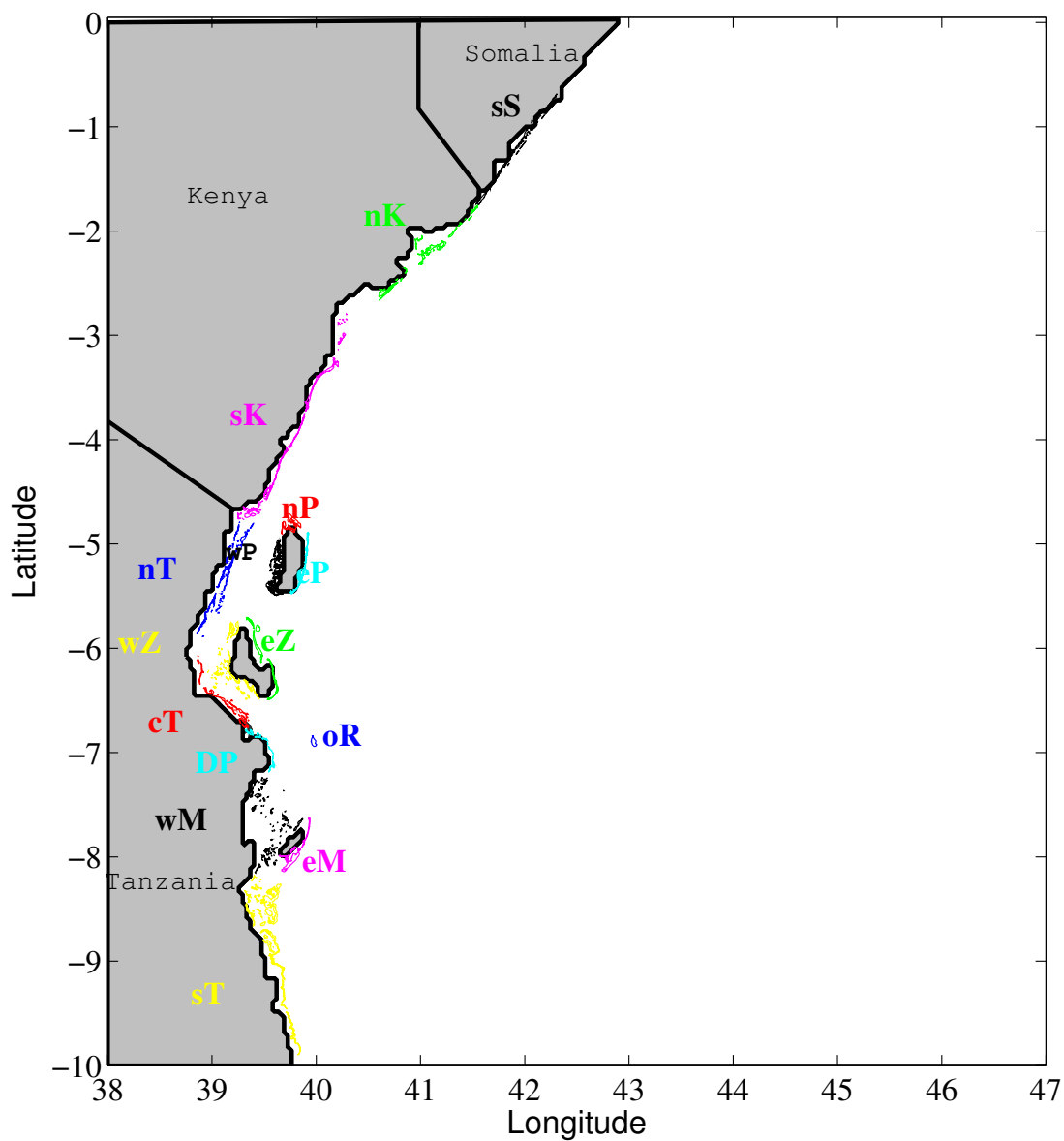
Figure 3.1: Study area with coral reefs grouped by color into 15 regions: sS=south Somalia, nK = north Kenya, sK = south Kenya, wP = west Pemba, eP = east Pemba, nP = north Pemba, nT = north Tanzania, wZ = west Zanzibar, eZ = east Zanzibar, cT = central Tanzania, DP = Dar es Salaam Peninsula, oR = offshore Reef, wM = west Mafia, eM = east Mafia, and sT = south Tanzania.
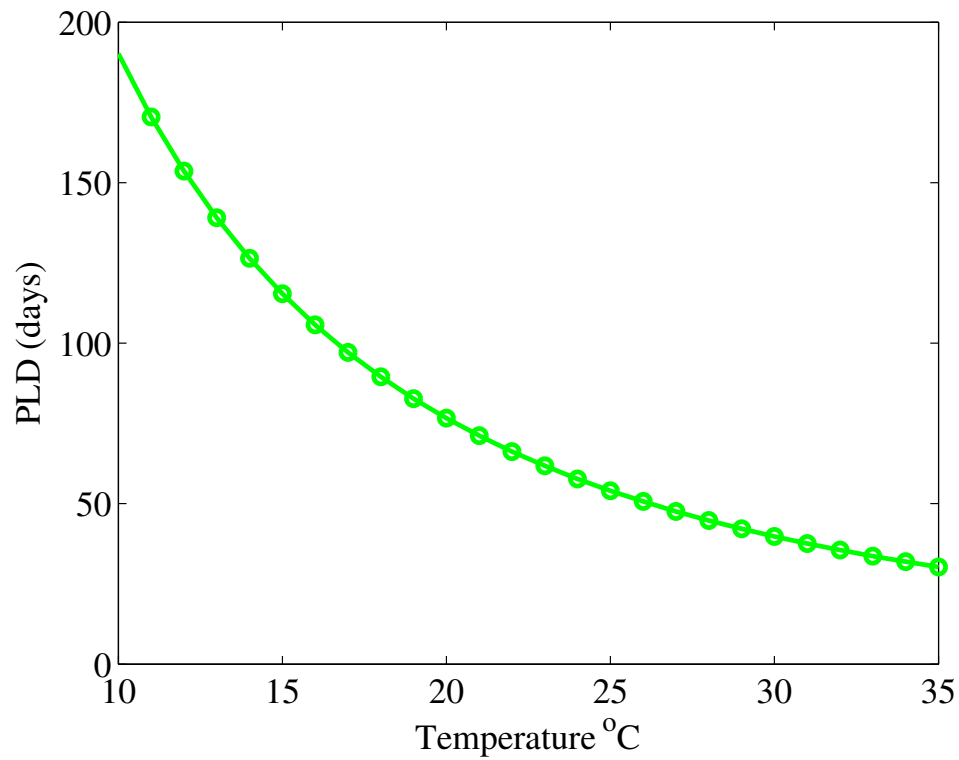
Figure 3.2: Pelagic Larval Duration (PLD) at different temperatures estimated using the O'Connor relationship fitted to represent reported PLDs of *Acanthurus* surgeonfish at typical environmental temperatures (Eq. 1.).

a) *Acanthurus*
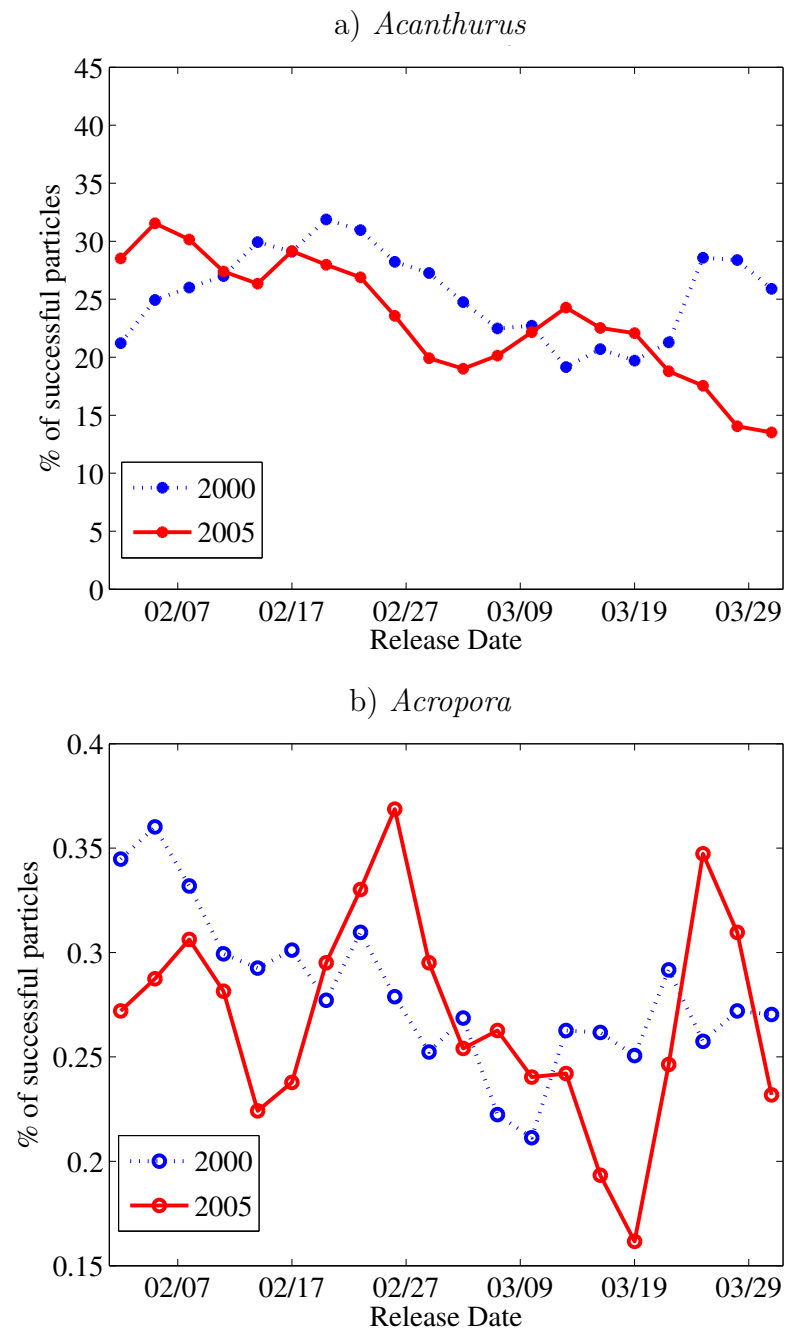
b) *Acropora*

Figure 3.3: Percentage of settlement success per each simulated release date during 2000 and 2005 for the a) *Acanthurus* and b) *Acropora* genera.

a) *Acanthurus* 2000

b) *Acropora* 2000

c) *Acanthurus* 2005

d)*Acropora* 2005
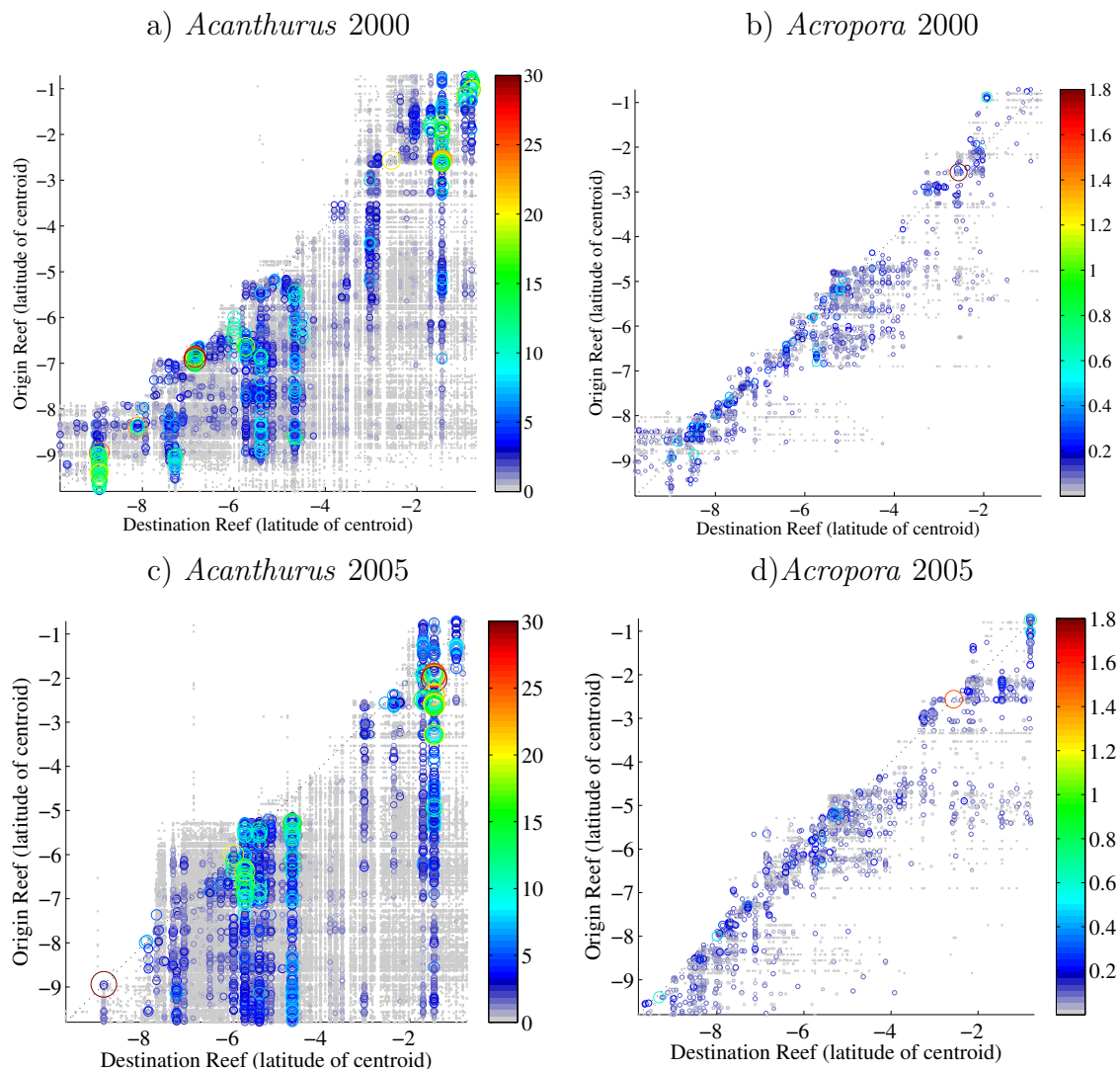
Figure 3.4: Reef to reef connectivity matrices with reefs organized by the latitude of their centroids. Color and size of the circles are proportional to the percentage of successful connections from origin to destination reefs according to the colorbar.
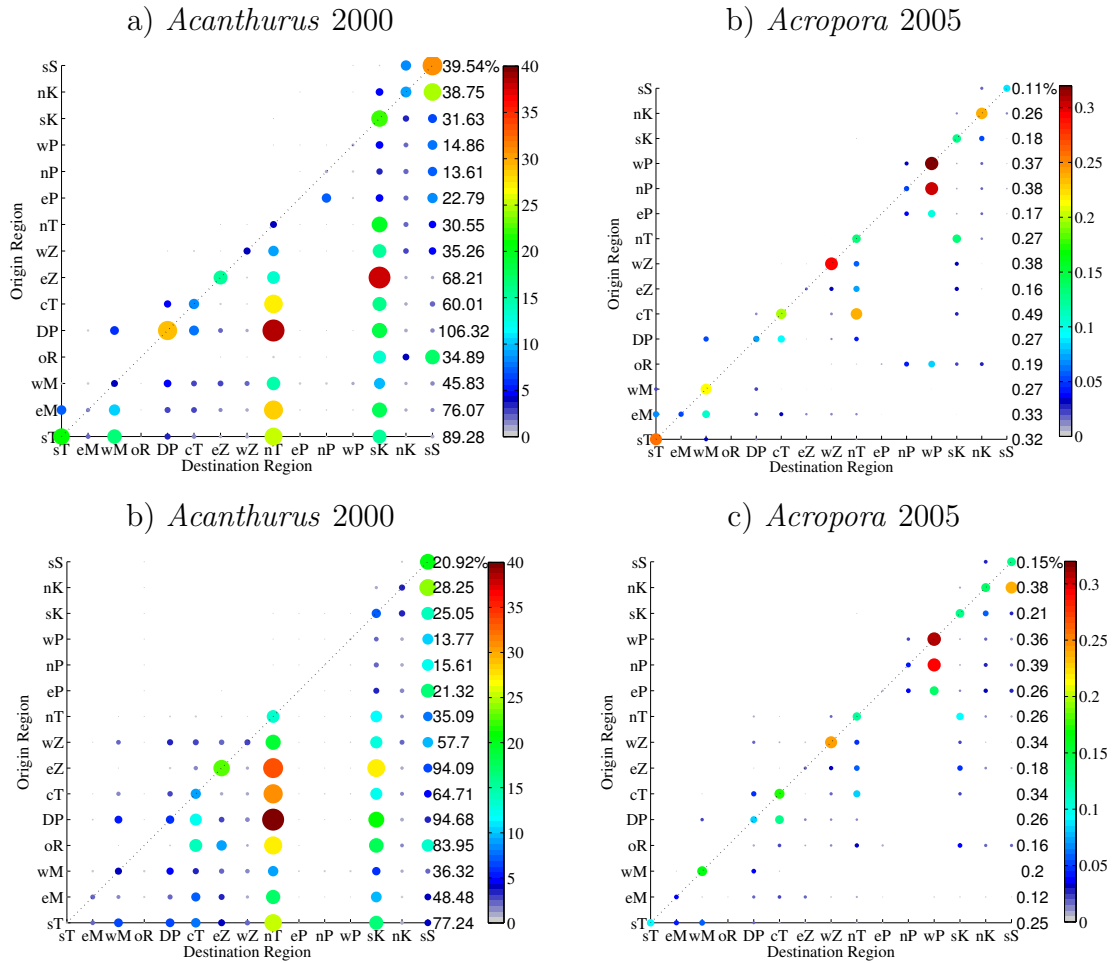
Figure 3.5: Region to region connectivity matrices with reefs grouped into 15 regions marked with different colors in Fig. 3.1 and identified as sS=south Somalia, nK = north Kenya, sK = south Kenya, wP = west Pemba, nP = north Pemba, eP = east Pemba, nT = north Tanzania, wZ = west Zanzibar, eZ = east Zanzibar, cT = central Tanzania, DP = Dar es Salaam Peninsula, oR = offshore Reef, wM = west Mafia, eM = east Mafia, and sT = south Tanzania. Color and size of the circles are proportional to the percentage of successful connections from origin to destination reefs according to the colorbar.
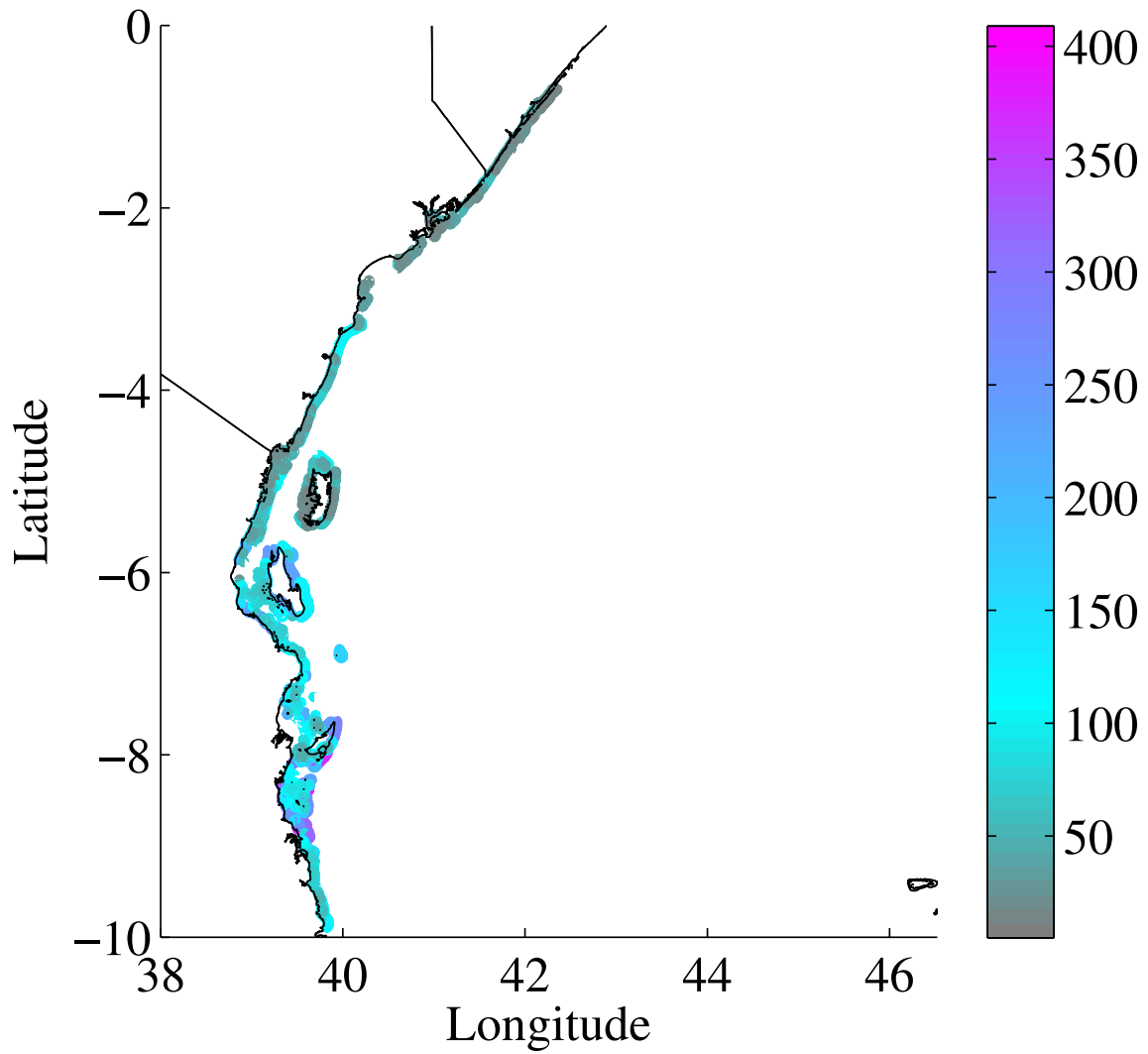
Figure 3.6: Reefs color coded by the number of different reefs reached by *Acanthurus* virtual larvae originated on them on both simulated years to identify the best origin reefs.
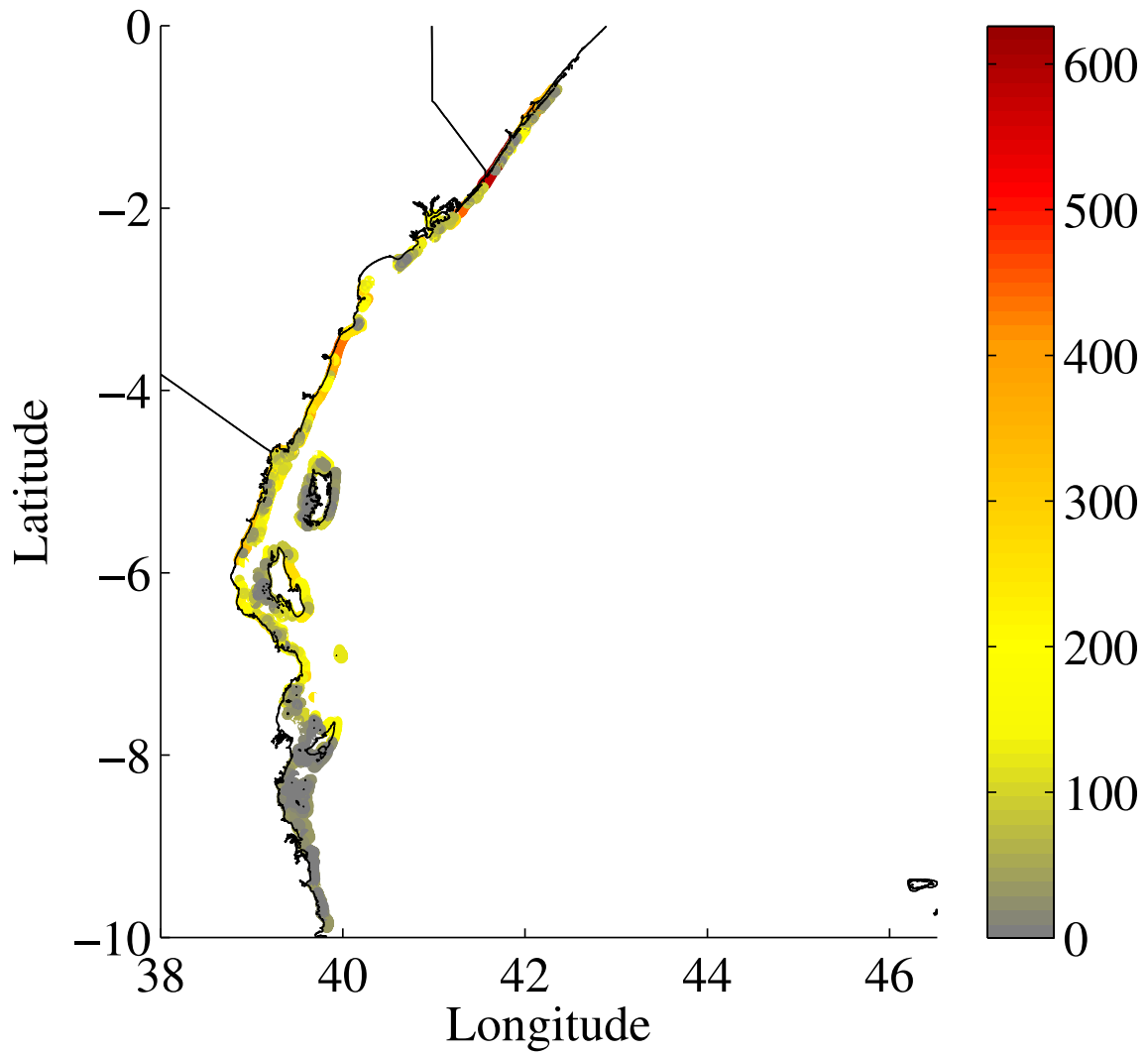
Figure 3.7: Reefs color coded by the number of different reefs it received *Acanthurus* virtual larvae from, on both simulated years to identify the best destination reefs.
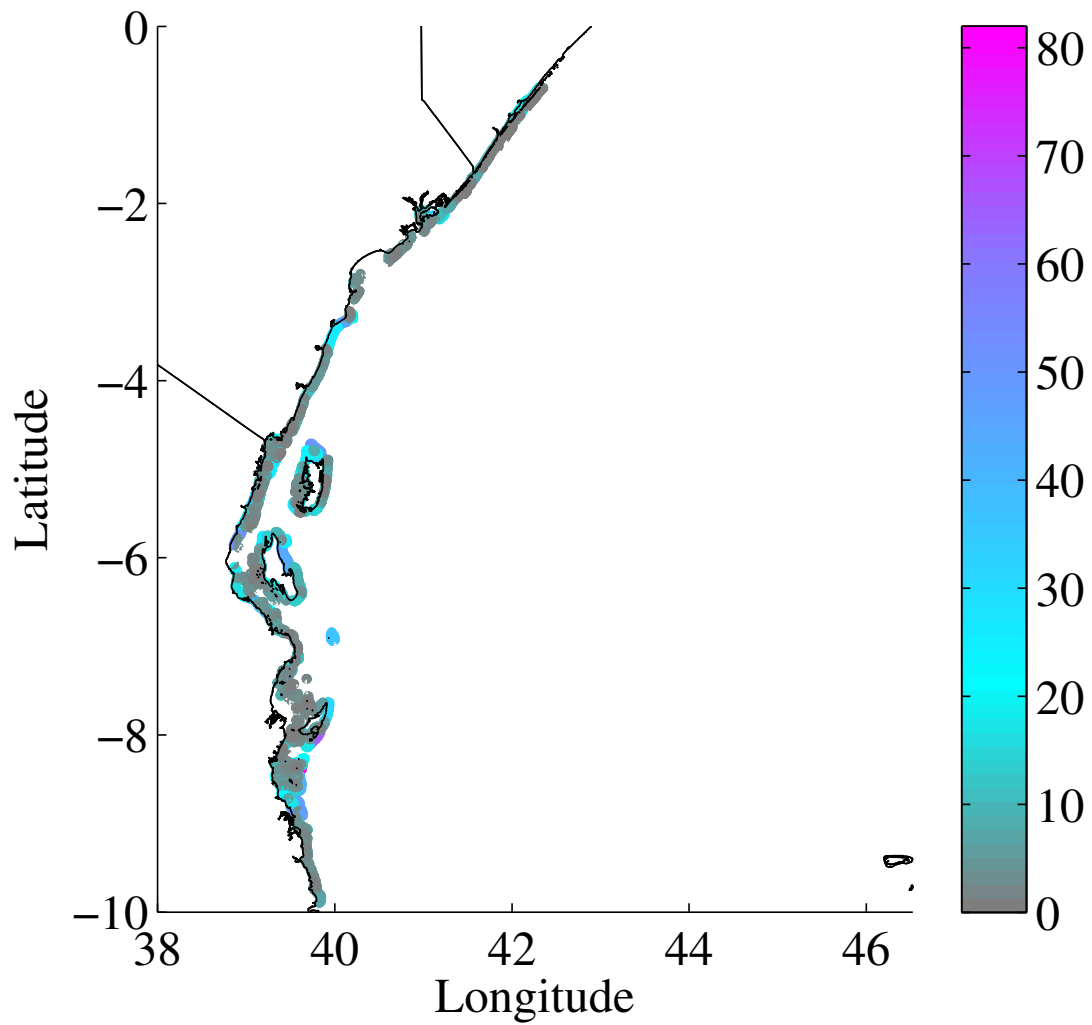
Figure 3.8: Reefs color coded by the number of different reefs reached by *Acropora* virtual larvae originated on them on both simulated years to identify the best origin reefs.
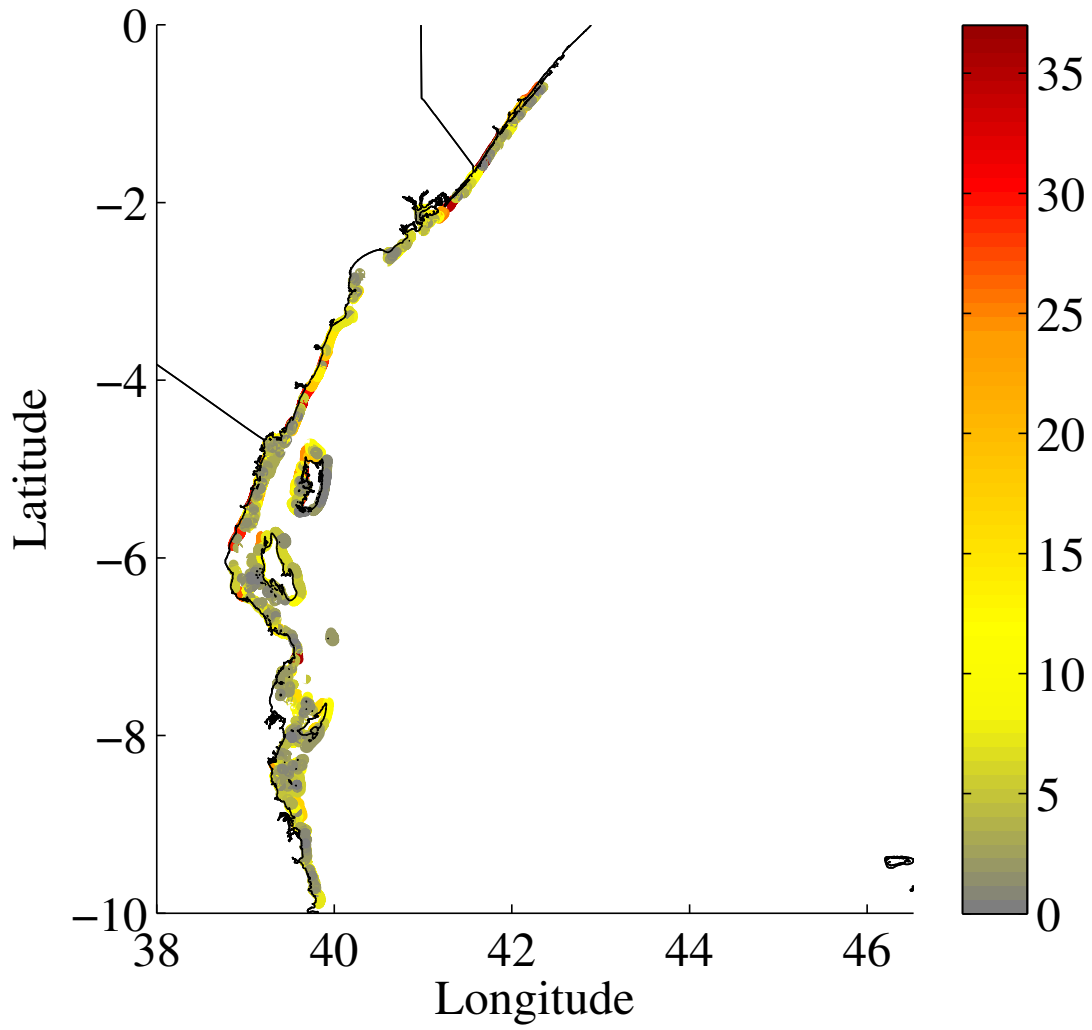
Figure 3.9: Reefs color coded by the number of different reefs it received *Acropor* virtual larvae from, on both simulated years to identify the best destination reefs.
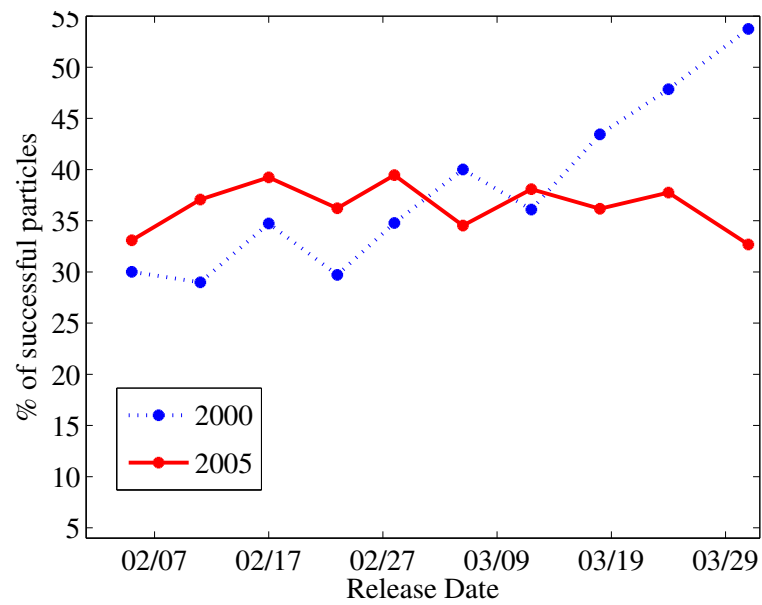
Figure 3.10: Percentage of settlement success per each simulated release date during 2000 and 2005 for *Acanthurus* virtual larvae with an idealized Ontogenetic Vertical Migration (OVM).

a) 2000

b) 2005
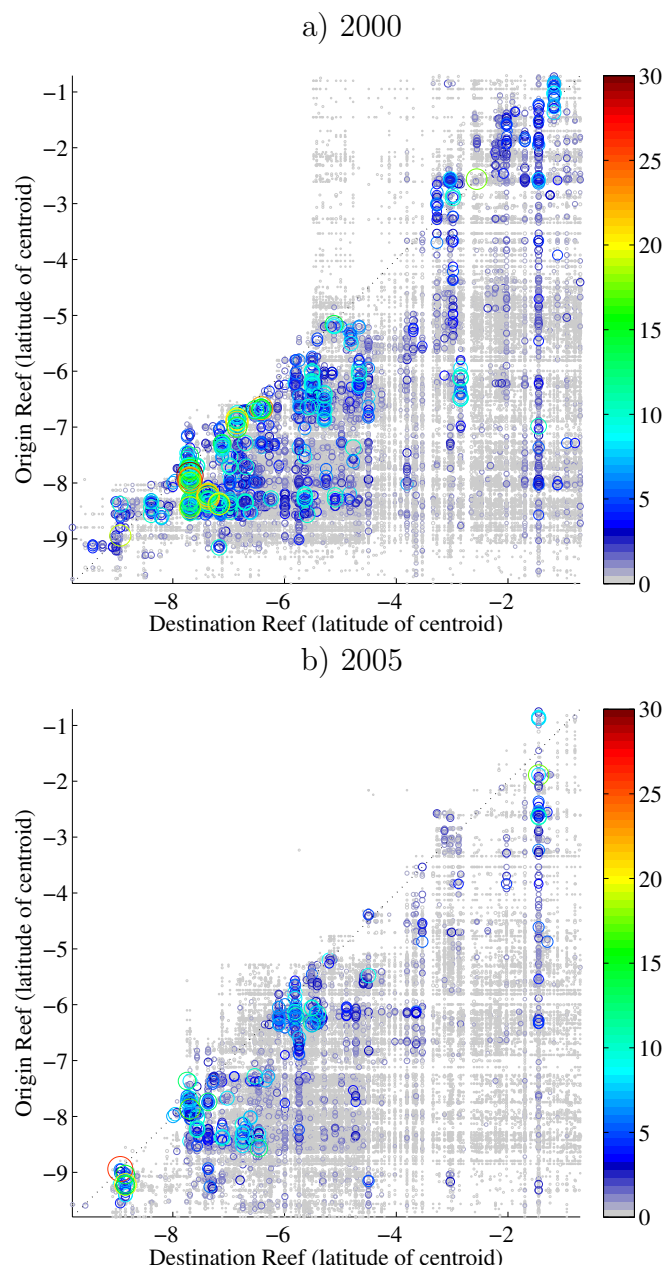
Figure 3.11: Reef to reef connectivity matrices for *Acanthurus* with OVM with reefs organized by the latitude of their centroids. Color and size of the circles are proportional to the percentage of successful connections from origin to destination reefs according to the colorbar.
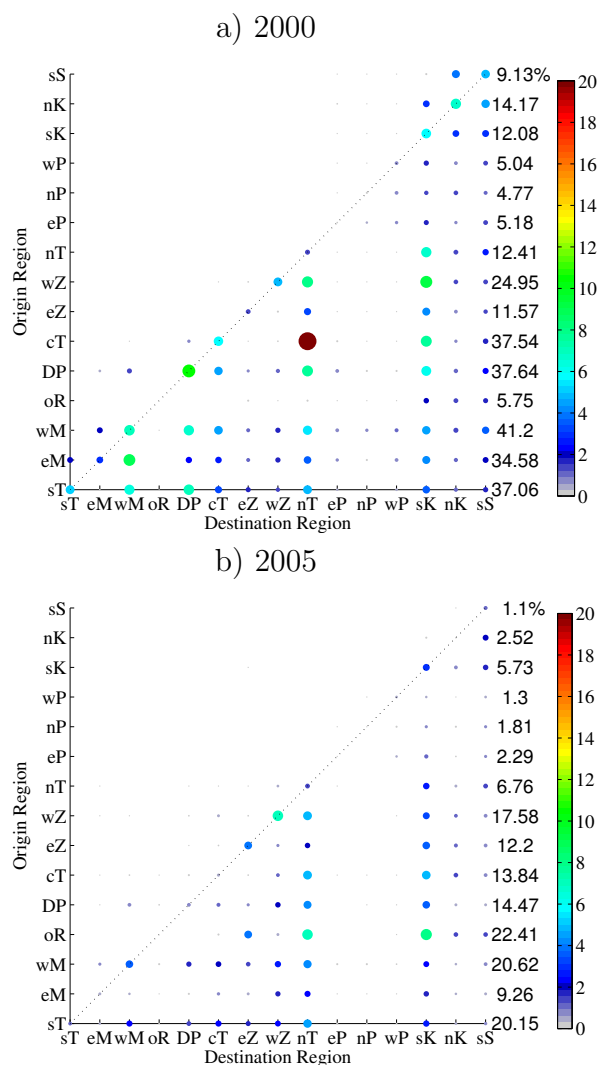
Figure 3.12: Region to region connectivity matrices for *Acanthurus* virtual larvae with OVM. Reefs were grouped into 15 regions identified by two letters in Fig. 3.1. Color and size of the circles are proportional to the percentage of successful connections from origin to destination reefs according to the colorbar.
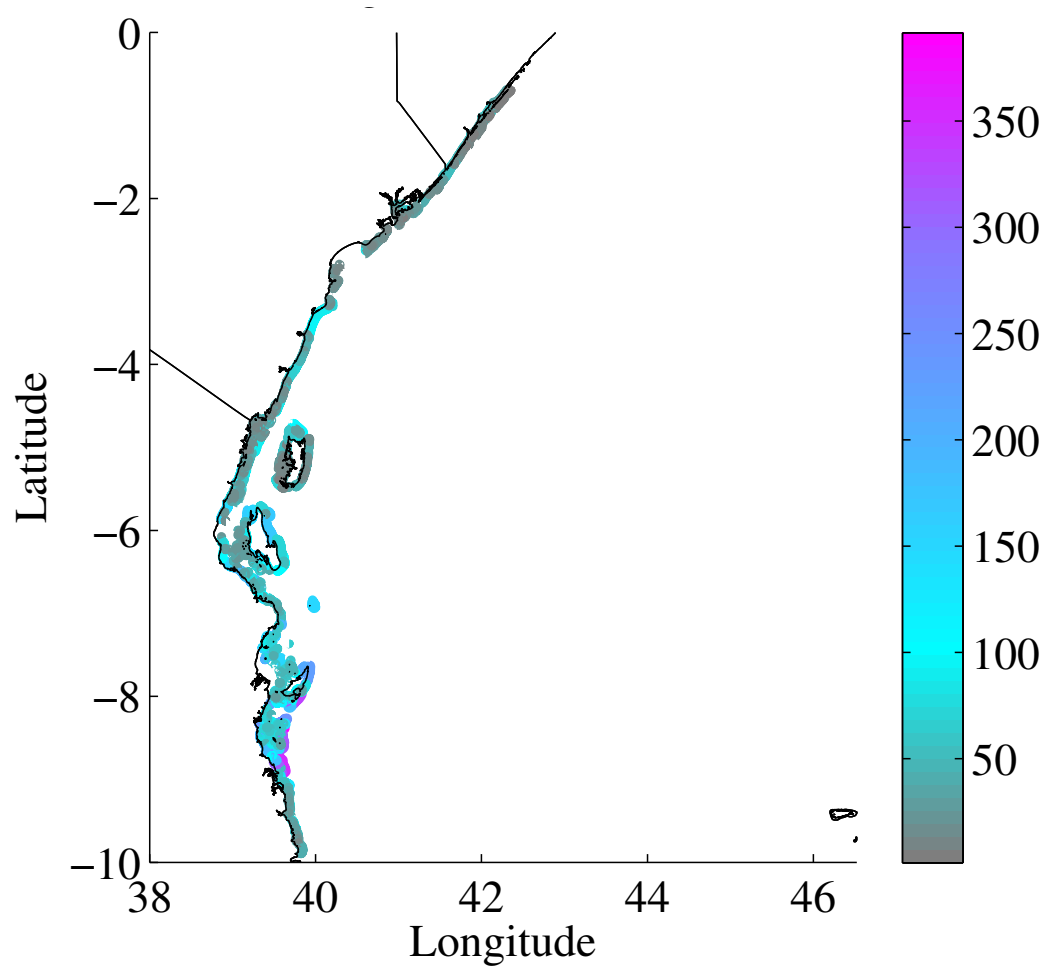
Figure 3.13: Reefs color coded by the number of different reefs reached by *Acanthurus* virtual larvae with OVM originated on them on both simulated years to identify the best origin reefs.
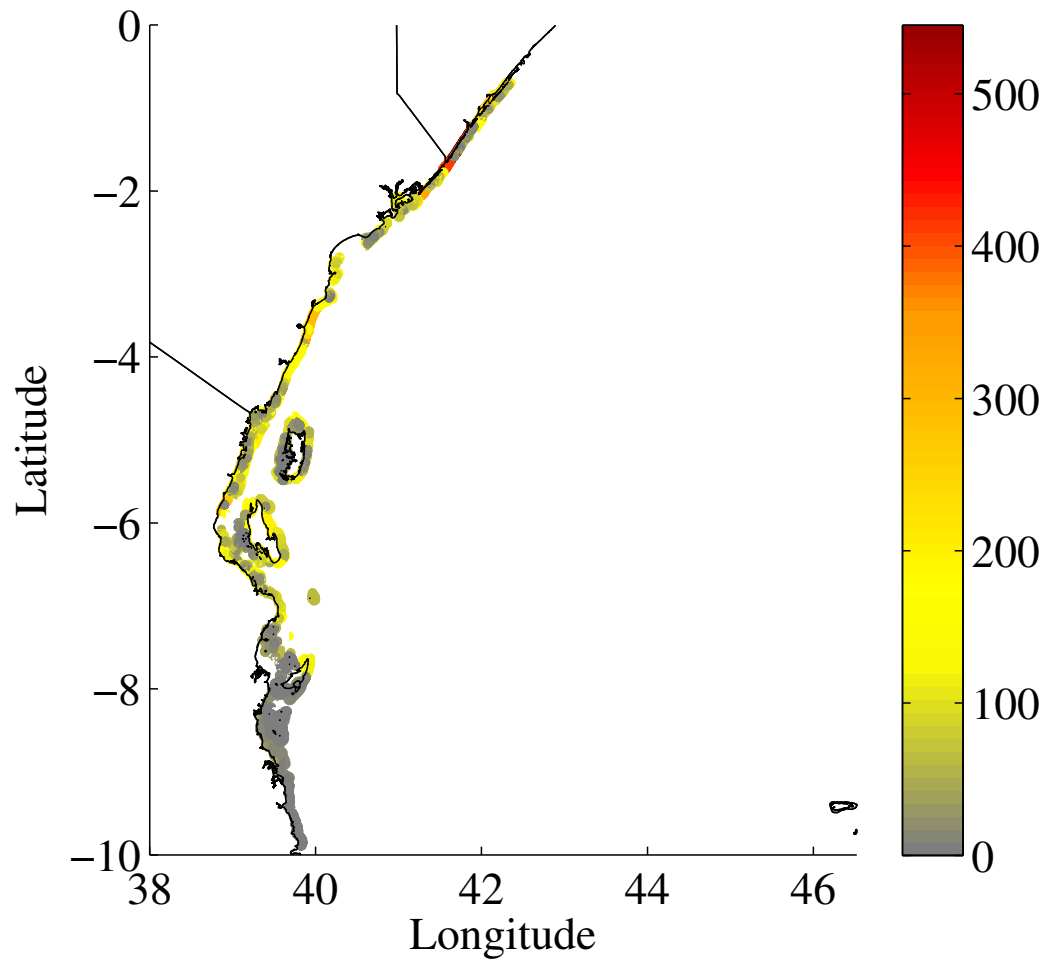
Figure 3.14: Reefs color coded by the number of different reefs it received *Acanthurus* virtual larvae with OVM from, on both simulated years to identify the best destination reefs.
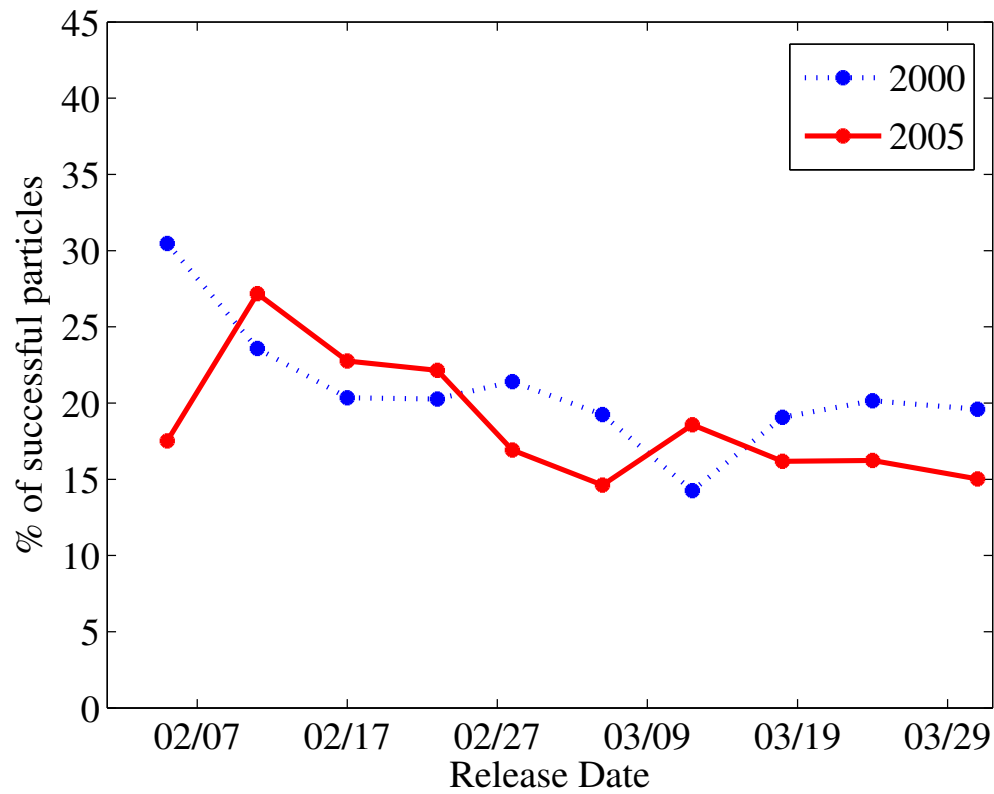
Figure 3.15: Percentage of settlement success per each simulated release date during 2000 and 2005 for *Acanthurus* virtual larvae with temperature dependent PLD.

a) 2000

b) 2005
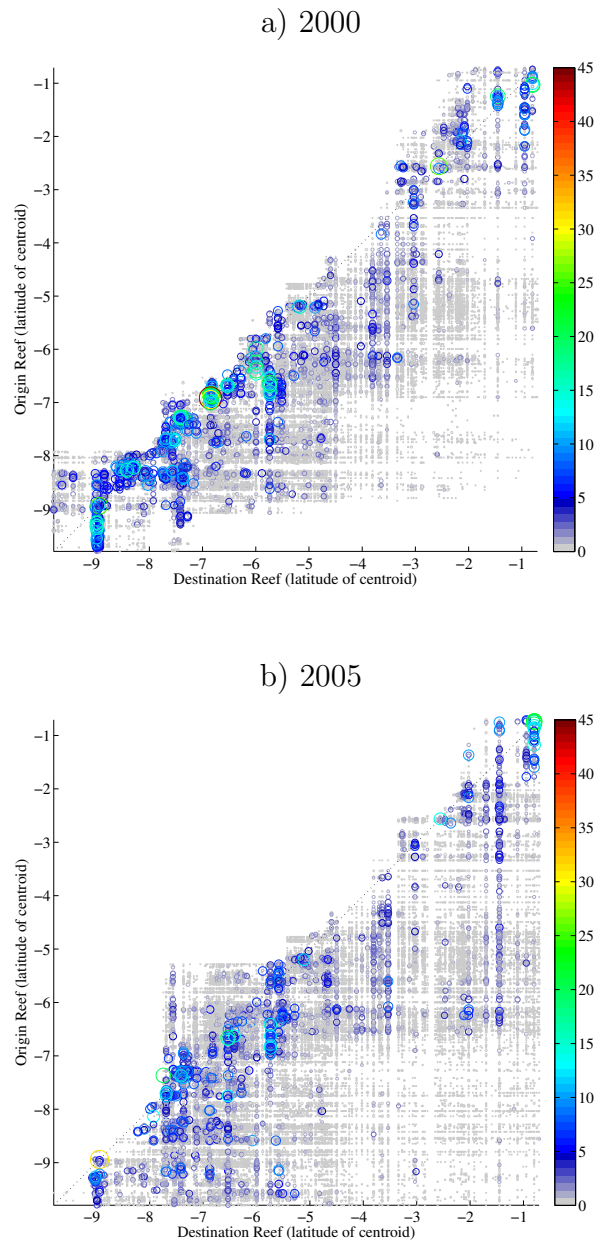
Figure 3.16: Reef to reef connectivity matrices for *Acanthurus* temperature dependent PLD with reefs organized by the latitude of their centroids. Color and size of the circles are proportional to the percentage of successful connections from origin to destination reefs according to the colorbar.
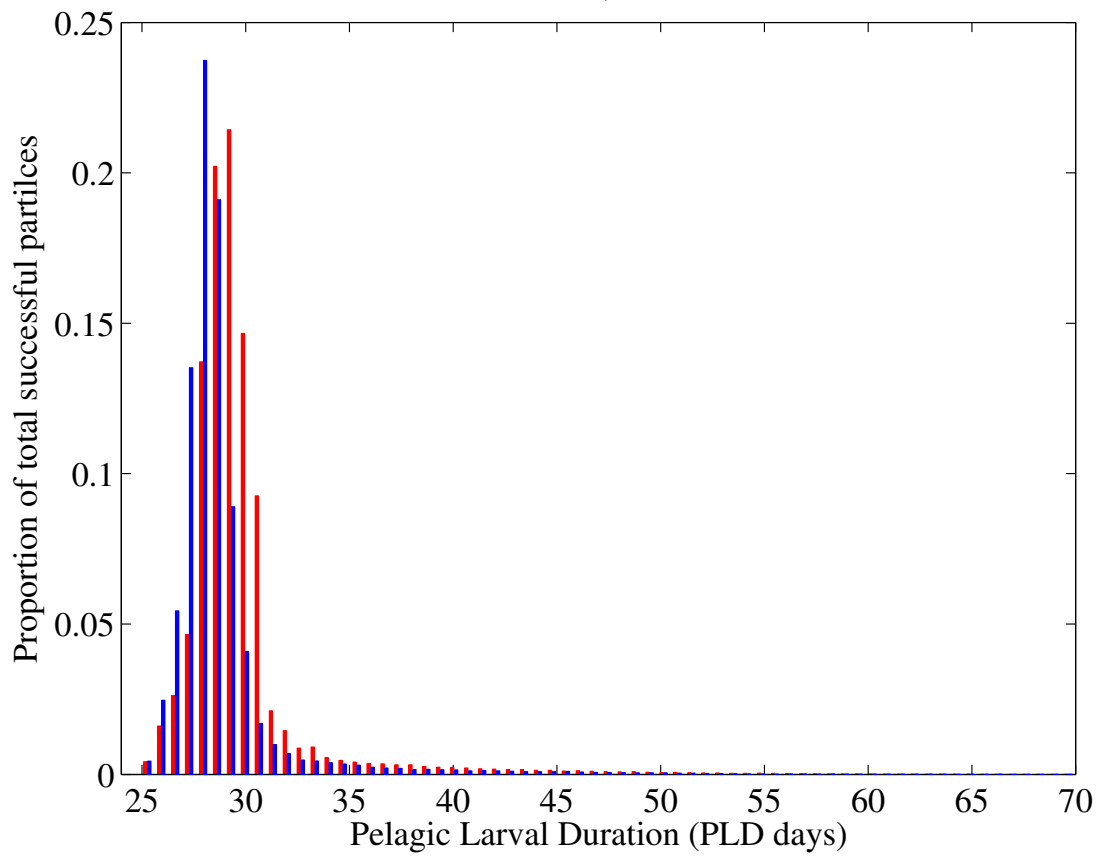
Figure 3.17: Histograms showing the distribution of pelagic larval durations of the succesful *Acanthurus* virtual larvae for the 2000 (blue) and 2005 (red) temperature dependent PLD simulations.
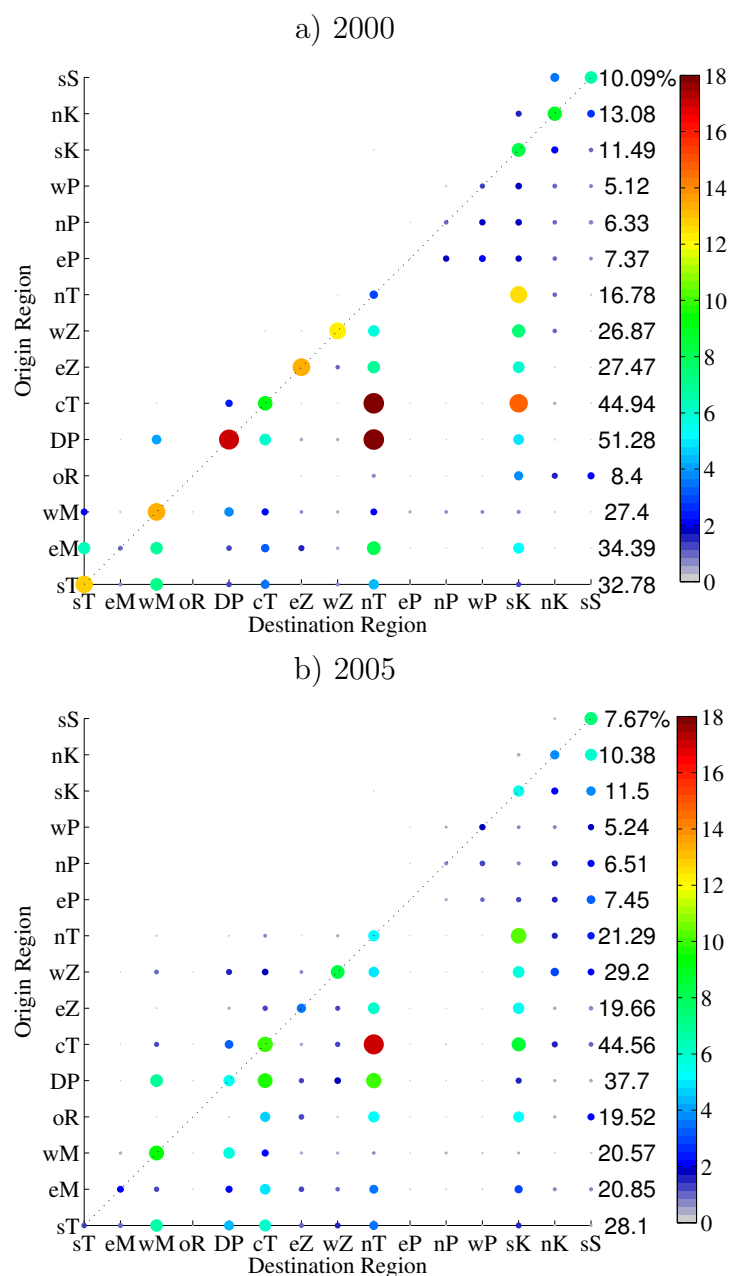
Figure 3.18: Region to region connectivity matrices for *Acanthurus* virtual larvae with temperature dependent PLD. Reefs were grouped into 15 regions identified by two letters in Fig. 3.1. Color and size of the circles are proportional to the percentage of successful connections from origin to destination reefs according to the colorbar.
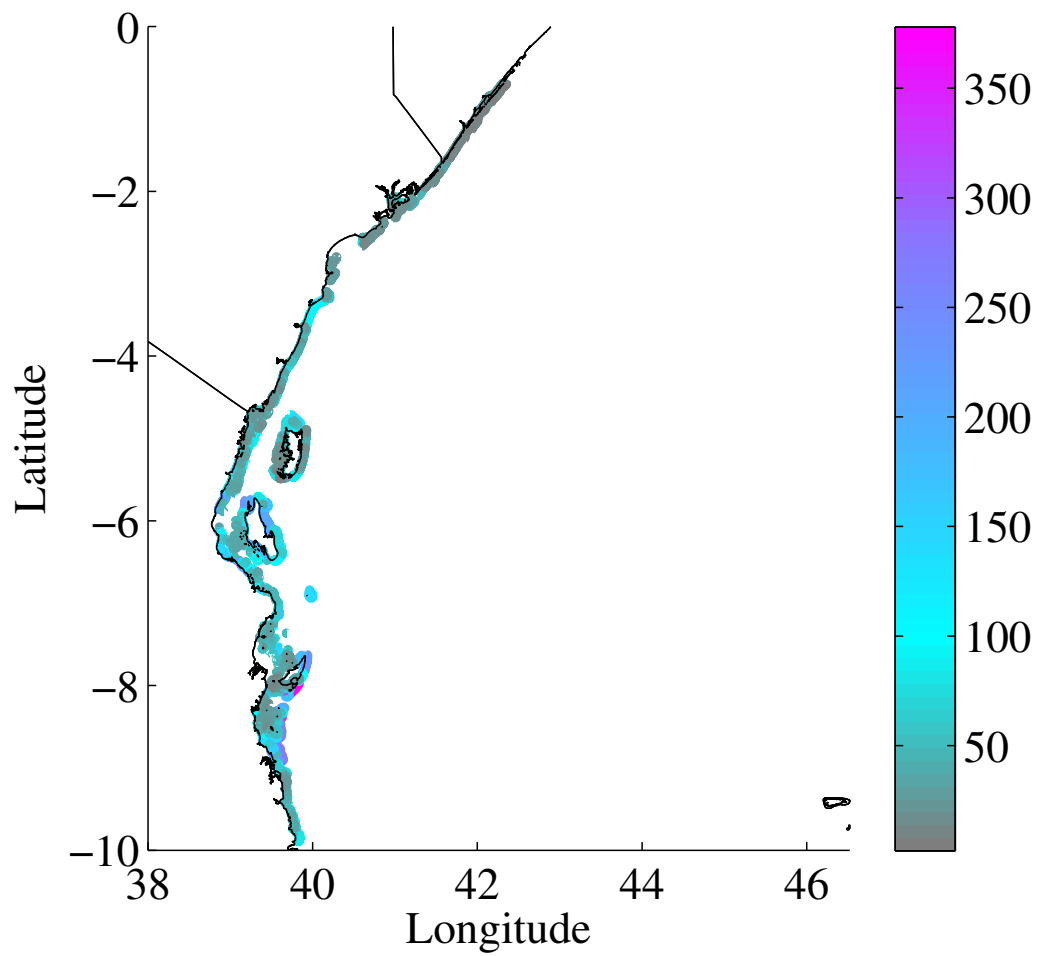
Figure 3.19: Reefs color coded by the number of different reefs reached by *Acanthurus* virtual larvae with temperature dependent PLD originated on them on both simulated years to identify the best origin reefs.
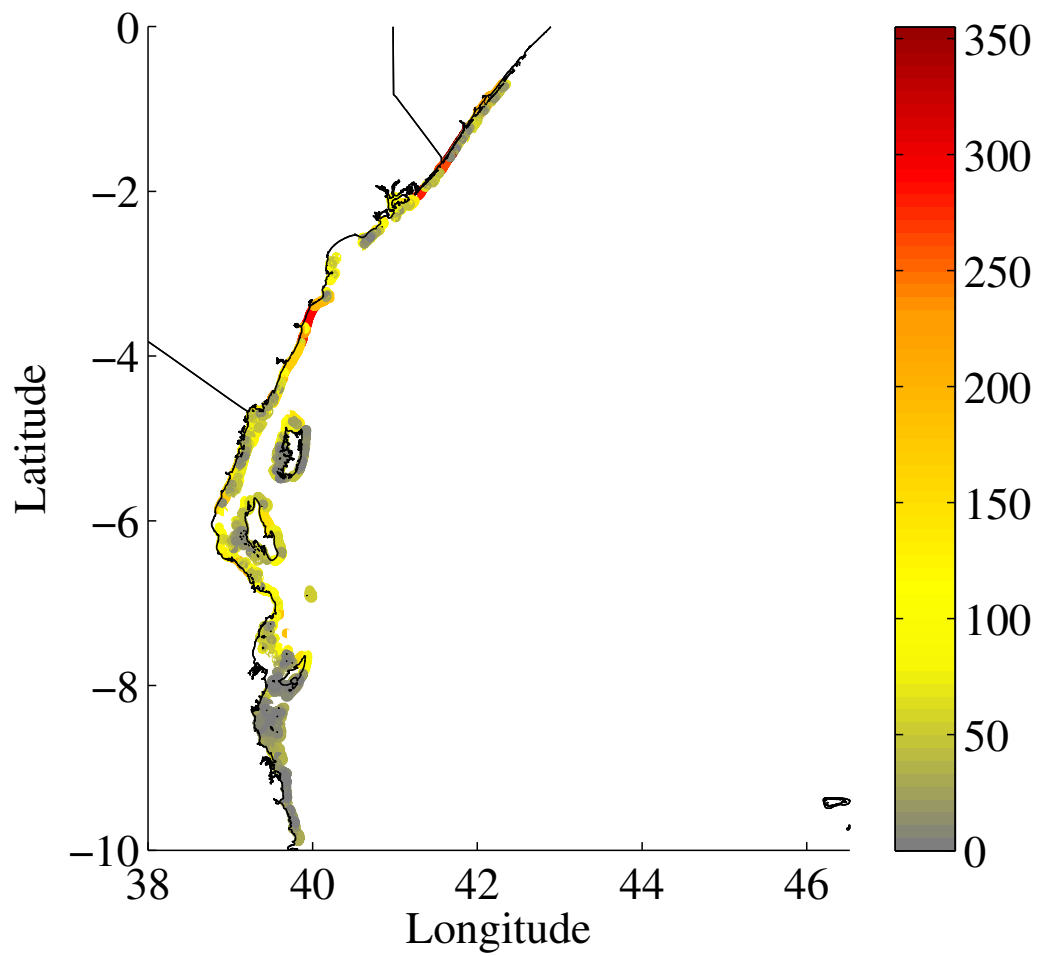
Figure 3.20: Reefs color coded by the number of different reefs it received *Acanthurus* virtual larvae with temperature dependent PLD from, on both simulated years to identify the best destination reefs.
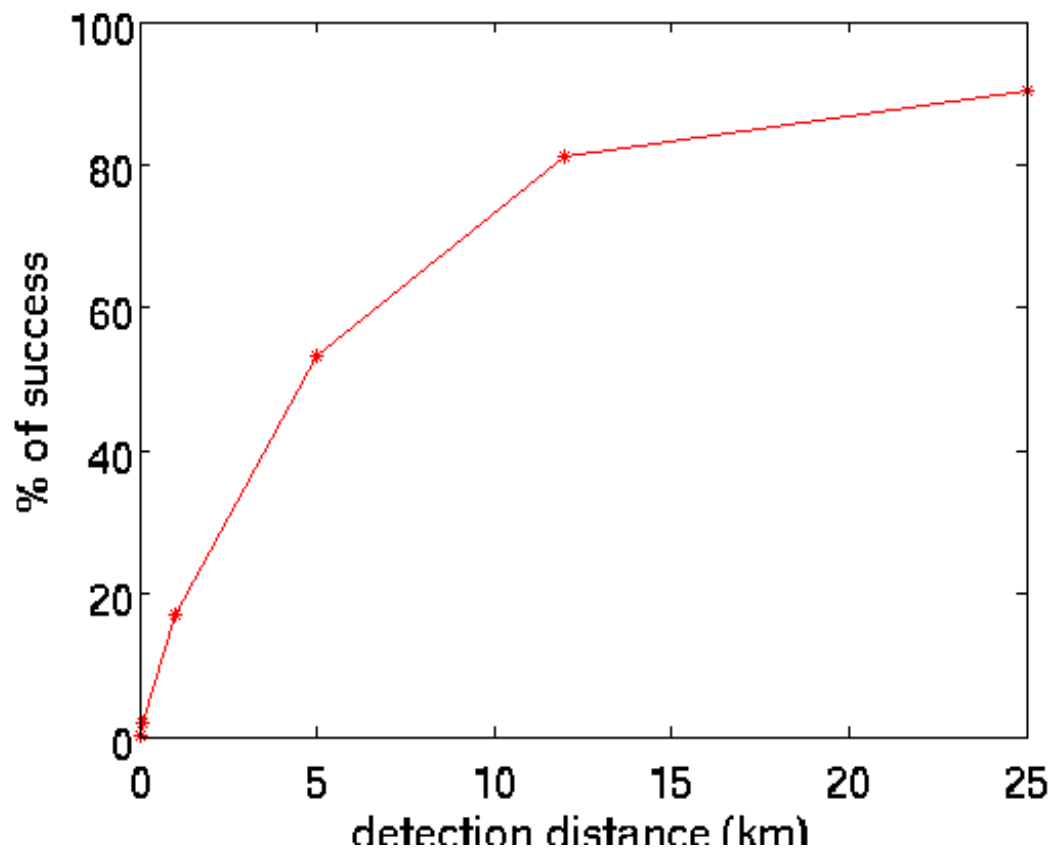
Figure 3.21: Settlement success for *Acropora* larvae with different perception distances.

Chapter 4: Mesoamerican Coastal Circulation Model

4.1   Introduction

The Mesoamerican Region in the Western Caribbean consists of the Atlantic coastal oceans off Honduras, Guatemala, Belize and Mexico. It contains the second largest barrier reef in the world; the Mesoamerican Barrier Reef System (MBRS) and landward, one of the largest watershed networks of the Caribbean. The hydrography of the region is dominated by the seasonal inflow of the North Equatorial Current through the passages connecting the Atlantic and the Caribbean Sea [Johns et al., 2001, as cited in Escobar-Briones, 2004] and by local winds [Gallegos and Czitrom, 1997].

   The large scale circulation of the Western Caribbean is dominated by the inflow of the Caribbean Current (CC), which continues northward along the eastern coast of the Yucatan Peninsula as the Yucatan Current (YC) and exits into the Gulf of Mexico through the Yucatan Channel (Fig. 4.1). The CC is a strong and persistent flow of relatively warm water from the East to Northwest, which speed increases gradually from the Antillean Arch to the Yucatan Channel [Gordon, 1967]. The core of this geostrophic current is approximately 20 km wide, extends from the surface to 150 m depth and is found ($\sim$250 km offshore of the coast of Venezuela [Fairbridge, 1966]. Its main branch turns northwestward and flows along the outer flank of the Nicaraguan Rise (between Jamaica and Nicaragua) to form a narrow offshore flow running westward and then northward to enter the Gulf of Mexico through the Yucatan Channel. The CC has a mean annual transport of 30 Sv [Gordon, 1967;Kinder et al., 1985] with a mean annual velocity of 0.5 m s^{-1}, being faster and better defined in spring-summer (0.8 m s^{-1}) than in fall-winter (0.4 m s^{-1}), when it is heavily influenced by mesoscale features (eddies, fronts and filaments) and by northerly winds, tropical storms and intense hurricanes that intermittently affect the Caribbean Sea [Gallegos and Czitrom, 1997]. Speeds greater than 1 m s^{-1} are common in the Yu-

catan Current [Richardson, 2005], and maximum surface velocities of 2.5 m s^{-1} have been measured [Kinder, 1983]. Current intensity decreases with depth to less than 0.05 m s^{-1} at 1000 m depth. The YC exits the Yucatan Basin near the surface at the western side of the Yucatan Channel and flows into the Gulf of Mexico where it feeds the Loop Current. The circulation in the Yucatan Channel is characterized by the surface-intensified Yucatan Current flowing into the Gulf of Mexico from the Caribbean Sea in the upper layer, weak Yucatan Countercurrent flowing southward beneath it over the western side of the Strait, and southward flows at the surface and at depth on the Cuban side [Sheinbaum et al., 2002; Ezer et al., 2002; Bunge, 2002. The annual mean section of temperature across the Yucatan Channel shows isotherms curving upward in the top 500 m associated with the northward Yucatan Current on the Mexican side. The change in curvature of the isotherms in the layers deeper than 800 m is associated with the Yucatan Countercurrent and the Cuban Countercurrent on the western and eastern sides of the Yucatan Channel [Sheinbaum et al., 2002; Fig. 4.2].

The trade winds of the northern hemisphere are the main wind system over the North Atlantic. They blow from the east/northeast in winter and from the east/southeast in summer, with an intensity of 3.5 to 10.5 m s^{-1} [Tucker and Barry, 1984 as cited in Gallegos and Czitrom, 1997]. This wind system is associated with the North Atlantic Subtropical High and the migration of the Intertropical Convergence Zone. The northeasterly trades intensify near the Caribbean Sea, forming the easterly Caribbean low-level jet (12.5 -15.5 ^{o}N and 70-80°W). Winds in the Yucatan Basin are northeasterly from October to January and easterly or southeasterly the rest of the year. Wind speed maxima are observed during June and November. Average satellite wind speed of 6.5 m s^{-1} with a maximum of 27.3 m s^{-1} has been recorded. Strong deviations from the monthly mean climatological winds are more common in winter due to air-sea interactions that generate a complex configuration of high and low smaller scale pressure cells identified, depending on their size and intensity, as fronts, tropical depressions, tropical storms and hurricanes. Every winter the trade winds are interrupted 2 to 3 times due to the eastward movement of atmospheric fronts that generate southward wind bursts known as "Nortes". From mid summer

through the end of fall tropical storms and hurricanes are dominant. September is known as the hurricane month because tropical storms that occur then have a 70% chance of strengthening into hurricanes [Colon, 1952 as cited in Gallegos and Czitrom, 1997].

Wind-driven upwelling affects the upper 200 m of the water column in the Mesoamerican region. Ekman transport accounts for 93% and Ekman pumping for 7% of the total wind driven vertical transport [Prez-Santos et al., 2010]. The northeast Yucatan Shelf is one of the most important upwelling sites in the Intra American Seas and the western oceanic margins [Merino, 1997]. Subsurface Caribbean water upwells along the eastern slope of the Yucatan shelf at 0.1 cm s^{-1} into the mixed layer following a seasonal pattern, as described by Merino [1997]. During spring and summer the upwelled water intrudes onto the bottom Yucatan shelf, causing stratification of the Caribbean surface water over the Yucatan upwelled water (YUW). The subsruface YUW layers moves westward across the shelf and contributes to the formation of a cyclonic gyre north of Cape Catoche, at the northern tip of the Yucatan Peninsula. In this manner, upwelling also affects the horizontal circulation. Coastal upwelling and high productivity along the southern Belize Barrier Reef and Gulf of Honduras has also been reported [Harborne et al., 2001].

The net heat flux in the region indicates that the ocean is heating from March to September with two local maxima in April and August, and cooling from October to February with a minimum in December [Coln, 1963]. The climatological rain pattern of the Western Caribbean is characterized by maxima in May-June and September-October separated by a midsummer drought in July-August [Gamble and Curtis, 2008]. In the Yucatan Basin the mean annual precipitation is 2250 mm/year with maximum and minimum monthly mean of ($\sim$200 and 65 mm in August and February, respectively. Spatially, there is a southeast to northwest gradient with higher precipitation in the southeast region [Sukhovey, 1980 as shown in Fig. 9 in Gallegos and Czitrom, 1997].

River discharges in the Mesoamerican region peak in August. Chrubin et al. [2008] report that the reefs of the MBRS are influenced by terrestrial runoff seasonally, with maximum effect during October to January, and minimum from March

to April. The region is influenced also by remote freshwater sources. Chrubin and Richardson [2007] used Sea Surface Salinity (SSS) maps and SeaWiFs color images to show that the freshwater plume from the Orinoco and Amazon rivers extend seasonally northwestward across the Caribbean basin from August to November, 3 to 4 months after the peak of the rain season in north-east South America. The plume is sustained by inflow from the North Brazilian Current (NBC) and its current rings. The main contribution of Amazon water by rings is during the summer and fall when most of the NBC retroflects into the Equatorial Countercurrent. The CC is intensified seasonally near 14ºN partly by the inflow of the river plumes. The number of anticyclonic eddies doubles during August-December, compared to January-July, since the buoyant plume promotes barotropic and baroclinic instabilities that lead to the formation of eddies [Chrubin and Richardson, 2007].

Eddies are important and ubiquitous features in the Western Caribbean, continually modifying the direction of the main flows (i.e. CC, YC). Both the Caribbean basin and the Gulf of Mexico are known for their mesoscale eddies with diameters of 100 km or more. The warm features have elevated central sea surface heights and thus rotate in a clockwise, anticyclonic direction. The warm eddies induce cool cyclonic eddies forming dipole like features, clearly seen in satellite sea surface height anomaly and temperature observations. Maximum surface currents around eddies can be several 100s cm s^{-1} [Zavala-Hidalgo et al., 2003; Andrade and Barton, 2000]. Eddy kinetic energy (EKE), also indicative of the eddy formation potential of a region, is large throughout the Western Caribbean, particularly in the Yucatan coasts and north of Cozumel Island (EKE >800 cm^2 s^{-2}) [Richardson, 2005] .

The objective of this research is to compare and contrast the coral reef connectivity patterns in two regional ecosystems The Western Caribbean region of the North Atlantic and the Kenyan-Tanzanian region of the Western Indian Ocean. Numerous investigators have previously developed ocean circulation models of the Western Caribbean [e.g. Chrubin et al., 2008; Treml et al., 2008; Paris et al., 2007; Cowen et al., 2006; Baums et al., 2006; Tang et al., 2006; Paris et al., 2005; Sheng and Tang, 2003]. However no other study covered the present study domain and had the temporal and spatial resolution necessary to generate the temperature and

flow field for the particle tracking experiments. Therefore we developed a Regional Ocean Model System (ROMS) application for the Western Caribbean, referred to as Mesoamerican Coastal Circulation Model (MCCM), with the same configuration as the Kenyan-Tanzanian counterpart (the Kenyan-Tanzanian Coastal Model (KTCM); see Chapters 2 and 3). In this chapter climatological model results are compared to observations, other model results and what is known about the regional circulation to verify that this physical model adequately represents the main characteristics of the hydrography and coastal circulation. Model results are then used to describe the ocean conditions, especially velocity fields and temperatures, which will be used to drive particle tracking experiments reported in Chapter 5.

4.2   Methods

The Mesoamerican Coastal Circulation Model (MCCM) is a ROMS [Haidvogel et al., 2008] application developed after the Kenyan-Tanzanian Coastal Model (KTCM; see Chapter 2). However, MCCM has enhanced horizontal resolution of ($\sim$2 km as does 2KTCM (see Chapter 3). The model domain is a rectangular grid extending from 83.3 to 89°W and from 15 to 22.5^{o}N (Fig. 4.1). It has 31 terrain following vertical levels with maximum and minimum depths of 5800 m and 5 m, respectively. The model bathymetry comes from the 30 arc-second grid product GEBCO_ 08, version 20100927 [http://www.gebco.net]. The model coastline was manually modified to retain as many features as the 2 km resolution allowed. From the many islands in the Western Caribbean region, only Contoy, Mujeres and Cozumel Islands off Mexico, the Bay Islands (Utila, Santa Elena, Barbareta and Guanaja) off Honduras and the northwest tip of Cuba are included as dry cells in the model land mask. North, East and West Boundaries are open using the Chapman condition for the free surface and Flather condition for the depth averaged velocities normal to the open boundaries [Marchesiello et al., 2001]. The generic length scale closure scheme [Warner et al., 2005; Umlauf and Burchard, 2003] with k-kl (Mellor-Yamada level 2.5) parameters [Mellor and Yamada, 1982] is used for vertical mixing. Type 1 water was used to represent clear waters and deep penetration of solar radiation [Jerlov,

1976]. The atmospheric forcing (wind stress, heat and freshwater fluxes) is calculated by ROMS bulk formulation using daily NCEP/NCAR reanalysis [Kalnay et al., 1996] atmospheric variables. To eliminate unrealistic transient behaviors, the model was initialized from the October field of a spin-up simulation initialized using fields from the Ocean General Circulation Model for the Earth Simulator (OFES) [Sasaki et al., 2006] and forced with climatological fields until it produced a repeatable seasonal cycle. Boundary forcing for MCCM was provided by OFES monthly outputs. An 8.25 year (October 1999 to December 2007) simulation of MCCM was obtained.

To verify MCCM's representation of the main oceanographic features of the region, climatological monthly model results are compared with monthly climatologies of satellite data of the modeled years (2000-2007) of Pathfinder v5 satellite Sea Surface Temperature (SST) [`http://www.nodc.noaa.gov/sog/pathfinder4km/`] and altimeter sea level anomaly (SLA) fields from AVISO v1.0 (2014) [Archiving, Validation and Interpretation of Satellite Oceanographic data, `http://www.aviso.altimetry.fr/`]. The higher resolution model results were interpolated to the coarser resolutions of the satellite gridded products using bilinear interpolation (Pathfinder v5 SST is 4 km; AVISO SLA is $1/4^o$ ($\sim$30 km). Agreement on the interannual variability pattern was assessed by comparing Hvmuller diagrams of modeled and satellite SST along a north-south transect in the middle of the domain (dashed line in Fig. 4.1) as well as SST time series at various locations (indicated by asterisks (*) in Fig. 4.1). AVISO SLA and model Sea Surface Height anomaly (SSHa) fields are not usually directly comparable because the subtracted mean sea level (mean dynamic topography (MDT) for AVISO and the climatological mean SSH for the model) are not identical; however, in this case the subtracted means are very similar and therefore the bias of the direct comparison is minimal. Agreement between model and satellite SSHa was examined using an Empirical Orthogonal Functions (EOF) analysis of the model and altimeter SSHa. Climatological surface salinity and velocity patterns and vertical sections of temperature and velocity across the Yucatan Channel were compared with figures and descriptions available in the literature.

When performing model-data comparisons, possible sources of error in the construction of the SST satellite fields should be considered. Indeed, there are several

problems with infrared retrievals of SST in the tropics: the formation of an anoma-
lously warm surface layer (<1 cm thick) during calm periods; the ocean skin layer,
errors caused by small scale clouds and the edges of clouds, and high humidity in
the lower atmosphere. The warm ocean skin layer hides the SST signature of more
dynamical feature beneath it. The sub-pixel scale clouds and cloud edges create
incorrect SST retrievals and atmospheric water vapor absorbs infrared radiation and
may not be adequately accounted for in the atmospheric corrections [Barale et al.,
2010; Martin, 2014; Wentz et al., 2000].

4.2.1 Validation of the Mesoamerican Coastal Circulation Model Cli-matology

4.2.1.1 SST model-data comparison

The monthly mean climatology Sea Surface Temperature (SST) of the modeled years
(2000-2007) is within the 22 - 31°C range (Fig. 4.3), in agreement with values
published in the literature [i.e. Gallegos and Czitrom, 1997] and the Pathfinder
satellite product [Fig. 4.4]. The annual variation of the spatial mean SST also
compares well with the Pathfinder SST (Fig. 4.5). However the model results show
more spatial variability than the satellite product; the model contains more and
better defined mesoscale features than the SST from satellite. Mesoscale features
may be smeared in the satellite gridded product due to its coarser resolution, or
not distinguishable due to AVHRR's inability to measure gradients below the upper
millimeters of the ocean surface, which may be constantly reheated by the strong solar
radiation in the tropics [Wentz et al., 2000]. The first discrepancy is that the satellite
product shows cooler temperatures north of the Yucatan Peninsula due to local
upwelling all year, while this feature is hardly noticeable in August and September
in the modeled field. In contrast, intense upwelling off the coast of Honduras is
evident in the model throughout the year, while this cool feature can only be seen in
the Pathfinder SST in May, July and November (Figs. 4.3 and 4.4). If the quality
control of the satellite data is relaxed to include all measurements, a pattern similar

to the model emerges, with cold temperatures in the Gulf of Honduras and a narrow cold band along the Honduras coasts during all months (Fig. 4.66). It is possible that accurate satellite measurements of cold SST are being flagged as clouds for being anomalously cold in comparisons to surrounding measurements.

4.2.1.2 Interannual variability of Sea Surface Temperature

The Hövmuller diagram in Figure 4.5 shows the comparison between satellite and modeled monthly SST time series for a north-south transect at 85.94^oW (dashed line in Fig. 4.1) for the 8 years modeled. The main feature observed is the annual cycle of heating and cooling. The timing of warming transition agrees well between satellite and model SST, however cooling happens earlier in the modeled SST than in the satellite observations. Both modeled and satellite SST show interannual variability in the timing and intensity of the seasonal warm and cool periods: 2005 displays the least intense cooling in the first half of the year and 2000 shows the most winter cooling of the 8 years modeled. The satellite SST is more uniform latitudinally (N-S) (Fig. 4.4), while the modeled field is more heterogeneous showing some mesoscale features like the large warm eddy centered in the NE corner of the domain and the warm core anticyclone in the Bay Islands region (Fig. 4.3). Upwelling adjacent to the coasts of Honduras and Guatemala (South of 17^oN) is also evident in the modeled SST fields from October to July but not perceptible in the satellite field.

Time series comparisons (Fig. 4.7) at various points in the domain (numbered * in Fig. 1) reveal that in general the model SST matches well the temporal changes at the selected sites, which are distributed broadly across the model domain. While the timing of the maximum and minimum temperatures of the model agrees with the satellite SST peaks, the model amplitude for peak to valley SST slightly exceeds the satellite range (by ($\sim 1^oC$) for some stations (*1, *2, *3). In the southern half of the domain (south of ($\sim 19^oN$, i.e. locations 4, 5 and 6) the model temperatures are up to 2^oC colder than the satellite SSTs. This difference points to the coastal upwelling along the Honduras and Guatemala coasts being too strong in the model and/or misrepresented in the satellite product.

4.2.1.3 Temperature and velocity transects across the Yucatan Channel

The modeled vertical distribution of annual mean temperature across the Yucatan Channel (Fig. 4.8a) agrees well with the observations of Sheinbaum, et al. [2002]. Modeled isotherms in the upper 600m are at the same depths as those observed in the CANEK Program (1996-2001) [Sheinbaum et al., 2002]. Below this depth MCCM temperatures are slightly warmer than the observations. The isotherms in the upper 1000 m tilt up in the western side of the strait as expected from the fast flowing Yucatan Current exiting to the Gulf of Mexico in that side of the channel, however the modeled tilt is more gentle than that shown by the observations, with no isotherms outcropping. The change in curvature of the isotherms below 800 m is associated with the southward flowing Yucatan counter-current in the western side of the channel and the Cuban counter-current in the eastern side Sheinbaum et al. [2002]. The along-channel velocity transect shows the surface intensified Yucatan Current flowing into the Gulf of Mexico in the western side of the channel, and the weak opposite flow of the Yucatan Countercurrent beneath it. The Cuban Countercurrent flows southward both at the surface and at depth in the eastern side of the channel (Fig. 4.8b). The velocity pattern agrees well with [Sheinbaum et al., 2002] observations, however the model-calculated Yucatan Current and both the Yucatan and Cuban Countercurrents are slightly weaker than the observations.

4.2.1.4 Sea Surface Salinity model-data comparison

The modeled Sea Surface Salinity (SSS) ranges between <35.0-36.4, in agreement with values reported for the region in Gallegos and Czitrom [1997]. The model also reflects the observed temporal variability with lowest salinities in winter and highest in spring. The spatial pattern shows high salinities in the nearshore region north of the Yucatan Peninsula, and lower salinities along the Guatemala and Honduras coasts. The main seasonal SSS variability is in the northward and offshore extent of the low salinity waters in the southwestern corner of the domain. The location with

highest SSS variability is the east coast of the Yucatan Peninsula, which is saltier from February to May, and fresher the rest of the year (Fig. 9). These seasonal patterns are in agreement with the SSS maps for winter and summer reported by Sukhovey [1980, Fig. 8 in Gallegos and Czitrom, 1997].

4.2.1.5   Sea Surface Height Anomalies model-data comparison

AVISO sea level anomaly (SLA) and modeled Sea Surface Height anomaly (SSHa) might not be directly comparable because of the different horizontal resolutions and because the Mean sea surface height subtracted from the AVISO and the model are different (corresponding to the mean of a different set of years: 1993 for AVISO and 2000 to 2007 for the model). Despite this potential problem, there is good qualitative agreement between the mesoscale features observed in the monthly anomaly means of AVISO (Fig. 4.10) and modeled (Fig. 4.11) SSHa fields. Both satellite SLA and model SSHa show negative anomalies along the east coast of the Yucatan peninsula, Guatemala and Honduras during the period of January to July, and positive anomalies along the coast the rest of the year. The central part of the domain has mostly negative SSHa values from November to April and positive values from June to October in both model and satellite observations. Stronger gradients and better defined eddy features are observed in the modeled fields. The size and specific locations of various eddies vary between the satellite and the model SSHa fields. However, positive and negative eddy anomalies are in relatively good agreement regarding the timing and general location in AVISO SLA and the model SSHa in figures 4.10 and 4.11. A cyclonic eddy is found south of the Cuban tip in August, later replaced by an anticyclone in December-January. However, AVISO shows more positive SLA in this region during March and April and negative SLA from July to October. At times (e.g., August), this eddy is part of a dipole, with an opposite sign eddy to the southwest. Another eddy with positive SSHa is present at the northern boundary of the domain (22ºN, 86ºW), in the middle of the Yucatan Channel. This eddy is evident in AVISO observations from January to May and in the model results from January to July. In the model SSHa this feature is replaced by a negative anomaly from

October to December; negative values are hinted in AVISO SLA during September and October.

4.2.1.6   Sea Surface Height anomaly EOF modes

The spatial patterns and time series of the first 3 EOF modes of variability of the AVISO SLA and modeled SSHa are similar (Figs. 4.12 - 4.14). The first mode explains 45% and 51% of the satellite and modeled SSHa variability, respectively. Its spatial pattern shows negative values in most of the domain. The first EOF of both AVISO SLA and modeled SSHa show a slightly positive feature in the center of the northern boundary. The time series of this mode shows an annual signal with a main peak in the first half of each year. The mean of the modeled amplitude time series for this mode is, however, larger than that of AVISO (Fig. 4.12). EOF 2 explains 15% and 22% of the satellite and modeled SSHa variability, respectively. The spatial pattern shows a positive feature in the middle of the domain (Fig. 4.13), and the time series an annual signal with 2 to 4 local peaks, which are better defined in the model time series. EOF 3 explains 10% and 9% of the satellite and modeled SSHa variability, respectively. Its spatial pattern shows a dipole with negative values in the northeast region and positive values in the western region. The time series of EOF 3 exhibit high frequency fluctuations ($\sim$ 4 months) better defined for the model (Fig. 4.14).

4.2.2   MCCM climatological surface velocity patterns

The Caribbean Current flows through the eastern open boundary (into the domain) year-round, except in the northern part where eddies in the region south of Cuba sometimes cause flow exiting through the eastern boundary (Fig. 4.15). The northward component of the CC varies throughout the year in the southern part of the domain, altering the flow direction from directly westward during summer and fall to northwestward during winter and spring. This variability and the interactions of the CC with eddies in the southern part of the domain change the latitude where the

flow impinges on the Yucatan coast (around 18°N), turns northward and becomes known as the Yucatan Current. There is a "shadow" region of slower velocities south of this latitude and to the southwest of the CC flow where eddy activity dominates. This region is rectangular from June to November covering a 1 to 2° band off the coast of Guatemala and Honduras and triangular the rest of the year covering the Gulf of Honduras and a variable region along the Honduras coast. During May and June the low energy triangular region is restricted to the Gulf of Honduras. D'Croz et al. [1998, as cited inHarborne et al., 2001] reports a small cyclonic counterclockwise eddy that affects the Bay Islands, particularly from January to March. The eddy causes a decrease in sea surface temperatures product of local upwelling. In the model surface velocity field, a cyclonic eddy with slightly cooler SST is observed year-round surrounding the Bay Islands. The feature seems to be locked to the islands and is likely generated by topographically steered instabilities. The strength of its marginal velocity seems to be associated with that of the CC, which, at times, advects the feature westward. The cyclone in the Gulf of Honduras is a permanent feature as well, but in this model is weaker and smaller than the cyclone around the Bay Islands. In the northeast region of the domain, south of the Cuban coast, there is a dipole with a cyclonic eddy nearshore (to the north) and an anticyclone farther south. The anticyclone is large year-round, with a diameter of ($\sim$150 to 220 km, but is not fully in the domain during May and June. The cyclonic eddy to the north is smaller, with a diameter fluctuating between ($\sim$55 and 110 km, compressed between the southern coast of Cuba and the anticyclone. Both features are present year round but are larger and stronger during August with maximum marginal velocities of 1.9 m s^{-1}. Strong upwelling occurs along the coast of Guatemala and Honduras during spring and the cool water is transported northward by eddies in the low velocity region (Fig. 4.15).

4.2.3   Contrasting Ocean Conditions

As mentioned in section 4.3.2, 2005 displays the least intense cooling in the first half of the year and in contrast 2000 shows the most winter cooling of the 8 years

modeled (Figs. 4.16 and 4.17). These two years also experience enhanced eddy activity, especially in the Golf of Honduras and around the Bay Islands. Eddy activity in this region seems to be related to the strength and direction of the CC flow coming in through the southern part of the eastern open boundary.

During 2000 (Fig. 4.16) the SST range is very similar to that of the climatology, even slightly cooler. Upwelling in the Guatemala and Honduras coast is intense during 2000, stronger than in the climatology and 2005, with water colder than 25^oC reaching 17.5^oN along the Yucatan peninsula from January to June. Monthly mean surface velocities are similar to the climatological values during all months (¡ 2cm s^{-1}), but higher in September and December (Fig. 4.16). During this year the main direction of the CC in the domain fluctuates almost month to month being northwestward during January, October, April and December, southwestward in February, June and September, and westward in March, May, July, August and November. There are fewer and weaker eddies in the southern part of the domain compared to the climatology and 2005. The anticyclone around the Bay Islands dominates during the first half of the year and is greatly intensified during February and May, minimizing other eddy features around it. The dipole south of Cuba is weak during 2000. The cyclonic eddy is dominant during June and December.

During 2005 (Fig. 4.17), SST is warmer than the climatology (up to 2^oC) from March to September, especially along the east coast of the Yucatan peninsula and the region occupied by the anticyclonic eddy south of Cuba. Upwelling in the Guatemala and Honduras coast is weaker than in the climatology with the cold water signal extending less than half a degree latitude ($\sim$50km) offshore. Mean surface velocities in the region are higher than climatological and 2000 values. The CC flow is mainly westward during January and February and again from July to November. During March, April and December it has a northwestward direction across the domain and a slight southwestward direction in the eastern boundary region between 17° and 18^oN in May and June. From July to November the westward flow of the CC enters the domain north of 17.2^oN, allowing slower velocities and eddy activity in the southern part of the domain. Four to five small eddies are observed along the coasts of Guatemala and Honduras during January and February. In March a larger

cyclonic eddy forms east of the Bay Islands and is advected towards the Yucatan peninsula in April. The Bay Island's cyclone forms in April, strengthens in May and is advected westward in June. The cyclonic eddy south of Cuba is greatly intensified during January and May, compared to 2000 and the climatology, while the cyclonic counterpart strengthens greatly in August and September.

2000 and 2005 will be the two extreme years considered to study coral reef connectivity patterns in the Western Caribbean region (Chapter 5). Spawning is modeled from February to March, and connectivity for species with long pelagic larval durations (72 days) is determined by ocean conditions from the February to mid July period, during which the two considered years display the largest difference in terms of circulation and water temperature.

4.2.4   Discussion

Unlike the Kenya-Tanzania region (Chapters 2 and 3), the wider Caribbean, including the western Caribbean region being modeled here, has been the subject of quite a few earlier numerical models of physical conditions and dynamics [Chrubin et al., 2008; Paris et al., 2007; Tang et al., 2006; Cetina et al., 2006; Sheng and Tang, 2003; Ezer et al., 2002. However, in order to provide a suitable basis for comparison of the reef-to-reef and subregion-to-subregion connectivity provided by pelagic larval stages (Chapter 5), we opted to develop a new numerical model of ocean physics for the western Caribbean. This model shares most of the important characteristics (horizontal resolution; number of vertical levels; shared global model source for initial and time-varying boundary conditions; atmospheric variable forcing) implemented in the physical model of the Kenya-Tanzania region, which enables a potentially less biased and fairer comparison of the two regions. It is worth noting here that the MCCM qualitatively shows the main features reported in observational studies [e.g. Richardson, 2005; Sheinbaum et al., 2002] and other models of the WC region [e. g.Chrubin et al., 2008; Tang et al., 2006; Johns et al., 2002; Ezer et al., 2002]. The strong westward flow of the Caribbean Current, the intensified northward flow of the Yucatan Current, slower flows in the vicinity of the Guatemala-Honduras

shelf, and eddies in the northeast region of the domain are present in observations, previous models and shared by this model. Based on satellite color imagery and their coastal model, Chrubin et al. [2008] reported that the river plume from the Honduras-Guatemala outflows is transported out of the Mesoamerican waters by a cyclonic gyre located north of Honduras between October and December, with part of the freshwater runoff from Honduras transported towards Chinchorro Banks and the Yucatan Channel, part re-circulated into the Gulf of Honduras, and part transported outside of the Mesoamerican Barrier Reef System. This circulation pattern is in agreement with the MCCM circulation pattern in the eddy dominated region southwest of the CC flow. Based on drifter analysis, Richardson [2005] identified a region of slower velocities to the south of the CC on the Honduras-Guatemala shelf. He reported strong eddy activity in the modeled region with numerous cyclones and anticyclones southwest of Cuba in the northeast corner of the domain, where the MCCM climatology shows a dipole [Richardson, 2005]. The larger anticyclone in MCCM (centered at 84^oW, 20.5^o N) was identified by Johns et al. [2002] as a permanent regional feature responsible for much of the transport in the upper 1000 m. Vertical temperature and velocity structure in the Yucatan Channel of our model show better agreement to Sheinbaum et al.'s [2002] observations than does the similar resolution nested model of Tang et al. [2006], or the high frequency (6-hourly) wind stress forced POM application described by Ezer et al. 2002. This generates confidence in the ability of MCCM to represent the regional circulation and hydrography at depth, where fewer observations have been made.

As expected from any ocean circulation model, the MCCM has its caveats. The surface water is slightly fresher than the summer/winter SSS from Sukhovey maps [1980, shown in Gallegos and Czitrom, 1997], particularly in the Honduras coasts. However, Sukhovey's maps are based on observations made two decades before the modeled period and the amount of observations used to create these maps is most likely limited. The SST difference between modeled and satellite observations along the Honduras and Guatemala coasts points to the coastal upwelling being too strong in the model and/or misrepresented in the satellite product. When all AVHRR satellite measurements are included, even those flagged as clouds, cold temperature

patterns similar to those in the model are observed in the satellite SST (Fig. 4.6). Resolution of the SST fields in the "shadow" region will require in situ near surface measurements of the region. It is possible that the AVHRR data require a different post-processing to generate a more realistic SST product for the tropics and the Western Caribbean than that used for the Pathfinder global product. Another potential explanation of the SST discrepancy in that region is the lack of river discharge in the model simulation. The buoyant plume created by the riverine discharge in the Gulf of Honduras might inhibit vertical mixing and upwelling, or form a fast warming layer in the upper ocean, resulting in warmer SST observations. This issue requires further investigation. At this point there is not enough evidence to support any of these hypotheses regarding the SST difference between MCCM model fields and Pathfinder. Another slight discrepancy of MCCM with satellite observations is the persistent difference in the magnitude of SSHa gradients, with the model showing stronger gradients than the satellite product. This is perhaps due to the higher spatial and temporal resolution of the model compared to the remote sensed observations of AVISO. The good agreement in the first 3 EOF mode's spatial and temporal patterns indicates that the model reproduces the main modes of SSHa variability from AVISO.

In conclusion MCCM shows similar capabilities to represent the main circulation features as other regional models and good agreement with available satellite SST and SSHa fields. This model system is, therefore, considered suitable to address coral reef connectivity patterns in the Western Caribbean region and to perform the corresponding Lagrangian particle tracking experiments using its three dimensional temperature and velocity fields (Chapter 5).
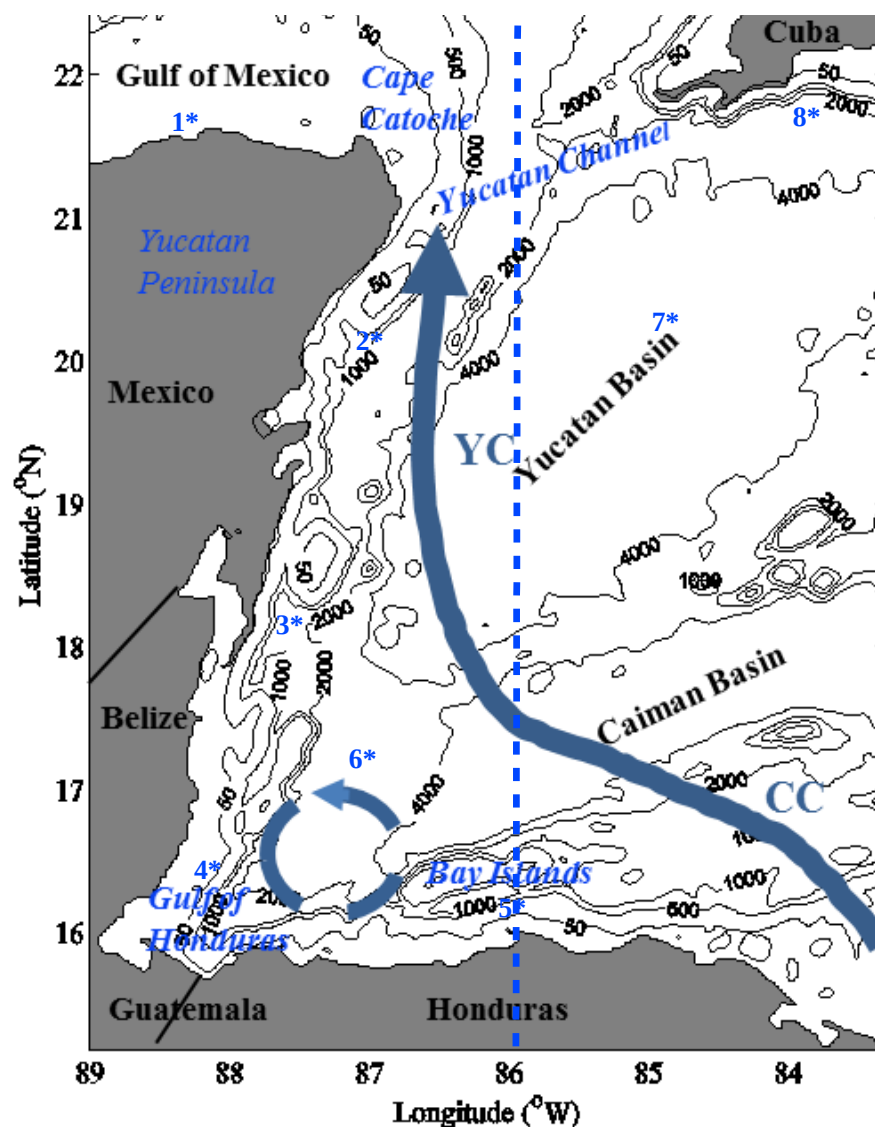
Figure 4.1: Model domain with schematic arrows showing the main surface currents, solid lines represent permanent features: the Caribbean Current (CC) and the Yucatan Current (YC), dasead line the seasonal cyclonic eddy in the Gulf of Honduras. The model coastline and bathymetry are shown, along with locations named in the text. Blue dash lines and numbered * mark locations examined for model validation. Bathymetric contours are: 50, 500, 1000 and 4000 m.
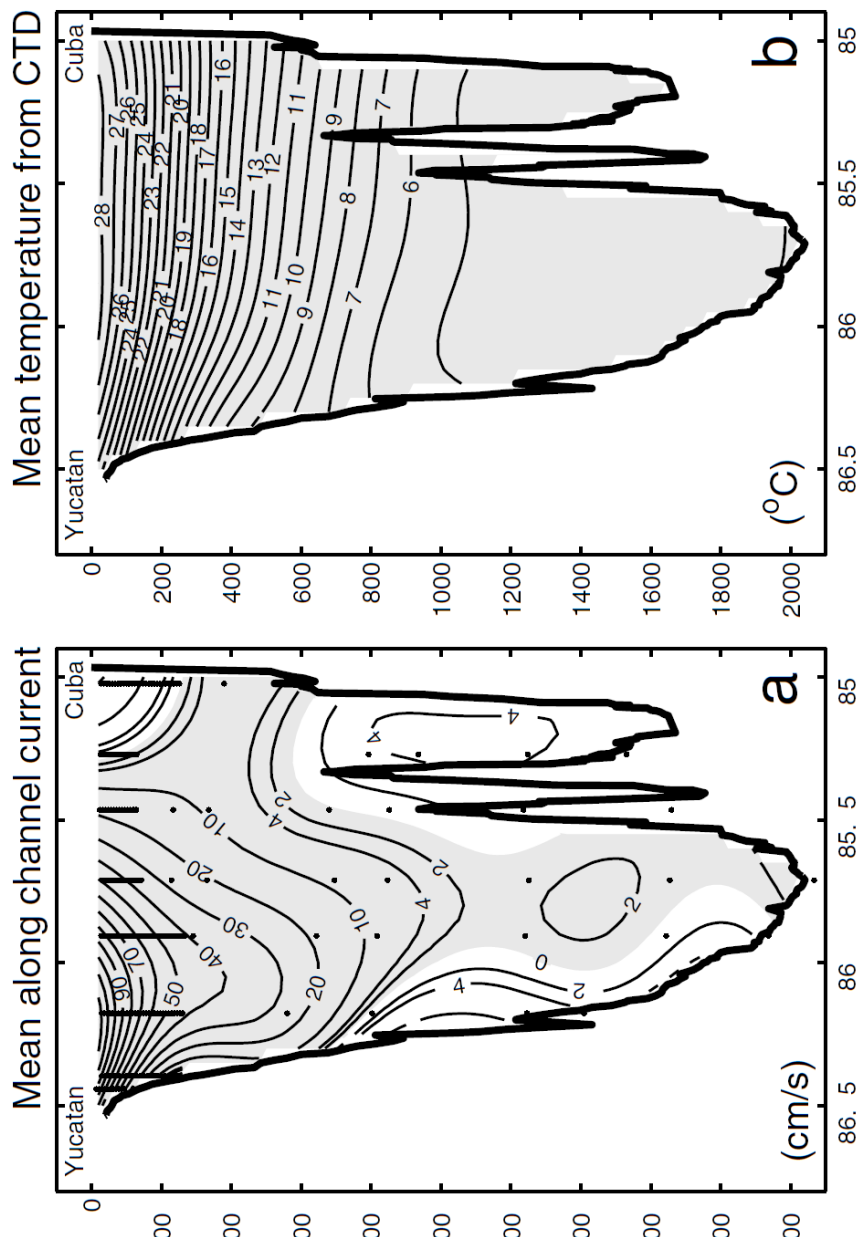
Figure 4.2: a) Structure of the mean along-channel velocity field for the full observational period (1996-2001). Shading indicates flow into the Gulf of Mexico. Counterflows into the Caribbean (unshaded) occur at depth on both sides of the Channel. b). Mean temperature structure in the Yucatan Channel from CTD profiles computed from 14 objective maps of crossings made at various times of the year straddling all seasons, during the Canek program. From Sheinbaum et al, 2002.
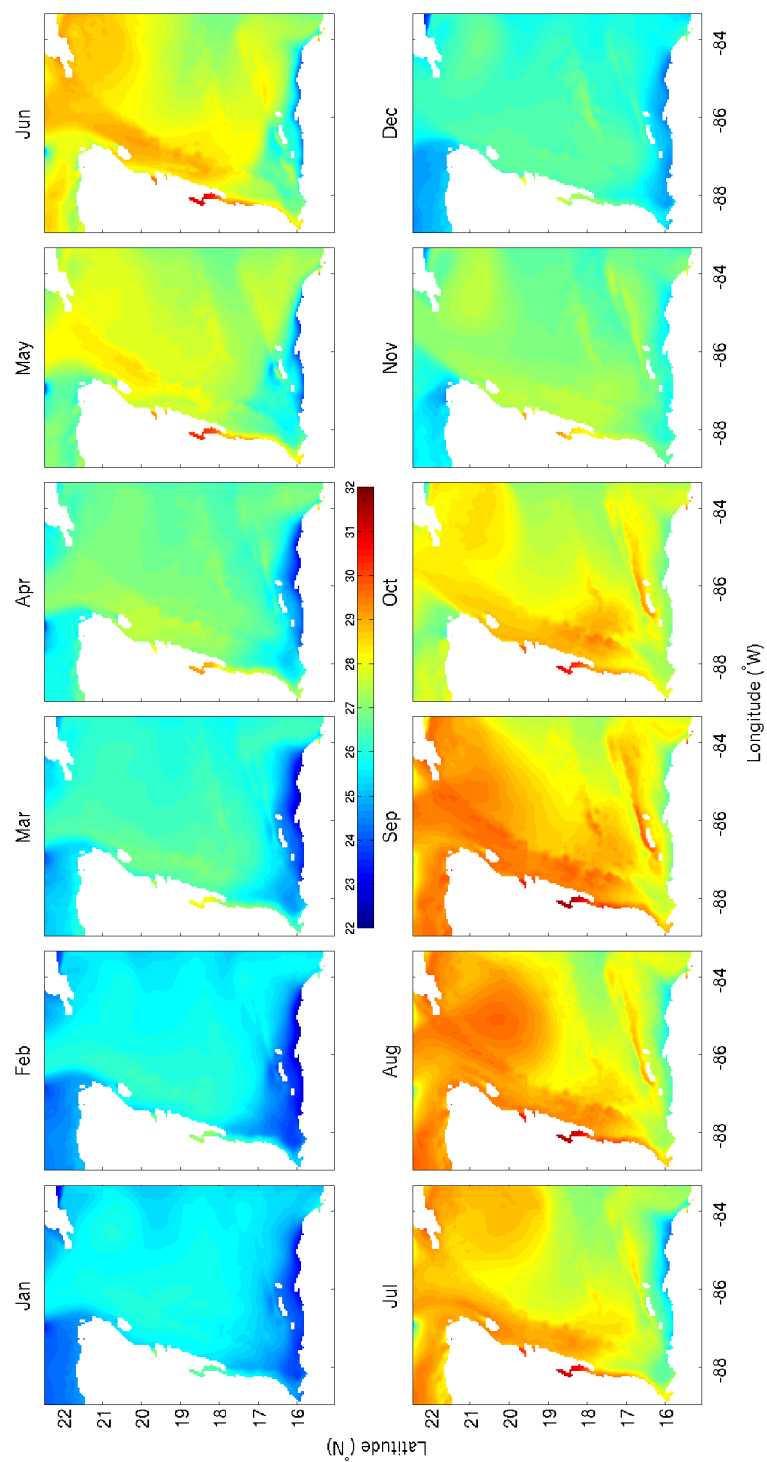
Figure 4.3: Monthly climatology of modeled SST in °C.
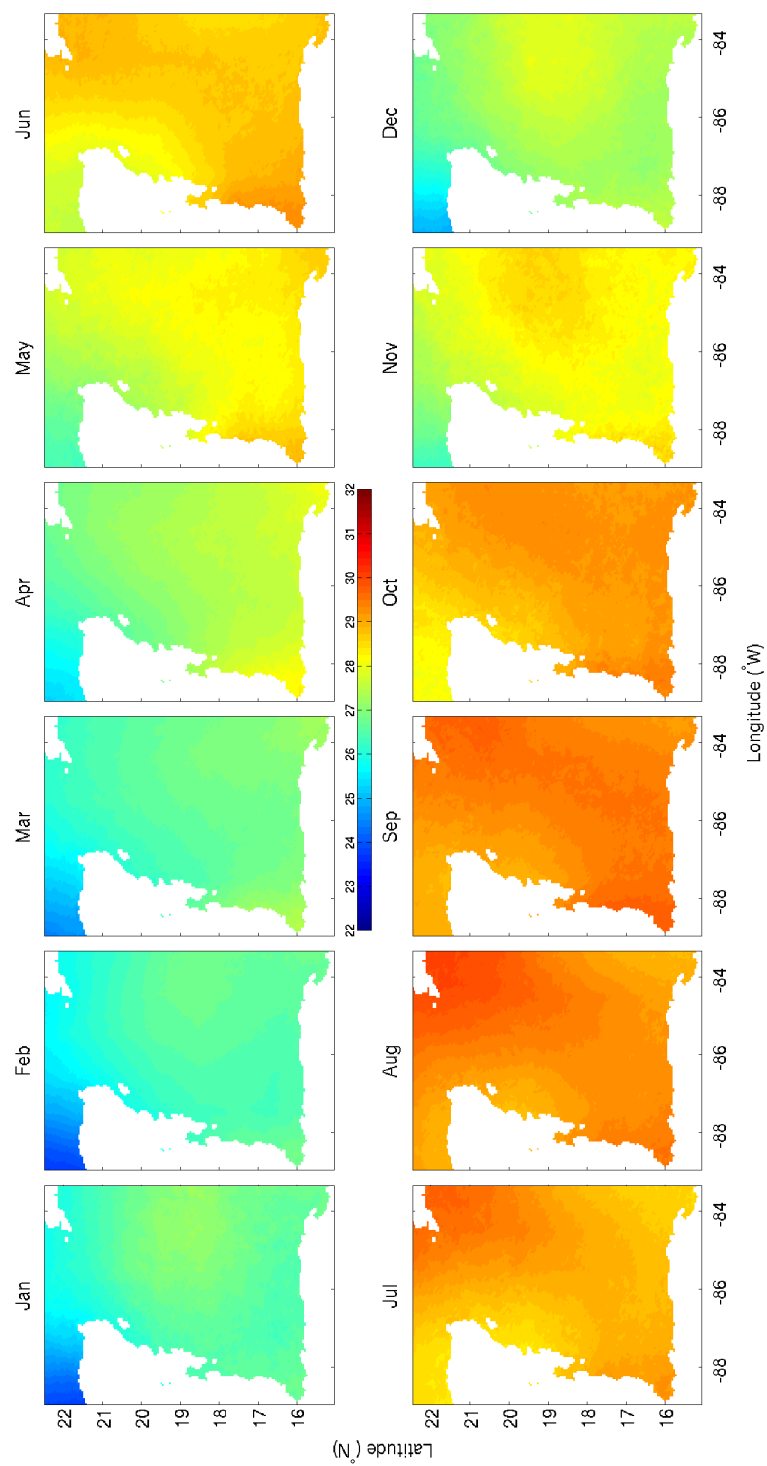
Figure 4.4: Monthly climatology of Pathfinder SST in °C.
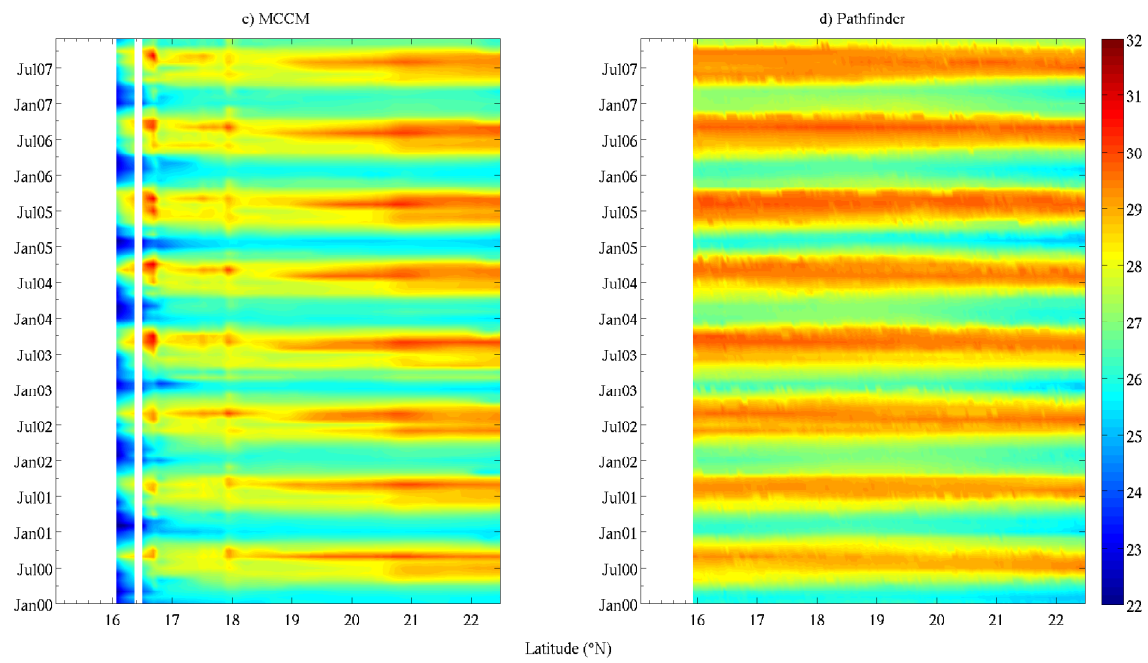
Figure 4.5: Hoffmuller Diagram of the SST transect along 86°W.
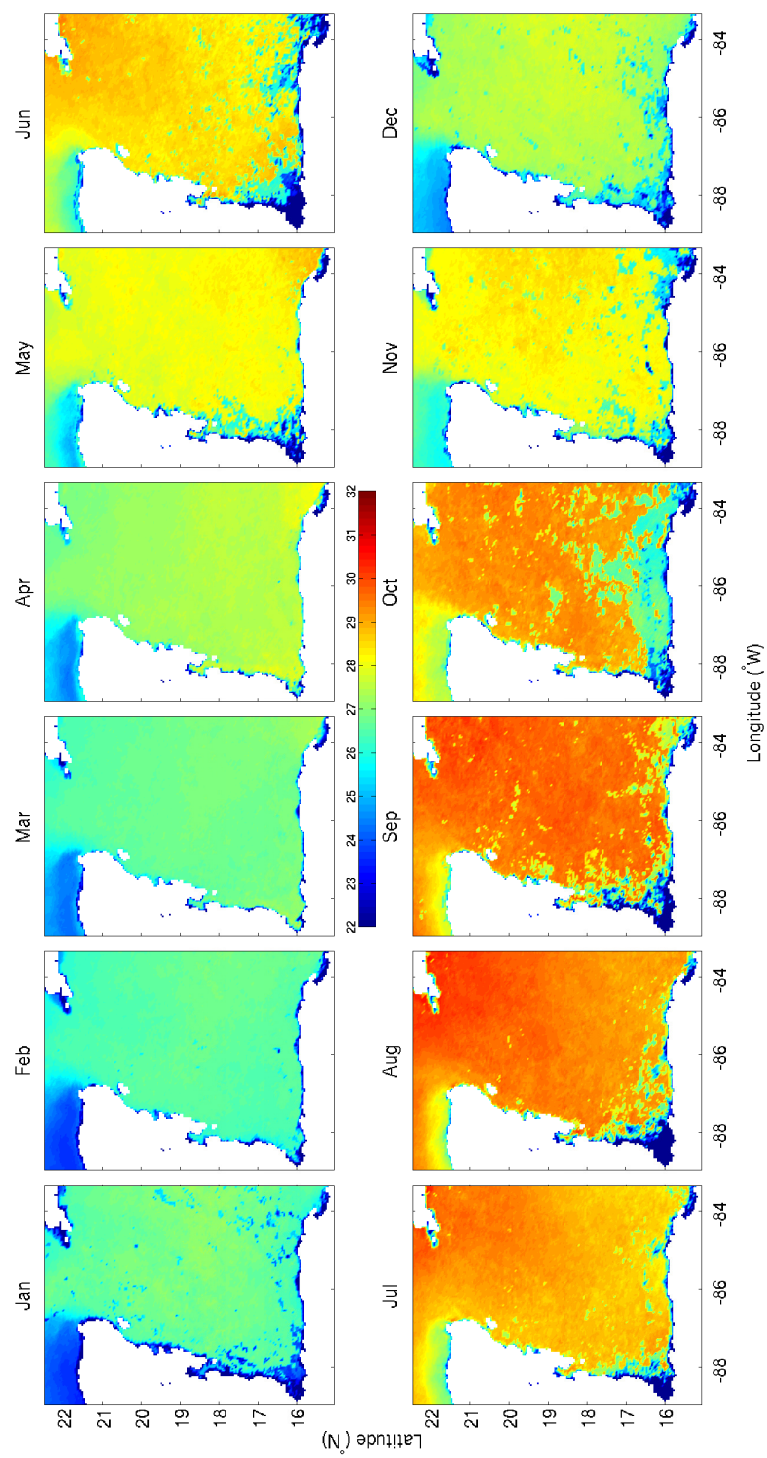
Figure 4.6: Monthly climatology of Pathfinder SST (°C) including all observations flagged as clouds.
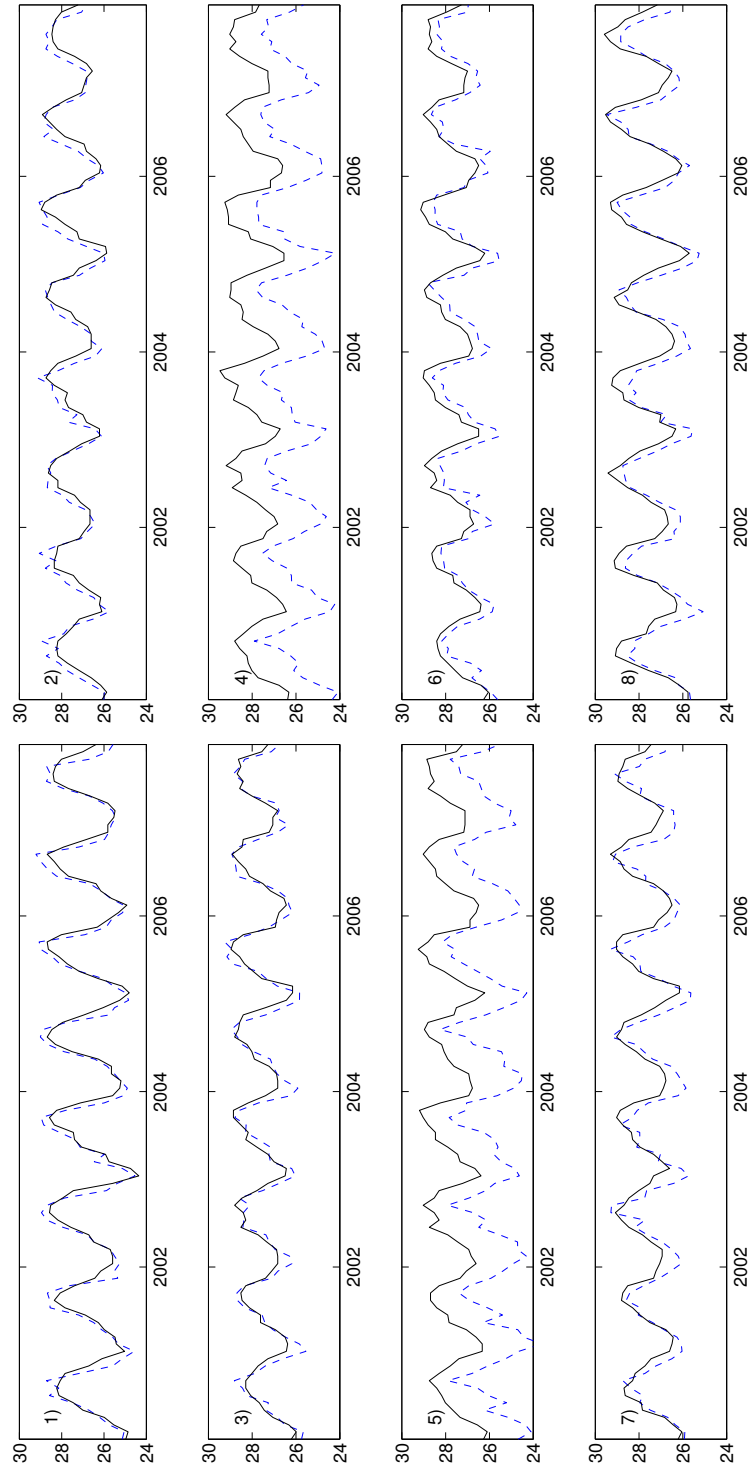
Figure 4.7: Time series of Pathfinder (solid line) and modeled (dashed line) SST (°C) at 8 different locations marked with * in Figure 1.

(b) Along-channel velocity (m s $^{-1}$)

(a) Temperature (°C)
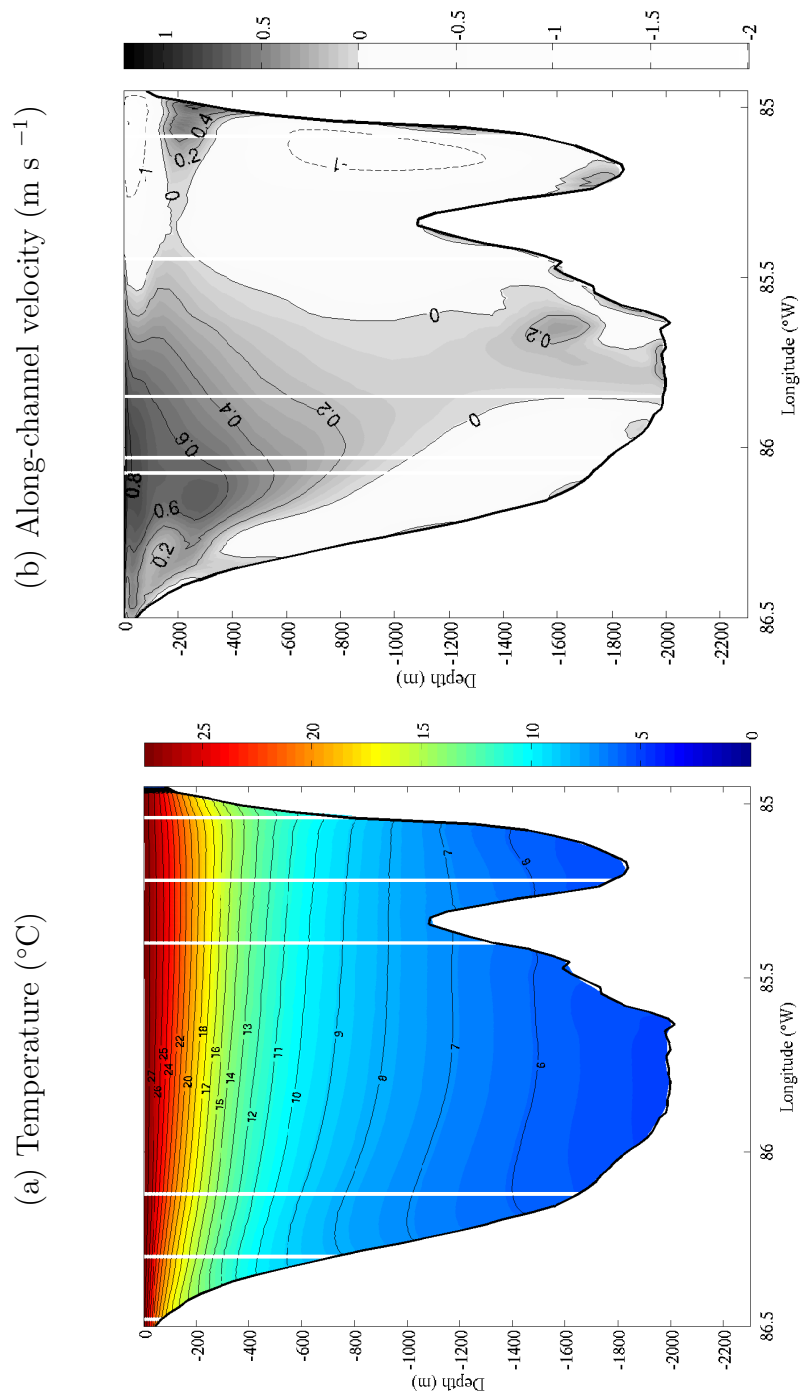
Figure 4.8: Transects across the Yucatan Channel with Cuba to rigth and the Yucatan Peninsula to the left.
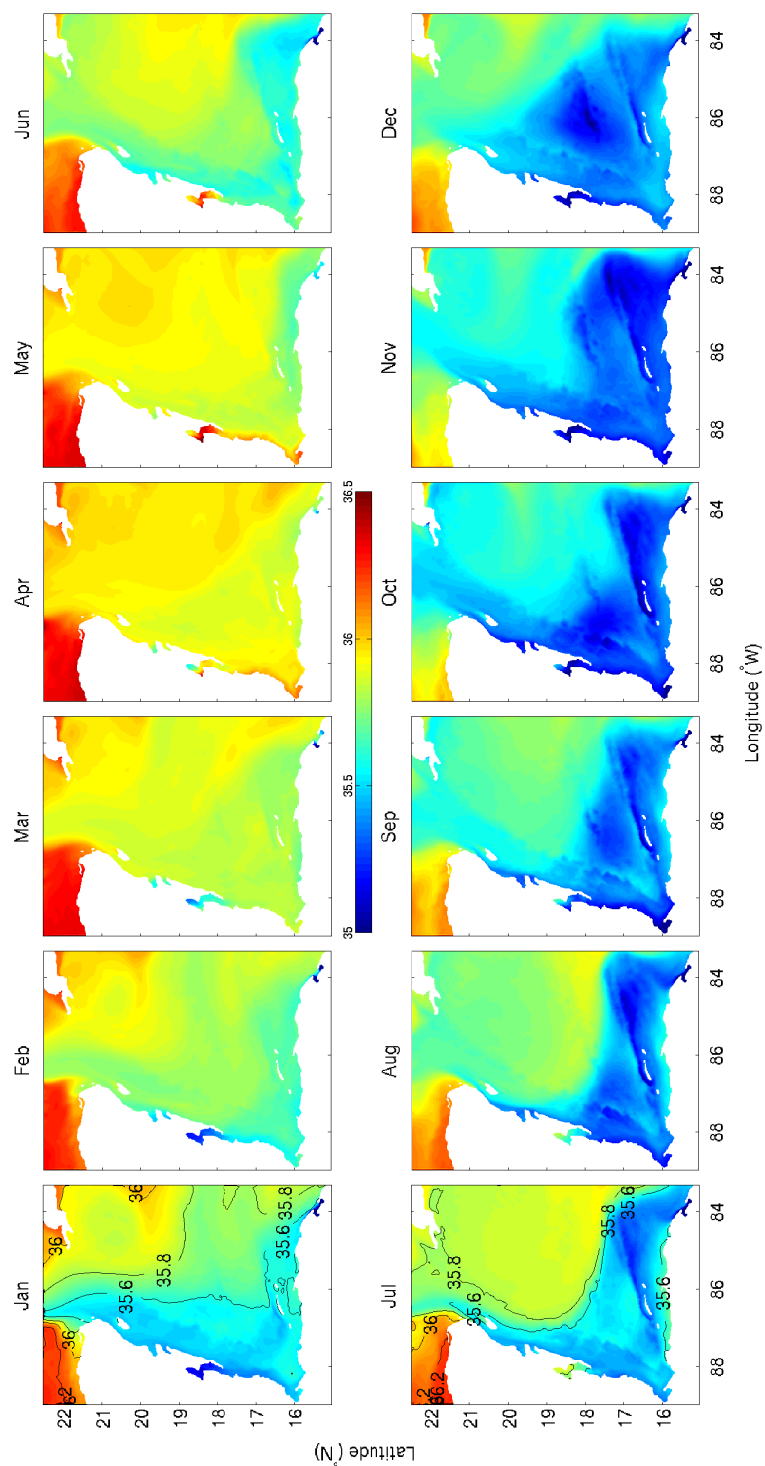
Figure 4.9: Modeled climatological monthly Sea Surface Salinity (PSU)
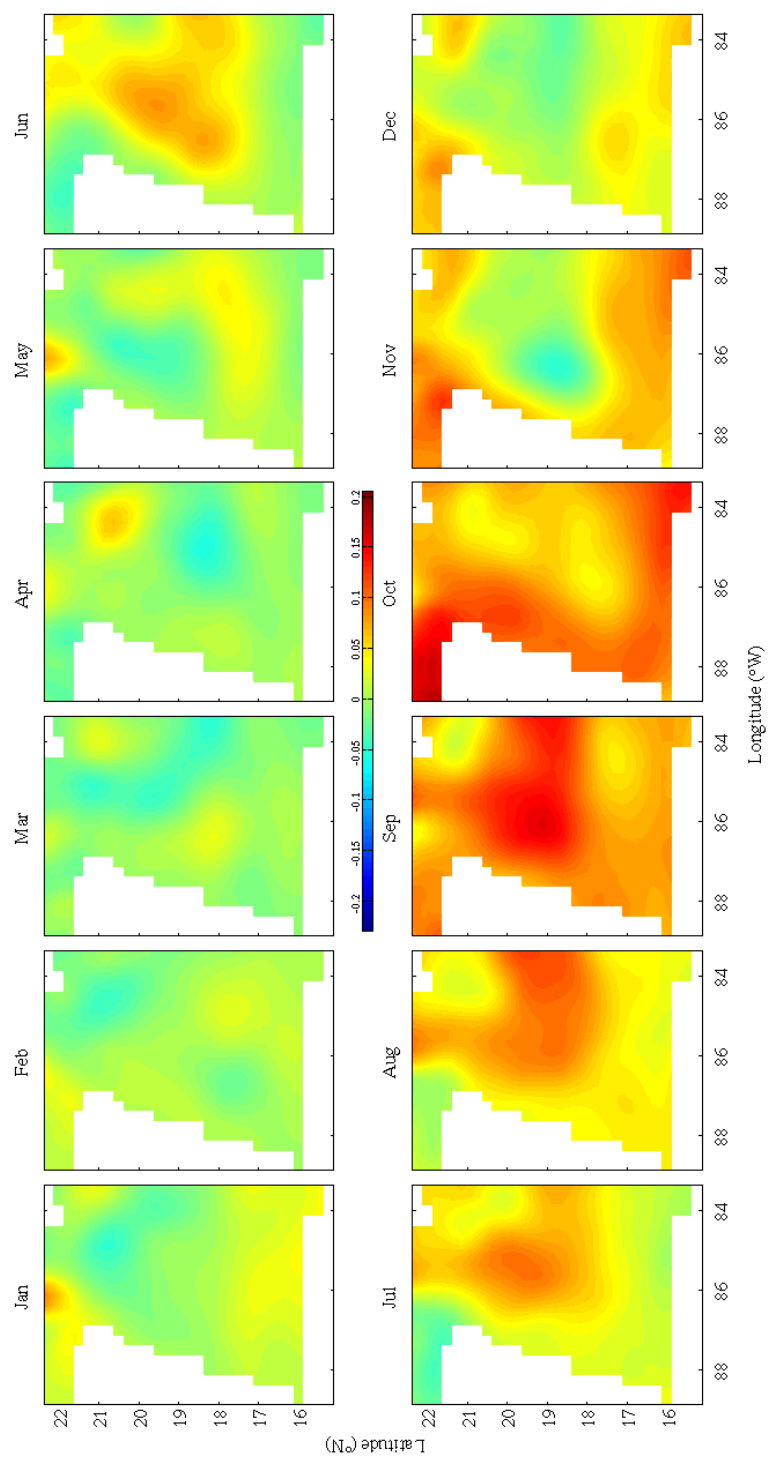
Figure 4.10: AVISO monthly climatological Sea Surface Height anomaly (m).
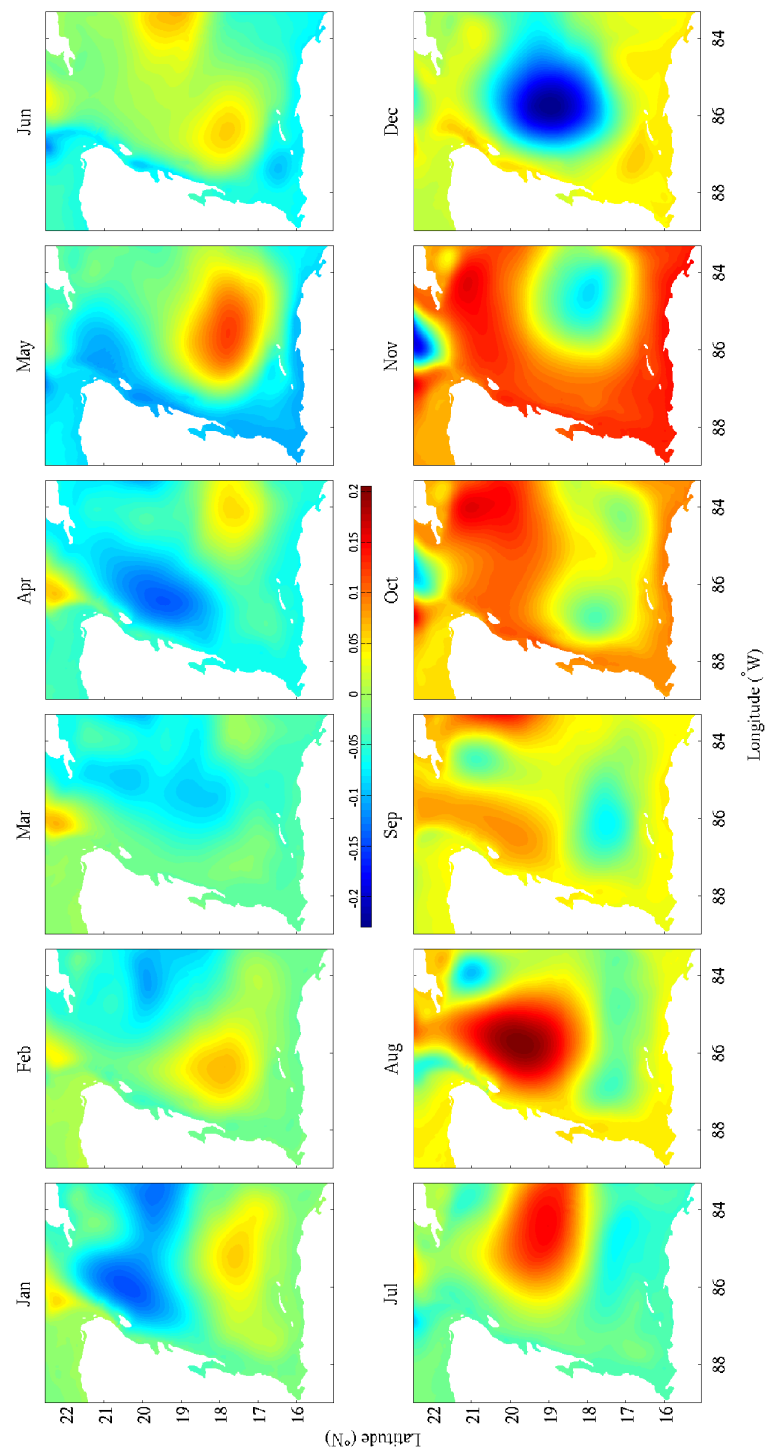
Figure 4.11: Modeled monthly climatological Sea Surface Height anomaly (m).
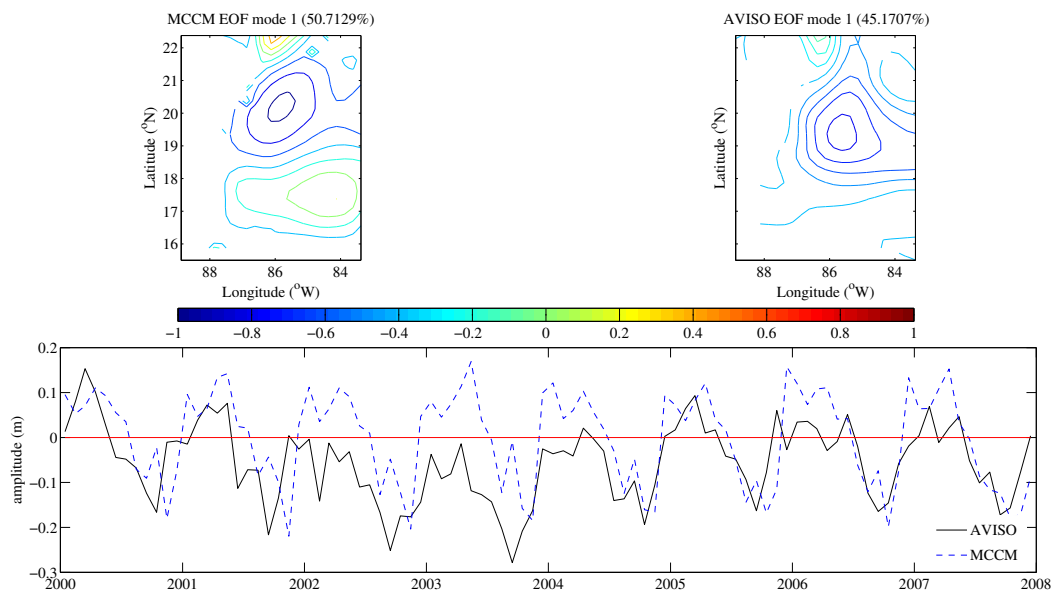
Figure 4.12: Sea level anomaly (m) EOF mode 1 spatial patterns and amplitude time series for MCCM and AVISO.
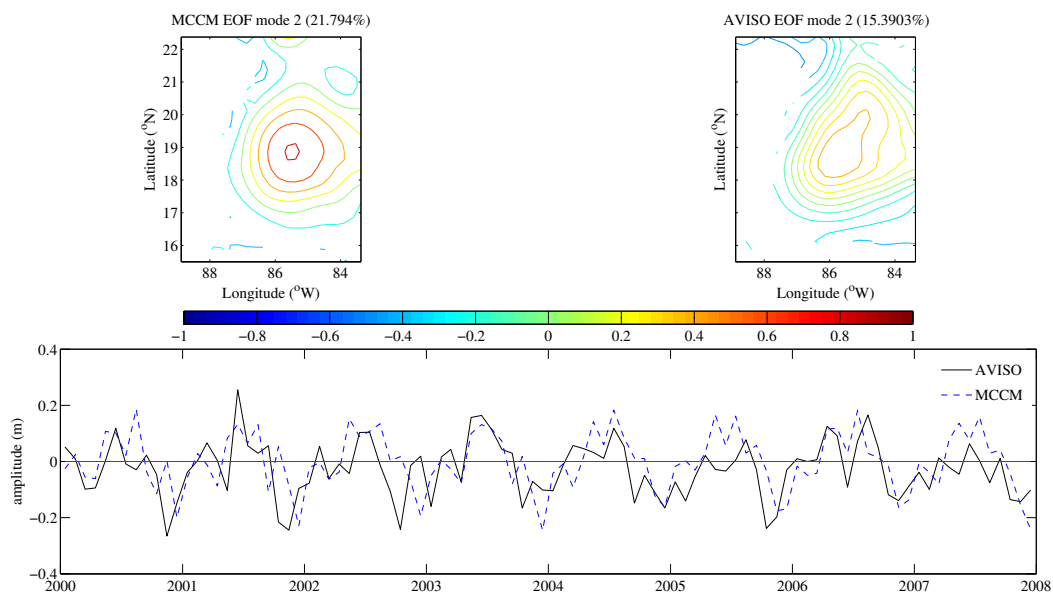
Figure 4.13: Sea level anomaly (m) EOF mode 2 spatial patterns and amplitude time series for MCCM and AVISO.
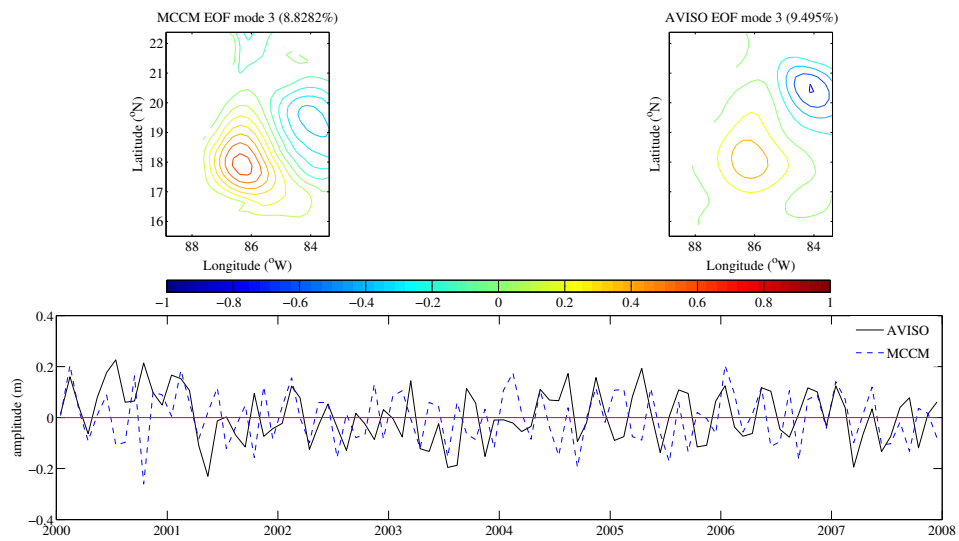
Figure 4.14: Sea level anomaly (m) EOF mode 3 spatial patterns and amplitude time series for MCCM and AVISO.
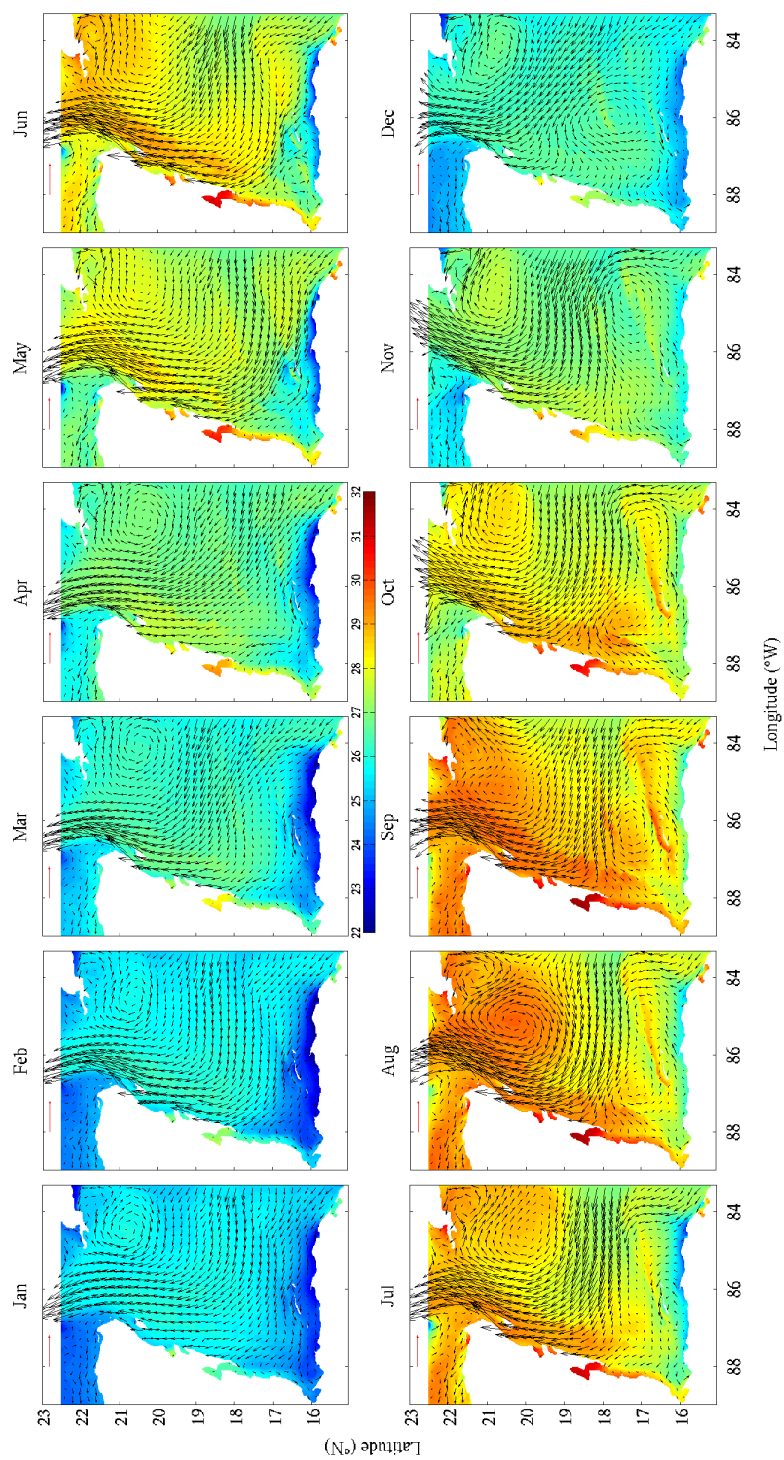
Figure 4.15: Modeled climatological sea surface temperature (°C) and surface velocity vectors (m.s^{-1}).
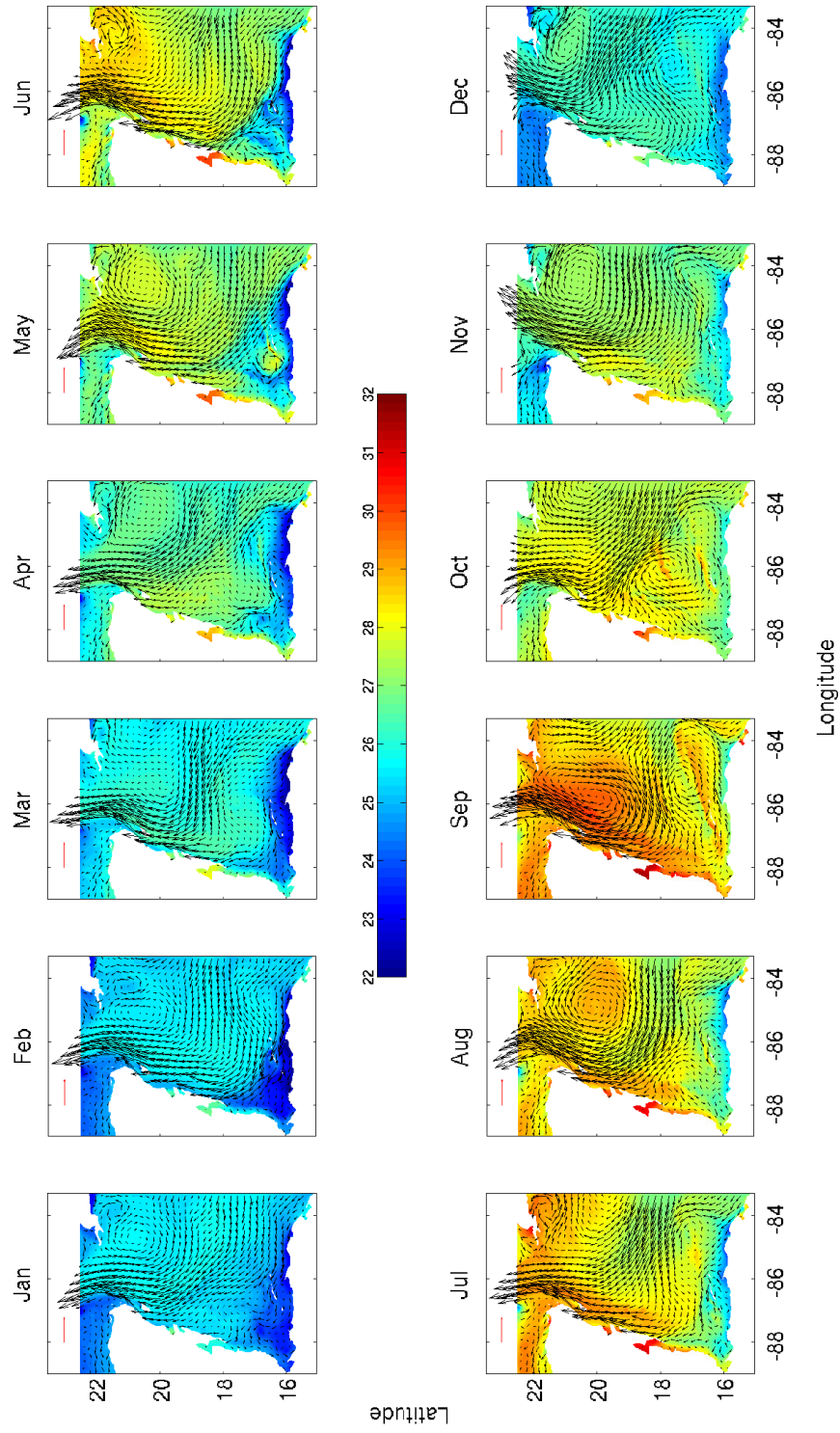
Figure 4.16: 2000 modeled sea surface temperature (°C) and surface velocity vectors (m.s^{-1}).
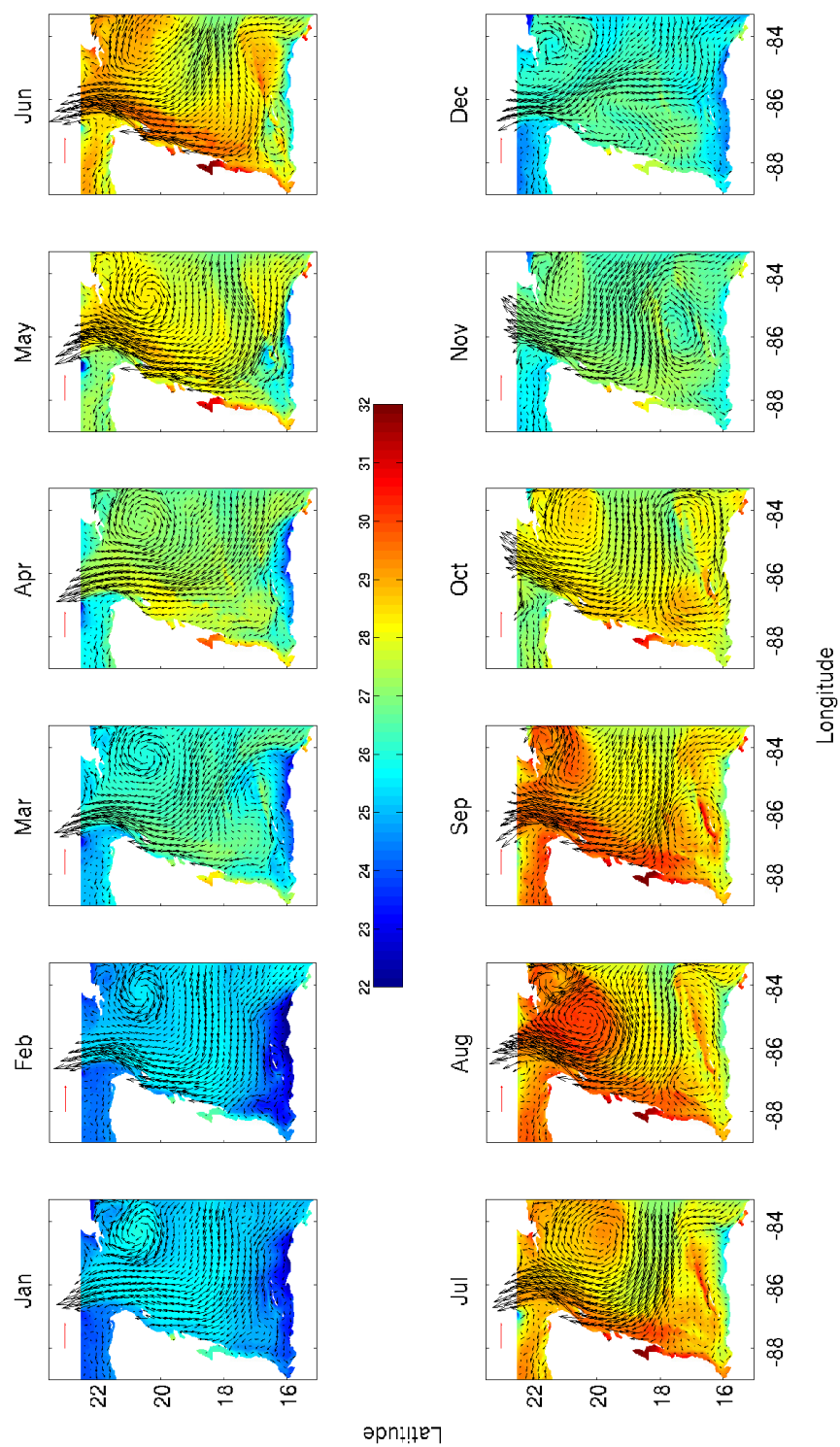
Figure 4.17: 2005 modeled sea surface temperature (°C) and surface velocity vectors (m.s^{-1}).

Chapter 5: Modeling potential connectivity among coral reefs in the Western Caribbean region

5.1 Introduction

The Western Caribbean (WC) hosts the Mesoamerican Barrier Reef, one of the largest barrier reefs in the world, second only to the Great Barrier Reef in Australia. Reef habitat in the Western Caribbean is very diverse, with fringing and barrier reefs virtually continuous along the east coast of the Yucatan Peninsula, and large offshore atolls and islands [Wallace, 2011]. The Mexican Caribbean has well developed reef structures and lacks river discharges [Soto et al., 2009], while the Belize Barrier reef is heavily influenced by the discharge of various rivers in the Gulf of Honduras [Chrubin et al., 2008; Paris and Chrubin, 2008]. According to Chrubin et al. [2008] even offshore reefs of the Western Caribbean region are seasonally affected by river runoff. The Caribbean coral reef ecosystem has low biodiversity in comparison to Indo-Pacific reefs [Hopley, 2011; Burke et al., 2011; Spalding et al., 2001]. Caribbean reefs are highly affected by the strongly variable environmental conditions of the region. They are frequently exposed to strong warming events associated with El Nio Southern Oscillation (ENSO) events, which cause coral bleaching and widespread coral mortality [Wilkinson et al., 2008]. Hurricane damage occurs almost every year at different locations. Mesoamerican Reefs experienced geographically widespread bleaching events in 1995, 1998 and 2005. Belize reefs lost on average 50% of coral cover in 1998 due to ENSO related bleaching followed by damages from Hurricane Mitch [Wilkinson et al., 2008]. Similar circumstances occurred again in late 2005 when large scale bleaching affected most Mesoamerican reefs and Hurricanes Wilma and Emily hit the Mexican coast. These events, however, resulted in lower coral mortality than in previous ENSO years [Wilkinson et al., 2008].

Diseases are another threat affecting corals and other organisms including keystone species like the long-spined sea urchin *Diadema antillarum* [Burke et al., 2011].

This herbivore helped prevent the transition from coral dominated to algal dominated reefs despite the overfishing of herbivorous fishes, but a disease outbreak in the 1980's resulted in a 95% decline of the Caribbean population [Carpenter, 1990]. *Acropora* coverage in the Caribbean has decreased dramatically since the 1970's linked to the impact of white band disease [Spalding et al., 2001]. Extraction activities, mainly fishing and shell collection, were common on Caribbean reefs long before pre-hispanic times. Today, most fish and invertebrates stocks are depleted due to systematic over-harvest going back centuries [Pandolfi et al., 2003; Burke et al., 2011]. The ecologic cascading effects of overfishing and environmental pressure on corals are leading the Caribbean reef ecosystem to become a fleshy algal dominated system [McManus and Polsenberg, 2004; McCook et al., 2014]. Invasive species are a newer and unexpected threat to the Caribbean ecosystem. Invasive Indo-Pacific lionfish species (*Peterois volitans and P. miles*) spread across the Western Atlantic after incidental releases of aquarium specimens in Florida waters [Betancur-R. et al., 2011]. The invasive lion fish population reached the Caribbean in 2007 and abundance has increased rapidly since then [Betancur-R. et al., 2011]. This voracious predator now comprises an important proportion of the total predator biomass on invaded reefs, which is having detrimental effects on recruitment of native coral reef fishes [Albins and Hixon, 2008] and causing further declines in depleted fish populations [Green et al., 2012] with potentially catastrophic long term effects [Albins and Hixon, 2013].

Local anthropogenic threats to the coral reef ecosystem vary regionally but fishing, sedimentation, agrochemicals, sewage, solid wastes and dredging are among the most widespread [Burke et al., 2011]. Tourism related damage mainly due to anchoring and divers is an issue in several places in the Caribbean and has lead to the complete degradation of several small reefs in the Cancun region [Spalding et al., 2001]. Despite the potentially negative effects of all of these cumulative stressors on reef systems, Caribbean coral reefs are very important for the regional economy. The value of ecosystem services and goods they provided, including tourism, fisheries and shoreline protection was estimated above $5 billion dollars in 2010 [Burke et al., 2011].

Marine Protected Areas (MPAs) have been implemented in the Caribbean region

as a conservation measure in the past 50 years [Selig and Bruno, 2010]. According to the Protected Planet database [http://www.protectedplanet.net/; accessed February 2013] there are 99 MPAs in the Caribbean, most of them encompassing coral reefs. The effectiveness of their protection varies widely. There are examples of very effective no-take zones that have significantly increased the biomass and number of fish and demonstrably increased fish yields from surrounding areas like the Hol Chan Marine Reserve in north Belize [Polunin and Roberts, 1993]. But there are many other MPAs with little to no effect on the ecosystem they are trying to protect. 61% of MPAs in the Atlantic Ocean attempting to protect coral reefs are rated as ineffective [Burke et al., 2011]. A comprehensive understanding of the connectivity among coral reefs in a region is a pre-requisite to design effective MPAs [Botsford et al., 2009; Almany et al., 2009; Steneck et al., 2009; Fogarty and Botsford, 2007; Sale et al., 2005] and could be helpful to elucidate the reasons of the variability in effectiveness of the existing Western Caribbean MPAs. Individual based models (IBMs) coupled to realistic high resolution ocean circulation models are critical tools to address the complex interdisciplinary issue of population connectivity in marine environments [Werner et al., 2007].

Some coral reefs in the Caribbean have been extensively studied, with surveys dating back to the 1950's [Selig and Bruno, 2010; Spalding et al., 2001]. Connectivity studies are much more recent, but already extensive for the wider Caribbean, which has been the focus of connectivity studies of multiple species at different spatial and temporal scales using genetics-based [Shulman and Bermingham, 1995; Goodbody-Gringley, 2010; Goodbody-Gringley et al., 2012], biomarkers [Chittaro and Hogan, 2012], and numerical modeling techniques [Cowen et al., 2006; Kettle and Haines, 2006; Kool et al., 2010].

Some genetic and biomarker studies of connectivity focus specifically in the Western Caribbean. Hogan et al. [2012] and Villegas Snchez et al. [2014] use genetic techniques to study demographic connectivity of the bicolor damselfish (*Stegastes partitus*) in different areas of the Western Caribbean. Hogan et al. [2012] found strong interannual variability, among the three years studied, in dispersal distances, self recruitment and patterns of connectivity of *S. partitus* from seven monitored

sites in south Mexico and Belize. However, in all 3 years and sampled sites, more than 80% of the juveniles were assignable to monitored sites, which provides a scale to the connectivity in this particular region. Villegas Snchez et al. [2014] studied the connections of northern Western Caribbean Mexican reefs with reefs in the Gulf of Mexico, reporting stronger within region differences in the Mexican Caribbean than between the Veracruz Reef System in the Gulf of Mexico and the Mexican Caribbean. [Chittaro and Hogan, 2012] use otolith microchemistry, a technique that uses the chemical signal of the environment recorded into the calcium carbonate balance organs (otoliths) of fish as a natural marker [Thorrold et al., 1998], to determine the natal origin of newly settled bicolor damselfish (*S. partitus*) and investigate the patterns of connectivity among populations in Mesoamerican reefs over two years.

Cowen et al. [2006] generated an IBM for larval dispersal to evaluate the spatial scales of dispersal at ecologically significant levels of reef fish populations in the wider Caribbean, including the Bahamas and Florida. With 5 years of simulations they determined that a typical larval dispersal distance capable of providing ecologically significant numbers of settlers (enough to replenish local populations) was on the scale of 50 to 100 km for most species. Paris et al. [2007] used nested ocean circulation models with maximum horizontal resolution of 2 km and Lagrangian stochastic models to study the relative influence of the physical environment and biological processes (i.e. vertical movement, mortality) on connectivity patterns of coral reef fish in the Western Caribbean. Similarly, Kough et al. [2013] used multiscale biophysical modeling techniques coupled with empirical estimates of larval behavior and gamete production to describe the pattern of larval connectivity for the Caribbean spiny lobster (*Panulirus argus)* in the wider Caribbean, including reefs in Mexico, Belize and Honduras. In general, modeling studies of connectivity identify the Western Caribbean as a strongly interconnected region but with substantial variability among locations [Kough et al., 2013; Paris et al., 2007; Cowen et al., 2006]. Strong larval retention and high levels of self-recruitment are often reported [Hogan et al., 2012; Cowen et al., 2006], as is an increase in successful settlement when Ontogenetic Vertical Migration (OVM) behavior is included [Paris et al., 2007].

The objective of this study is to investigate connectivity in the Western Caribbean

region with experiments parallel to those performed in the Kenyan-Tanzanian region in order to have directly comparable results that could help identify similar and dissimilar mechanisms driving connectivity patterns in these two coral reef regions (as described in Chapter 1). Unlike previous published numerical model estimated connectivities, such as those described above, this study focuses on the Western Caribbean at a fine spatial scale, depicting reef to reef connections.

Most studies on coral reef larval connectivity for particular species have focused on brooders or demersal spawners having short pelagic larval durations (PLDs). The family Pomacentridae is particularly well studied. This group of coral reef fish is relatively easy to sample due to their territorial site fidelity, which facilitates repeated sampling. However, most coral species are broadcast spawners and the majority of coral reef fish are pelagic spawners. In this modeling study *Acropora* corals and *Acanthurus* surgeonfish genera were selected to examine the connectivity among Western Caribbean reefs, since they encompass a wide range of PLD and larval capabilities observed in coral reef organisms. *Acropora* are representative of short PLD (12 days) passive larvae with limited reef perception skills, while *Acanthurus* have long PLD (72 days) larvae with strong perception and swimming abilities. This modeling study will benefit from the extensive existing literature on connectivity in the Caribbean region to compare results and build confidence on the applied methods that could extend to the parallel study done in the Kenyan Tanzanian region (Chapter 3), where connectivity studies at ecological time scales are scarce.

5.2 Methods

5.2.1 Hydrodynamic model

The Mesoamerican Coastal Circulation Model (hereafter MCCM), a 2 km horizontal resolution Regional Ocean Model System (ROMS) [Haidvogel et al., 2008] application of the Western Caribbean region was developed to provide 3-dimensional ocean velocity and temperature fields for the particle tracking experiments presented here. The configuration of MCCM is similar to the model developed for

the Kenyan-Tanzanian coastal region (see Chapter 2). The MCCM domain is a rect-angular grid extending from 83.3 to 89°W and 15 to 22.5^{o}S with 31 terrain following vertical levels. The model bathymetry is from the 30 sec global GEBCO product [`www.gebco.net/data_and_products/gridded_bathymetry_data/`; accessed April 2011]. The model coastline was manually edited to retain as many features as the 2 km resolution allowed. Only the Bay Islands (Utila, Roatan, Isla Barbareta and Guanaja) off Honduras, and Cozumel, Mujeres, Contoy and Holbox Islands in the northern Yucatan Peninsula are included as dry cells in the land mask (Fig. 1, Chap-ter 4). The atmospheric forcing (wind stress, heat and freshwater fluxes) is calculated by ROMS bulk formulation using atmospheric variables from daily NCEP/NCAR re-analysis [Kalnay et al., 1996]. The model is initialized from fields of the 1/10° global model OFES (Ocean General Circulation Model for the Earth Simulator, [Sasaki et al., 2006] and forced at the open boundaries by monthly OFES fields and tides from the TPXO6 global tidal model [Egbert et al., 1994;Egbert and Erofeeva, 2002. Freshwater inflows and diurnal wind variability are not included in the model. The MCCM was run continuously for 8.25 years from October 1999 to December 2007. Three-hourly averaged velocity and temperature fields for 2000 and 2005 are used for the particle tracking experiments. The MCCM is described in detail and validated against available observations in Chapter 4.

5.2.2   Lagrangian particle tracking experiments

Lagrangian particle tracking experiments parallel to those carried out for the Kenyan-Tanzanian (KT) region (see Chapter 3 for more details) were run for the Western Caribbean Region. The advection only version of Batchelder's IBM [Batchelder, 2006] used for the KT was used to track forward in time the dispersal of virtual larvae originating at WC reef polygons. The IBM runs offline using previously stored 3-hour averages of the 3-dimensional MCCM velocity and temperature fields. No explicit diffusion (e.g. random walk applied to the individual's position) is invoked. The tracking was done using a 30 min time step and the resulting particle trajectories were stored every 2 hrs. The February-March spawning period was simulated with

daily releases every 3 days for the 3-dimensional passive experiments, for a total of 20 releases during the two months. A total of ($\sim$200 000 particles were released per simulated day, at a density of 50 particles/km ^{2} from a total of 1003 reefs.

Two types of larvae were modeled representing *Acropora* coral larvae and *Acanthurus* surgeonfish. *Acropora* larvae are characterized by short (12 days) PLD. They reach competency after the first 4 days and are assumed to have minimal mobility and habitat recognition capabilities, represented by a reef perception distance of only 10 m. *Acropora* coral larvae were tracked only under the 3-dimensional passive advection scenario.

Acanthurus surgeonfish virtual larvae have a long (72 days) PLD, reaching competency after 50 days. Because of their strong swimming ability and developed sensory systems, *Acanthurus* larvae were assumed to have a 4 km reef perception distance. They were tracked under 3 different scenarios: (1) 3-dimensional passive, (2) idealized ontogenetic vertical migration and (3) temperature dependent PLD scenario. In the ontogenetic vertical migration scenario, 20 days after spawning a migration to deeper water is simulated by shifting the vertical position of the particles to 50 m depth where they are retained until competency. In the temperature dependent PLD scenario, rather than being fixed duration, PLD is assumed to change with temperature according to a quasi-universal relationship for marine organisms [O'Connor et al., 2007] adjusted for *Acanthurus* (Eq. 1, chapter 3). Due to limited computing resources, release of *Acanthurus* virtual larvae was performed only every 6 days for the non-passive scenarios, providing information from 10 release dates during February and March.

5.2.3   Seascape and visualization analysis

The Western Caribbean continental shelf is very narrow ($\sim$2 km wide) in the northern (Yucatan peninsula) region. Belize and the Honduras region south of the Bay Islands have a wider shelf ($\sim$30 km wide). Coral reefs are virtually continuous along the eastern shores of the Yucatan Peninsula. The Belize barrier reef is the longest ($\sim$230 km) in the Caribbean; in the north it joins the mainland at Ambergris Cay,

the southerly extension of the Yucatan Peninsula. From this point northward the reef system becomes fringing. There are very dense patches of small reefs inshore of the barrier reef in south Belize and at offshore banks (Chinchorro Bank, Gladen Spit and Lighthouse reefs). Patch and fringing reefs occur around the Tuneffe Atoll, Cozumel, the Bay Islands and Cayos Cochinos in central Honduras, and Misquitia Cays near the eastern boundary of our model domain. Cabo Corrientes, the southwest tip of Cuba is included in the northeast corner of our model domain. It has fringing reefs in the south and barrier reefs in the north [Spalding et al., 2001]. For the particle tracking experiments reef habitat suitable for larval settlement was represented by a total of 1003 simplified individual reef polygons extracted from the Global Distribution of Coral Reefs 2010 database [`http://data.unep-wcmc.org/`] (Fig. 5.1).

The reef to reef connectivity matrices with reefs organized by the latitude of their centroid are not very informative regarding across-shore connections, since they do not differentiate between neighbor reefs and reefs that are located at similar latitudes but are very distant in the east-west direction. This could be an important issue in the WC region due to the L shape of the coast, the complexity of the reef habitat with offshore reefs surrounding multiple islands, and the wide across-shore area covered by reefs in south and central Belize. For this reason after organizing the reefs by the latitude of their centroid, they were reorganized to cluster offshore groups of reefs at similar latitudes. The latitude axis of the reef to reef connectivity matrices is therefore a crude indication of the north-south locations of the grouped reefs. In order to synthesize the information from the reef to reef connectivity matrices and visualize the results in a more meaningful way, we grouped reefs into 22 geographical subregions, which are marked in different colors in Figure 5.1. The regional connectivity matrices are presented for all simulations. In all connectivity matrices, the number of particles that successfully settled on a reef was normalized by the number of particles released at the source reef or region and is shown as percentage.

5.3   Results

5.3.1   Passive particles

5.3.1.1   Settlement success

During 2000, *Acanthurus* settlement success experiences a steady increase from 18% to (∼30% at the end of the release period. The annual mean settlement success is 25.6% with 12.5% is due to self-recruitment. In 2005 there is a steady increase in *Acanthurus* settlement during the first 6 release dates, from <18% in February 2nd, the first release date, to (∼33% in February 17th. After that a steady decline in settlement success is observed for the following 6 release dates, to (∼25% in March 6th. Some fluctuations are observed in the remainder of release dates, but the declining pattern prevails with settlement declining to (∼22% on the last release date (March 30th) (Fig. 5.2a).Mean settlement success for 2005 is 27.1%, with 20.4% of the successful larvae self-recruiting.

Acropora virtual larvae have much lower settlement success ranging from 0.11% to 0.33% (Fig. 5.2b). Both modeled years show high variability among the 20 release dates. Fluctuations in 2000 have a smaller range, while 2005 has the lowest observed settlement success at the beginning of the modeled spawning season (February 2nd) and the highest in March 16th. This temporal pattern over the spawning period is the opposite of the pattern for *Acanthurus* settlement. Mean settlement success is 0.18% for 2000 and 0.21% for 2005, with 27.8 and 16.7% of the successful virtual larvae settling at their origin reef (self-recruiting), respectively.

5.3.1.2   Reef to reef connectivity matrices

The Gulf of Honduras region shows a distinctly different connectivity pattern from the rest of the modeled region and can be identified in the reef to reef connectivity matrices of both species groups as a high connectivity region in the SW corner (Fig. 5.3). Outside of the Gulf of Honduras successful connections for both species groups are more scattered. Differences between the 2000 and 2005 connectivity patterns are

minimal for both genera. For *Acanthurus* the intensity of connections among reefs is slightly lower in 2005.

In the *Acanthurus* passive experiment Gulf of Honduras (south of 17.8^{o}S) larvae successfully connect to reefs both northward and southward of their reef of origin as indicated by the square shape of the high connectivity region (Fig. 5.3a and c). This pattern is consistent with long PLD larvae of *Acanthurus* circulating around a permanent cyclonic eddy in a region with suitable habitat and spawning metapopulations to the south and east divided by a region without suitable habitat for settlement. Long PLD is a requirement for this pattern to exist since larvae need to have enough time to be transported through regions lacking suitable habitat in the NE and SW regions of the eddy. Slightly more north to south connections are observed, particularly in 2005. This pattern is likely due to the high density of reefs in southern Belize releasing many virtual larvae, compared to the smaller reef areas and fewer virtual larvae released from the Honduras Islands region. The Gulf of Honduras reefs also provide recruits to reefs north of the Gulf, in smaller proportions, particularly to reefs between 20.1 and 22.2^{o}S. Northward connecting larvae come from reefs at the northern and eastern Honduras Islands (Fig. 5.3) which are less likely to be entrained in the recirculating eddy feature. The high connectivity band between 18.4 and 18.7^{o}S indicates successful settlement within the reefs of Chinchorro Bank. Reefs between 20.3 and 21.6^{o}S, in the vicinity of Cozumel Island connect in high proportions ($\sim$50%) to a reef centered around 20°S, this southward transport is due to a local reversal of the northward current in the deeper strata at the southern entrance of the Cozumel Channel where a topographically steered cyclonic eddy forms [Muhling et al., 2013; Chapter 4]. Very high (> 80%) self-recruitment occurs at some reefs in the southernmost region of the Gulf of Honduras, and at Cuban reefs.

Recruitment in the *Acropora* passive experiments is very localized (Fig. 5.3b and d). Successful connections occur by self-seeding at Cuban reefs in the northern part of the domain, and north to south (or west to east) connections in the Gulf of Honduras. Connections are relatively week for reefs in the rest of the domain, except for some settlement at Chinchorro Bank. For short PLD larvae organisms, considering the configuration of reef habitat and the cyclonic eddy circulation, suc-

cessful connections are likely only along the Belize barrier reefs. The circulation promotes connections between the Belize and Bay Island reefs in the south and vice-versa in the north of the Gulf of Honduras. However, these connections are unlikely for short PLD larvae since the reef habitat gap is too large for them to move between regions. Larvae transported offshore, past the Belize barrier reefs and those transported northwestward off the Bay Islands by the cyclonic eddy circulation are lost due to the lack of habitat along the dominant flow paths during their short competency period.

5.3.1.3   Regional connectivity matrices

The regional connectivity matrices help synthesize the information from the reef to reef connectivity matrices and visualize the results in the context of known geographical regions. They are also useful to identify across-shore connections, which are difficult to discern from the reef to reef connectivity matrices organized by latitude, where north to south connections are indistinguishable from west to east connections.

Acanthurus larvae from the north (nM1, nM2) and central (cM1, cM2) Mexico regions as well as the east and west Cozumel regions (eCO, wCO) have high probabilities of connecting to central Mexico1 (Fig. 5.4a and c), due to the subsurface coastal recirculation pattern in the southern entrance of the Cozumel Channel [Muhling et al., 2013; MCCM Chapter 4)]. The eddy circulation in the Gulf of Honduras connects the three south Belize regions and Glovers and Lighthouse reefs to the Bay Islands in Honduras (nHo, sHO). The connection is bidirectional but southward and eastward connections are stronger. The three north Belize regions connect among themselves in both modeled years. In 2000 the south Mexico region has few connections to other reefs (Fig. 5.4a), while in 2005 it connects to sB3, nB2 and nB3 (Fig. 5.4c). High probabilities of settlement success at the Cuba, east Cozumel, north Honduras and north Belize 2 regions are due to within region settlement. Cuban reefs also get small proportions of recruits from all three groups of Honduras Islands as well as Glover and Lighthouse reefs. Alacranes reefs (ALA), to the north of the Yucatan peninsula get minimal settlers in both simulated years, indicating low larval

exchange from the Caribbean to other reefs in the northern Campeche Bank.

Connections for the *Acropora* larval type, even when reefs are grouped into sub-regions, are not widespread (Fig. 5.4b and d). South to north connections are more common and stronger, while north to south connections are fewer and weaker. Strong connections for *Acropora* are localized in a few areas. Similarly to *Acanthurus*, the central Mexico region gets *Acropora* virtual larvae from mainland (south Mexico region, sME) and offshore reefs around the Cozumel area (nM1, nM2, eCO, wCO). *Acropora* larvae from Chinchorro bank successfully connect to the other offshore reefs Turneffe, Glover reef, and Lighthouse reef, as well as south Belize1 and north Belize3 regions. The strongest connections for *Acropora* occur between regions to the south of Turneffe Atoll, including inshore and offshore reefs and the south Belize regions (sB1, sB2, sB3, but mainly sB2 and sB3). Strong within region connections are observed at south Belize regions 1 and 2 and at north Belize region 1. The connectivity pattern changes very little between the two modeled years, with only small variations in the strength of the connections.

5.3.1.4 Multiple origin and destination maps

The south Belize barrier reef receives and provides *Acanthurus* virtual larvae from/to more different reefs than any other region in the Western Caribbean region (Fig. 5.5 and 5.6), sourcing connections to more than 70% of the reefs and getting propagules from a slightly greater proportion of reefs. The northern shore of Roatan and Barbareta Islands in the north Honduras region provide *Acanthurus* virtual larvae to multiple different reefs. This region, however, is not well connected to source reefs, as it receives settlers from less than 2% of the reefs. The rest of the reefs in the north of Honduras region provide *Acanthurus* virtual larvae to approximately half of the reefs of the region and are also excellent sinks, receiving propagules from more than 75% of the reefs. The rims of the offshore atolls off the Yucatan peninsula, Chinchorro Bank, Turneffe Island, Lighthouse Reef and Glover Reef provide and receive *Acanthurus* larvae from more than 60% of the reefs. The southern Honduras Islands provide and receive *Acanthurus* larvae from very few reefs. Mexican coast and the

northern Cuban reefs seed less than 30% of the reefs. From them, southern Mexico reefs receive propagules from multiple sources, central Mexico reefs from slightly less and northern Mexico and northern Cuba from only a few different source reefs. North Belize reefs provide and receive *Acanthurus* larvae to/from 25% of the reefs in the region. Reefs at Alacranes, Cozumel, southern Cuba, inshore of the Belize Barrier reef and inside the atolls rims provide *Acanthurus* larvae to less than 5% of the reefs.

The south Belize barrier reef is also the best provider and receiver of Acropora providing larvae to ∼30% of the reefs in the region and receiving settlers from 47 reefs (∼0.5%) (Figs. 5.7 and 5.8). Turneffe Island reefs provide propagules to 20% of the reefs and receive larvae from around 20 different reefs. The rims of the offshore atolls provide propagules for 10% of the reefs, and are the second best destinations, receiving virtual larvae from different reefs. North Belize barrier reefs (nB1), the south Mexico and northern Cuba reefs provide *Acropora* virtual larvae to less than 5% of the reefs and receive propagules from only 15 reefs. Central Mexico reefs receive *Acropora* virtual larvae from multiple different reefs but provide larvae to very few reefs.

5.3.2   Ontogenetic Vertical Migration experiments

5.3.2.1   Settlement success

The OVM scenario generates higher settlement success than the passive scenario on all release dates, with a range between 30 and 53.7% for both years. Self-recruitment levels are highly enhanced, accounting for 54.3% of the total successful settlers in 2000 and 30.4% in 2005. Annual means for 2000 and 2005 are 37.5 and 36.4% for 2000 and 2005 respectively. In 2000, settlement success continuously increases after March 10th, reaching 53.7% in the last release date (March 30th). Smaller fluctuations among the release dates are observed in 2005 (Fig. 5.9).

5.3.2.2   Reef to reef connectivity matrices

In general, connectivity patterns in the OVM scenario are similar to the passive scenario, but the strength of the connectivity is largely different, particularly in 2005 (Fig. 5.10). In both modeled years, the Gulf of Honduras and Chinchorro Bank at 18.6ºS continue to stand out as a region of high connectivity. The Mexican Caribbean north of Chinchorro Bank and the rest of the region show opposite patterns.

North to south connections from larvae originating south of Chinchorro Bank were stronger in 2000 than in 2005, while north to south connection in the northern Mexican reefs were weaker in 2000 than in 2005. In both years a reef in the Cozumel area ($\sim$21ºN) has the strongest connections due to self-recruitment of up to 60% of the released larvae. Another region of strong connections is observed in the south at ($\sim$16.7ºN in 2000, which shifts to the corner of the Gulf of Honduras in 2005. Cuba is a strong hot-spot of connections, stronger in 2000 than in 2005.

5.3.2.3   Regional connectivity matrices

Within region recruitment is common (Fig. 5.11); it varies interannually being stronger in 2000 for the Belize reefs. The north Belize barrier reef (nB1) replenishes mainly due to self-recruitment in both modeled years. In 2000 larvae arriving into two other north Belize regions (nB2 and nB3) connect mainly among themselves with a small contribution from the south Mexico region (sME), while in 2005 they also receive virtual larvae from northern regions. The east Honduras region did not show self-recruitment and is deprived of larvae from all other regions. Its larvae, however, get entrained in the Caribbean Current and connect to most regions, but mainly the north Honduras region and regions to the north of Chinchorro Bank. The south Mexico (sME) region gets settlers from all other regions except Cuba, Alacranes and east Honduras Islands, the contribution from the three north Belize regions being minimal. Cozumel, central and northern Mexico regions connect mainly among themselves in 2000, while they show more southward connections in 2005. The Bay Islands (nHO and sHO) receive larvae from all other regions except Cuba, Alacranes and north Belize 1 and 2 in 2005, but only from reefs south of sME

in 2000.

5.3.2.4 Multiple origin and destination maps

In the OVM scenario the spatial distribution of origin reefs providing *Acanthurus* larvae to multiple reefs (Fig. 5.12) is very similar to that of the passive scenario. However origin reefs connect to fewer different reefs than in the passive scenario, with the reef with most different connections sourcing only 68% of the reefs in the region. In the case of destination reefs receiving virtual larvae from multiple different reefs (Fig. 5.13), the magnitude is very similar to that of the passive scenario but the spatial pattern changes. The reefs receiving virtual larvae from the greater number of origin reefs are now located in the south Mexico region, followed by Chinchorro Bank and the Bay Islands. Similarly to the passive scenario the south Belize reefs, Lighthouse Reef and Glover reefs are common destination. The cM1 region receives *Acanthurus* virtual larvae from more different origin reefs in this scenario than in the passive one, conversely to the southern Cuba reefs that have fewer sources.

5.3.3 Temperature dependent Pelagic Larval Duration Experiments

5.3.3.1 Settlement success

The temperature dependent PLD scenario produces the lowest settlement success of all *Acanthurus* scenarios with a range of 5.3% to 17.8% (Fig. 5.14). Variability among the release dates was low, with both years showing the lowest settlement success at the beginning of the spawning season. Mean settlement success was very similar for the two modeled years; 11.3% and 12.3% for 2000 and 2005, respectively. In this scenario settlement success is slightly higher than in the passive scenario, accounting for 18.6% of the successful settlers in 2000 and 17.9% in 2005.

5.3.3.2   Reef to reef connectivity matrices

The connectivity pattern of the temperature dependent PLD scenario shows that in general long distance connections decrease (Fig. 5.15) due to the reduction in larval duration caused by warm temperatures. Under the temperature dependent scenario the mean precompetency period decreases to 37 days instead of the 50 days for the passive scenario (Fig. 5.16). North to south connections on reefs to the north of Chinchorro Bank and south to north connections in the Gulf of Honduras decrease in comparison to the passive scenario, especially in 2000. For short PLD organisms, the habitat distribution favors north to south connections in the Gulf of Honduras more than the reciprocal south to north connections, as seen for *Acropora*. This is also true for *Acanthurus* virtual larvae with shorter PLD due to the temperature dependence. Self-recruitment continues to be important in some regions, producing the strong settlement hot-spots in the Cozumel region and south in the Gulf of Honduras.

5.3.3.3   Regional connectivity matrices

When grouped by region (Fig. 5.17) the predominance of north to south connections in the temperature dependent PLD scenario becomes more evident, as well as the reduction in dispersal distance. Self-recruitment is the most important source of recruits for the nHO, nB1, nB3, eCO, nM1, sME regions in both modeled years. The self-recruitment contribution is also important for the sB3 and cM1 regions. The strongest connections in both years are from the north Mexico region to cM1. Other strong connections occur between Chinchorro Bank reefs and the sB2 and sB3 regions. In this scenario the east Honduras Islands are relatively isolated from all other regions having only very weak connections with the south Mexico region. This connection is slightly stronger in 2005.

5.3.3.4   Multiple origin and destination maps

The spatial pattern of reefs receiving virtual larvae from multiple origins (Fig. 5.18) is very similar under the temperature dependent PLD scenario and the passive scenario. The number of reefs reached by strong *Acanthurus* origin reefs decreases slightly in comparison to the passive scenario, with a single origin reef connecting to at most 63% destination reefs. This is also true for reefs receiving propagules from multiple origin reefs (Fig. 3.20), the spatial pattern persists and the number of different reefs connecting to them decreases to 78% of the reefs for the reef with more different sources, the south Belize Barrier Reef.

5.4   Discussion

The circulation of the Gulf of Honduras, driven by complex eddy interactions (Fig. A.7 and A.9), creates strong connectivity for both *Acropora* and *Acanthurus* larval types. In the case of *Acanthurus* virtual larvae the connections are bidirectional in the north-south and east-west directions, while for the *Acropora* north to south connections are the most common (Fig. 5.4). Long distance connections are common in *Acanthurus* (Fig. 5.3). *Acropora* connections are very sparse and concentrated only in a few spots; Cuban reefs, Chinchorro Bank and the Gulf of Honduras (Fig. 5.3). *Acropora* dispersal distance is much shorter than *Acanthurus*, settling more often within $1/2^o$($\sim$50 km) of their natal reef, except at the Chinchorro Bank and Gulf of Honduras where they recruit up to 3^o ($\sim$300 km) away from their natal reefs.

The general patterns of connectivity of the different larval types and the different scenarios for *Acanthurus* (OVM and temperature dependent PLD) did not change dramatically between the two modeled years (2000 and 2005). The magnitude of the connections however shows important variations between the two modeled years with the location of connectivity hot-spots changing between the 2000 and 2005 simulations.

The ontogenetic vertical migration consistently increased settlement success in comparison with the passive scenario, in agreement with results from previous modeling studies in the Caribbean [Paris et al., 2007] and the California Current [Drake

et al., 2013]. The increase in settlement success was, however, not as large as that reported by Paris et al., [2007] for other regions of the wider Caribbean.

Self-recruitment is an important mechanism for both larval types accounting for an average of 22.3% of the *Acropora* successful settlers and 16.3% of the *Acanthurus* in the passive scenario. A great increase in self-recruitment is observed for *Acanthurus* under the OVM scenario, with an average of 42.4% of successful settlers returning to their reef of origin. High levels of self-recruitment have been reported for several species of coral reef fish using both otolith tagging [i.e. Amphiprion polymnus, Jones et al. [2005]; Amphiprion percula and Chaetodon vagabundus, Almany et al. [2007] and genetic techniques (*S. partitus*, Christie et al. [2010a]; Thalassoma bifasciatum, Swearer et al. [1999]). The level of self-recruitment for *Acanthurus* virtual larvae fluctuates among the different modeled scenarios with a minimum of 12.5% in the 2005 passive simulation and a maximum of 54.3% in the 2000 OVM simulation. Median values from this modeling study are lower than empirical estimates for different coral reef fish. There are multiple reasons for this discrepancy; 1) *Acanthurus* is a pelagic spawner, adults release their gametes near the surface at the reef edges, which promotes their dispersal since the egg stage. 2) They are a long PLD species, modeled here with a maximum PLD of 72 days (50 day pre-competency). 3) *Acanthurus* have been observed to settle near conspecifics [Lecchini et al., 2005], but their habitat requirements are not as specific as for the commonly studied anemonefish and damselfish, which may not find many options for suitable settlement far away from their birth place. From an ecological perspective, larval behaviors are intended to reduce dispersal distance and increase settlement success. Since the particle tracking model scenarios presented here are still highly idealized, it is likely that these results represent an upper bound for the dispersal capabilities of *Acanthurus* and the lower bound of their self-recruitment capabilities. Tagging techniques have not been applied to long PLD pelagic spawners and unlikely to work for *Acanthurus* larvae. Genetic techniques would be the most adequate methods to elucidate the scale of dispersal of *Acanthurus* and their self-recruitment probability. Genetic studies of contemporary connectivity for a long PLD and therefore long distance dispersing species would imply a great sampling effort and have not been conducted for this

genus to date.

Several genetic studies have focused on the damselfish Stegastes partitus to study connectivity at ecological time scales in the Western Caribbean region. Studies using microsatellites as genetic markers reported a weak but significant large scale genetic structure for the *S. Partitus* Caribbean population, on the order of 1 000 km or greater [Purcell et al., 2006; [Salas et al., 2010]]. The model scenario that would best compare to these studies of damselfish, which is a brooder species with PLD ranging between 24 and 40 days [Wellington and Victor, 1989], is the one including temperature dependent PLD. The environmental temperature indeed shortened the PLD of the *Acanthurus* virtual larvae, with the majority of them reaching competency before 40 days in the pelagic environment (Fig. 5.16). Under this scenario the long distance connections reported here for *Acanthurus* virtual larvae agree with the large scale genetic structure reported for the shorter PLD (∼30 days) damselfish.

Hogan et al. [2012] sampled juvenile and adult *S. partitus* in 7 coral reef sites in south Mexico and Belize from 2005 to 2007 and used genetic fingerprinting to assign juveniles to their site of origin. Their sampled sites correspond to the sME, nB1, TUR and sB1 regions presented here. They were able to assign 35% of the sampled juveniles to a particular sample site. From those, 15% were found to be self-recruits, while 85% came from other sampled sites. They reported strong interannual and spatial variability of their results, concluding that there was no predictability in the larval dispersal pathways from one year to the next. In 2005 enhanced local retention was reported as well as bidirectional connectivity with slightly stronger north to south connections. According to their estimates, *S. partitus* traveled an average of 77 km ± 6 km during their ∼30 days larval duration, with the majority of assignable juveniles recruiting within a radius of 60 km or less of the natal reef but 5% of the assignable larvae traveled across the full extent of their sampling region (∼200 km). There was no decline of connectivity strength with distance among sites. At the site level, a temporal mean of 65% of self-recruitment is reported for Turneffe Atoll, while 1.7% juveniles of the atoll come from external, unsampled sites. Results of our passive and OVM scenarios for *Acanthurus* showed bidirectional connectivity with stronger north to south connections for sME, nB1, TUR and sB1 regions, in

agreement with the general pattern described by Hogan et al. [2012]. However, our temperature dependent scenario for *Acanthurus*, the most similar to *S. partitus* regarding PLD shows minimal south to north connections. The modeled results with *Acanthurus* in regions sampled by Hogan et al. [2012] present some self-recruitment, but it represents the greatest proportion of *Acanthurus* settlers only for the sB1 region. Most of the modeled connections for *Acanthurus* fall within the ($\sim$200 km long dispersal distance reported by Hogan et al. [2012] for S. partitus, however long distance connections for *Acanthurus* spanned the full modeled domain ($\sim$650 km).

The otolith microchemistry study by Chittaro and Hogan [2012] identified the source locations of S. partitus collected at Chinchorro Bank and Turneffe Island based on the natal isotopic signal of the otholit's postcore and the chemical maps of potential source population generated from the isotopic signal of the otholit's edge, representative of the current environment. 26% of their sampled fish originated from unsampled source locations, beyond the Mexican and Belize Barrier reefs. 66% of the collected organisms at both offshore atolls came from Turneffe, indicating that S. partitus larvae commonly travel the 146 km between the two sites. They reported high levels ($>$74%) of self-recruitment for both Turneffe Atoll and Chinchorro Bank but highlighted the substantial temporal variability in recruit composition and connectivity among S. partitus populations. Only in the OVM simulated scenario, did more than 3% of the released *Acanthurus* virtual larvae released in Turnaffe Atoll connect to Chinchorro Bank and vice-versa. Simulated self-recruitment was more important at Chinchorro Bank than at Turnaffe Atoll. In this simulation, the main reefs providing *Acanthurus* larvae to Chinchorro Bank and Turnaffe Atoll were Lighthouse Reef, Glover Reef and the Honduras Islands, to the south of Chittaro and Hogan [2012] sample sites.

Villegas Sanchez et al. [2013] investigated the connectivity between *S. partitus* populations in the Mexican Caribbean region and the Veracruz Reef System (VRS) in the Gulf of Mexico using microsatellites as genetic markers. Chinchorro Bank and Cozumel exhibited restricted gene flow with Puerto Morelos, a reef in the nM2 model region. The population of this later reef was, however, genetically similar to the S. partitus population of a reef of the VRS. In this modeling study there was minimal

connectivity among the Cozumel, Chinchorro Bank and nM2 regions. The westward extension of the model domain used in this study does not allow to investigate the connections of Caribbean and Gulf of Mexico reefs. Connections to the reefs in the northern coast of the Yucatan Peninsula, near Alacranes Atoll would be the only indication of a connection to the Gulf of Mexico. The Alacranes region, however, does not get recruits from any other region within the model domain, indicating that larvae connecting the MC and the VRS are not likely to travel through the Campeche Bank nor use it as a stepping stone to connect to coral reef populations in the Gulf of Mexico. S. partitus larvae connecting from the MC to the VRS could be transported instead in the Loop Current, which flows northward past the Campeche Bank and into the Gulf of Mexico as the trajectories of the Lagrangian drifters deployed by Muhling et al. [2013] suggest.

The genetic similarity between a reef in the Gulf of Mexico and Puerto Morelos, and the difference between these two and other Mexican Caribbean reefs sites to the south (Cozumel and Chinchorro Bank) reported by [Villegas-Snchez et al., 2010] indicate a discontinuity in the connectivity of reef fish populations along the eastern shores of the Yucatan Peninsula. In our simulations, the nM2 region, which includes Puerto Morelos, has minimal connections with the Cozumel and Chinchorro Bank regions. Virtual larvae from the bank and the island are mainly influenced by the offshore Yucatan Current, while the larvae in the nM2 region are subject to small scale coastal flows that often recirculate (Fig. A.6 and A.8).[Purcell et al., 2006] also found significant genetic differences between S. partitus populations from Puerto Morelos (nM2) and Mahaual in the sME region. The results of the *Acanthurus* simulations similarly indicate a discontinuity in connectivity at the sME, which gets recruits from both southward and northward reefs.

In these simulations, bidirectional connectivity is common for regions to the south of sME, while reefs to the north show more unidirectional southward connections. The trajectory of drifter buoys analyzed by Muhling et al. [2013] also confirms this pattern. Drifter released at the Chinchorro Bank region showed bidirectional dispersal along the coast after 1 week. After 2 weeks, 42.9% of the drifters were retained south of 21ºN, while 53.6% had reached the Gulf of Mexico. Drifters released at the

Western Gulf of Honduras were retained south of 20°N after 1 week and remained in the Western Caribbean region after 2 weeks. Drifters passing through the Cozumel region tend to continue northward with 72.3% of them leaving the Western Caribbean after 2 weeks (their Fig. 6). The majority of successful larvae from the Cozumel region connect southward, which seems counterintuitive, considering the direction of the main flow and the trajectory of drifter buoys released in the region. Many virtual larvae travel to the north with the main flow, but they do not successfully settle since most of them leave the model domain before reaching competency. The successful larvae accounted for in the connectivity matrices are those retained very close to shore, subject to return flows that do not influence drifter buoys deployed offshore.

The location of the discontinuity in alongshore connectivity reported by genetic studies, drifter buoys trajectories and this modeling study coincides roughly with the region where the Caribbean Current impinges in the eastern Yucatan shelf and turns northward to form the Yucatan Current. The latitude of this location varies interannually depending on the angle of the CC (Chapter 4). This seems to be an oceanographic barrier to dispersal, detected by both genetic studies and the present modeling study. To the north of this location the offshore flow is mainly northward but there are southward coastal return flows (Figs. A.6 and A.8) connecting the north Mexico (nM1 and nM2) regions with the central and south Mexico (sME, cM2, cM1) regions. To the south of these locations eddy activity prevails creating a complex bidirectional connectivity pattern (Figs. A.7 and A.9).

Kough et al. [2013] described the Caribbean-wide connectivity pattern of the long PLD (5-9 months) Caribbean spiny lobster (*Panulirus argus*) using a multi-scale biophysical model coupled to empirical estimates of larval behavior and gamete production. Their results indicate that the lobster populations of Cuba are largely self-recruiting while the Honduras population depends on larval subsidies from other countries. This model for *Acanthurus* also shows Cuban reefs as strongly self-recruiting, while the Honduras reefs receive additional recruits from other regions. This difference could be simply due to the spatial scale of the models used. Many possible sources of larvae for the Honduras Island are excluded from our domain since they represent the easternmost reef habitat included. Larvae from sources

not included in this model but present in the Kough et al. [2013] model may account for a large proportion of the Honduras recruits. Similar to the findings of Kough et al. [2013] for the Wider Caribbean, international connections among Western Caribbean reefs were very common in this study, particularly between Honduras and Belize reefs. This highlights the importance of international collaborations to protect the interconnected coral reef ecosystems of the region.

The connectivity patterns and scale of dispersal for *Acanthurus* larvae resulting from this modeling study agree with the general patterns previously reported for other coral reef fish species with shorter PLD. Levels of recruitment are low in comparisons to other studies, but considering the long larval duration and the spawning behavior of the genus, this could illustrate a real interspecific difference among coral reef fish.

This study provides connectivity patterns for two ecologically important coral reef genera (*Acropora* and *Acanthurus*) in the Western Caribbean region. The subregional focus of this study and high horizontal resolution (2 km) of the ocean circulation model used provide a level of details greater than previous modeling studies for the Wider Caribbean that include this region [i.e. Paris et al., 2007; Cowen et al., 2006]. This information is relevant to developing spatial management strategies and conservation efforts at the national and international level. After evaluating the robustness of these results by assessing the sensitivity of the connectivity patterns to the various assumptions made in these simulations, the results presented could be further analyzed in the context of Marine Protected Area management to generate specific recommendations for local communities, managers and government agencies addressing the multiple local and global threats affecting the Western Caribbean reefs.
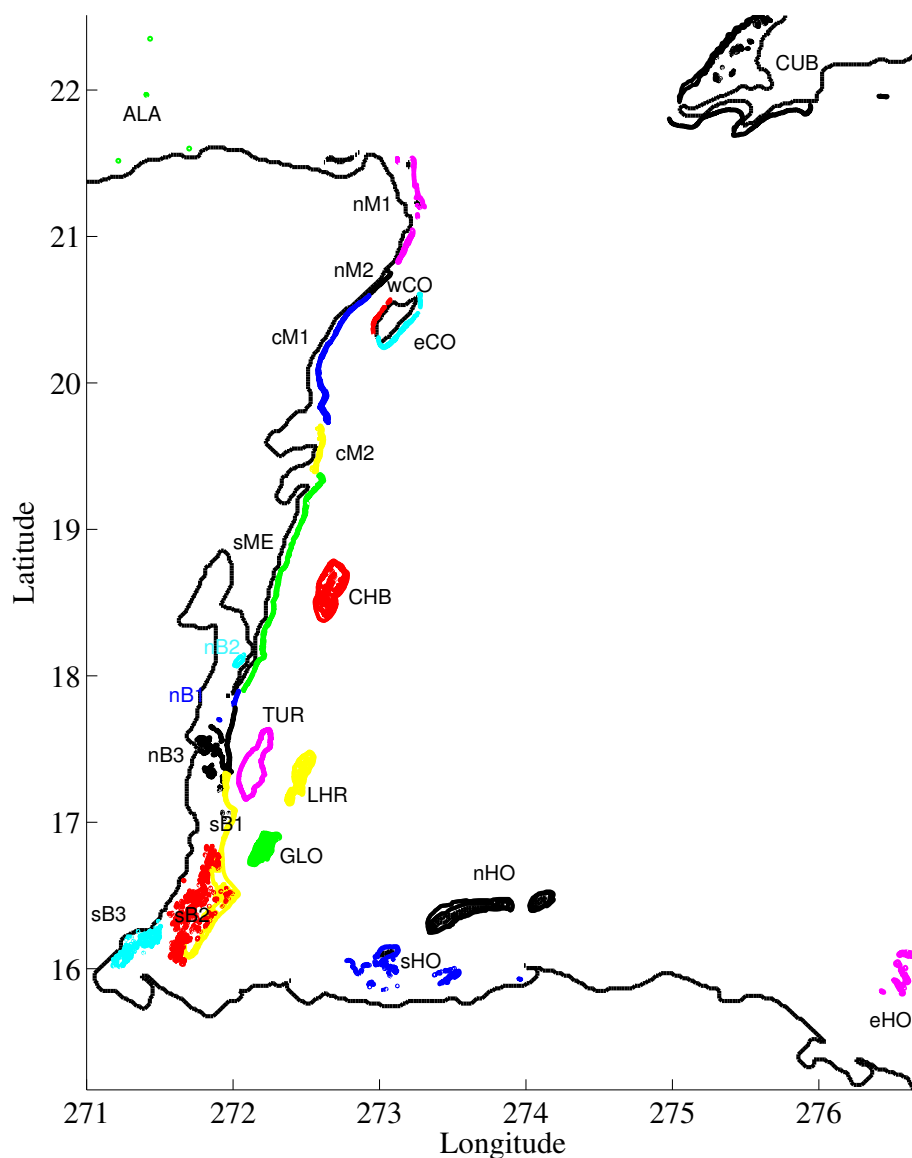
Figure 5.1: Study area with coral reefs grouped by color into 22 regions: CUB=Cuba, ALA=Alacranes reefs, CHB=Chinchorro Bank, TUR=Turneffe Atoll, LHR=Ligth House Reef, GLO=Glober Reef. The rest of the regions are labelled by 2 letters, one indicating north-south location: n=north, c=central, s=south, e=east, w=west, another one indicating country: M=Mexico, B=Belize and H=Honduras, and a number that when there are various regiones at the same latitude indicates 1=offshore, 2=mid-shelf, 3=inner shelf.
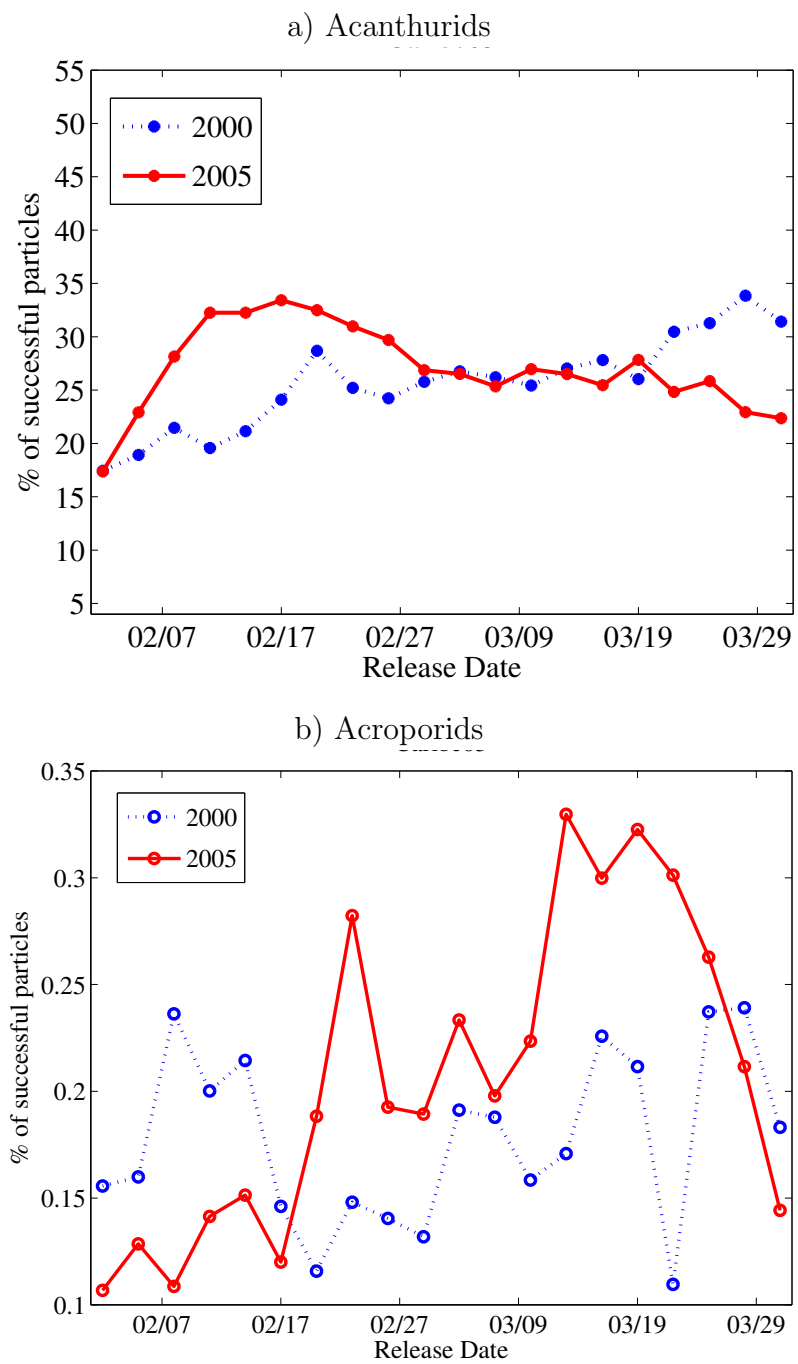
Figure 5.2: Percentage of settlement success per each simulated release date during 2000 and 2005 for the a) Acanthurids and b) Acroporids species groups.
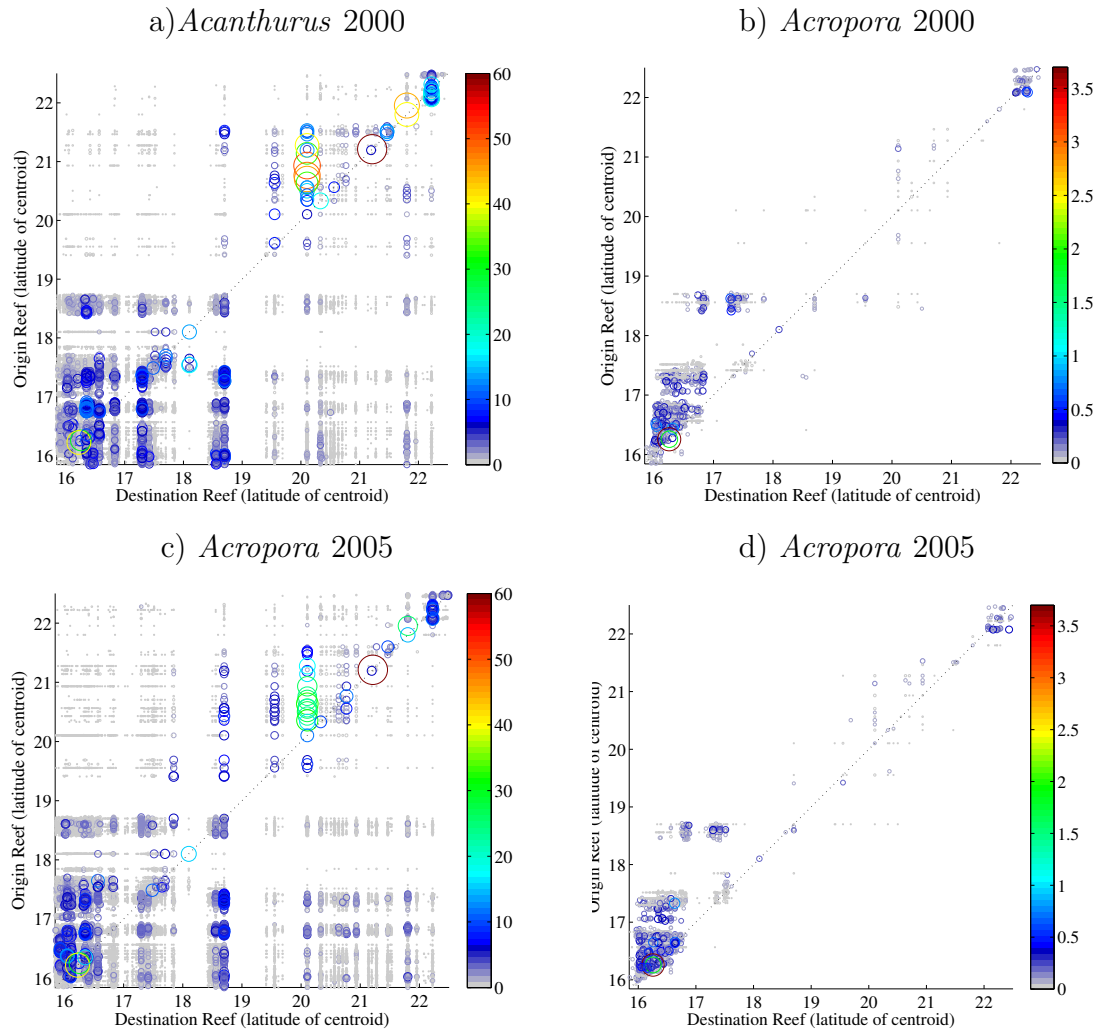
Figure 5.3: Reef to reef connectivity matrices with reefs organized by the latitude of their centroids. Color and size of the circles are proportional to the percentage of successful connections from origin to destination reefs according to the colorbar.
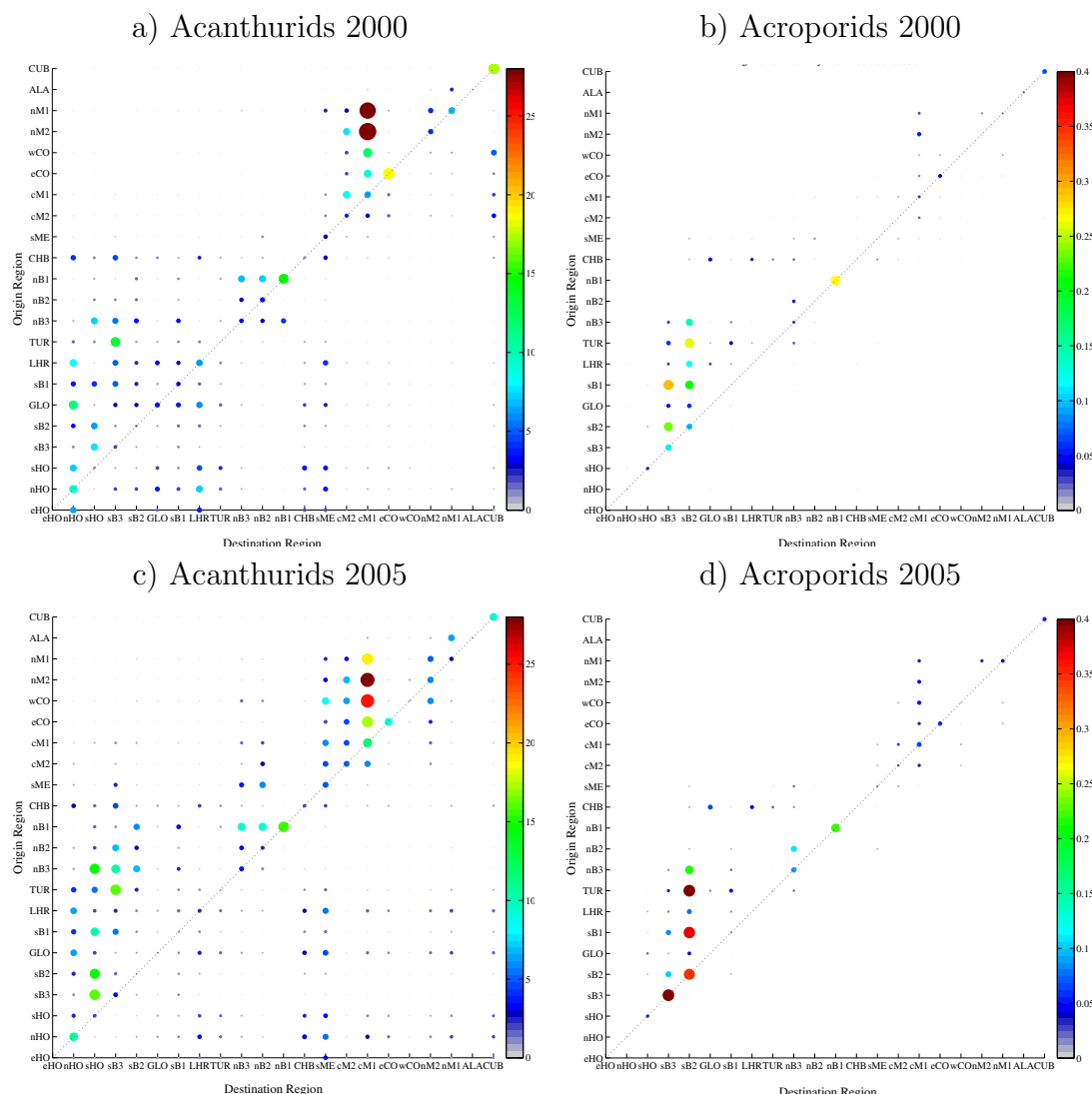
Figure 5.4: Region to region connectivity matrices with reefs grouped into 22 regions according to Fig. 5.1: CUB=Cuba, ALA=Alacranes reefs, CHB=Chinchorro Bank, TUR=Turneffe Atoll, LHR=Ligth House Reef, GLO=Glober Reef. The rest of the regions are labelled by 2 letters, one indicating north-south location: n=north, c=central, s=south, e=east, w=west, another one indicating country: M=Mexico, B=Belize and H=Honduras, and a number that when there are various regiones at the same latitude indicates 1=offshore, 2=mid-shelf, 3=inner shelf. Color and size of the circles are proportional to the percentage of successful connections from origin to destination reefs according to the colorbar.
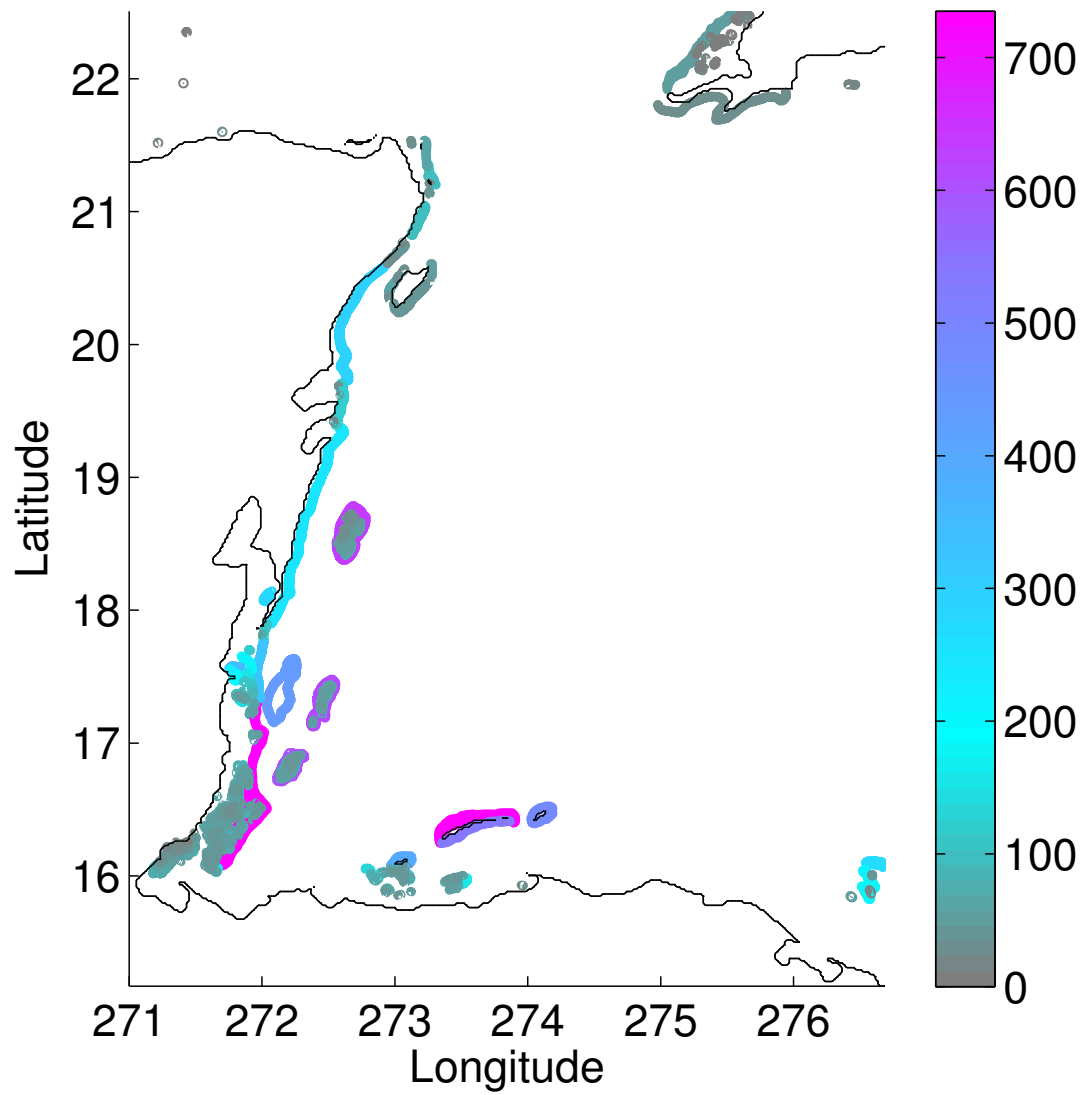
Figure 5.5: Reefs color coded by the number of different reefs reached by *Acanthurus* virtual larvae originated on them on both simulated years to identify the best destination reefs.
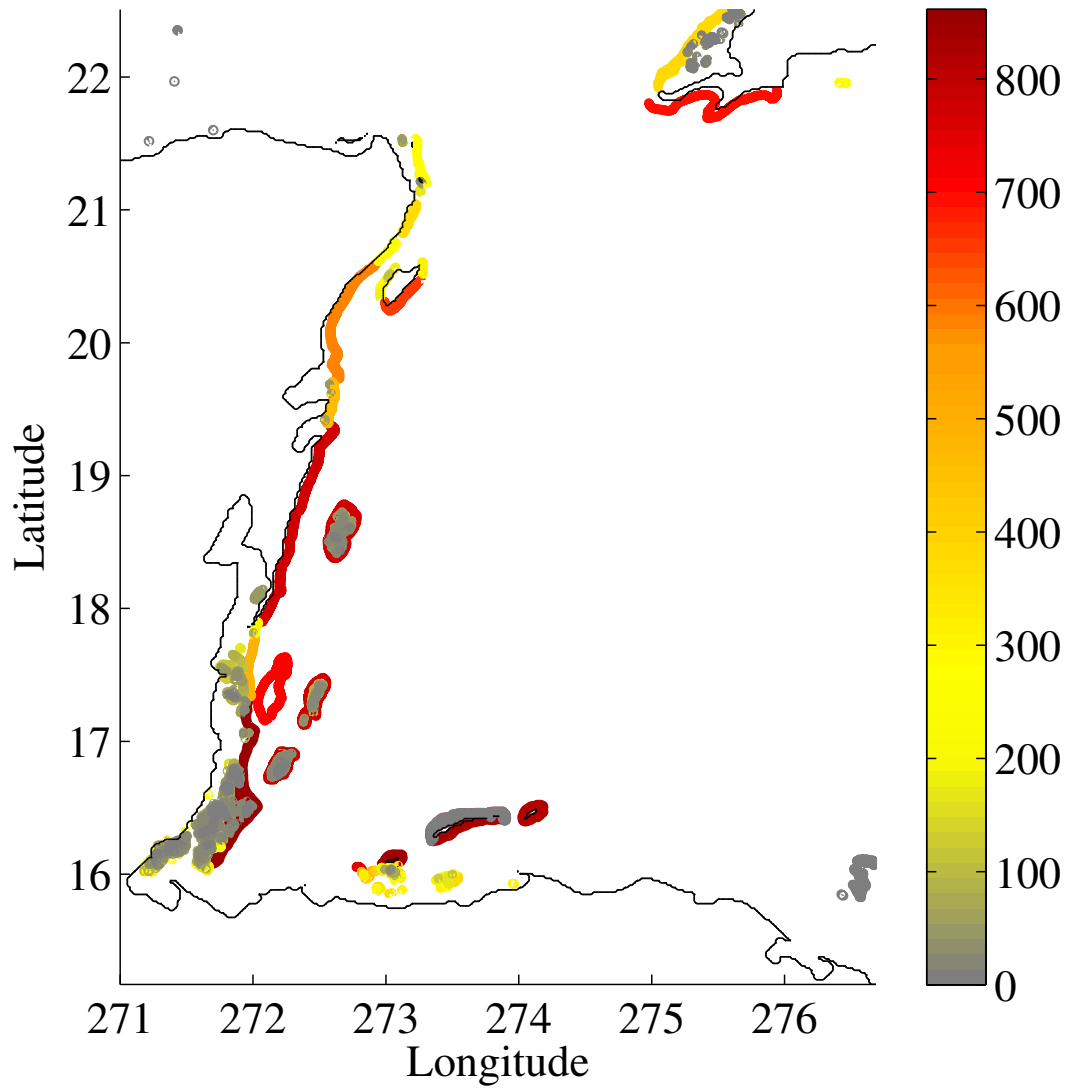
Figure 5.6: Reefs color coded by the number of different reefs it received *Acanthurus* virtual larvae from, on both simulated years to identify the best destination reefs.
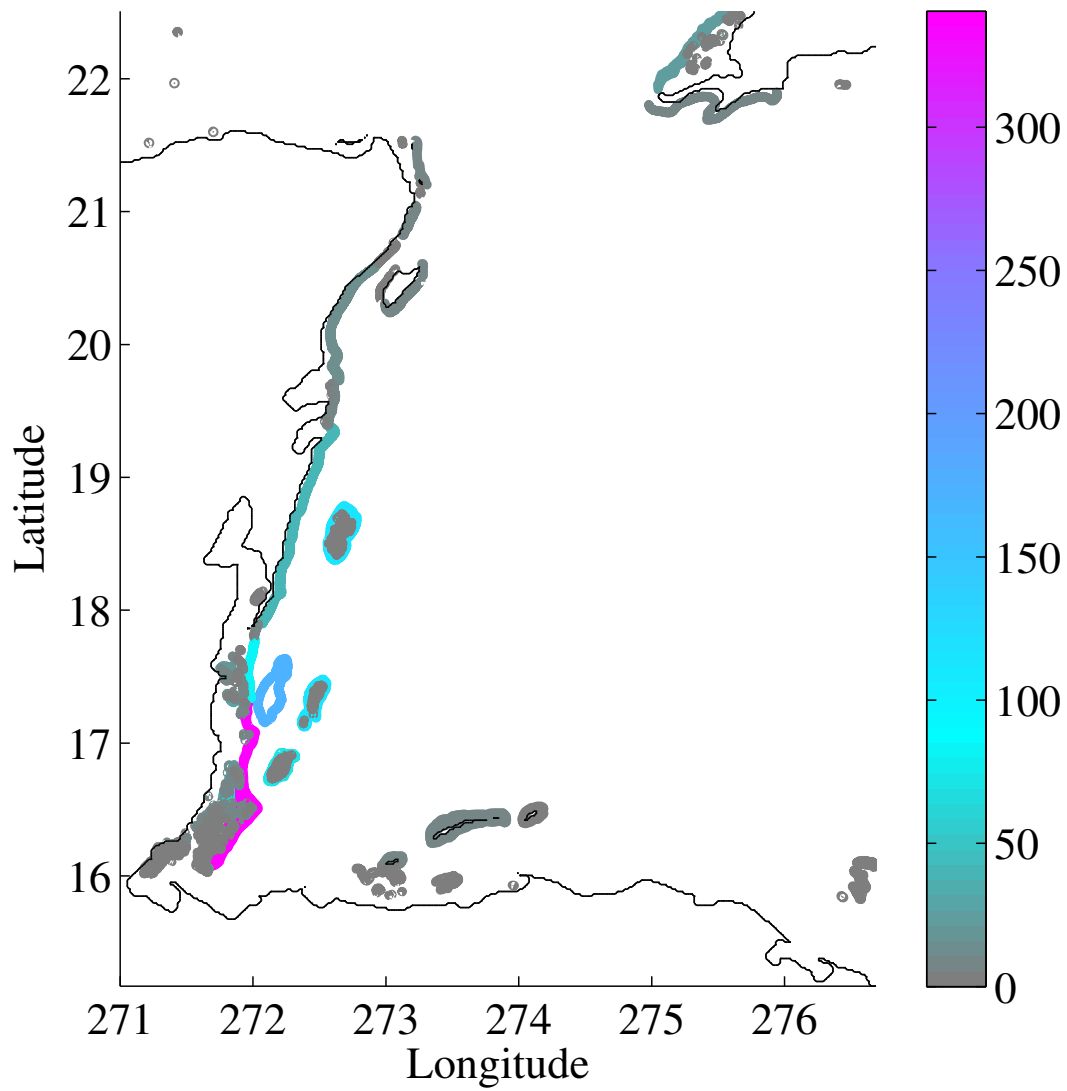
Figure 5.7: Reefs color coded by the number of different reefs reached by *Acroporids* virtual larvae originated on them on both simulated years to identify the best origin reefs.
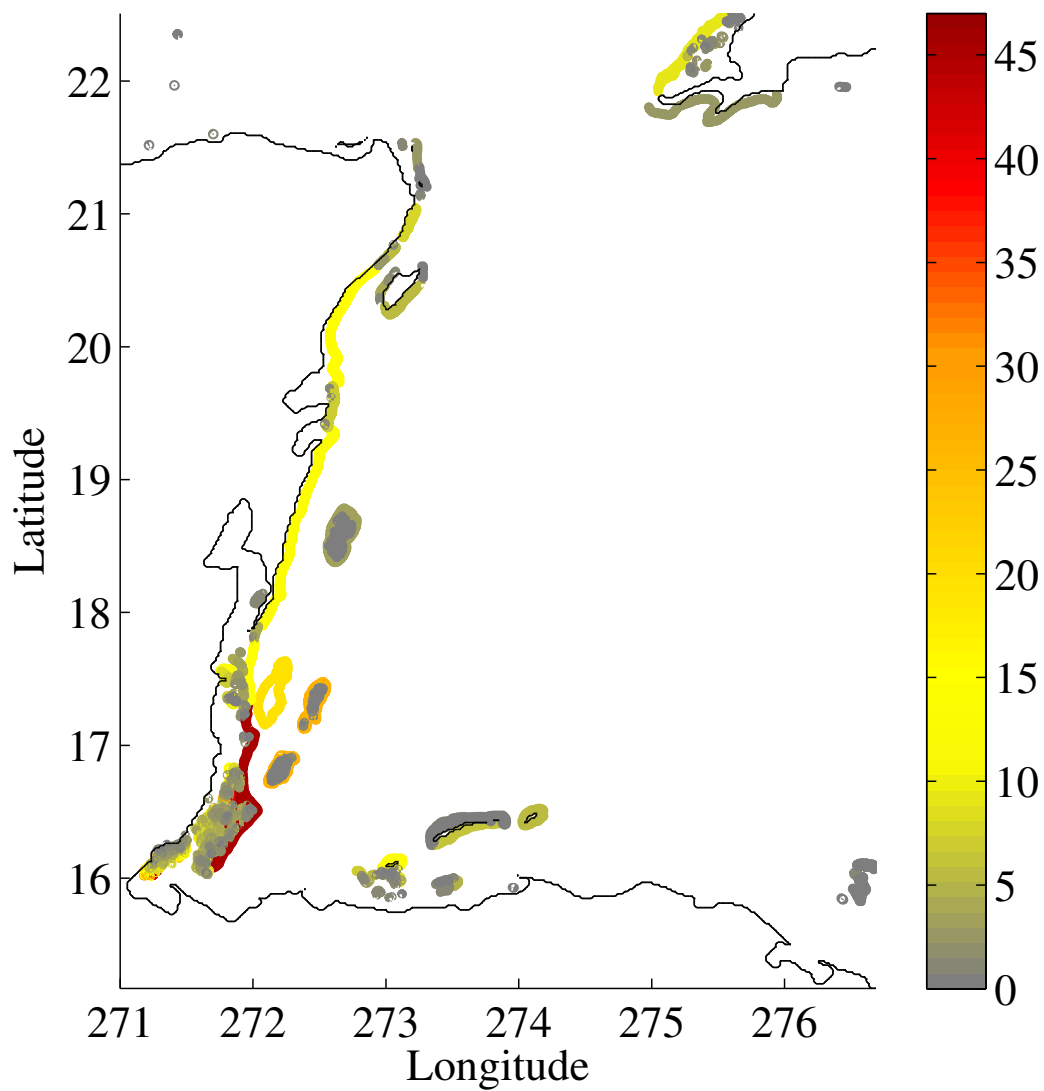
Figure 5.8: Reefs color coded by the number of different reefs it received *Acroporids* virtual larvae from, on both simulated years to identify the best destination reefs.
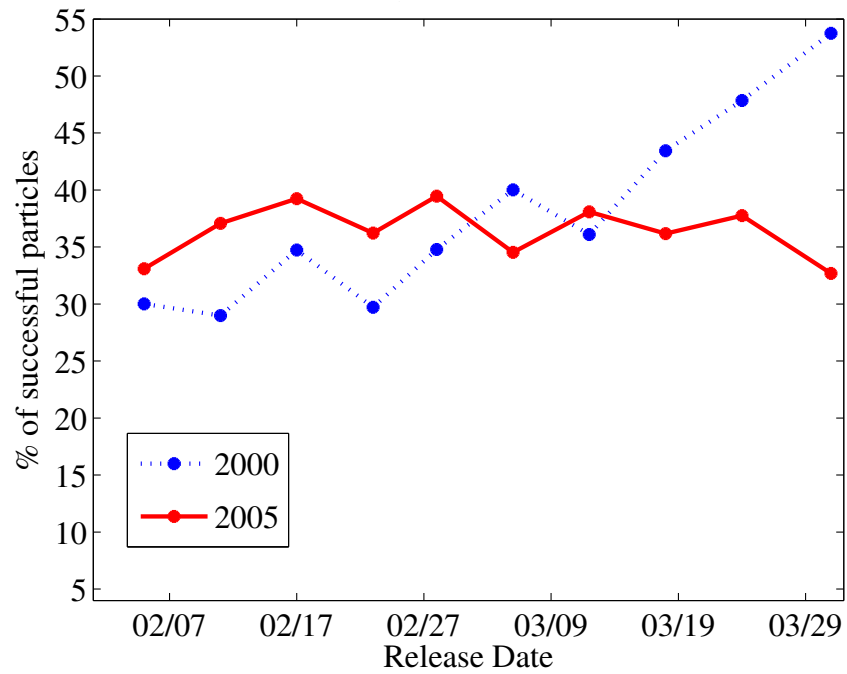
Figure 5.9: Percentage of settlement success per each simulated release date during 2000 and 2005 for *Acanthurus* virtual larvae with an idealized Ontogenetic Vertical Migration (OVM).
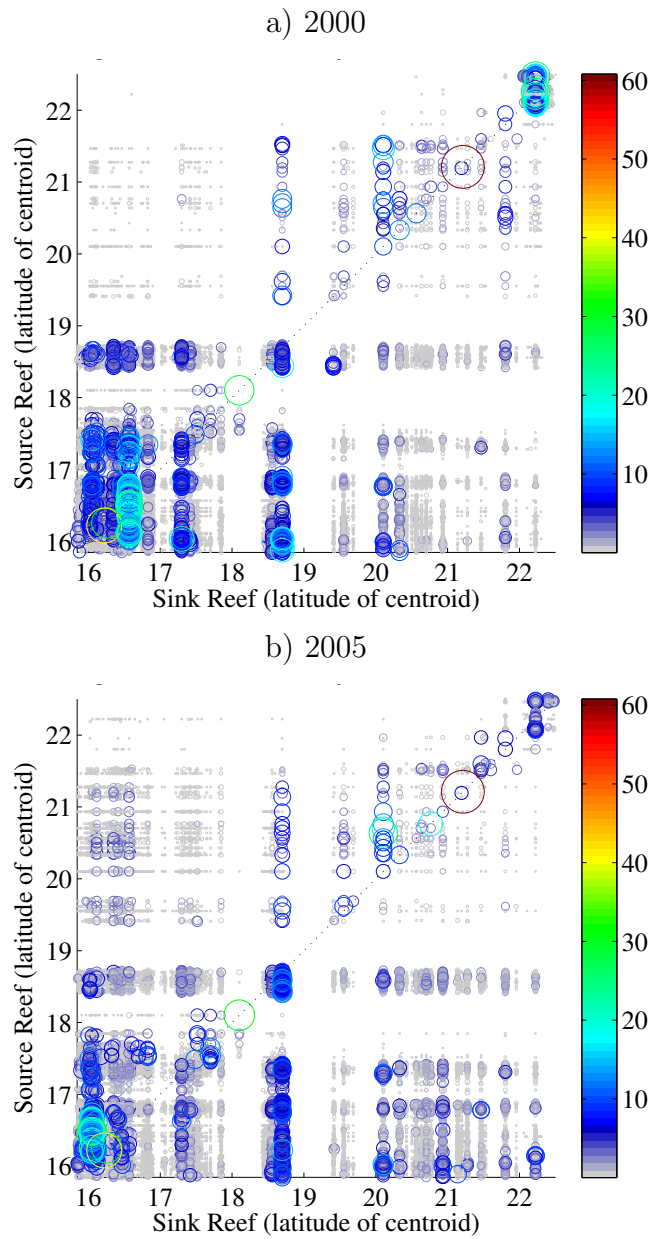
Figure 5.10: Reef to reef connectivity matrices for *Acanthurus* with OVM with reefs organized by the latitude of their centroids. Color and size of the circles are proportional to the percentage of successful connections from origin to destination reefs according to the colorbar.
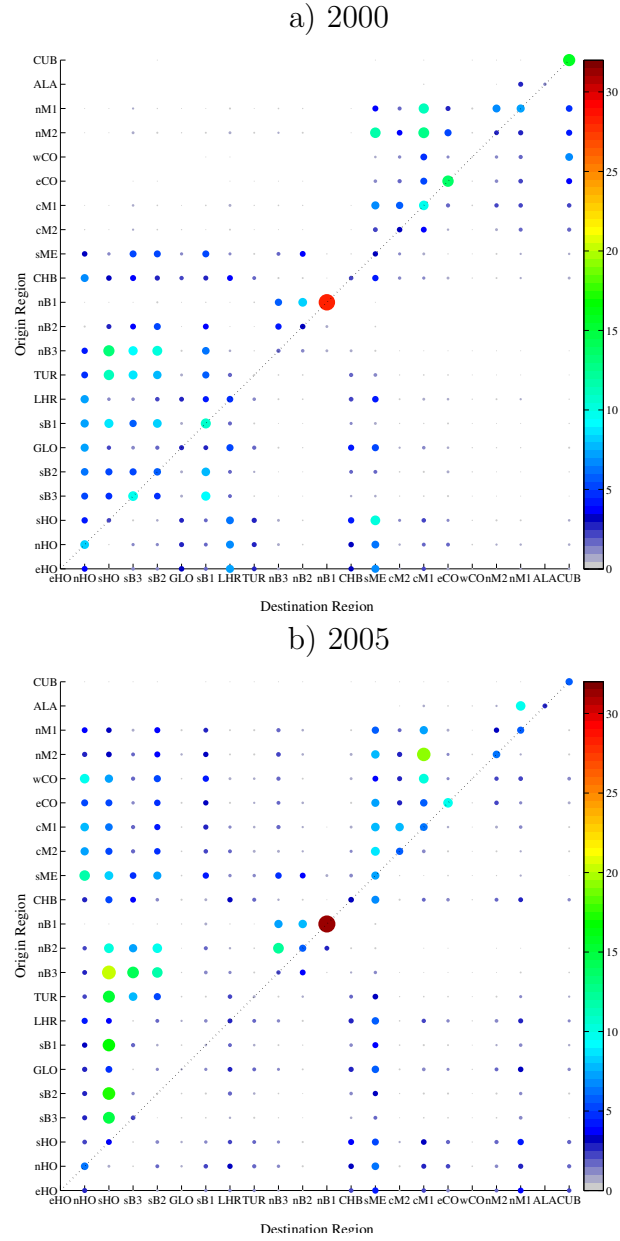
Figure 5.11: Region to region connectivity matrices for *Acanthurus* virtual larvae with OVM. Reefs were grouped into 22 regions identified by two letters in Fig. 5.1. Color and size of the circles are proportional to the percentage of successful connections from origin to destination reefs according to the colorbar.
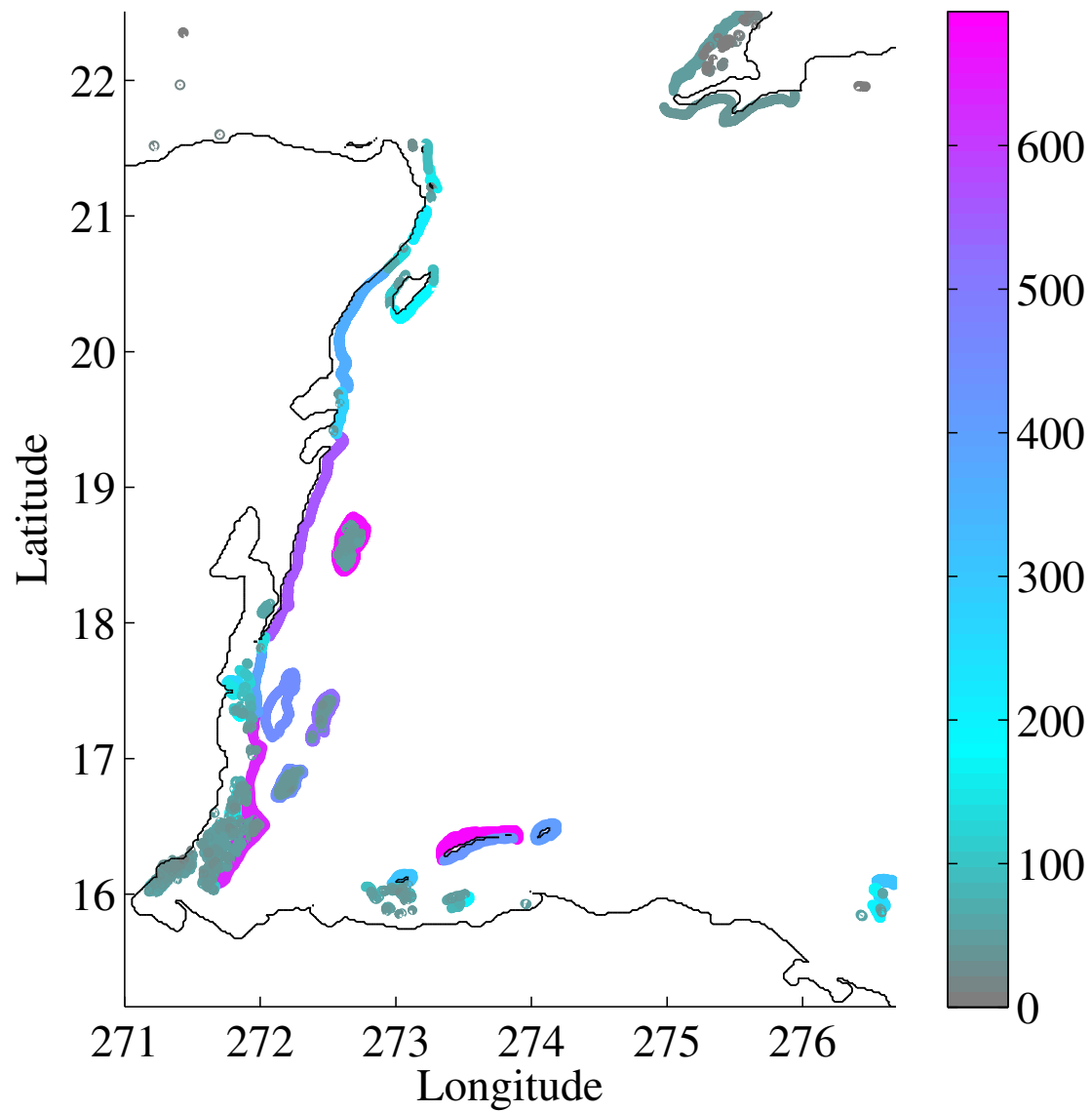
Figure 5.12: Reefs color coded by the number of different reefs reached by *Acanthurus* virtual larvae with OVM originated on them on both simulated years to identify the best origin reefs.
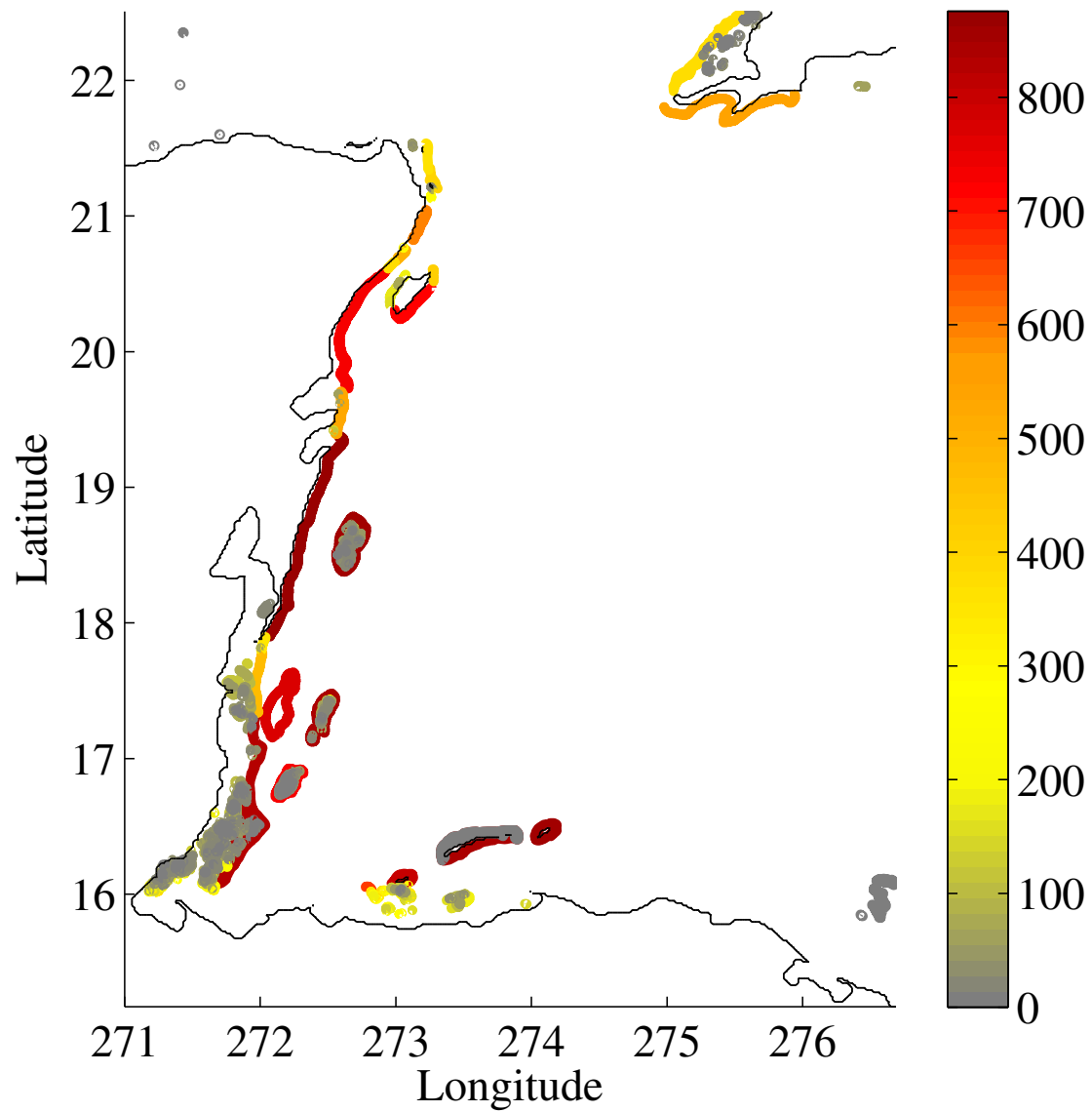
Figure 5.13: Reefs color coded by the number of different reefs it received *Acanthurus* virtual larvae with OVM from, on both simulated years to identify the best destination reefs.
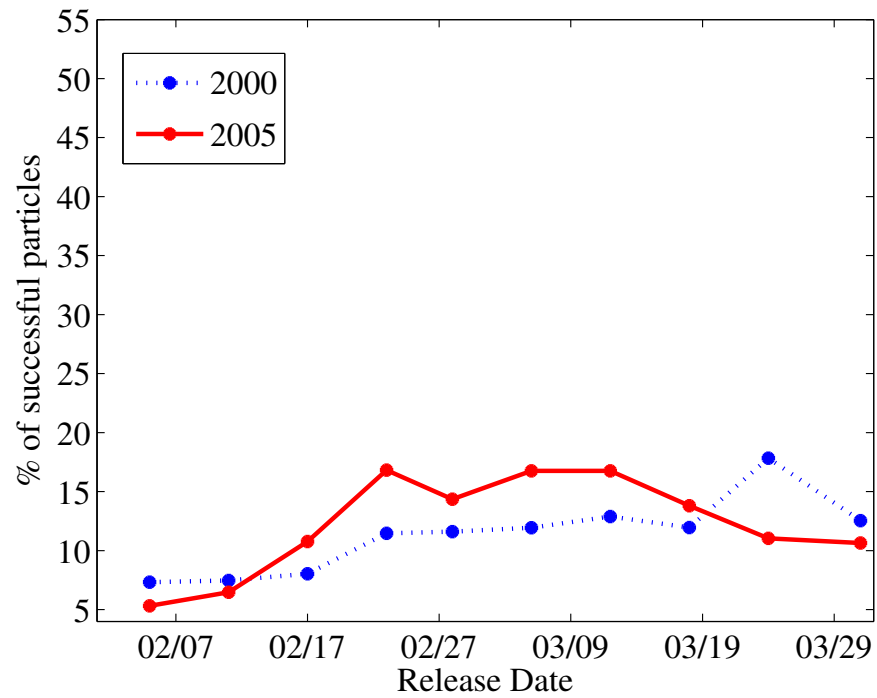
Figure 5.14: Percentage of settlement success per each simulated release date during 2000 and 2005 for *Acanthurus* virtual larvae with temperature dependent PLD.

a) 2000

b) 2005
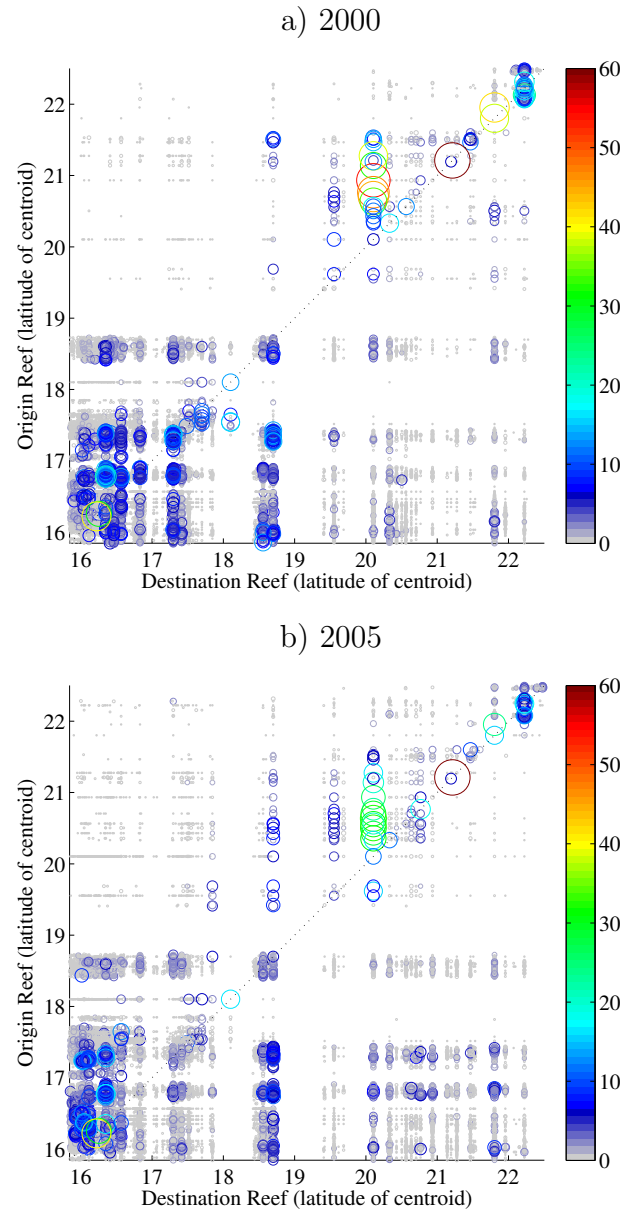
Figure 5.15: Reef to reef connectivity matrices for *Acanthurus* with temperature dependent PLD with reefs organized by the latitude of their centroids. Color and size of the circles are proportional to the percentage of successful connections from origin to destination reefs according to the colorbar.
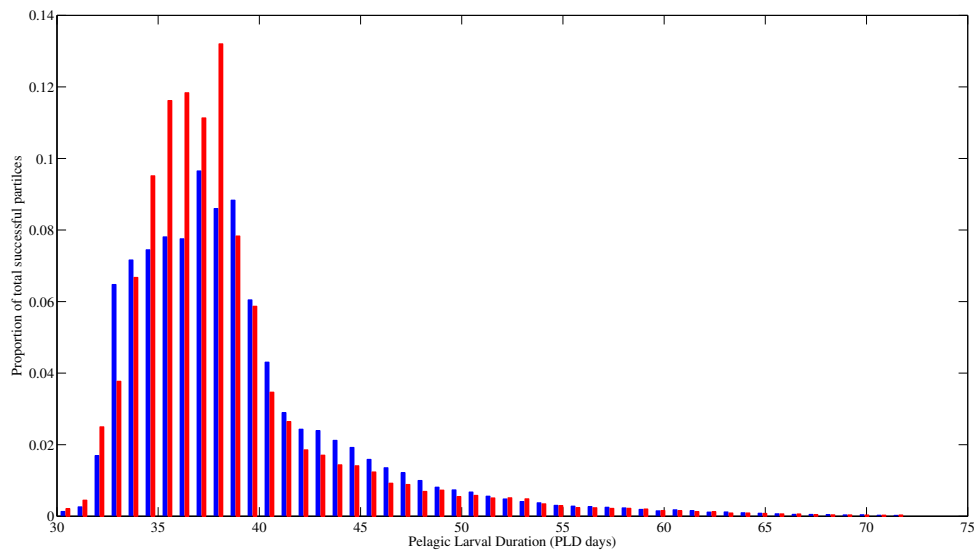
Figure 5.16: Histograms showing the distribution of pelagic larval durations of the succesful *Acanthurus* virtual larvae for the 2000 (blue) and 2005 (red) temperature dependent PLD simulations.
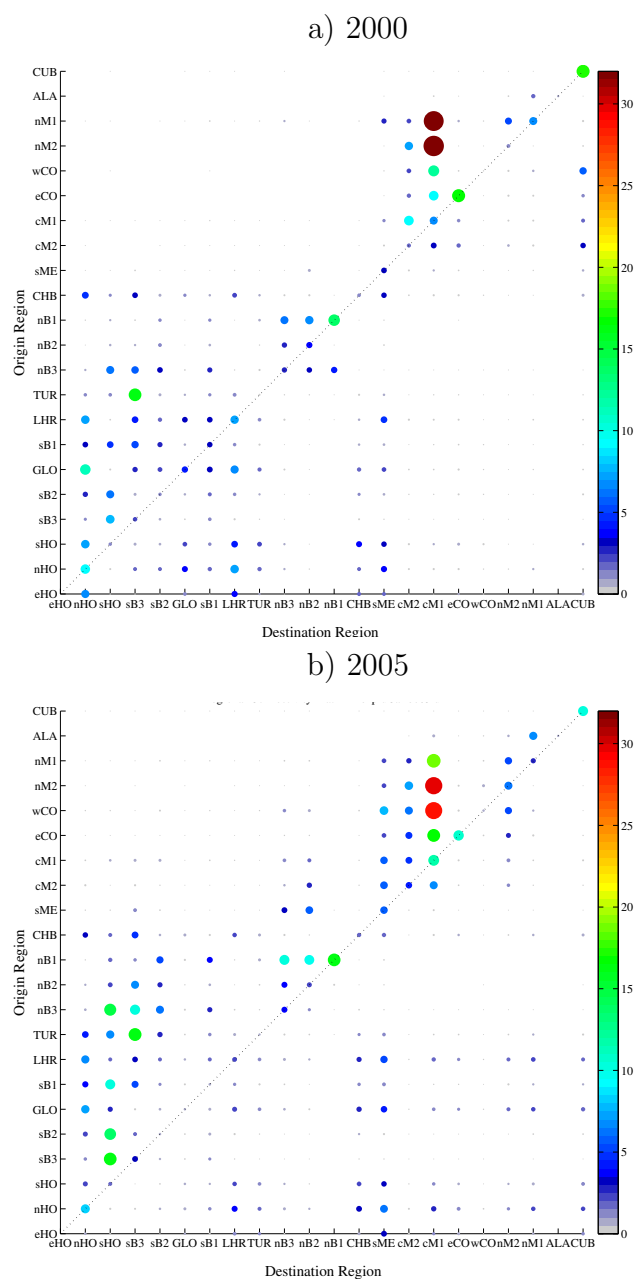
Figure 5.17: Region to region connectivity matrices for *Acanthurus* virtual larvae with temperature dependent PLD. Reefs were grouped into 22 regions identified in Fig. 5.1. Color and size of the circles are proportional to the percentage of successful connections from origin to destination reefs according to the colorbar.
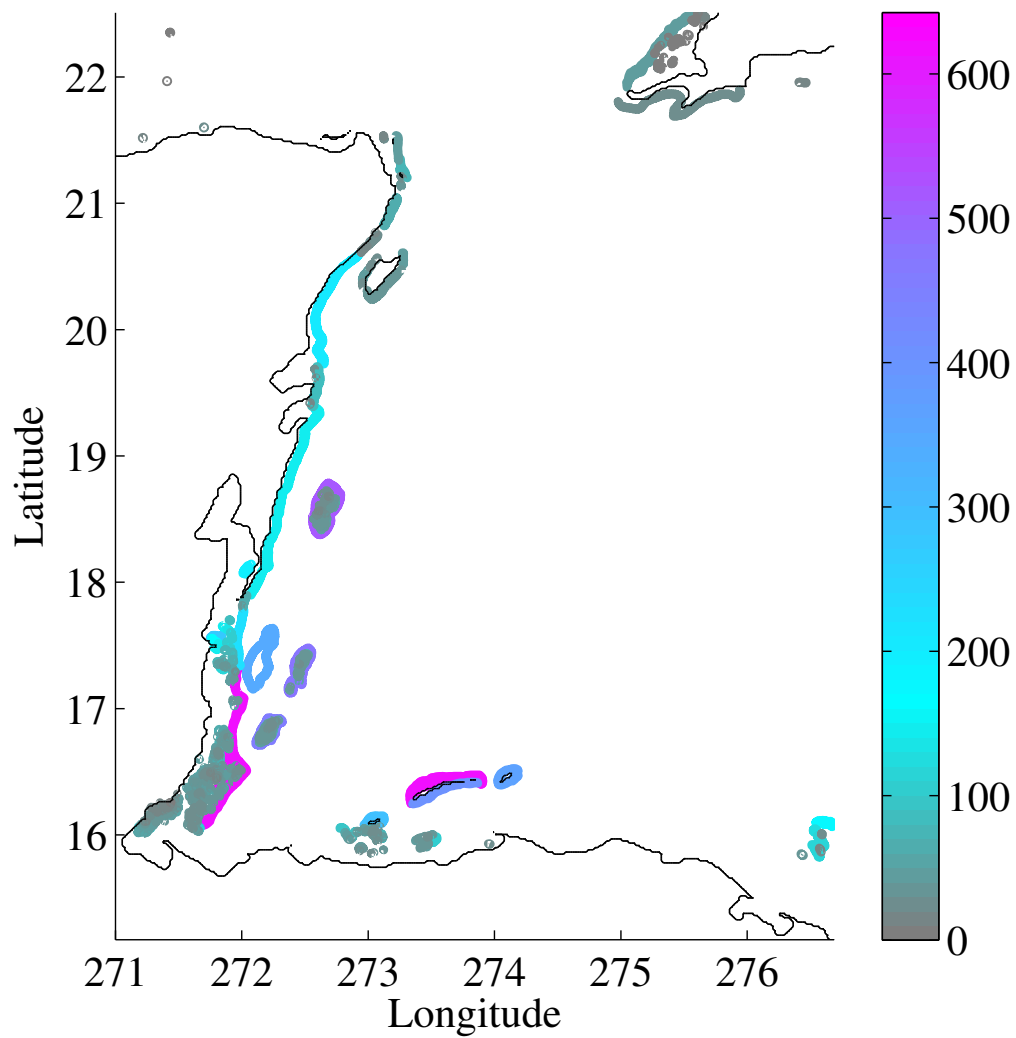
Figure 5.18: Reefs color coded by the number of different reefs reached by *Acanthurus* virtual larvae with temperature dependent PLD originated on them on both simulated years to identify the best origin reefs.
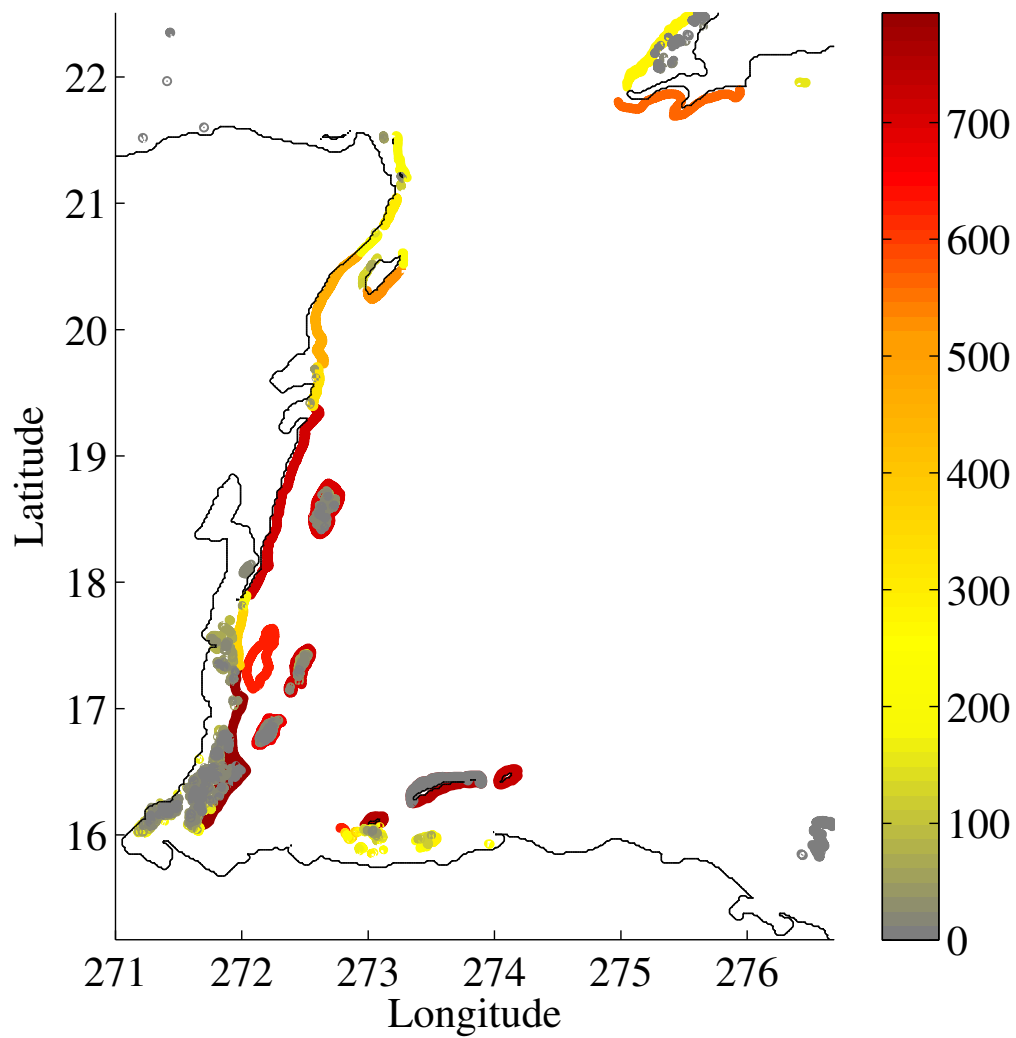
Figure 5.19: Reefs color coded by the number of different reefs it received *Acanthurus* virtual larvae with temperature dependent PLD from, on both simulated years to identify the best destination reefs.

Chapter 6: Conclusions

In this chapter, I compare the seascape, ocean circulation regimes and connectivity patterns in the Kenya-Tanzania and Western Caribbean coral reef regions. Important considerations regarding the capabilities of the models, application of these results and future directions are discussed. Special attention is provided to some of the assumptions made in the model, and the caveats these impose in applying the models to spatial marine management in the regions. Some examples of the implications for Marine Protected Area Management of the connectivity matrices derived from the models are given. General conclusions and implications of the main findings of this research are summarized.

6.1 Seascapes and ocean circulation regimes

The seascape, specifically the distribution, size and spacing of reef habitat, are important factors that differ between the Kenya-Tanzania (KT) and Western Caribbean (WC) regions. A total of 661 reefs for the KT region and 1003 for the WC region were included in this study, with a total reef area of 7165 km^2 for the KT region and 6907 km^2 for the WC. Even though the number of reefs is higher in the WC the total reef area is 258 km^2 less than the reef area of the KT region. There are many more small reefs in the WC region (Fig. 6.1). More than 75% percent of the reefs in both regions are smaller than 5 km^2. The WC region has a higher proportion of reefs in the 6-11 km^2 size range. Coral reef habitat area is important because in the model set up used here virtual larvae were released at a constant density (50 virtual larvae km^{-2}) on all reefs. This is the simplest assumption when the spatial variability of the spawning population size is unknown. Reef area is also important during settlement because large reefs have higher probability of being perceived by competent larvae. To eliminate the bias on connection strength introduced by larger reefs having more seeding locations, connectivity strength was presented as the percentage of the to-

tal larvae released from each reef or region. No correction was applied to eliminate the bias introduced by larger reefs having a higher probability of being perceived by recruits and therefore getting more settlers. The distance between adjacent reefs is another factor that influences the likelihood of larvae finding suitable settlement habitat during their competency period. This is particularly important for *Acropora* larvae that have both a short perception distance and short PLD. Coral reefs in the WC region are more clustered spatially than are KT reefs, with more than half of the reefs separated from the perimeter of their closest neighbor by less than 0.5 km, compared to 3.5 km for the majority of the KT reefs (Fig. 6.2). All other conditions being similar, *Acropora* larvae in the WC, where reefs are closer together, would have a higher probability of finding suitable settlement habitat. However, the settlement success for *Acropora* in the WC region (0.11-0.33%) is, counterintuitively, similar and even slightly lower than in the KT region (0.16-0.37%). The explanation for this is that for passively advected larvae, distance is also controlled by current speed. *Acropora* larvae in the KT region are on average exposed to higher water velocities, due to the strong northward flow of the East African Coastal Current along the KT coastal region; *Acropora* larvae in the southern part of the WC (Gulf of Honduras) experience slower and more variable flows, resulting in very similar settlement success for this genus in both regions. The differences in the velocity of the main flows also impact self recruitment. Levels of self recruitment are low in the KT region with an average for *Acropora* of 8.2% and less than 2% for *Acanthurus*. Self recruitment is much higher in the WC region with an average of 22.3% for *Acropora* and 16.3% for *Acanthurus* in the passive scenario and 42.4% in the OVM scenario.

The WC has a more complex spatial arrangement of reefs, with numerous small reefs inside barrier reefs in southern Belize, as well as inside the rims of Chinchorro Bank, Lighthouse and Glover reefs. The east-west oriented coastline of Honduras with islands surrounded by reefs, and the Cuban reefs in the northeast corner of the model domain have no counterpart in the KT region. The KT reef habitat is distributed mainly along the north to south oriented coastline, and around the islands. The Songo-Songo reef complex, south of Mafia Island, is the only area in the KT region with high densities of small reefs forming a spatially complex patchy

habitat similar to that found in southern Belize in the WC. Considering the reef distribution, the most similar (and therefore directly comparable) regions are the Mexican Caribbean region of the WC and the region north of the Dar es Salaam peninsula in the KT region.

The Kenya-Tanzania reef region and the region of the Western Caribbean north of 17^oN are similar in having north-south oriented coastlines, narrow shelves, offshore islands and atolls, and strong predominantly northward flows. Despite these geomorphological and circulation similarities, other regions, such as the eddy dominated region in the Gulf of Honduras in the WC and the monsoon-related flow reversal (Somali Current) in the northern part of the KT exhibit different dynamics that are clearly quantified by the Regional Ocean Circulation models of the two regions (Chapters 2 and 4). The depth distribution and vertical extent of alongshore velocities within the water column are very different in the two systems. The WC has a shallow shear layer separating a northward flowing surface layer in the upper 100 m, with peak velocities in the upper 15 m, which contrasts strongly from deeper southward flow (Figs. A.10, A.11, A.12, A.13). Conversely, the KT region, has coherent northward flow (EACC) extending to 300 m during the SW monsoon (May to October); during the NE monsoon (December to March), the region north of ($\sim3^oS$ (Figs. A.2 and A.4) reverses to southward flow (Somali Current) in the upper 100 m, while the predominantly northward flow continues at greater depths. The strong (monsoon) seasonal flows and tidal mixing prevent the formation of a shallow mixed layer.

Considering the ocean circulation regime, only the Mexican Caribbean region is similar to the Tanzanian region. Even though the width and depth of the channels vary, the flow dynamics around Mafia, Zanzibar and Pemba Islands in the KT region are similar to flows near Chinchorro Bank and Cozumel Island in the WC. Similar small scale circulation features are observed around these islands in both regions, such as topographically steered eddies at the southern entrances of Zanzibar Island (KT) and Cozumel Island (WC), although subsurface in the case of Cozumel, and(southwar) flows into the channels at the northern entrances of the Zanzibar, Pemba and Cozumel channels. These similar small scale circulation features associ-

ated with the islands in both regions suggests that such features may be common in regions of strong flow offshore of islands. Modeled connectivity patterns suggest that these recirculating dynamics are important for larval retention and connectivity.

6.2 Comparing connectivity patterns between the Kenya-Tanzania and the Western Caribbean regions

The Kenya-Tanzania connectivity patterns showed a predominantly south to north pattern for both the passive larvae of *Acropora* and all three model scenarios for *Acanthurus*. Connectivity in the Western Caribbean region, in contrast, was more bidirectional for all scenarios of the *Acanthurus* larval type and very localized and mainly south to north for *Acropora* virtual larvae. North to south connections in the KT region were fewer and weaker, interannually variable and generally restricted to specific regions such as Somalia (due to the influence of the Somali Current during the NE monsoon) and the Zanzibar Channel (due to eddy and coastal recirculation flows).

Acanthurus in the Gulf of Honduras, in the south WC region, had bidirectional connectivity facilitated by an eddy recirculation that connected both ways between Belize reefs in the west and Honduras reefs in the east. Bidirectional connectivity of *Acanthurus* was possible because the long PLD was sufficient at the relatively slow current speeds of the eddy for exchange between Belize and Honduras. Bidirectional connectivity was not possible for *Acropora*, which had only north to south connectivity in this region, because the assumed 12 day maximum PLD was too short at the current speeds present for the virtual coral larvae to cross the gap in coral reef habitat between the Belize reefs and the Bay Islands in Honduras.

The effects on connectivity of the different scenarios (3D passive, temperature dependent PLD, OVM) implemented for *Acanthurus* differed markedly between the KT and the WC region. The ontogenetic vertical migration scenario produced consistently higher settlement in the WC region, where the shallow shear layer assures a stronger positive effect of the OVM scenario, since virtual larvae that migrate down to 50 m are exposed to slower alongshore currents with an onshore component (Fig.

??fig:A11). In the KT region the effect of OVM on settlement was positive for larvae released early during the spawning season when NE monsoon conditions prevail and negative for larvae released later during the spawning season, during the transition and establishment of strong SW monsoon flows. The impact of OVM on larval connectivity is explained by the different vertical distributions of alongshore velocities. The KT region has unidirectional northward flow during the SW monsoon in the upper 300 m and southward flow in the upper 100 m during the NE monsoon. Beneath these seasonally changing currents a northward flow prevails during both phases of the monsoon. These deep unidirectional flows to depths beyond the 50 m assumed migration depth of the later stage larvae, prevented the larval OVM from having a strong and positive impact on connectivity and settlement of *Acanthurus* in the KT region. Moreover, the effects of the implementation of the OVM behavior in the KT differed between the two modeled years, due to the interannual variability of the monsoon seasons start and duration. The comparison illustrates how the same vertical behavior pattern can have opposite effects on connectivity and settlement success in different regions, depending of the details of the ocean circulation regime. This key finding of the present study emphasizes the importance of conducting regional-specific studies for understanding the interactions of ocean dynamics and biological processes, such as depth keeping OVM, or temperature-sensitive development times, that could dramatically alter estimates of inter-reef connectivity patterns.

The scenario that included temperature dependent PLD reduced settlement of *Acanthurus* in both regions, although the effect was more dramatic in the WC region where mean settlement decreased to less than half that observed in the passive scenario. The connectivity patterns showed a reduction in the number of long distance connections and a general decrease in dispersal distance. This was anticipated since the environmental temperatures shortened development time, resulting in a reduction of PLD from 50 pre-competency days assumed in the passive scenario to a mean of 30 days in the KT and WC regions. Reduced dispersal and lower settlement success is then a general response of *Acanthurus* in both study regions, under the simulated scenarios of warmer temperatures. This accords with previous studies that examined the effects of climate change on the connectivity of marine species [i.e. Lett

et al., 2010; Munday et al., 2009]. This finding has important implications for implementing adaptive management strategies that consider climate change predicted scenarios [McCook et al., 2009; Hughes et al., 2003].

6.3 Important considerations and future directions

Despite their apparent complexity, individual based models of larval connectivity are still, like most models, a mechanistic simplification of a very complex problem that involves a myriad of biophysical processes operating at different spatio-temporal scales [Jones, 2015; Largier, 2003; Pineda, 2000; Pineda et al., 2007]. The risk of oversimplifying a problem and excluding important components or processes of the studied phenomenon has to be constantly evaluated [i.e. Pineda et al., 2009]. It is fundamental to evaluate the validity of the assumptions on which models are based in comparison to the real phenomenon studied. The connectivity patterns resulting from individual based particle tracking models coupled to ocean circulation models as presented here for the Western Caribbean and the Kenyan-Tanzanian shelf, provide one realization of the likelihood of connections among reef habitats when all of the model assumptions are satisfied. In the simulations presented here, several biological assumptions were made (6.1). Most of these assumptions are based on relatively few observational studies, and in some cases are generalized from observations of different species in different study regions (see Introduction Chapter for details).

The perception distance assumption is based on the swimming and sensory capabilities of the larvae [Simpson et al., 2013] but the values used are often arbitrary (best guess). In this study perception distances are conservative compared to other modeling studies of coral reef fish: Cowen et al. [2006] used a 9 km perception distance; Paris et al. [2005] 9 to 19 km; Paris et al. [2007] up to 12 km. This assumption has an important effect on settlement as illustrated with the sensitivity analysis done for virtual *Acropora* larvae (Fig. 3.21), therefore its validity should be explored in light of recent studies on sensory biology and navigation behavior of coral reef fish larvae [Atema et al., 2015]. Sensitivity to perception distance for *Acanthurus* larvae should be explored as a logical next step of this research. In the modeled applications presented here, swimming and sensory abilities are only considered to have an effect at settlement during the competency period through the perception distance assumption. Ontogenetic changes of sensory skill, and swimming ability and directional swimming and spatially variable orientation clues [i.e. Staaterman et al., 2012; Wolanski et al., 1997; Wolanski and Kingsford, 2014] should be considered to increase the realism of the model.

The ontogenetic vertical migration scheme applied to the *Acanthurus* virtual larvae was highly idealized and could be improved by migrating only the virtual larvae that remain shallower than the migration depth 20 days after spawning (i.e. flexion). Since the vertical distribution of *Acanthurus* larvae through ontogeny is not well known, sensitivity to the migration depth should be investigated, as well as sensitivity to the length of the period that virtual larvae stay at depth. The combination of the temperature dependent pelagic larval duration scenario and the vertical migration scenario would be a more realistic scenario that should be explored.

The O'Connor relationship of PLD and temperature for *Acanthurus* (3.2) was fitted based on the maximum water temperature experienced by the virtual larvae in the KT region. Since *Acanthurus* is not an amenable aquarium species it is hard to experimentally obtain developmental series at different water temperatures. In situ temperature observations though ontogeny are not feasible due to the impossibility to track the very small larvae during their long PLD. Therefore, larval duration estimates using the fitted equation were compared to an *Acanthurus* development time

Table 6.1: Table 1. Biological assumptions implemented in the individual based model to characterize the two larval types. S1, S2, and S3 in the *Acanthurus* column refer to conditions assumed for scenario 1: 3D-passive, scenario 2: temperature dependent PLD, and scenario 3: ontogenetic vertical migration (OVM) scenarios, respectively.

	Acropora (Branching coral)	*Acanthurus* (Surgeonfish)
Initial Depth	3 m	3 m
Pre-competency period	4 days	S1 (50 days) S2 (temp-dependent)
Competency period	8 days	22 days
Pelagic Larval Duration	4-12 days	50-72 days
Perception Distance	10 m	4 km
Modeled spawning period	February-March	February-March
Vertical migration	None (3D passive)	S3 (Ontogenetic vertical migration to 50 m or 3 m above the bottom if at <50 m water depth between days 20 and 50 after spawning; individuals depth keep at 50 m for 30 days; on day 50 migrate to 3 m for subsequent 3D passive drift, until perceive nearby reef)

series reared at constant temperature provided by Frank Beansch (personal communication), who has successfully reared *Acanthurus* to pre-competent stages, and to some published larval age data from otolith aging associated to juvenile collection temperature. The PLD-temperature relationship (3.2) is therefore highly uncertain, not very robust, and perhaps unrealistic. Results from this scenario are only intended to be compared with the non-temperature controlled PLD experiments and between the two modeled years, which did differ in temperature, which is a fairer comparison.

Larval production in nature is proportional to the population density of reproductive adults and is therefore not uniform in the coral reef habitat. Several modeling studies [e.g., Kough et al., 2013; Watson et al., 2010] scaled estimates of potential connectivity, defined by Watson et al., 2010 as the probability of larval transport from a source to a destination location and is quantified using Lagrangian particle simulations by observed spatially variable larval production rates to obtain "realized connectivity" estimates that can be used to estimate larval settlement patterns [Watson et al., 2010]. In this study virtual larvae were released from randomly chosen locations within each reef, with the number of released larvae at an effective density of 50 per km^2, without considering variability in larval production. *Acropora* corals are a reef front species that are more abundant on the perimeter of coral reefs. *Acanthurus* surgeonfish may have a more uniform distribution on the reefs, mainly determined by the availability of leafy algae; however they swim to the reef edges to spawn. Even if no estimates of larval production exist for these genera in the modeled regions,

Observed patterns of settlement for a variety of coral reef fish species in the Great Barrier Reef showed strong interannual variability between 2 surveyed years [Williams et al., 1994]. This is common in marine organisms with long pelagic larval durations (e.g., spiny lobster,[Briones-Fourzn et al., 2008]; flatfish, Sohn et al, in prep.). In this study particle tracking experiments to estimate connectivity patterns of *Acanthurus* and *Acropora* virtual larvae were performed only for 2000 and 2005. These two years were chosen because the differences in temperature and velocity fields were the greatest from among the eight simulated years. Interannual variability in connectivity patterns between the two years was larger in the KT than in the

WC region, however this could easily change if more years were modeled. The 3-dimensional velocity and temperature fields from KTCM and MCCM exist for 6 additional years, since the ocean circulation models in both regions were run for 8 years, from 2000 to 2007. Conducting particle tracking experiments for the other 6 years would provide additional results that might lead to new insights on the interannual variability of connectivity in these two coral reef regions.

In this study, spawning in both the KT and WC region was assumed to be focused seasonally in February and March, but to be uniform in intensity within those two months. This may be realistic for *Acropora* corals in the KT region where spawning is thought to be linked to the marked seasonal monsoon conditions [Mangubhai, 2008], but it may not be realistic for *Acropora* spawning in the WC [Van Woesik et al., 2006]. In the Red Sea *Acanthurus* have been reported to spawn in pairs throughout the year, but in large spawning aggregations only during the northeast monsoon season [Myrberg et al., 1988]. The peak spawning months for coral reef fish in the Caribbean are March to May and August to November [Johannes, 1978]. Given the uncertainty of the seasonal spawning, sensitivity studies of the timing of spawning are needed to examine whether spawning at times other than the February-March period assumed here provides new connectivity between origins and destinations than are observed from the simulations reported here. Simulated spawning during some days on every month would be a suitable approach to investigate settlement success and connectivity pattern sensitivity to spawning day/season.

In this study, no mortality was applied to the modeled virtual larvae. The effect of mortality in the real ocean is to reduce larval connectivity among coral reefs and it may also decouple the larval supply from recruitment to the reef populations [Pineda, 2000; Doherty et al., 2004]. High, non-uniform larval mortality is common during early life stages of pelagic spawner fish [Reichert et al., 2010] . Mortality may vary spatially and temporally due to predation and food availability for feeding larvae. Mortality rates due to predation are difficult to estimate, and are influenced by the patchy distribution of predators, as well as the patchiness of eggs and larvae; and predation susceptibility, which varies among species and life stage [McGurk, 1986] . Realistic mortality rates are difficult to obtain for larvae of coral reef organisms,

but some mean estimates exist (i.e. McGurk [1986] for larval fish of some species). High mortality during settlement (recruitment to the reef leads to exposure to new predators than have been experienced during the pelagic phase) has been reported to be a population bottleneck for *Naso Unicronis* (a surgeonfish of a different genus) in Morea Island [Doherty et al., 2004].

There are several physical processes that are not represented or are not well resolved in the KTCM and MCCM ocean circulation models or the IBM (in the case of diffusion), which might have an important effect on larval transport. According to [Largier, 2003],"when considering dispersion parameters at the appropriate population scales, advection is usually weaker than initially anticipated, and diffusion is stronger than typically used in model studies". Vertical diffusion, often included explicitly in individual based models as a vertical random walk applied to the particles [Batchelder, 2006]; [Cowen et al., 2006]; [Paris et al., 2007], was not included in this study. Larval dispersal is due to a combination of advection; the mean transport of a group of particles originating at the same location, and diffusion which reflects the differences in transport of individual particles starting at the same location due to turbulent mixing at subgrid scales [Largier, 2003]. Often, diffusion acts to prevent "washout" of larvae away from suitable habitat, e.g., provides longer local retention times, and allows for more flexibility in the size and spacing of effective marine reserves [Largier, 2003]. The effects that diffusion might have on altering the non-diffusive results presented here should be assessed by additional simulations that include a random walk scaled by the local vertical diffusivity [Batchelder et al., 2002], at least as a sensitivity analysis.

Several physical processes can have an important role on bringing larvae onshore and closer to suitable habitat. Particles in steep non-linear waves move along nearly circular paths, but the orbits do not close this generates net transport in the direction of propagation of the waves known as Stokes drift [Stokes, 1847 in Kundu and Cohen, 2008]. Unstable surface breaking waves can travel 10s of meters transporting mass. Wave dynamics are not included in the ocean circulation models of this study. Similar to the surface dynamics, Ekman transport occurs in the bottom boundary layer in response to the stress generated by the flows above the still bottom. Ekman transport

in the bottom boundary layer is often in the opposite direction of the surface, wind induced, Ekman transport, having a net transport 45° to the left (right) of the mean flow in the northern (southern) hemisphere [Ekman, 1905 in Stewart, 1997]. Very high vertical resolution near the bottom is needed to accurately resolve the bottom Ekman layer. The vertical resolution of KTCM and MCCM is only appropriate to resolve it in very shallow waters, and is therefore not accurately represented all along the coast.

Internal waves and internal tidal bores may be important mechanisms transporting marine larvae across-shore [Pineda, 1999; Pineda, 1994; Shanks, 1983], often towards suitable settlement habitat. Internal waves are not adequately represented in the KTCM or MCCM since ROMS is a hydrostatic model, therefore ill-suited to resolve fine-scale internal waves [Chao et al., 2007], which require non constant density dynamics.

In the real ocean planktonic larvae are exposed to all of these unresolved physical processes, which could strongly alter their connectivity. Even relatively passive larvae like *Acropora*, that can only slightly control their vertical position during their settlement stage can interact with temporal and spatially variable currents generated by these processes to reach suitable habitat. More complex larvae of decapods and fishes (i.e. *Acanthurus*) have highly developed senses that allow them to detect variations in water chemistry, sound and vibration, light, current direction, magnetism and water pressure [Atema et al., 2015; Kingsford et al., 2002]. Integrated sensory responses may allow them to orient and effectively navigate towards suitable habitats by taking advantage of a variable flow environment.

Often, observed settlement does not correlate with larval supply [Pineda, 2000]. Settlement behavior, such as substrate discrimination and selection, can decouple larval supply, resulting from larval transport, from settlement patterns. This decoupling can significantly alter recruitment, modifying and likely minimizing the effects of larval transport and connectivity patterns on the dynamics of local subpopulations [Blythe and Pineda, 2009; Pineda, 2000; Pineda et al., 2010]. Post-settlement processes [i.e. interspecific competition, predation) can have a similar effect [Almany and Webster, 2005; Carr and Hixon, 1995; Caselle, 1999; Victor, 1986]. Therefore it

is not surprising that model derived estimates of settlement success and connectivity patterns do not consistently reproduce patterns observed in time series of settlement [Kough et al., 2013; Sponaugle et al., 2012] and much less patterns of recruitment to the spawning population [Pineda et al., 2006]. Obtaining observations of larval supply and settlement time series for the *Acropora* and *Acanthurus* genera at a few locations in the KT and WC regions would be useful to determine whether the modeled settlement time series are representative of observed patterns.

6.4 Implications of the modeled connectivity patterns for Marine Protected Area Management in the KT and WC regions

According to the Protected Planet database [`http://www.protectedplanet.net/`] there are 26 MPAs in the KT region and 99 in the WC (Figs. 6.3 and 6.4). These numbers include all MPAs, some of which are primarily targeted to mangroves or estuarine habitat preservation rather than coral reef conservation. Polygons that overlap in these figures indicate that there is more than one designation for the same region, such as a different level of protection (i.e. a no-take area within a marine reserve). As expected from the number of MPAs in the two regions, and considering that the WC region has a smaller area ($\sim$6.5^o alongshore) than the KT region (10° alongshore), the density of MPAs in the WC is much higher than in the KT region. Higher density of MPAs implies shorter distance among them, which enhances the probabilities of interconnectedness among MPAs, especially for genera like *Acropora* that have short PLDs. Enhanced connectivity is an important characteristic for the effectiveness of MPA networks [Botsford et al., 2008; Botsford et al., 2009; Almany et al., 2009; Underwood et al., 2013]. Edgar et al. [2014] reported that global conservation outcomes of MPAs depended on 5 key features:

"1) The degree of fishing permitted in the MPAs;

2) level of enforcement; 3) MPA age;

4) MPA size; and,

5) presence of continuous habitat allowing unconstrained movement of

fish across MPA boundaries".

In both regions, several MPAs cover a large ocean area but only a small reef area. Large protected areas around reefs act as spatial buffers isolating reefs from threats beyond the borders of the MPAs (i.e. fishing, diving), but the small reef area within the MPA implies that only a small fraction of the spawning populations is protected. Several MPAs in the KT region do not satisfy the 5th criterion, since often entire reefs are not encompassed within the MPA boundaries but divided by them. This is less frequent in the WC region. These simple considerations indicate that WC MPAs have the potential to be more efficient for conservation than those in the KT region.

Considering all of the caveats discussed above, the connectivity and origin and destination summaries from this research can be considered as working hypotheses to be further strengthened and explored with additional sensitivity analysis. The most critical need for validating the model results is more systematic collection of observations from the field; specifically needed are observations of settlement time series and comparable observations of connectivity, such as studies of genetic connectivity at ecological time scales [Christie et al., 2010b; Christie et al., 2010b; Pusack et al., 2014]. Model results can be cautiously interpreted in the context of the existing Marine Protected areas by identifying protected reefs or larger regions and assessing their role as origin or destinations of virtual larvae (i.e. Fig. 6.3 and 6.4) and the degree of connectivity or isolation they demonstrate in the connectivity matrices. The Pemba Channel MPA and the no-take zone inside it, for example, are unique within the KT reef system in being relatively isolated from other reef regions; thus, it is important to protect Pemba Channel reefs because any anthropogenic or natural environmental damage to these reef communities might have a potentially long term impact. According to the results of the present model, the probability of Pemba reefs receiving recruits from elsewhere is low, and therefore recovery would be slow. In this case local protection is a valid rationale for creating and enforcing a marine reserve (rather than as one node of a network) even if isolated from other reefs and MPAs.

The location of the Rufiji-Mafia-Kilwa MPA (8.3ºS, 39.5ºE, Fig. 6.3) to the south of Mafia Island is well placed according to the results of the modeling study,

as it encompasses reefs that provide *Acanthurus* virtual larvae to many different destination reefs. *Acanthurus* larvae from these reefs reached more than 350 other reefs within the region. Results of this model suggest that the enforcement and monitoring of this MPA should be a priority for local communities and national authorities in charge of environmental protection. As reported here trans-boundary exports of larvae are common between Tanzania and Kenya, therefore the importance of protecting key sites, like Juani reef inside the Rufiji-Mafia-Kilwa MPA, which are likely to provide larvae to most of the reefs in the region.

Connectivity matrices that consider protected reefs only as origins and destinations could be constructed from these particle tracking results to determine which reefs within the two studied regions are effectively being protected by the existing MPAs and to what extent MPAs are providing settlers to reefs beyond their boundaries. Connectivity matrices of protected reefs would also provide information on whether the existing MPAs form an effective network. Testing the effectiveness of alternative MPAs arrangements with experiments similar to those presented by Kough et al. [2013] for spiny lobster is another possibility. Results for *Acropora* (a reef builder) and *Acanthurus* (important herbivore group) would be highly relevant since they are important genera for preserving the integrity of the coral reef ecosystem, and therefore of great importance for both biodiversity conservation and fisheries enhancement purposes. These analyses will be more relevant once the robustness of the model results shown here have been better validated with additional sensitivity analysis.

6.5   Conclusions

The individual based particle tracking models of two ecologically important species coupled to ocean circulation models of the Kenyan-Tanzanian region and the Western Caribbean illustrate differences in connectivity of the two regions, and produce testable working hypotheses that should be considered when designing spatial management strategies to protect coral reef environments in these regions. The connectivity datasets enable further analysis to evaluate the performance of existing or

proposed MPAs, as well as the possibility of evaluating sites that may be vulnerable due to isolation, such as those of Pemba Island in the KT. Further simulations should be done to investigate the robustness of the presented results to variability in the biological assumptions, to investigate the persistence of the observed connectivity patterns through time, and to study the effects of increasing temperatures due to global warming on connectivity. Future studies of connectivity will benefit from enhanced observation and sampling of key taxa. Enhanced observation programs are needed to increase knowledge of key taxa larval ecology, such as ontogenetic depth preferences, thermal tolerances, species spawning schedules, and more realistic reef habitat perception skills.

The results presented here generally agree with the connectivity patterns of similar organisms described using empirical techniques for the KT [i.e. Souter et al., 2009] and WC region [Chittaro and Hogan, 2012; Villegas Sanchez et al., 2013; Hogan et al., 2012]. Due to the relatively small size of the modeled regions, the higher resolution results of this modeling study provide a level of detail greater than previous coupled IBMs that encompass larger regions and include the WC region [i.e. Kough et al., 2013; Paris et al., 2007; Cowen et al., 2006. Another characteristic that sets this study apart from previous studies is the focus on keystone genera of crucial ecological importance for coral reef ecosystems: *Acropora* branching corals and *Acanthurus* surgeonfish. Previous studies focused on economically important species (e.g. spiny lobster, [Kough et al., 2013], territorial demersal spawners that are easier to collect in the field [e.g. damselfish, [Sponaugle et al., 2012; Christie et al., 2010b; Christie et al., 2010a; Villegas-Snchez et al., 2010 Villegas-Sanchez et al, 2013] and brooding corals (e.g. *Pocillopora damicornis*, [Souter et al., 2013]) that have very short PLDs. Despite broadcast spawning species being more abundant in coral reef ecosystems, they have received little attention in connectivity studies. *Acropora* and *Acanthurus* have contrasting PLDs (12 days and 72 days, respectively), and very different habitat perception and swimming capabilities. Thus, these two genera illustrate extremes of the wide spectrum of larval duration, sensory and swimming capabilities observed in coral reef species. Simultaneously examining two species in the same modeling environment allows for a fair comparison of the connectivity patterns, knowing that the

observed differences emerge due to the characteristics defined for the virtual larvae, which is a more objective approach than comparing connectivity patterns of different species resulting from different physical models.

The existence of small scale circulation features with similar effects on connectivity in both study regions, like the topographically steered eddies in the southern entrances of the Cozumel channel in the WC and the Zanzibar Channels in the KT region, suggest that such features could be ubiquitous in other regions with similar coastal morphology and predominant flow direction. Our results highlight the importance of these small scale circulation features which are able to increase larval retention and modify the connectivity patterns. The high resolution ocean circulation model used in this study resolves these features and can serve as a link between larger mesoscale models and smaller scale studies [i.e. Sammarco and Andrews, 1988; Cowen and Castro, 1994; Hamner and Hauri, 1981] that have previously identified these features but are unable to quantify their impacts on regional connectivity due to their restricted spatial scale. Higher resolution models focused on small scale circulation and reef geometry [i.e. Cetina-Heredia and Connolly, 2011] would be useful to conduct detailed studies and further investigate the importance of specific small scale circulation features on larval retention, after features have been identified in ocean circulation models like KTCM and MCCM.

The results presented here are highly informative, particularly for the far less studied Kenya-Tanzania region. The integration of these results with local studies of MPA effectiveness [i.e.Maina et al., 2003;McClanahan and Mangi, 2000; McClanahan et al., 2006] should improve our understanding of the mechanisms behind the successes and failures of MPAs, generate further insights and strategies to maximize the effectiveness of the existing MPAs, and inform the design of new proposed ones. The information provided by coupled biophysical particle tracking models of *Acropora* and *Acanthurus* virtual larvae is expected to be helpful for scientists, that are working to understand the biophysical interactions affecting coral reef connectivity, and for managers and decision makers, that are tasked with protecting coral reef ecosystems.
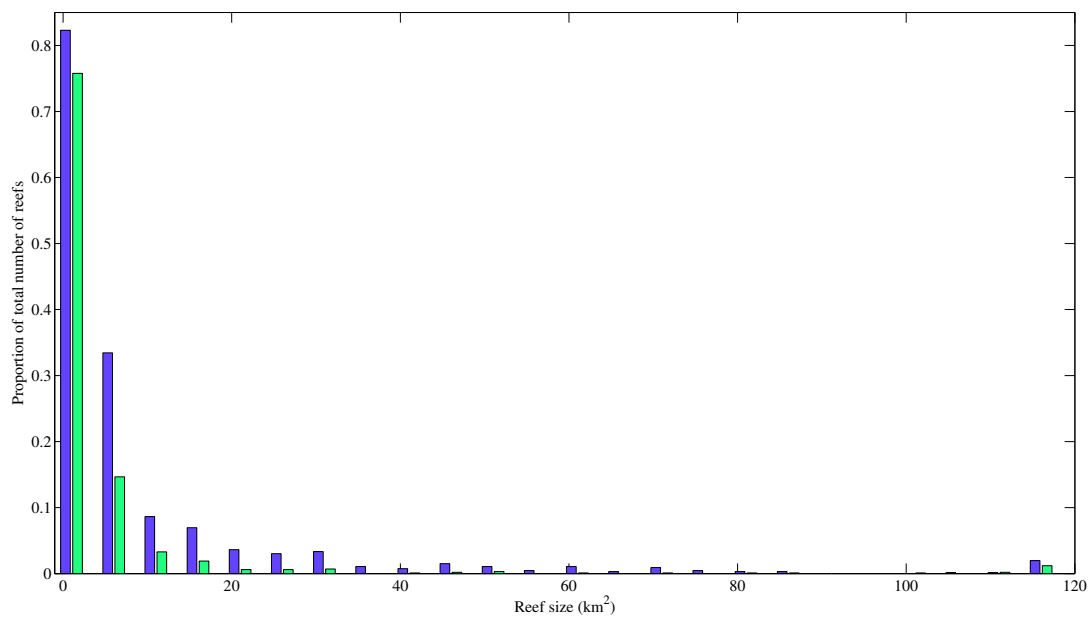
Figure 6.1: Histogram showing the reef size distribution for the Kenya-Tanzania (green) and Western Caribbean (purple) regions as a proportion of the total number of reefs on each region.
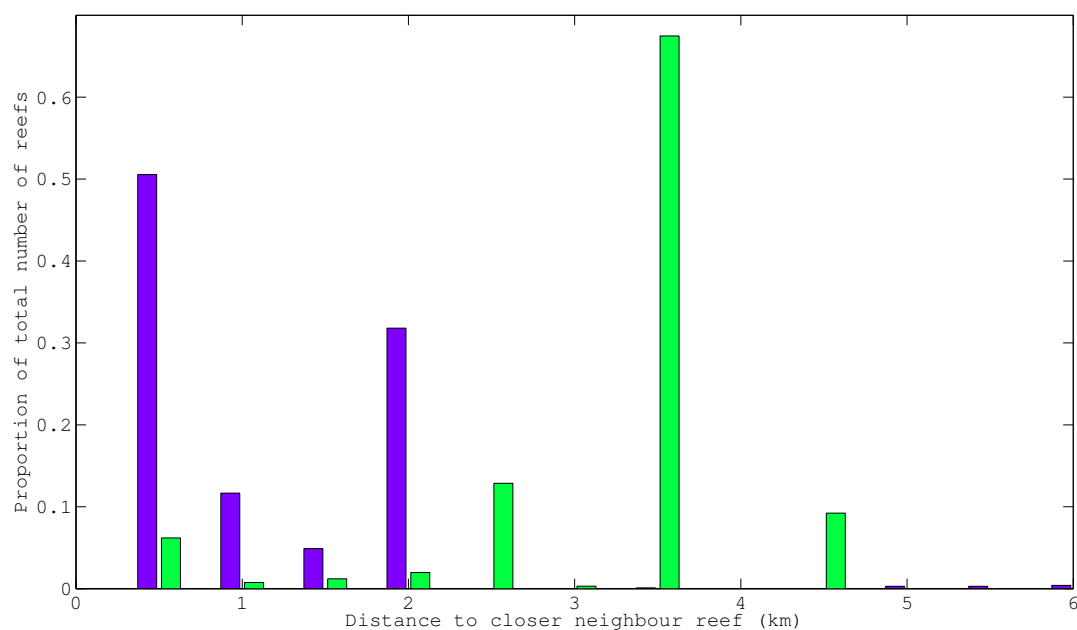
Figure 6.2: Marine Protected Areas in the Kenya-Tanzanian region (green polygons), coral reef habitat is marked in gray. Polygons that overlap in these figures indicate that there is more than one designation for the same region, such as a different level of protection (i.e. a no-take area within a marine reserve).
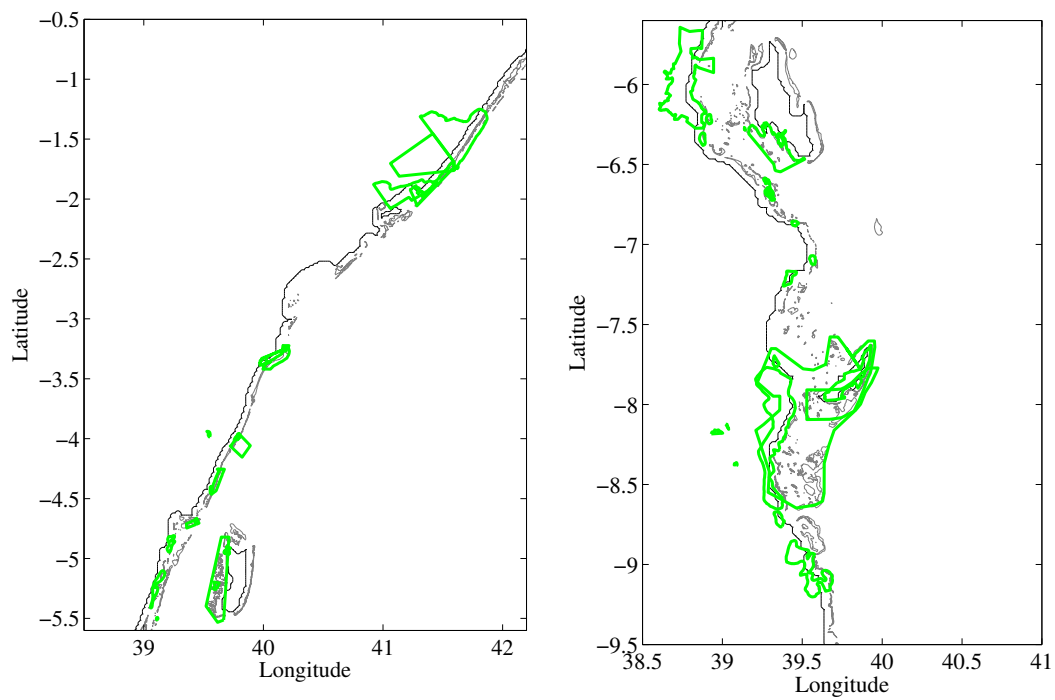
Figure 6.3: Histogram showing the reef size distribution for the Kenya-Tanzania (green) and Western Caribbean (purple) regions as a proportion of the total number of reefs on each region.
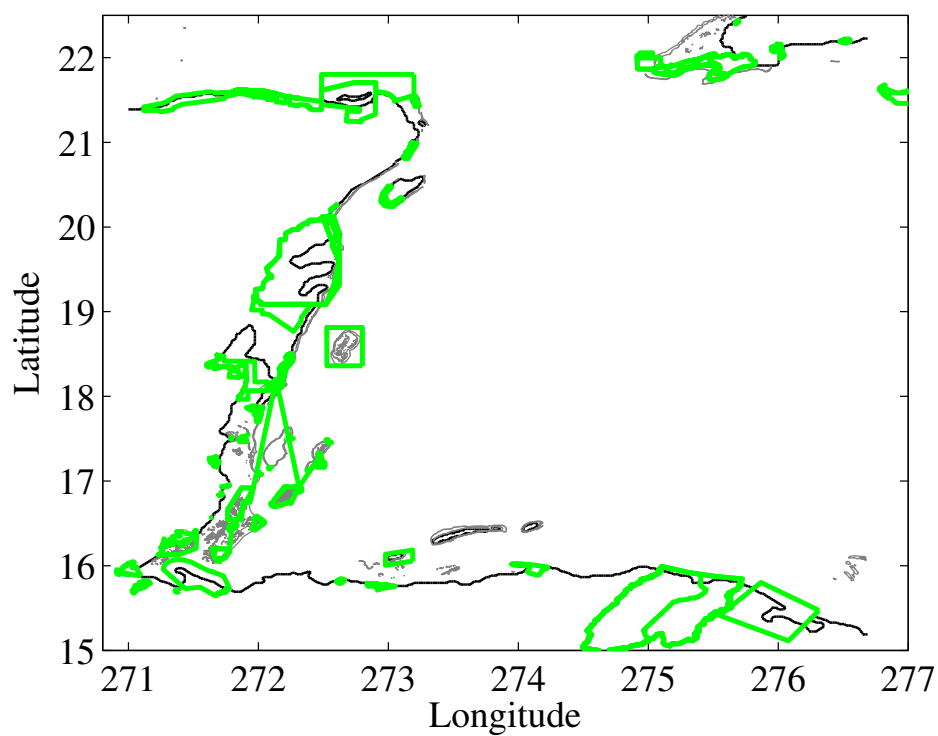
Figure 6.4: Marine Protected Areas in the Western Caribbean region (green polygons), coral reef habitat is marked in gray. Polygons that overlap in these figures indicate that there is more than one designation for the same region, such as a different level of protection (i.e. a no-take area within a marine reserve).

APPENDICES

Appendix A: Appendix

205
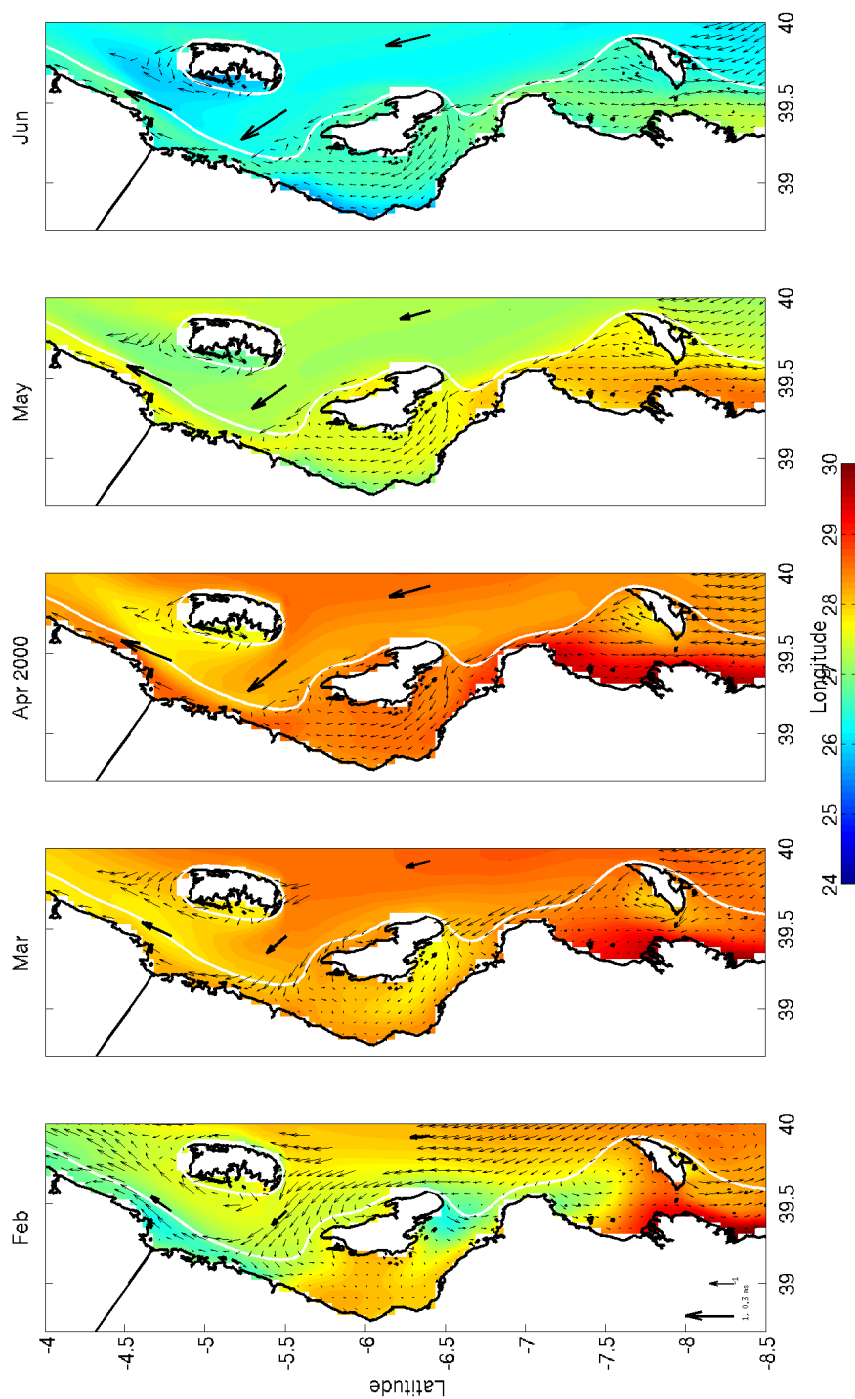
Figure A.1: 2000 SST with surface velocity vectors overlaid for the Tanzanian shelf region. The islands from north to south are Pemba, Zanzibar and Mafia. For clarity only every third vector is shown and vectors with a speed greater than 0.4 m s^{-1} were removed. Thick arrows show strong currents representing the removed vectors. Scale arrows in the left panel apply to all panels.

206
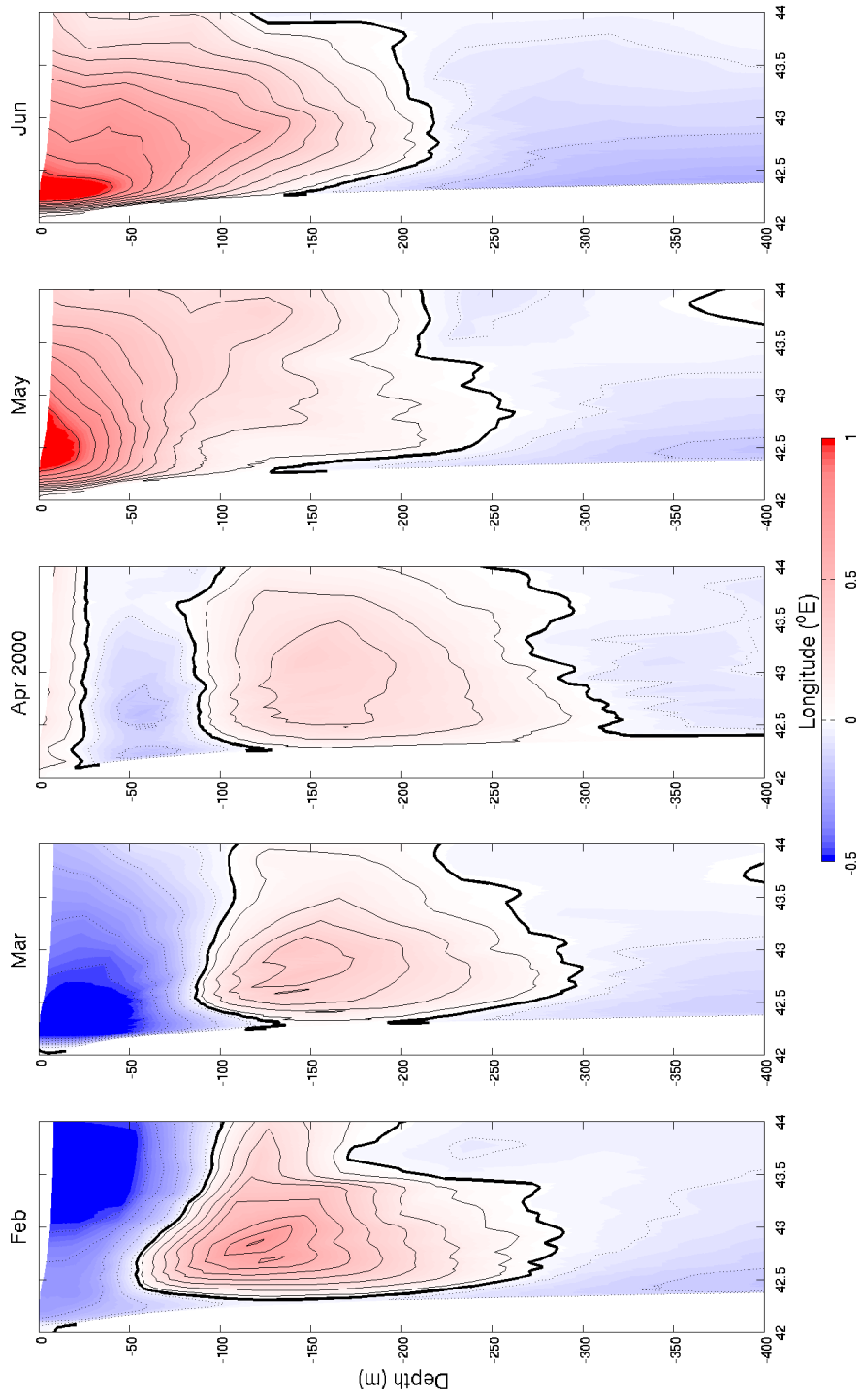
Figure A.2: 2000 north-south (v) velocity (m s^{-1}) at 1 °S, marked isotachs have a 10 cm s^{-1} interval starting from ± 5 cm s^{-1}; solid thick line is zero velocity, thin solid lines mark northward velocity contours, and dashed lines southward velocity contours.
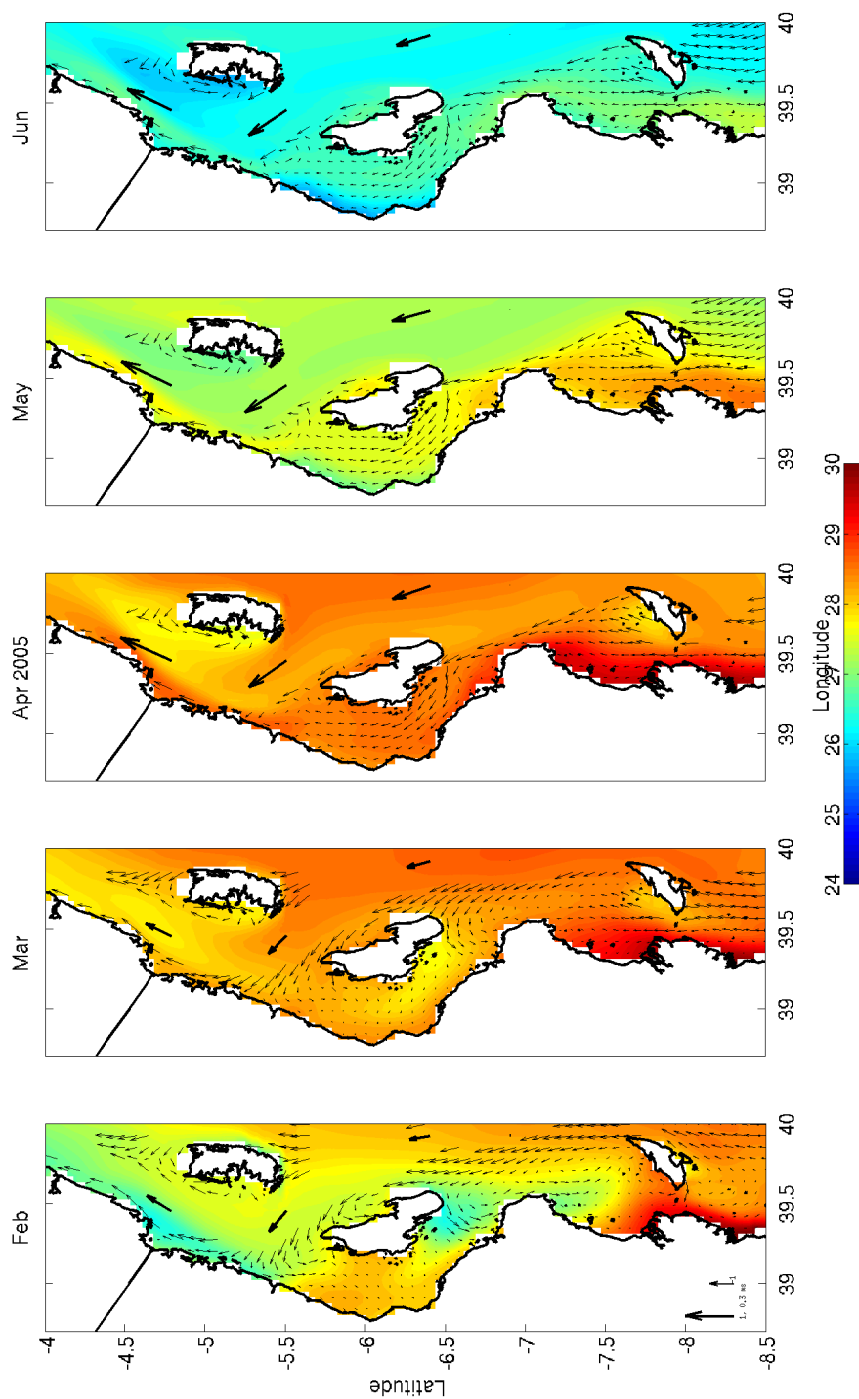
Figure A.3: 2005 SST with surface velocity vectors overlaid for the Tanzanian shelf region. The islands from north to south are Pemba, Zanzibar and Mafia. For clarity only every third vector is shown and vectors with a speed greater than 0.4 m s^{-1} were removed. Thick arrows show strong currents representing the removed vectors. Scale arrows in the left panel apply to all panels.

208
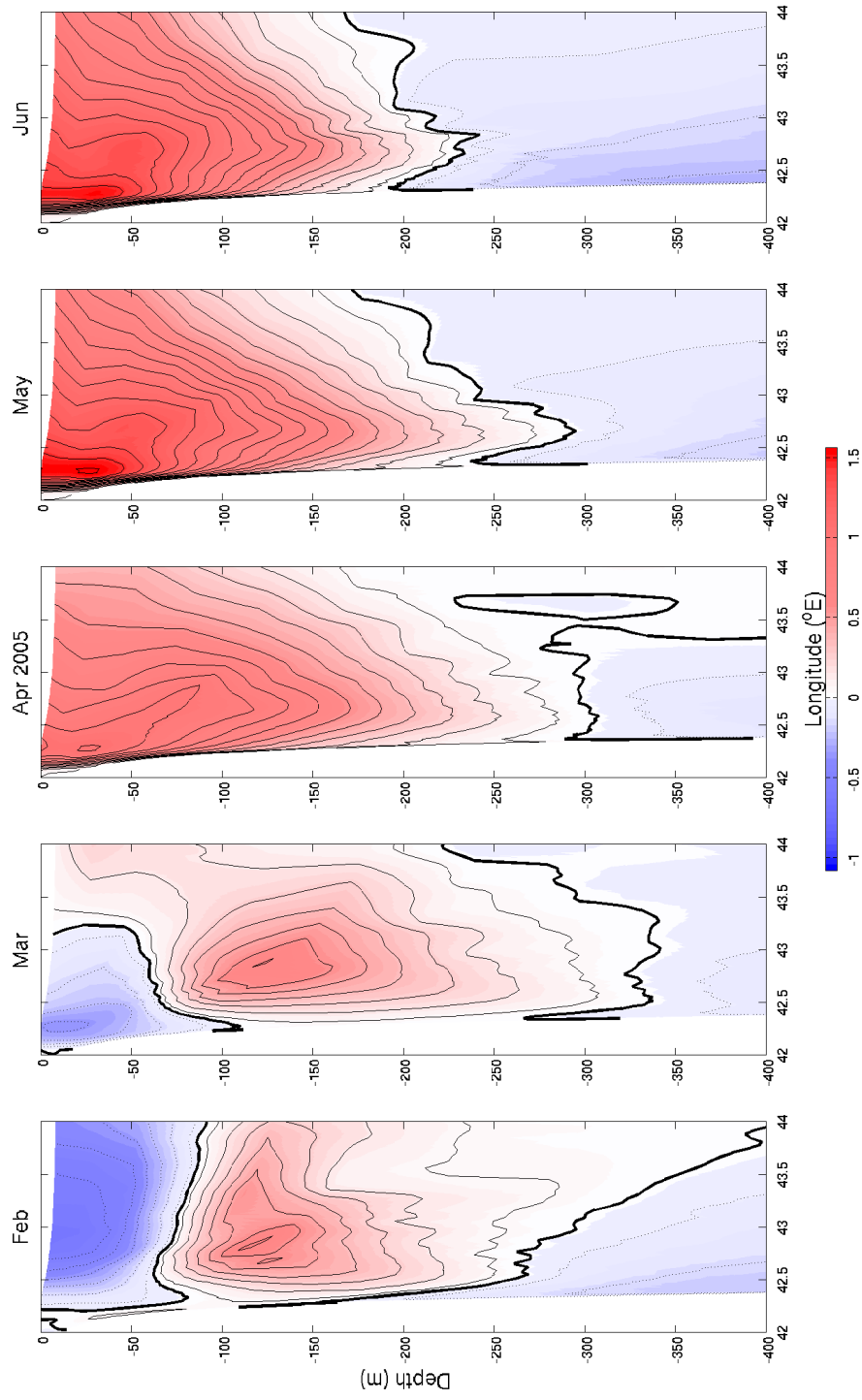
Figure A.4: 2005 north-south (v) velocity (m s^{-1}) at 1°S, marked isotachs have a 10 cm s^{-1} interval starting from +-5 cm s^{-1}; solid thick line is zero velocity, thin solid lines mark northward velocity contours, and dashed lines southward velocity contours.
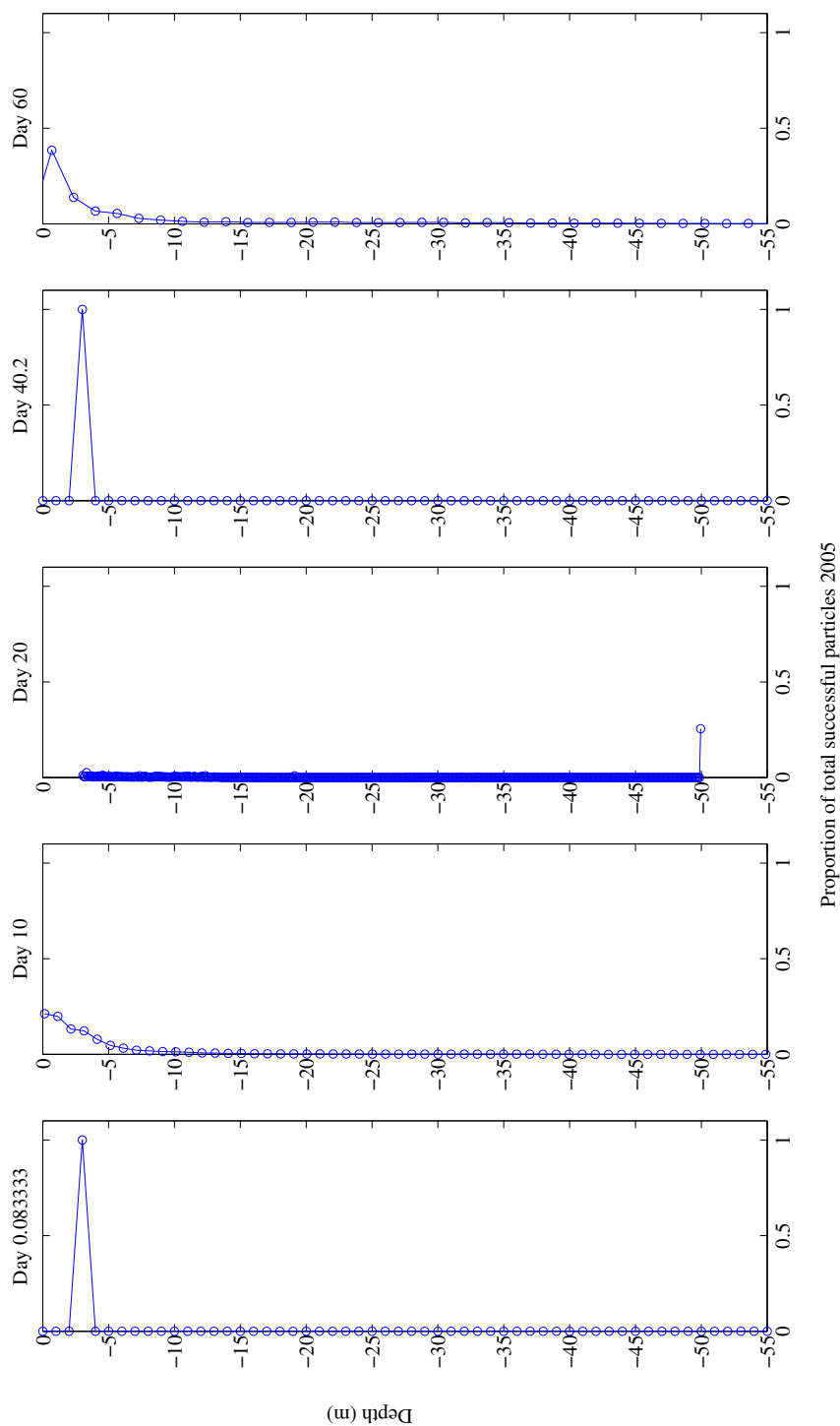
Figure A.5: Depth distribution of the successful particles of 2005 (as a proportion of the total) on different days after spwaning, to illustrate the ontogenetic vertical migration behavior applied to *Acanthurus*. Virtual larvae are spawned at 3 m depth and are advected passivly in the three dimensions for 20 days. On day 20 virtual larvae migrate down to 50 m depth or 3 m above the bottom. On day 40 they migrate back up to 3 m depth and are advected passively again until they settle.
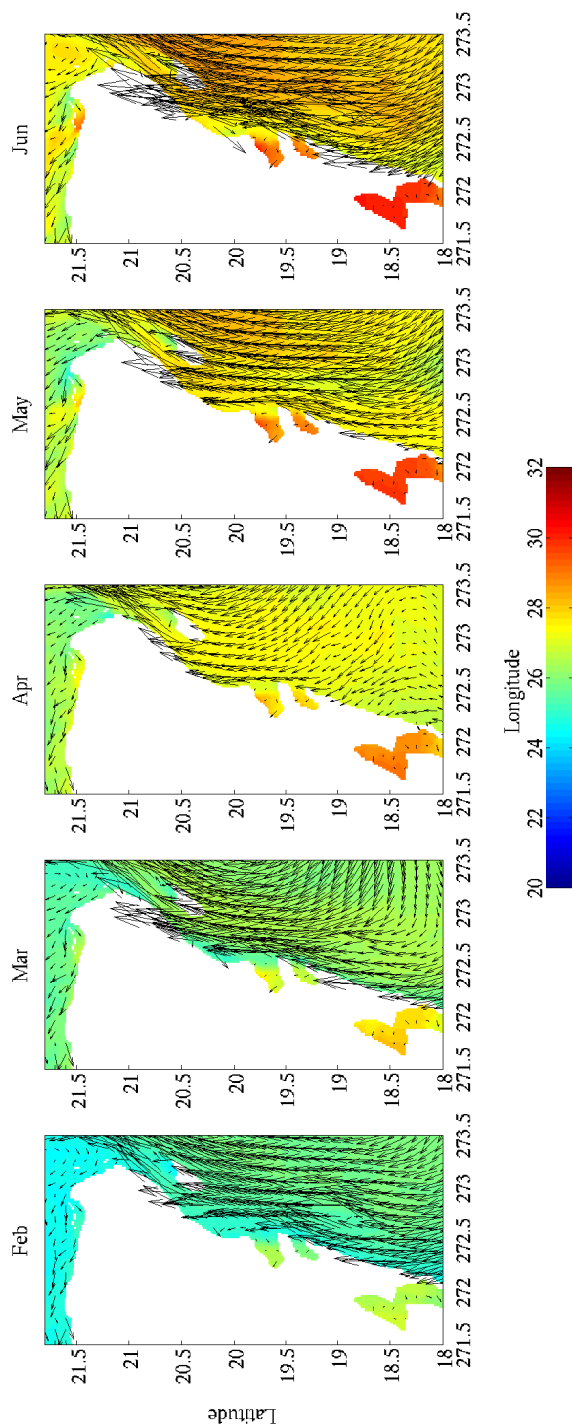
Figure A.6: 2000 SST with surface velocity vectors overlaid for the north Western Caribbean region.
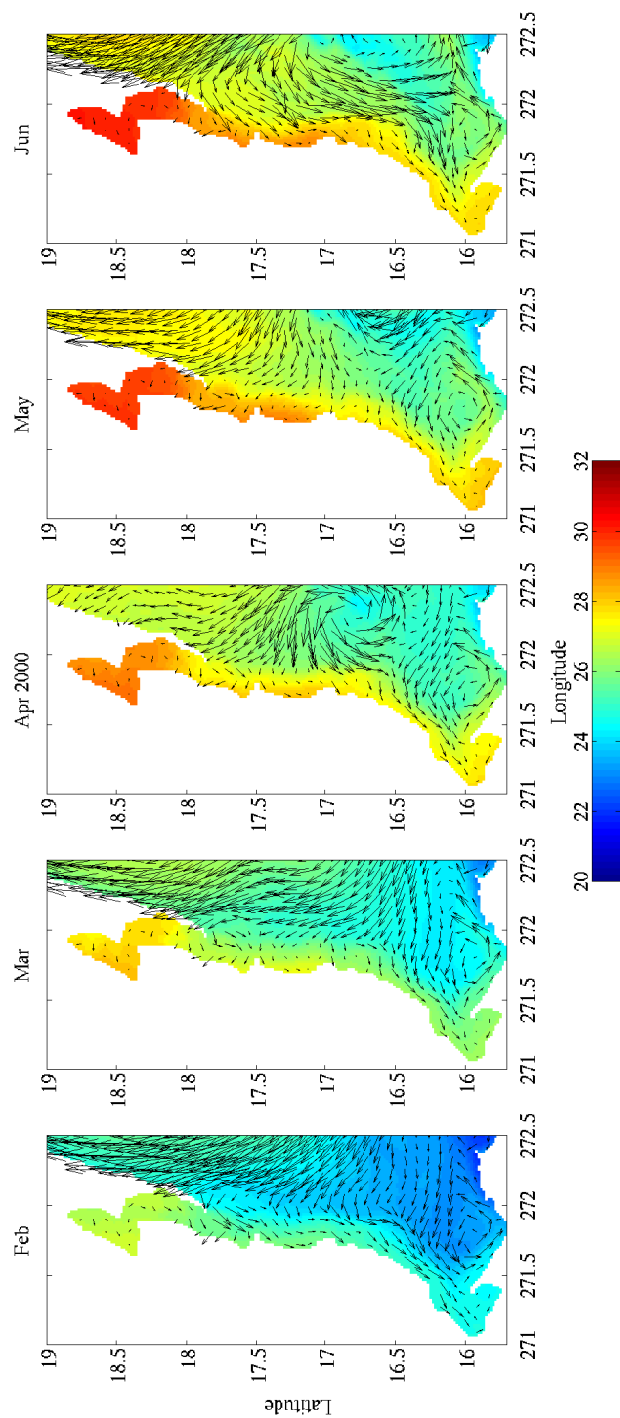
Figure A.7: 2000 SST with surface velocity vectors overlaid for the south Western Caribbean region.
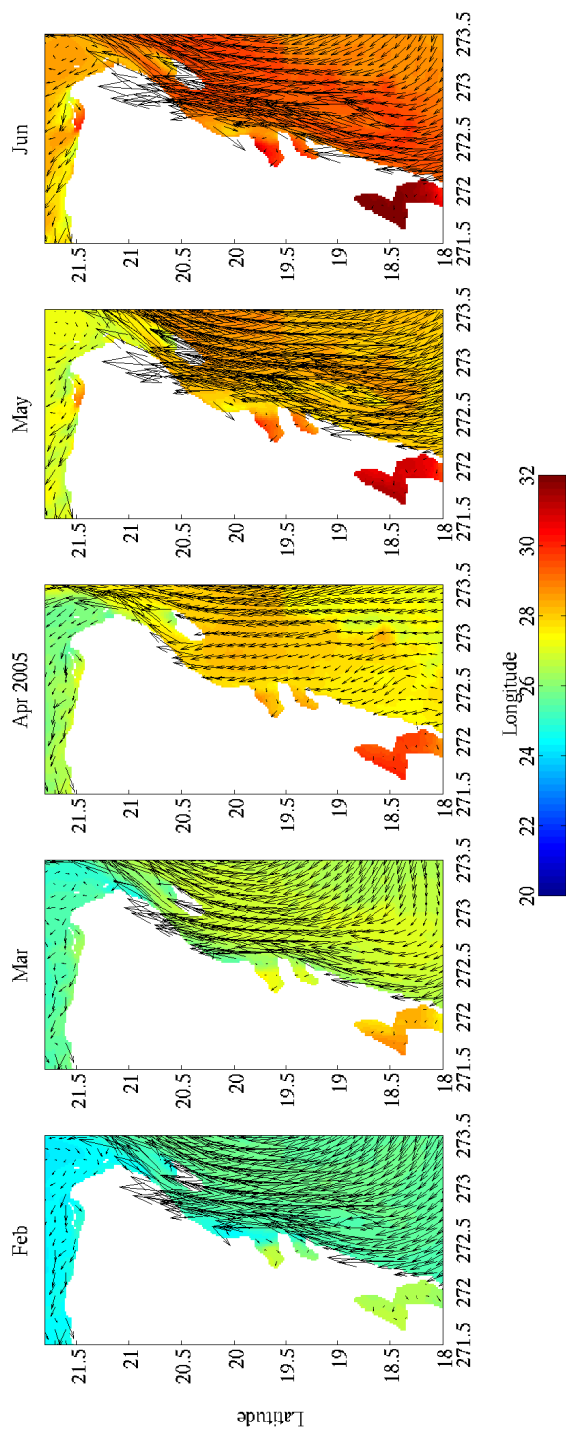
Figure A.8: 2005 SST with surface velocity vectors overlaid for the north Western Caribbean region.
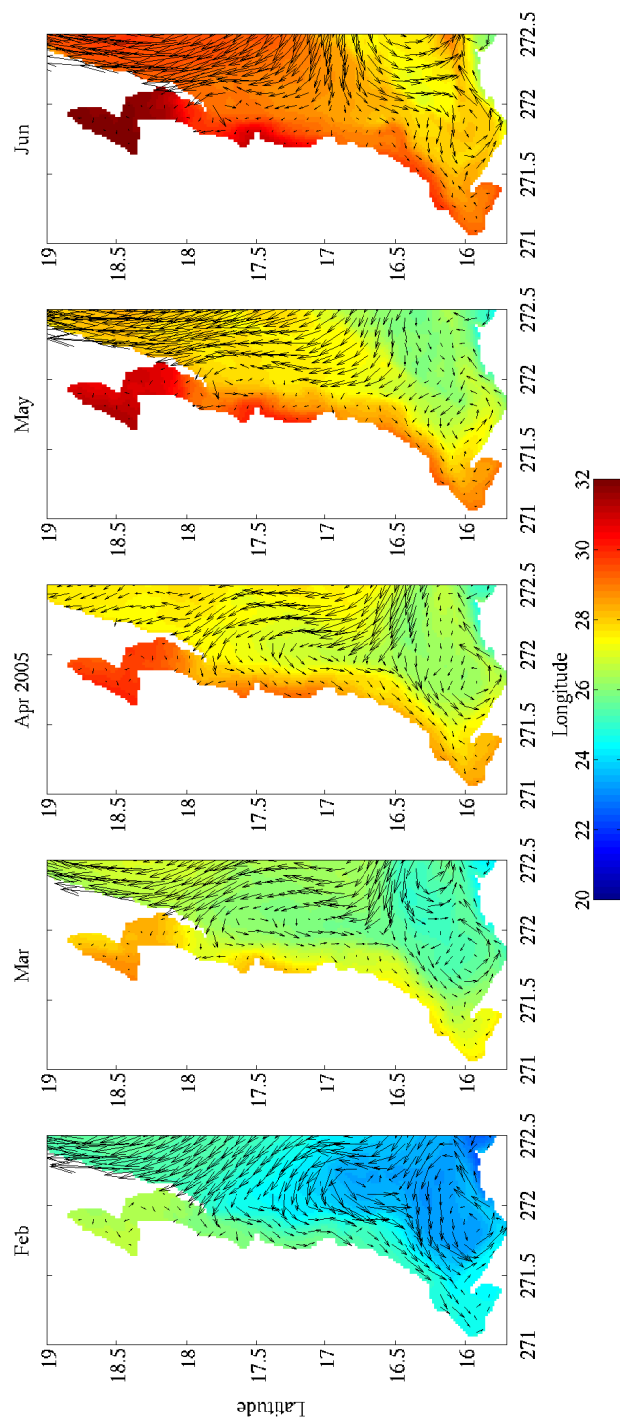
Figure A.9: 2005 SST with surface velocity vectors overlaid for the south Western Caribbean region.
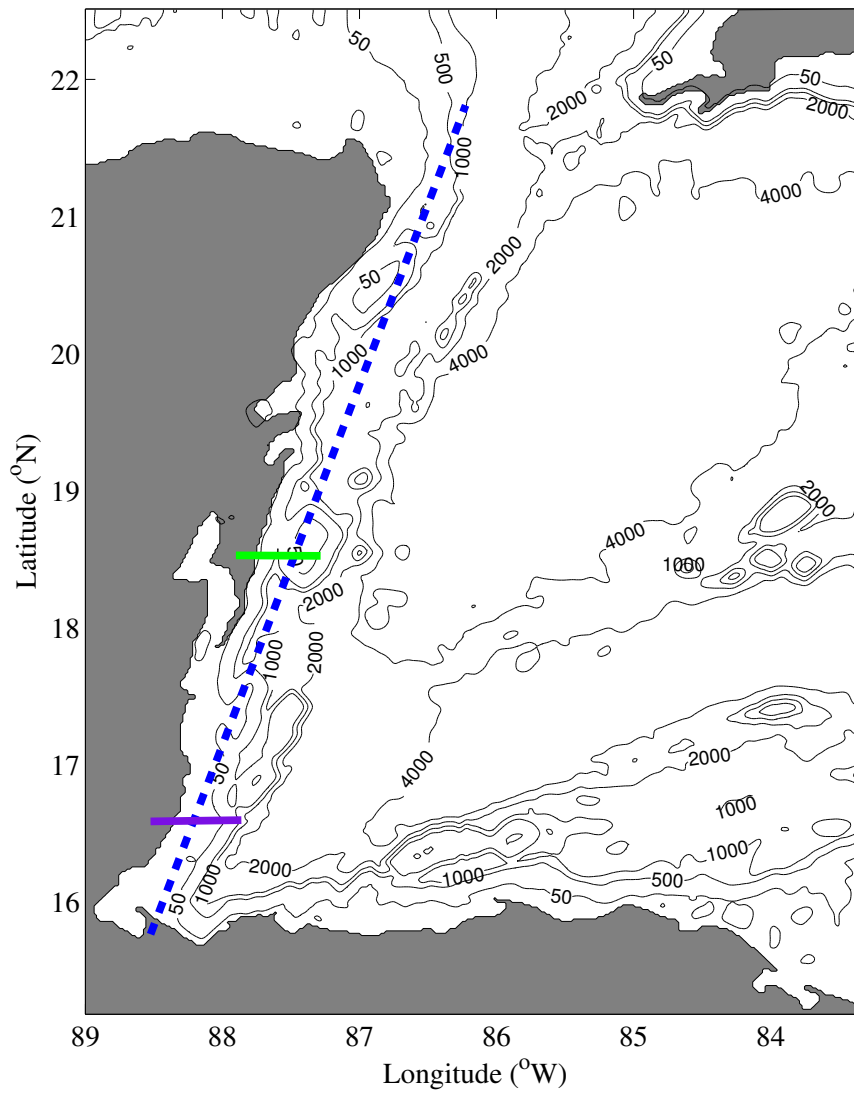
Figure A.10: Map showing the location of velocity sections on figures A6-A8.

215
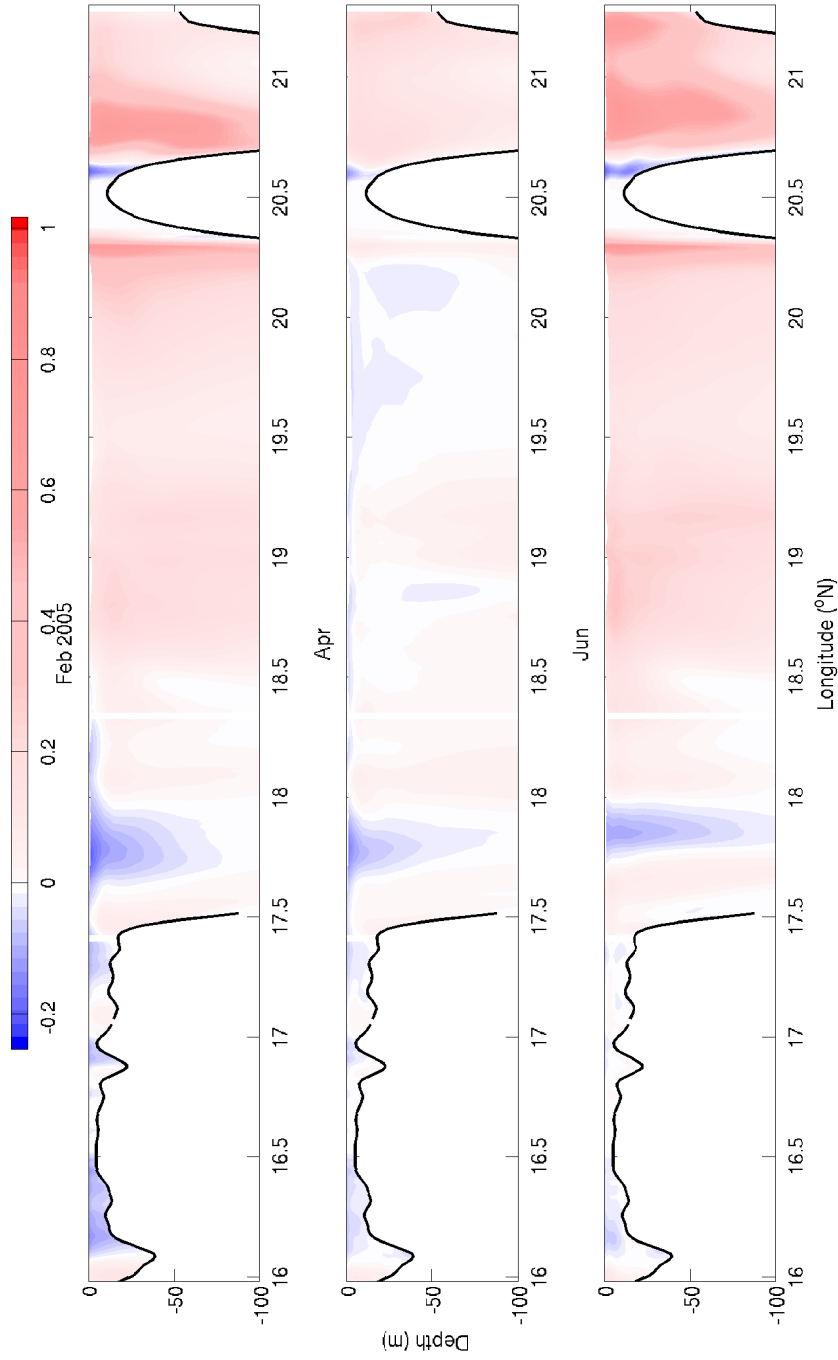
Figure A.11: East-West velocity section for 2005 at the transect marked with a dashed blue line A10. Blue shades are westward velocities (onshore), red shades are eastward velocities (offshore). Near zero velocities are blanked. Black contour marks the bottom.

216
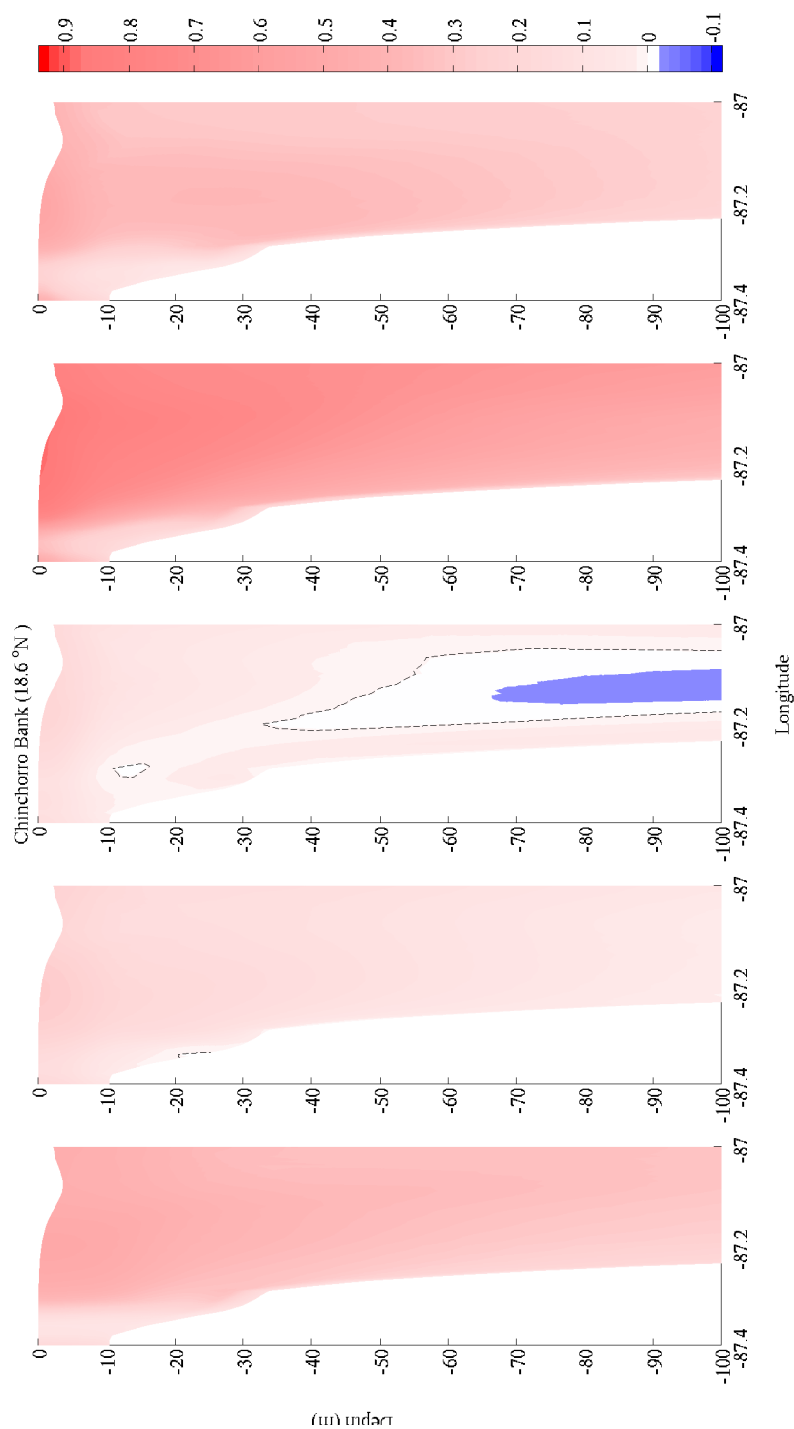
Figure A.12: North-southt velocity section for 2005 at green line marked in the map on figure A10. Blue shades are westward velocities (onshore), red shades are eastward velocities (offshore).

217
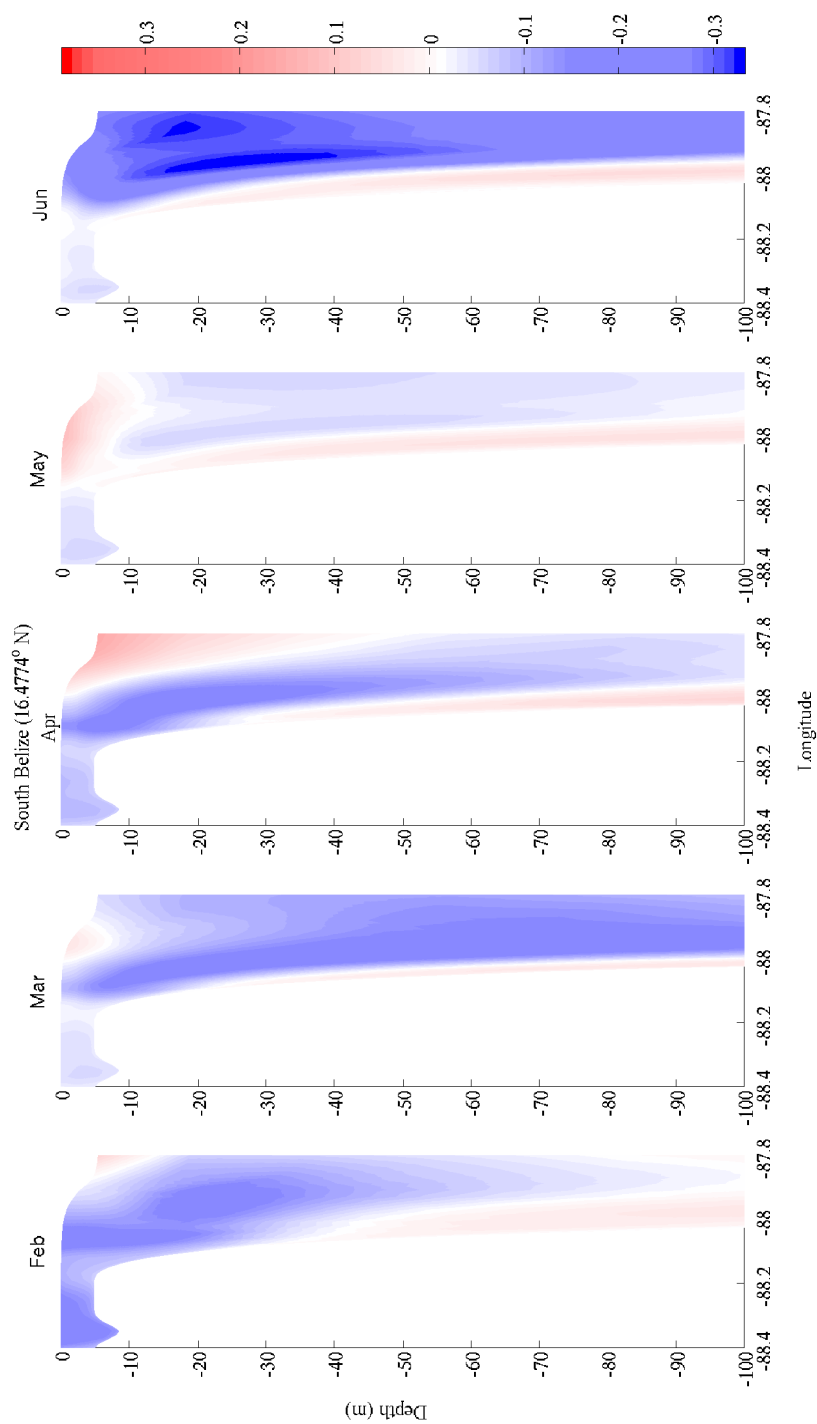
Figure A.13: North-southt velocity section for 2005 at green line marked in the map on figure A5. Blue shades are westward velocities (onshore), red shades are eastward velocities (offshore).

Bibliography

Albins, M. and Hixon, M. (2008). Invasive Indo-Pacific lionfish Pterois volitans reduce recruitment of Atlantic coral-reef fishes. *Marine Ecology Progress Series*, 367:233–238.

Albins, M. A. and Hixon, M. A. (2013). Worst case scenario: potential long-term effects of invasive predatory lionfish (Pterois volitans) on Atlantic and Caribbean coral-reef communities. *Environmental Biology of Fishes*, 96(10-11):1151–1157.

Almany, G. R., Berumen, M. L., Thorrold, S. R., Planes, S., and Jones, G. P. (2007). Local Replenishment of Coral Reef Fish Populations in a Marine Reserve. *Science*, 316(5825):742–744.

Almany, G. R., Connolly, S. R., Heath, D. D., Hogan, J. D., Jones, G. P., McCook, L. J., Mills, M., Pressey, R. L., and Williamson, D. H. (2009). Connectivity, biodiversity conservation and the design of marine reserve networks for coral reefs. *Coral Reefs*, 28(2):339–351.

Almany, G. R. and Webster, M. S. (2005). The predation gauntlet: early post-settlement mortality in reef fishes. *Coral Reefs*, 25(1):19–22.

Anderson, D., Carrington, D., Corry, R., and Gordon, C. (1991). Modeling the variability of the Somali Current. *Journal of Marine Research*, 49(4):659–696.

Andrade, C. A. and Barton, E. D. (2000). Eddy development and motion in the Caribbean Sea. *Journal of Geophysical Research: Oceans*, 105(C11):26191–26201.

Andrade, C. A., Barton, E. D., and Mooers, C. N. K. (2003). Evidence for an eastward flow along the Central and South American Caribbean Coast. *Journal of Geophysical Research: Oceans*, 108(C6):3185.

Atema, J., Gerlach, G., and Paris, C. B. (2015). Sensory biology and navigation behavior of reef fish larvae. In Mora, C., editor, *Ecology of Fishes on Coral Reefs*, number Cambridge University Press.

Atema, J., Kingsford, M. J., and Gerlach, G. (2002). Larval reef fish could use odour for detection, retention and orientation to reefs. *Marine Ecology Progress Series*, 241:151–160.

Babcock, R. C. and Heyward, A. J. (1986). Larval development of certain gamete-spawning scleractinian corals. *Coral Reefs*, 5(3):111–116.

Barale, V., Gower, J. F. R., and Alberotanza, L. (2010). *Oceanography from Space: Revisited*. Springer Science & Business Media.

Batchelder, H. P. (2006). Forward-in-Time-/Backward-in-Time-Trajectory (FITT/BITT) Modeling of Particles and Organisms in the Coastal Ocean*. *Journal of Atmospheric and Oceanic Technology*, 23(5):727–741.

Batchelder, H. P., Edwards, C. A., and Powell, T. M. (2002). Individual-based models of copepod populations in coastal upwelling regions: implications of physiologically and environmentally influenced diel vertical migration on demographic success and nearshore retention. *Progress in Oceanography*, 53(24):307–333.

Baums, I. B., Miller, M. W., and Hellberg, M. E. (2005). Regionally isolated populations of an imperiled Caribbean coral, Acropora palmata. *Molecular Ecology*, 14(5):1377–1390.

Baums, I. B., Paris, C. B., and Chrubin, L. M. (2006). A bio-oceanographic filter to larval dispersal in a reef-building coral. *Limnology and Oceanography*, 51(5):1969–1981.

Beckmann, A. and Haidvogel, D. B. (1993). Numerical simulation of flow around a tall isolated seamount. Part I: Problem formulation and model accuracy. *Journal of Physical Oceanography*, 23(8):1736–1753.

Bendekovic, J. and Vuletic, D. (2013). Piracy influence on the shipowners and insurance companies. *DAAAM International Scientific Book*.

Bergenius, M. A., Meekan, M. G., Robertson, R. D., and McCormick, M. I. (2002). Larval growth predicts the recruitment success of a coral reef fish. *Oecologia*, 131(4):521–525.

Betancur-R., R., Hines, A., Acero P., A., Ort, G., Wilbur, A. E., and Freshwater, D. W. (2011). Reconstructing the lionfish invasion: insights into Greater Caribbean biogeography. *Journal of Biogeography*, 38(7):1281–1293.

Blythe, J. and Pineda, J. (2009). Habitat selection at settlement endures in recruitment time series. *Marine Ecology Progress Series*, 396:77–84.

Boehlert, G. W. and Mundy, B. C. (1993). Ichthyoplankton assemblages at seamounts and oceanic islands. *Bulletin of Marine Science*, 53(2):336–361.

Botsford, L. W., Brumbaugh, D. R., Grimes, C., Kellner, J. B., Largier, J., OFarrell, M. R., Ralston, S., Soulanille, E., and Wespestad, V. (2008). Connectivity, sustainability, and yield: bridging the gap between conventional fisheries management and marine protected areas. *Reviews in Fish Biology and Fisheries*, 19(1):69–95.

Botsford, L. W., Micheli, F., and Hastings, A. (2003). Principles for the design of marine reserves. *Ecological Applications*, 13(sp1):25–31.

Botsford, L. W., White, J. W., Coffroth, M.-A., Paris, C. B., Planes, S., Shearer, T. L., Thorrold, S. R., and Jones, G. P. (2009). Connectivity and resilience of coral reef metapopulations in marine protected areas: matching empirical efforts to predictive needs. *Coral Reefs*, 28(2):327–337.

Briones-Fourzn, P., Candela, J., and Lozano-lvarez, E. (2008). Postlarval settlement of the spiny lobster Panulirus argus along the Caribbean coast of Mexico: patterns, influence of physical factors, and possible sources of origin. *Limnology and Oceanography*, 53(3):970–985.

Bunge, L. (2002). Deep flows in the Yucatan Channel and their relation to changes in the Loop Current extension. *Journal of Geophysical Research*, 107(C12).

Burke, L., Reytar, K., Spalding, M., and Perry, A. (2011). *Reefs at risk revisited*. World Resources Institute, Washington, DC.

Carpenter, R. C. (1990). Mass mortality ofDiadema antillarum. *Marine Biology*, 104(1):67–77.

Carr, M. H. and Hixon, M. A. (1995). Predation effects on early post-settlement survivorship of coral-reef fishes. *Marine ecology progress series. Oldendorf*, 124(1):31–42.

Caselle, J. E. (1999). Early post-settlement mortality in a coral reef fish and its effect on local population size. *Ecological Monographs*, 69(2):177–194.

Cetina, P., Candela, J., Sheinbaum, J., Ochoa, J., and Badan, A. (2006). Circulation along the Mexican Caribbean coast. *Journal of Geophysical Research: Oceans*, 111(C8):C08021.

Cetina-Heredia, P. and Connolly, S. R. (2011). A simple approximation for larval retention around reefs. *Coral Reefs*, 30(3):593–605.

Chao, S.-Y., Ko, D.-S., Lien, R.-C., and Shaw, P.-T. (2007). Assessing the west ridge of Luzon Strait as an internal wave mediator. *Journal of Oceanography*, 63(6):897–911.

Chassignet, E. P., Hurlburt, H. E., Smedstad, O. M., Halliwell, G. R., Hogan, P. J., Wallcraft, A. J., Baraille, R., and Bleck, R. (2007). The HYCOM (hybrid coordinate ocean model) data assimilative system. *Journal of Marine Systems*, 65(1):60–83.

Chittaro, P. M. and Hogan, J. D. (2012). Patterns of connectivity among populations of a coral reef fish. *Coral Reefs*, 32(2):341–354.

Choat, J. H. and Axe, L. M. (1996). Growth and longevity in acanthurid fishes; an analysis of otolith increments. *Oceanographic Literature Review*, 43(12):1263–1264.

Christie, M. R., Johnson, D. W., Stallings, C. D., and Hixon, M. A. (2010a). Self-recruitment and sweepstakes reproduction amid extensive gene flow in a coral-reef fish. *Molecular Ecology*, 19(5):1042–1057.

Christie, M. R., Tissot, B. N., Albins, M. A., Beets, J. P., Jia, Y., Ortiz, D. M., Thompson, S. E., and Hixon, M. A. (2010b). Larval Connectivity in an Effective Network of Marine Protected Areas. *PLoS ONE*, 5(12):e15715.

Chvez, G., Candela, J., and Ochoa, J. (2003). Subinertial flows and transports in Cozumel Channel. *Journal of Geophysical Research: Oceans*, 108(C2):3037.

Chrubin, L. M., Kuchinke, C. P., and Paris, C. B. (2008). Ocean circulation and terrestrial runoff dynamics in the Mesoamerican region from spectral optimization of SeaWiFS data and a high resolution simulation. *Coral Reefs*, 27(3):503–519.

Chrubin, L. M. and Richardson, P. L. (2007). Caribbean current variability and the influence of the Amazon and Orinoco freshwater plumes. *Deep Sea Research Part I: Oceanographic Research Papers*, 54(9):1451–1473.

Colin, P. L. and Clavijo, I. E. (1988). Spawning activity of fishes producing pelagic eggs on a shelf edge coral reef, southwestern Puerto Rico. *Bulletin of Marine Science*, 43(2):249–279.

Collins, C., Reason, C. J. C., and Hermes, J. C. (2012). Scatterometer and reanalysis wind products over the western tropical Indian Ocean. *Journal of Geophysical Research: Oceans*, 117(C3):C03045.

Coln, J. A. (1963). Seasonal Variations in Heat Flux from the Sea Surface to the Atmosphere over the Caribbean Sea. *Journal of Geophysical Research*, 68(5).

Cowen, R. K. and Castro, L. R. (1994). Relation of coral reef fish larval distributions to island scale circulation around Barbados, West Indies. *Bulletin of Marine Science*, 54(1):228–244.

Cowen, R. K., Gawarkiewicz, G. G., Pineda, J., Thorrold, S. R., and Werner, F. E. (2007). Population connectivity in marine systems: an overview.

Cowen, R. K., Paris, C. B., and Srinivasan, A. (2006). Scaling of Connectivity in Marine Populations. *Science*, 311(5760):522–527.

Cowen, R. K. and Sponaugle, S. (2009). Larval Dispersal and Marine Population Connectivity. *Annual Review of Marine Science*, 1(1):443–466.

Craig, P., Choat, H., Axe, L., and Saucerman, S. (1997). Population biology and harvest of the coral reef surgeonfish Acanthurus¡ meatus in American Samoa. *Fishery Bulletin*, 95:680–693.

Craig, P. C. (1998). Temporal Spawning Patterns of Several Surgeonfishes and Wrasses in American Samoa. *Pacific Science*, 52(1):35–39.

Da Silva, J. C. B., New, A. L., and Magalhaes, J. M. (2009). Internal solitary waves in the Mozambique Channel: Observations and interpretation. *Journal of Geophysical Research: Oceans (19782012)*, 114(C5).

Doherty, P. J., Dufour, V., Galzin, R., Hixon, M. A., Meekan, M. G., and Planes, S. (2004). High mortality during settlement is a population bottleneck for a tropical surgeonfish. *Ecology*, 85(9):2422–2428.

Domingues, C. P., Nolasco, R., Dubert, J., and Queiroga, H. (2012). Model-Derived Dispersal Pathways from Multiple Source Populations Explain Variability of Invertebrate Larval Supply. *PLoS ONE*, 7(4):e35794.

Dorenbosch, M., Pollux, B. J. A., Pustjens, A. Z., Rajagopal, S., Nagelkerken, I., Velde, G. v. d., and Staay, S. Y. M.-v. d. (2006). Population structure of the Dory snapper, Lutjanus fulviflamma, in the western Indian Ocean revealed by means of AFLP fingerprinting. *Hydrobiologia*, 568(1):43–53.

Drake, P. T., Edwards, C. A., Morgan, S. G., and Dever, E. P. (2013). Influence of larval behavior on transport and population connectivity in a realistic simulation of the California Current System. *Journal of Marine Research*, 71(4):317–350.

Dupont, T. M. and Thomas, S. M. (2004). Tourist development in Mexico: the case of Cancun Quintanta Roo.

Edgar, G. J., Stuart-Smith, R. D., Willis, T. J., Kininmonth, S., Baker, S. C., Banks, S., Barrett, N. S., Becerro, M. A., Bernard, A. T. F., Berkhout, J., Buxton, C. D., Campbell, S. J., Cooper, A. T., Davey, M., Edgar, S. C., Frsterra, G., Galvn, D. E., Irigoyen, A. J., Kushner, D. J., Moura, R., Parnell, P. E., Shears, N. T., Soler, G., Strain, E. M. A., and Thomson, R. J. (2014). Global conservation outcomes depend on marine protected areas with five key features. *Nature*, 506(7487):216–220.

Egbert, G. D., Bennett, A. F., and Foreman, M. G. G. (1994). TOPEX/POSEIDON tides estimated using a global inverse model. *Journal of Geophysical Research: Oceans*, 99(C12):24821–24852.

Egbert, G. D. and Erofeeva, S. Y. (2002). Efficient Inverse Modeling of Barotropic Ocean Tides. *Journal of Atmospheric and Oceanic Technology*, 19(2):183–204.

Escobar-Briones, E. (2004). Structure and function in the ecosystems of the intra-Americas sea (IAS). In Robinson, A. and Brink, K., editors, *The sea*, volume 14, pages 225–258. Harvard College.

Ezer, T., Oey, L.-Y., and Lee, H.-C. (2002). Simulation of velocities in the Yucatan Channel. In *OCEANS'02 MTS/IEEE*, volume 3, pages 1467–1471. IEEE.

Fairbridge, R. W. (1966). Caribbean Current. In Fairbridge, R. W., editor, *The encyclopedia of oceanography*, volume 1 of *Encyclopedia of Earth Sciences Series*, page 175.

Fieux, M. (2001). Somali Current. In Steele, J. H., Thorpe, S. A., and Turekian, K. K., editors, *Elements of physical oceanography: a derivative of the encyclopedia of ocean sciences*. Academic Press, San Diego, CA. USA.

Fieux, M. and Riverdin, G. (2001). Current Systems in the Indian Ocean. In Steele, J. H., Thorpe, S. A., and Turekian, K. K., editors, *Elements of physical oceanography: a derivative of the encyclopedia of ocean sciences*. Academic Press, San Diego, CA. USA.

Fogarty, M. and Botsford, L. W. (2007). Population connectivity. *Oceanography*, 20(3):112.

Fraschetti, S., Terlizzi, A., Ceccherelli, G., Addis, P., Murenu, M., Chemello, R., Milazzo, M., Spano, N., De Domenico, F., Mangialajo, L., and others (2006). Quantificazione degli effetti della protezione sul benthos di substrato duro: risultati di un esperimento condotto in 15 aree marine protette (AMP) italiane. *Biologia Marina Mediterranea*, 13(1):364–372.

Gallegos, A. and Czitrom, S. (1997). Aspectos de la oceanografa fsica regional del Mar Caribe. In *Contribuciones a la oceanografa fsica en Mxico*, number 3 in Monografa, pages 225–242. Unin Geofsica Mexicana.

Gamble, D. W. and Curtis, S. (2008). Caribbean precipitation: review, model and prospect. *Progress in Physical Geography*, 32(3):265–276.

Gawarkiewicz, G. G., Monismith, S. G., and Largier, J. (2007). Observing larval transport processes affecting population connectivity: progress and challenges.

Gell, F. R. and Roberts, C. M. (2003). Benefits beyond boundaries: the fishery effects of marine reserves. *Trends in Ecology & Evolution*, 18(9):448–455.

Gerlach, G., Atema, J., Kingsford, M. J., Black, K. P., and Miller-Sims, V. (2007). Smelling home can prevent dispersal of reef fish larvae. *Proceedings of the National Academy of Sciences*, 104(3):858–863.

Gommenginger, C., Thibaut, P., Fenoglio-Marc, L., Quartly, G., Deng, X., Gmez-Enri, J., Challenor, P., and Gao, Y. (2011). Retracking Altimeter Waveforms Near the Coasts. In Vignudelli, S., Kostianoy, A. G., Cipollini, P., and Benveniste, J., editors, *Coastal Altimetry*, pages 61–101. Springer Berlin Heidelberg, Berlin, Heidelberg.

Goodbody-Gringley, G. (2010). Diel planulation by the brooding coral Favia fragum (Esper, 1797). *Journal of Experimental Marine Biology and Ecology*, 389(12):70–74.

Goodbody-Gringley, G., Woollacott, R. M., and Giribet, G. (2012). Population structure and connectivity in the Atlantic scleractinian coral Montastraea cavernosa (Linnaeus, 1767). *Marine Ecology*, 33(1):32–48.

Gordon, A. L. (1967). Circulation of the Caribbean Sea. *Journal of Geophysical Research*, 72(24):6207–6223.

Graham, E. M., Baird, A. H., and Connolly, S. R. (2008). Survival dynamics of scleractinian coral larvae and implications for dispersal. *Coral Reefs*, 27(3):529–539.

Green, S. J., Akins, J. L., Maljkovi, A., and Ct, I. M. (2012). Invasive Lionfish Drive Atlantic Coral Reef Fish Declines. *PLoS ONE*, 7(3):e32596.

Haidvogel, D. B., Arango, H., Budgell, W. P., Cornuelle, B. D., Curchitser, E., Di Lorenzo, E., Fennel, K., Geyer, W. R., Hermann, A. J., Lanerolle, L., Levin, J., McWilliams, J. C., Miller, A. J., Moore, A. M., Powell, T. M., Shchepetkin, A. F., Sherwood, C. R., Signell, R. P., Warner, J. C., and Wilkin, J. (2008). Ocean forecasting in terrain-following coordinates: Formulation and skill assessment of the Regional Ocean Modeling System. *Journal of Computational Physics*, 227(7):3595–3624.

Halpern, B. S. (2003). The impact of marine reserves: do reserves work and does reserve size matter? *Ecological Applications*, 13(sp1):117–137.

Hamilton, H. G. and Brakel, W. H. (1984). Structure and coral fauna of East African reefs. *Bulletin of Marine Science*, 34(2):248–266.

Hamner, W. M. and Hauri, I. R. (1981). Effects of island mass: Water flow and plankton pattern around a reef in the Great Barrier Reef lagoon, Australia1. *Limnology and Oceanography*, 26(6):1084–1102.

Harborne, A. R., Afzal, D. C., and Andrews, M. J. (2001). Honduras: Caribbean Coast. *Marine Pollution Bulletin*, 42(12):1221–1235.

Harrison, H., Williamson, D., Evans, R., Almany, G., Thorrold, S., Russ, G., Feldheim, K., vanHerwerden, L., Planes, S., Srinivasan, M., Berumen, M., and Jones, G. (2012). Larval Export from Marine Reserves and the Recruitment Benefit for Fish and Fisheries. *Current Biology*, 22(11):1023–1028.

Harrison, P. L. (2011). Sexual Reproduction of Scleractinian Corals. In Dubinsky, Z. and Stambler, N., editors, *Coral Reefs: An Ecosystem in Transition*, pages 59–85. Springer Netherlands.

Harrison, P. L., Babcock, R. C., Bull, G. D., Oliver, J. K., Wallace, C. C., and Willis, B. L. (1984). Mass Spawning in Tropical Reef Corals. *Science*, 223(4641):1186–1189.

Hawkins, J. P. and Roberts, C. M. (2004). Effects of Artisanal Fishing on Caribbean Coral Reefs. *Conservation Biology*, 18(1):215–226.

Heenan, A., Simpson, S. D., and Braithwaite, V. A. (2009). Testing the generality of acoustic cue use at settlement in larval coral reef fish. *Proceedings of the 11th International Coral Reef Symposium, International Society for Reef Studies*.

Hermes, J. C. and Reason, C. J. C. (2008). Annual cycle of the South Indian Ocean (Seychelles-Chagos) thermocline ridge in a regional ocean model. *Journal of Geophysical Research: Oceans*, 113(C4):C04035.

Hogan, J. D., Thiessen, R. J., Sale, P. F., and Heath, D. D. (2012). Local retention, dispersal and fluctuating connectivity among populations of a coral reef fish. *Oecologia*, 168(1):61–71.

Hopley, D., editor (2011). *Encyclopedia of Modern Coral Reefs*. Encyclopedia of Earth Sciences Series. Springer Netherlands, Dordrecht.

Huebert, K. B., Cowen, R. K., and Sponaugle, S. (2011). Vertical migrations of reef fish larvae in the Straits of Florida and effects on larval transport. *Limnology and Oceanography*, 56(5):1653–1666.

Hughes, T. P., Baird, A. H., Bellwood, D. R., Card, M., Connolly, S. R., Folke, C., Grosberg, R., Hoegh-Guldberg, O., Jackson, J. B. C., Kleypas, J., Lough, J. M., Marshall, P., Nystrm, M., Palumbi, S. R., Pandolfi, J. M., Rosen, B., and Roughgarden, J. (2003). Climate Change, Human Impacts, and the Resilience of Coral Reefs. *Science*, 301(5635):929–933.

Irisson, J.-O., Paris, C. B., Guigand, C., and Planes, S. (2010). Vertical distribution and ontogenetic "migration" in coral reef fish larvae. *Limnology and Oceanography*, 55(2):909–919.

James, M. K., Armsworth, P. R., Mason, L. B., and Bode, L. (2002). The structure of reef fish metapopulations: modelling larval dispersal and retention patterns. *Proceedings of the Royal Society of London B: Biological Sciences*, 269(1505):2079–2086. An improved understanding of the dispersal patterns of marine organisms is a prerequisite for successful marine resource management. For species with dispersing larvae, regionalscale hydrodynamic models provide a means of obtaining results over relevant spatial and temporal scales. In an effort to better understand the role of the physical environment in dispersal, we simulated the transport of reef fish larvae among 321 reefs in and around the Cairns Section of the Great

Barrier Reef Marine Park over a period of 20 years. Based on regionalscale hydrodynamics, our models predict the spatial and temporal frequency of significant selfrecruitment of the larvae of certain species. Furthermore, the results suggest the importance of a select few local populations in ensuring the persistence of reef fish metapopulations over regional scales.

Jerlov, N. G. (1976). *Marine Optics*. Elsevier.

Johannes, R. E. (1978). Reproductive strategies of coastal marine fishes in the tropics. *Environmental Biology of Fishes*, 3(1):65–84.

Johns, W. E., Townsend, T. L., Fratantoni, D. M., and Wilson, W. D. (2002). On the Atlantic inflow to the Caribbean Sea. *Deep Sea Research Part I: Oceanographic Research Papers*, 49(2):211–243.

Jones, G. P. (2015). Mission imposible: unlocking the secret of coral reef fish dispersal. In Mora, C., editor, *Ecology of Fishes on Coral Reefs*, number Cambridge University Press.

Jones, G. P., Planes, S., and Thorrold, S. R. (2005). Coral Reef Fish Larvae Settle Close to Home. *Current Biology*, 15(14):1314–1318.

Kalnay, E., Kanamitsu, M., Kistler, R., Collins, W., Deaven, D., Gandin, L., Iredell, M., Saha, S., White, G., Woollen, J., Zhu, Y., Leetmaa, A., Reynolds, R., Chelliah, M., Ebisuzaki, W., Higgins, W., Janowiak, J., Mo, K. C., Ropelewski, C., Wang, J., Jenne, R., and Joseph, D. (1996). The NCEP/NCAR 40-Year Reanalysis Project. *Bulletin of the American Meteorological Society*, 77(3):437–471.

Kaunda-Arara, B., Mwaluma, J. M., Locham, G. A., resland, V., and Osore, M. K. (2009). Temporal variability in fish larval supply to Malindi Marine Park, coastal Kenya. *Aquatic Conservation: Marine and Freshwater Ecosystems*, 19(S1):S10–S18.

Kettle, A. J. and Haines, K. (2006). How does the European eel (Anguilla anguilla) retain its population structure during its larval migration across the North Atlantic Ocean? *Canadian Journal of Fisheries and Aquatic Sciences*, 63(1):90–106.

Kiflawi, M. and Mazeroll, A. I. (2006). Female Leadership During Migration and the Potential for Sex-Specific Benefits of Mass Spawning in the Brown Surgeonfish (Acanthurus nigrofuscus). *Environmental Biology of Fishes*, 76(1):19–23.

Kinder, T. H. (1983). Shallow currents in the Caribbean Sea and Gulf of Mexico as observed with satellite-tracked drifters. *Bulletin of Marine Science*, 33(2):239–246.

Kinder, T. H., Heburn, G. W., and Green, A. (1985). Some aspects of the Caribbean circulation. *Marine Geology*, 68:25–52.

Kingsford, M. J., Leis, J. M., Shanks, A., Lindeman, K. C., Morgan, S. G., and Pineda, J. (2002). Sensory environments, larval abilities and local self-recruitment.

Kool, J. T., Paris, C. B., Andrfout, S., and Cowen, R. K. (2010). Complex migration and the development of genetic structure in subdivided populations: an example from Caribbean coral reef ecosystems. *Ecography*, 33(3):597–606.

Kough, A. S., Paris, C. B., and Butler, IV, M. J. (2013). Larval Connectivity and the International Management of Fisheries. *PLoS ONE*, 8(6):e64970.

Kruse, M., Taylor, M., Muhando, C. A., and Reuter, H. (2015). Lunar, diel, and tidal changes in fish assemblages in an East African marine reserve. *Regional Studies in Marine Science*.

Kundu, P. K. and Cohen, I. M. (2008). *Fluid mechanics. 4th Edition*. ELSEVIER, Oxford.

Largier, J. L. (2003). Considerations in estimating larval dispersal distances from oceanographic data. *Ecological Applications*, 13(sp1):71–89.

Lecchini, D. (2005). Spatial and behavioural patterns of reef habitat settlement by fish larvae. *Marine Ecology Progress Series*, 301:247–252.

Lecchini, D., Shima, J., Banaigs, B., and Galzin, R. (2005). Larval sensory abilities and mechanisms of habitat selection of a coral reef fish during settlement. *Oecologia*, 143(2):326–334.

Lee, T. and Marotzke, J. (1998). Seasonal cycles of meridional overturning and heat transport of the Indian Ocean. *Journal of Physical Oceanography*, 28(5):923–943.

Leis, J. M. and Carson-Ewart, B. M. (1999). In situ swimming and settlement behaviour of larvae of an Indo-Pacific coral-reef fish, the coral trout Plectropomus leopardus (Pisces: Serranidae). *Marine Biology*, 134(1):51–64.

Leis, J. M., Carson-Ewart, B. M., Hay, A. C., and Cato, D. H. (2003). Coral-reef sounds enable nocturnal navigation by some reef-fish larvae in some places and at some times. *Journal of Fish Biology*, 63(3):724–737.

Leis, J. M. and Fisher, R. (2006). Swimming speed of settlement-stage reef-fish larvae measured in the laboratory and in the field: a comparison of critical speed and in situ speed. In *Proceedings of the 10th international coral reef symposium, Okinawa*, pages 438–445. Coral Reef Society of Japan Tokyo.

Leis, J. M., Wright, K. J., and Johnson, R. N. (2007). Behaviour that influences dispersal and connectivity in the small, young larvae of a reef fish. *Marine Biology*, 153(1):103–117.

Lester, S., Halpern, B., Grorud-Colvert, K., Lubchenco, J., Ruttenberg, B., Gaines, S., Airam, S., and Warner, R. (2009). Biological effects within no-take marine reserves: a global synthesis. *Marine Ecology Progress Series*, 384:33–46.

Lett, C., Ayata, S.-D., Huret, M., and Irisson, J.-O. (2010). Biophysical modelling to investigate the effects of climate change on marine population dispersal and connectivity. *Progress in Oceanography*, 87(14):106–113.

Longenecker, K. and Langston, R. (2008). Life History Compendium of Exploited Hawaiian Fishes.

Mahongo, S. B. and Shaghude, Y. W. (2014). Modelling the dynamics of the Tanzanian coastal waters. *Journal of Oceanography and Marine Science*, 5(1):1–7.

Maina, J., Muthiga, N., and McClanahan, T. R. (2003). The effectiveness of management of marine protected areas in Kenya.

Maina, J., Venus, V., McClanahan, T. R., and Ateweberhan, M. (2008). Modelling susceptibility of coral reefs to environmental stress using remote sensing data and GIS models. *Ecological Modelling*, 212(34):180–199.

Mangubhai, S. (2008). Spawning patterns of Acropora species in the Mombasa lagoon in Kenya. *Ten years after bleachingfacing the consequences of climate change in the Indian Ocean*, pages 213–221.

Mangubhai, S. and Harrison, P. (2008). Asynchronous coral spawning patterns on equatorial reefs in Kenya. *Marine Ecology Progress Series*, 360:85–96.

Manyilizu, M., Dufois, F., Penven, P., and Reason, C. (2014). Interannual variability of sea surface temperature and circulation in the tropical western Indian Ocean. *African Journal of Marine Science*, 36(2):233–252.

Marchesiello, P., McWilliams, J. C., and Shchepetkin, A. (2001). Open boundary conditions for long-term integration of regional oceanic models. *Ocean Modelling*, 3(12):1–20.

Martin, S. (2014). *An Introduction to Ocean Remote Sensing.* Cambridge University Press.

Matano, R. P., Beier, E. J., and Strub, P. T. (2008). The seasonal variability of the circulation in the South Indian Ocean: Model and observations. *Journal of Marine Systems*, 74(1):315–328.

Matano, R. P., Beier, E. J., Strub, P. T., and Tokmakian, R. (2002). Large-Scale Forcing of the Agulhas Variability: The Seasonal Cycle. *Journal of Physical Oceanography*, 32(4):1228–1241.

Mayorga Adame, C. G. (2007). Ocean circulation of the Zanzibar Channel: A modeling approach, Outreach program final report. Summer Internship Final Report, Theiss Research Corporation, La Jolla, CA. USA.

Mayorga Adame, C. G. (2010). Development, performance evaluation and application of a physical model of the Kenyan-Tanzanian coastal region.

McClanahan, T. R. (1994). Kenyan coral reef lagoon fish: effects of fishing, substrate complexity, and sea urchins. *Coral Reefs*, 13(4):231–241.

McClanahan, T. R. and Mangi, S. (2000). Spillover of exploitable fishes from a marine park and its effect on the adjacent fishery. *Ecological Applications*, 10(6):1792–1805.

McClanahan, T. R., Marnane, M. J., Cinner, J. E., and Kiene, W. E. (2006). A Comparison of Marine Protected Areas and Alternative Approaches to Coral-Reef Management. *Current Biology*, 16(14):1408–1413.

McClanahan, T. R., Muthiga, N. A., Kamukuru, A. T., Machano, H., and Kiambo, R. W. (1999). The effects of marine parks and fishing on coral reefs of northern Tanzania. *Biological Conservation*, 89(2):161–182.

McClanahan, T. R., Nugues, M., and Mwachireya, S. (1994). Fish and sea urchin herbivory and competition in Kenyan coral reef lagoons: the role of reef management. *Journal of Experimental Marine Biology and Ecology*, 184(2):237–254.

McCook, L., Jompa, J., and Diaz-Pulido, G. (2014). Competition between corals and algae on coral reefs: a review of evidence and mechanisms. *Coral Reefs*, 19(4):400–417.

McCook, L. J., Almany, G. R., Berumen, M. L., Day, J. C., Green, A. L., Jones, G. P., Leis, J. M., Planes, S., Russ, G. R., Sale, P. F., and Thorrold, S. R. (2009). Management under uncertainty: guide-lines for incorporating connectivity into the protection of coral reefs. *Coral Reefs*, 28(2):353–366.

McCormick, M. I. (1999). Delayed metamorphosis of a tropical reef fish (Acanthurus triostegus): a field experiment. *Marine Ecology Progress Series*, 176:25–38. WOS:000078918200004.

McGurk, M. D. (1986). Natural mortality of marine pelagic fish eggs and larvae: role of spatial patchiness. *Marine ecology progress series*, 34(3):227–242.

McLeod, E., Salm, R., Green, A., and Almany, J. (2009). Designing marine protected area networks to address the impacts of climate change. *Frontiers in Ecology and the Environment*, 7(7):362–370.

McManus, J. W. and Polsenberg, J. F. (2004). Coralalgal phase shifts on coral reefs: Ecological and environmental aspects. *Progress in Oceanography*, 60(24):263–279.

Mellor, J. L. and Yamada, T. (1982). Development of a Turbulence Closure Model for Geophysical Fluid Problems. *Reviews of Geophysics and Space Physiscs*, 20(4):851–875.

Merino, M. (1997). Upwelling on the Yucatan Shelf: hydrographic evidence. *Journal of Marine Systems*, 13(14):101–121.

Micheli, F., Saenz-Arroyo, A., Greenley, A., Vazquez, L., Espinoza Montes, J. A., Rossetto, M., and De Leo, G. A. (2012). Evidence That Marine Reserves Enhance Resilience to Climatic Impacts. *PLoS ONE*, 7(7):e40832.

Mishra, A. P., Rai, S., and Pandey, A. C. (2007). Ocean Model Simulation of Southern Indian Ocean Surface Currents. *Marine Geodesy*, 30(4):345–354.

Muhling, B. A., Smith, R. H., VsquezYeomans, L., Lamkin, J. T., Johns, E. M., Carrillo, L., Sosa-Cordero, E., and Malca, E. (2013). Larval fish assemblages and mesoscale oceanographic structure along the Mesoamerican Barrier Reef System. *Fisheries Oceanography*, 22(5):409–428.

Munday, P. L., Leis, J. M., Lough, J. M., Paris, C. B., Kingsford, M. J., Berumen, M. L., and Lambrechts, J. (2009). Climate change and coral reef connectivity. *Coral Reefs*, 28(2):379–395.

Munro, J. L., Gaut, V. C., Thompson, R., and Reeson, P. H. (1973). The spawning seasons of Caribbean reef fishes. *Journal of Fish Biology*, 5(1):69–84.

Muthiga, N., Costa, A., Motta, H., Muhando, C., Mwaipopo, R., and Schleyer, M. (2008). Status of coral reefs in East Africa: Kenya, Tanzania, Mozambique and South Africa. *Status of coral reefs of the world*, pages 91–104.

Muths, D., Gouws, G., Mwale, M., Tessier, E., and Bourjea, J. (2012). Genetic connectivity of the reef fish Lutjanus kasmira at the scale of the western Indian Ocean. *Canadian Journal of Fisheries and Aquatic Sciences*, 69(5):842–853.

Myrberg, A. A., Montgomery, W. L., and Fishelson, L. (1988). The Reproductive Behavior of Acanthurus nigrofuscus (Forskal) and other Surgeonfishes (Fam. Acanthuridae) off Eilat, Israel (Gulf of Aqaba, Red Sea). *Ethology*, 79(1):31–61.

Nauw, J. J., Van Aken, H. M., Webb, A., Lutjeharms, J. R. E., and De Ruijter, W. P. M. (2008). Observations of the southern East Madagascar Current and undercurrent and countercurrent system. *Journal of Geophysical Research: Oceans (19782012)*, 113(C8).

Nishikawa, A., Katoh, M., and Sakai, K. (2003). Larval settlement rates and gene flow of broadcast-spawning (Acropora tenuis) and planula-brooding (Stylophora pistillata) corals. *Marine ecology. Progress series*, 256:87–97.

Nishikawa, A. and Sakai, K. (2005). Settlement-competency Period of Planulae and Genetic Differentiation of the Scleractinian Coral Acropora digitifera. *Zoological Science*, 22(4):391–399.

Nozawa, Y. and Harrison, P. L. (2008). Temporal patterns of larval settlement and survivorship of two broadcast-spawning acroporid corals. *Marine Biology*, 155(3):347–351.

O'Connor, M. I., Bruno, J. F., Gaines, S. D., Halpern, B. S., Lester, S. E., Kinlan, B. P., and Weiss, J. M. (2007). Temperature control of larval dispersal and the implications for marine ecology, evolution, and conservation. *Proceedings of the National Academy of Sciences*, 104(4):1266–1271.

Odido, M. and Mazzilli, S. (2009). African oceans and coasts.

Oxenford, H. A., Fanning, P., and Cowen, R. K. (2008). Spatial Distribution of Surgeonfish (Acanthuridae) Pelagic Larvae in the Eastern Caribbean. Proceedings of a Special Symposium, 9-11 November 2006, 59th Annual Meeting of the Gulf and Caribbean Fisheries Institute, Belize City, Belize. In Grober-Dunsmore, R. and Keller, B. D., editors, *Caribbean Connectivity: Implications fo r Marine Protected Area Management*, page 195. Marine Sanctuaries Conservation Series ONMS-08-07. U.S. Department of Commerce, National Oceanic and Atmospheric Administ ration, Office of Nationa l Marine Sanctuaries, Silver Spring, MD.

Pandey, A. C. and Rai, S. (2008). Sensitivity of the Indian Ocean circulation to surface wind stress. *Indian Journal of Marine Sciences*, 37(1):55–61.

Pandolfi, J. M., Bradbury, R. H., Sala, E., Hughes, T. P., Bjorndal, K. A., Cooke, R. G., McArdle, D., McClenachan, L., Newman, M. J. H., Paredes, G., Warner, R. R., and Jackson, J. B. C. (2003). Global Trajectories of the Long-Term Decline of Coral Reef Ecosystems. *Science*, 301(5635):955–958.

Paris, C., Chrubin, L., and Cowen, R. (2007). Surfing, spinning, or diving from reef to reef: effects on population connectivity. *Marine Ecology Progress Series*, 347:285–300.

Paris, C. B. and Chrubin, L. M. (2008). River-reef connectivity in the Meso-American Region. *Coral Reefs*, 27(4):773–781.

Paris, C. B. and Cowen, R. K. (2004). Direct evidence of a biophysical retention mechanism for coral reef fish larvae. *Limnology and Oceanography*, 49(6):1964–1979.

Paris, C. B., Cowen, R. K., Claro, R., and Lindeman, K. C. (2005). Larval transport pathways from Cuban snapper (Lutjanidae) spawning aggregations based on biophysical modeling. *Marine Ecology Progress Series*, 296:93–106.

Pastorok, R. A. and Bilyard, G. R. (1985). Effects of sewage pollution on coral-reef communities. *Marine ecology progress series. Oldendorf*, 21(1):175–189.

Payet, R. and Obura, D. (2004). The negative impacts of human activities in the Eastern African region: An international waters perspective. *AMBIO: A Journal of the Human Environment*, 33(1):24–33.

Pineda, J. (1994). Internal tidal bores in the nearshore: Warm-water fronts, seaward gravity currents and the onshore transport of neustonic larvae. *Journal of Marine Research*, 52(3):427–458.

Pineda, J. (1999). Circulation and larval distribution in internal tidal bore warm fronts. *Limnology and Oceanography*, 44(6):1400–1414.

Pineda, J. (2000). Linking larval settlement to larval transport: assumptions, potentials, and pitfalls. *Oceanography of the Eastern Pacific*, 1(2000):84–105.

Pineda, J., Hare, J. A., and Sponaungle, S. (2007). Larval transport and dispersal in the coastal ocean and consequences for population connectivity.

Pineda, J., Porri, F., Starczak, V., and Blythe, J. (2010). Causes of decoupling between larval supply and settlement and consequences for understanding recruitment and population connectivity. *Journal of Experimental Marine Biology and Ecology*, 392(1-2):9–21.

Pineda, J., Reyns, N. B., and Starczak, V. R. (2009). Complexity and simplification in understanding recruitment in benthic populations. *Population Ecology*, 51(1):17–32.

Pineda, J., Starczak, V. R., and Stueckle, T. A. (2006). Timing of successful settlement: demonstration of a recruitment window in the barnacle Semibalanus balanoides.

Polunin, N. V. C. and Roberts, C. M. (1993). Greater biomass and value of target coral-reef fishes in two small Caribbean marine reserves. *Marine Ecology-Progress Series*, 100:167–167.

Purcell, J. F. H., Cowen, R. K., Hughes, C. R., and Williams, D. A. (2006). Weak genetic structure indicates strong dispersal limits: a tale of two coral reef fish. *Proceedings of the Royal Society of London B: Biological Sciences*, 273(1593):1483–1490.

Pusack, T., Christie, M. R., Johnson, D. W., Stallings, C. D., and Hixon, M. A. (2014). Spatial and temporal patterns of larval dispersal in a coral-reef fish metapopulation: evidence of variable reproductive success - Pusack - 2014 - Molecular Ecology - Wiley Online Library. *Molecular Ecology*, 23(14):3396–3408.

Prez-Santos, I., Schneider, W., Sobarzo, M., Montoya-Snchez, R., Valle-Levinson, A., and Garcs-Vargas, J. (2010). Surface wind variability and its implications for the Yucatan basin-Caribbean Sea dynamics. *Journal of Geophysical Research*, 115(C10).

Randall, J. E. (1961). A Contribution to the Biology of the Convict Surgeonfish of the Hawaiian Islands, Acanthurus triostegus sandvicensis.

Reichert, J. M., Fryer, B. J., Pangle, K. L., Johnson, T. B., Tyson, J. T., Drelich, A. B., and Ludsin, S. A. (2010). River-plume use during the pelagic larval stage benefits recruitment of a lentic fish. *Canadian Journal of Fisheries and Aquatic Sciences*, 67(6):987–1004.

Reid, J. L. (2003). On the total geostrophic circulation of the Indian Ocean: flow patterns, tracers, and transports. *Progress in Oceanography*, 56(1):137–186.

Richardson, P. L. (2005). Caribbean Current and eddies as observed by surface drifters. *Deep Sea Research Part II: Topical Studies in Oceanography*, 52(34):429–463.

Richmond, M. D. (2002). *A field guide to the seashores of eastern Africa and the western Indian Ocean islands.* Swedish International Development Cooperation Agency.

Ridderinkhof, H., Van der Werf, P. M., Ullgren, J. E., Van Aken, H. M., Van Leeuwen, P. J., and De Ruijter, W. P. M. (2010). Seasonal and interannual variability in the Mozambique Channel from moored current observations. *Journal of Geophysical Research: Oceans (19782012)*, 115(C6).

Roberts, C. (2012). Marine Ecology: Reserves Do Have a Key Role in Fisheries. *Current Biology*, 22(11):R444–R446.

Roberts, C. M., Hawkins, J. P., and Gell, F. R. (2005). The role of marine reserves in achieving sustainable fisheries. *Philosophical Transactions of the Royal Society of London B: Biological Sciences*, 360(1453):123–132.

Robertson, D. R. (1983). On the spawning behavior and spawning cycles of eight surgeonfishes (Acanthuridae) from the Indo-Pacific. *Environmental Biology of Fishes*, 9(3-4):193–223.

Rocha, L. A., Bass, A. L., Robertson, D. R., and Bowen, B. W. (2002). Adult habitat preferences, larval dispersal, and the comparative phylogeography of three Atlantic surgeonfishes (Teleostei: Acanthuridae). *Molecular Ecology*, 11(2):243–251.

Roman, R. E. and Lutjeharms, J. R. E. (2009). Red Sea Intermediate Water in the source regions of the Agulhas Current. *Deep Sea Research Part I: Oceanographic Research Papers*, 56(6):939–962.

Salas, E., Molina-Urea, H., Walter, R. P., and Heath, D. D. (2010). Local and regional genetic connectivity in a Caribbean coral reef fish. *Marine Biology*, 157(2):437–445.

Sale, P. F., Cowen, R. K., Danilowicz, B. S., Jones, G. P., Kritzer, J. P., Lindeman, K. C., Planes, S., Polunin, N. V. C., Russ, G. R., Sadovy, Y. J., and Steneck, R. S. (2005). Critical science gaps impede use of no-take fishery reserves. *Trends in Ecology & Evolution*, 20(2):74–80.

Sammarco, P. W. and Andrews, J. C. (1988). Localized Dispersal and Recruitment in Great Barrier Reef Corals: The Helix Experiment. *Science*, 239(4846):1422–1424.

Sasaki, H., Sasai, Y., Nonaka, M., Masumoto, Y., and Kawahara, S. (2006). An eddy-resolving simulation of the quasi-global ocean driven by satellite-observed wind field. *Journal of the Earth Simulator*, 6:35–49.

Schott, F. A., Dengler, M., and Schoenefeldt, R. (2002). The shallow overturning circulation of the Indian Ocean. *Progress in Oceanography*, 53(1):57–103.

Schott, F. A. and McCreary, J. P. (2001). The monsoon circulation of the Indian Ocean. *Progress in Oceanography*, 51(1):1–123.

Schott, F. A., Xie, S.-P., and McCreary, J. P. (2009). Indian Ocean circulation and climate variability. *Reviews of Geophysics*, 47(1):RG1002.

Schultz, E. T. and Cowen, R. K. (1994). Recruitment of coral reef fishes to Bermuda: Local retention or long-distance transport? *EEB Articles*, page 15.

Selig, E. R. and Bruno, J. F. (2010). A Global Analysis of the Effectiveness of Marine Protected Areas in Preventing Coral Loss. *PLoS ONE*, 5(2):e9278.

Shaghude, Y. W., Wannas, K. O., and Mahongo, S. B. (2002). Biogenic assemblage and hydrodynamic settings of the tidally dominated reef platform sediments of the Zanzibar Channel.

Shaghude, Y. W. and Wanns, K. O. (2000). Mineralogical and Biogenic Composition of the Zanzibar Channel Sediments, Tanzania. *Estuarine, Coastal and Shelf Science*, 51(4):477–489.

Shanks, A. (1983). Surface slicks associated with tidally forced internal waves may transport pelagic larvae of benthic invertebrates and fishes shoreward. *Marine Ecology Progress Series*, 13:311–315.

Shanks, A. L. (2009). Pelagic Larval Duration and Dispersal Distance Revisited. *The Biological Bulletin*, 216(3):373–385.

Sheinbaum, J., Julio, C., Badan, A., and Ochoa, J. (2002). Flow structure and transport in the Yucatan Channel. *Geophysical Research Letters*, 29(3).

Sheng, J. and Tang, L. (2003). A Numerical Study of Circulation in the Western Caribbean Sea. *Journal of Physical Oceanography*, 33(10):2049–2069.

Shulman, M. J. and Bermingham, E. (1995). Early Life Histories, Ocean Currents, and the Population Genetics of Caribbean Reef Fishes. *Evolution*, 49(5):897–910.

Simpson, S. D., Meekan, M., Montgomery, J., McCauley, R., and Jeffs, A. (2005). Homeward Sound. *Science*, 308(5719):221–221.

Simpson, S. D., Piercy, J. J. B., King, J., and Codling, E. A. (2013). Modelling larval dispersal and behaviour of coral reef fishes. *Ecological Complexity*, 16:68–76.

Smith, S. L., Codispoti, L. A., Morrison, J. M., and Barber, R. T. (1998). The 1994-1996 Arabian Sea Expedition: An integrated, interdisciplinary investigation of the response of the northwestern Indian Ocean to monsoonal forcing. *Deep-sea research. Part II, Topical studies in oceanography*, 45(10-11):1905–1915.

Sobel, J. and Dahlgren, C. (2004). *Marine Reserves: A Guide to Science, Design, and Use.* Island Press.

Soto, I., Andrfout, S., Hu, C., Muller-Karger, F. E., Wall, C. C., Sheng, J., and Hatcher, B. G. (2009). Physical connectivity in the Mesoamerican Barrier Reef System inferred from 9 years of ocean color observations. *Coral Reefs*, 28(2):415–425.

Souter, P., Henriksson, O., Olsson, N., and Grahn, M. (2009). Patterns of genetic structuring in the coral Pocillopora damicornis on reefs in East Africa. *BMC Ecology*, 9(1):19.

Spalding, M., Ravilious, C., and Green, E. P. (2001). *World Atlas of Coral Reefs*. University of California Press.

Sponaugle, S., Paris, C., Walter, K., Kourafalou, V., and DAlessandro, E. (2012). Observed and modeled larval settlement of a reef fish to the Florida Keys. *Marine Ecology Progress Series*, 453:201–212.

Staaterman, E., Paris, C. B., and Helgers, J. (2012). Orientation behavior in fish larvae: A missing piece to Hjort's critical period hypothesis. *Journal of Theoretical Biology*, 304:188–196.

Steneck, R. S., Paris, C. B., Arnold, S. N., Ablan-Lagman, M. C., Alcala, A. C., Butler, M. J., McCook, L. J., Russ, G. R., and Sale, P. F. (2009). Thinking and managing outside the box: coalescing connectivity networks to build region-wide resilience in coral reef ecosystems. *Coral Reefs*, 28(2):367–378.

Stewart, R. H. (1997). Introduction to physical oceanography. *American Journal of Physics*, 65(10):1028.

Stobutzki, I. C. and Bellwood, D. R. (1997). Sustained swimming abilities of the late pelagic stages of coral reef fishes. *Oceanographic Literature Review*, 9(44):986.

Swallow, J. C., Schott, F., and Fieux, M. (1991). Structure and transport of the East African coastal current. *Journal of Geophysical Research: Oceans (19782012)*, 96(C12):22245–22257.

Swearer, S. E., Caselle, J. E., Lea, D. W., and Warner, R. R. (1999). Larval retention and recruitment in an island population of a coral-reef fish. *Nature*, 402(6763):799–802.

Tang, L., Sheng, J., Hatcher, B. G., and Sale, P. F. (2006). Numerical study of circulation, dispersion, and hydrodynamic connectivity of surface waters on the Belize shelf. *Journal of Geophysical Research: Oceans*, 111(C1):C01003.

Taylor, K. E. (2000). *Summarizing multiple aspects of model performance in a single diagram.* Program for Climate Model Diagnosis and Intercomparison, Lawrence Livermore National Laboratory, University of California.

Thorrold, S. R., Jones, C. M., Swart, P. K., and Targett, T. E. (1998). Accurate classification of juvenile weakfish Cynoscion regalis to estuarine nursery areas based on chemical signatures in otoliths. *Marine Ecology Progress Series*, 173:253–265.

Tolimieri, N., Jeffs, A. G., and Montgomery, J. C. (2000). Ambient sound as a cue for navigation by the pelagic larvae of reef fishes.

Treml, E. A., Halpin, P. N., Urban, D. L., and Pratson, L. F. (2008). Modeling population connectivity by ocean currents, a graph-theoretic approach for marine conservation. *Landscape Ecology*, 23(1):19–36.

Umlauf, L. and Burchard, H. (2003). A generic length-scale equation for geophysical turbulence models. *Journal of Marine Research*, 61(2):235–265.

Underwood, J. N., Wilson, S. K., Ludgerus, L., and Evans, R. D. (2013). Integrating connectivity science and spatial conservation management of coral reefs in northwest Australia. *Journal for Nature Conservation*, 21(3):163–172.

Van der Werf, P. M., Van Leeuwen, P. J., Ridderinkhof, H., and De Ruijter, W. P. M. (2010). Comparison between observations and models of the Mozambique Channel transport: Seasonal cycle and eddy frequencies. *Journal of Geophysical Research: Oceans (19782012)*, 115(C2).

Van Katwijk, M. M., Meier, N. F., Van Loon, R., Van Hove, E. M., Giesen, W., Van der Velde, G., and Den Hartog, C. (1993). Sabaki River sediment load and coral stress: correlation between sediments and condition of the Malindi-Watamu reefs in Kenya (Indian Ocean). *Marine Biology*, 117(4):675–683.

Van Woesik, R., Lacharmoise, F., and Kksal, S. (2006). Annual cycles of solar insolation predict spawning times of Caribbean corals. *Ecology Letters*, 9(4):390–398.

Victor, B. C. (1986). Larval Settlement and Juvenile Mortality in a Recruitment-Limited Coral Reef Fish Population. *Ecological Monographs*, 56(2):145–160.

Villegas Snchez, C. A., Perez Espaa, H., Rivera Madrid, R., Salas Monreal, D., and Arias Gonzlez, J. E. (2014). Subtle genetic connectivity between Mexican Caribbean and south-western Gulf of Mexico reefs: the case of the bicolor damselfish, Stegastes partitus. *Coral reefs*, 33(1):241–251.

Villegas-Snchez, C. A., Rivera-Madrid, R., and Arias-Gonzlez, J. E. (2010). Small-scale genetic connectivity of bicolor damselfish (Stegastes partitus) recruits in Mexican Caribbean reefs. *Coral Reefs*, 29(4):1023–1033.

Vimal Kumar, K. G., Dinesh Kumar, P. K., Smitha, B. R., Habeeb Rahman, H., Josia, J., Muraleedharan, K. R., Sanjeevan, V. N., and Achuthankutty, C. T. (2008). Hydrographic characterization of southeast Arabian Sea during the wane of southwest monsoon and spring intermonsoon. *Environmental Monitoring and Assessment*, 140(1-3):231–247.

Visram, S., Yang, M.-C., Pillay, R. M., Said, S., Henriksson, O., Grahn, M., and Chen, C. A. (2010). Genetic connectivity and historical demography of the blue

barred parrotfish (Scarus ghobban) in the western Indian Ocean. *Marine Biology*, 157(7):1475–1487.

Wallace, C. C. (2011). Acropora. In Hopley, D., editor, *Encyclopedia of Modern Coral Reefs*, Encyclopedia of Earth Sciences Series. Springer Netherlands, Dordrecht.

Warner, J. C., Sherwood, C. R., Arango, H. G., and Signell, R. P. (2005). Performance of four turbulence closure models implemented using a generic length scale method. *Ocean Modelling*, 8(1-2):81–113.

Watson, J., Mitarai, S., Siegel, D., Caselle, J., Dong, C., and McWilliams, J. (2010). Realized and potential larval connectivity in the Southern California Bight. *Marine Ecology Progress Series*, 401:31–48.

Wellington, G. M. and Victor, B. C. (1989). Planktonic larval duration of one hundred species of Pacific and Atlantic damselfishes (Pomacentridae). *Marine Biology*, 101(4):557–567.

Wentz, F. J., Gentemann, C., Smith, D., and Chelton, D. (2000). Satellite Measurements of Sea Surface Temperature Through Clouds. *Science*, 288(5467):847–850.

Werner, F. E., Cowen, R. K., and Paris, C. B. (2007). Coupled biological and physical models present capabilities and necessary developments for future studies of population connectivity. *Oceanography*, 20(3):54–69.

Werner, F. E., Quinlan, J. A., Lough, R. G., and Lynch, D. R. (2001). Spatially-explicit individual based modeling of marine populations: a review of the advances in the 1990s. *Sarsia*, 86(6):411–421.

Whittick, A. (2007). Western Indian Ocean Marine Science Association Annual Report 2006. page 26.

Wilkinson, C. R., Souter, D., and Network, G. C. R. M. (2008). *Status of Caribbean coral reefs after bleaching and hurricanes in 2005*. Global Coral Reef Monitoring Network.

Williams, D. M., English, S., and Milicich, M. J. (1994). Annual recruitment surveys of coral reef fishes are good indicators of patterns of settlement. *Bulletin of Marine Science*, 54(1):314–331.

Willis, B. L. and Oliver, J. K. (1990). Direct tracking of coral larvae: Implications for dispersal studies of planktonic larvae in topographically complex environments. *Ophelia*, 32(1-2):145–162.

Willis, T., Millar, R., Babcock, R., and Tolimieri, N. (2003). Burdens of evidence and the benefits of marine reserves: putting Descartes before des horse? *Environmental Conservation*, null(02):97–103.

Winterbottom, R. and McLennan, D. A. (1993). Cladogram Versality: Evolution and Biogeography of Acanthuroid Fishes. *Evolution*, 47(5):1557–1571.

Wolanski, E., Doherty, P., and Carleton, J. (1997). Directional Swimming of Fish Larvae Determines Connectivity of Fish Populations on the Great Barrier Reef. *Naturwissenschaften*, 84(6):262–268.

Wolanski, E. and Kingsford, M. J. (2014). Oceanographic and behavioural assumptions in models of the fate of coral and coral reef fish larvae. *Journal of The Royal Society Interface*, 11(98):20140209.

Wyrtki, K. (1973). An equatorial jet in the Indian Ocean. *Science*, 181(4096):262–264.

Xie, S.-P., Annamalai, H., Schott, F. A., and McCreary Jr, J. P. (2002). Structure and mechanisms of south indian ocean climate variability*. *Journal of Climate*, 15(8):864–878.

Yahya, S. A. S., Muhando, C., and Gullstrm, M. (2011). Fish and sea urchin community patterns and habitat effects on Tanzanian coral reefs.

Zavala-Garay, J., Theiss, J., Moulton, M., Walsh, C., van Woesik, R., Mayorga-Adame, C. G., Garca-Reyes, M., Mukaka, D. S., Whilden, K., and Shaghude, Y. W. (2015). On the dynamics of the Zanzibar Channel. *Journal of Geophysical Research: Oceans*, pages n/a–n/a.

Zavala-Hidalgo, J., Morey, S. L., and O'Brien, J. J. (2003). Cyclonic eddies northeast of the Campeche Bank from altimetry data. *Journal of physical oceanography*, 33(3):623–629.